NUMERICAL TIDAL MODELS WITH UNEQUAL GRID-SPACING

RECOMMENDED:

Patrick Kinsey

Chairman, Advisory Committee

W. S. Reff
Department Head

APPROVED:

Dean of the College of Mathematics, Physical Sciences
and Engineering.

Dec. 14, 1972
Date

Vice President for Research and Advanced Study

Dec 14 1972
Date

NUMERICAL TIDAL MODELS WITH UNEQUAL GRID-SPACING

A

DISSERTATION

Presented to the Faculty of the

University of Alaska in Partial Fulfillment

of the Requirements

for the Degree of

DOCTOR OF PHILOSOPHY

By

John Christian Hartley Mungall,

B.Sc., M.Sc., M.Sc.

Fairbanks, Alaska

May, 1973

ABSTRACT

A two-dimensional alternating-direction implicit numerical tidal model with unequal grid-spacing is developed and successfully tested. The method is essentially an extension into two dimensions of a one-dimensional implicit method in which tide heights and flow rates are evaluated on the same cross-sections, an approach which permits a river to be schematized into a number of sections of differing lengths.

The two-dimensional scheme gives the user considerable control over the density of the computation points in a region by virtue of the fact that heights and depth-mean currents are evaluated midway between the points of intersection of a grid constructed from orthogonal lines, the spacing between which may be chosen at will.

The method is applied initally to the Irish Sea using a grid of constant spacing. The effects of increasing time step and friction on stability and accuracy are investigated, and the model is proved to be unconditionally stable. The results match those of previous investigators, and some new information on the M_2 currents of the region is obtained. The second application of the model is to a 'rectangular' North Sea, a favorable comparison being obtained when the region is schematized by two grids of equal and unequal spacing. Finally, the model is applied to Cook Inlet, Alaska, a region of complexity sufficient to warrant the use of a scheme possessing the unequal grid-spacing feature. Satisfactory results are obtained after tuning the model by adjustment of the friction coefficient.

Movie films were made in order to conceptually clarify the tidal behaviors of the Irish Sea and Cook Inlet. Each film shows as functions of time, perspective views of the sea surface, and current vectors superimposed on a contour map of the sea surface.

ACKNOWLEDGEMENTS

Particular thanks are due to

Mrs. Lavonia Wiele who typed the entire dissertation, and

uncovered many slips and inconsistencies in the process.

Lastly, this dissertation could not have been produced except for

the generous support of the United States Office of Naval Research

under contract N00014-67-A-0317-0002.

TABLE OF CONTENTS

TABLE OF CONTENTS
(cont'd)

LIST OF TABLES

LIST OF FIGURES

LIST OF FIGURES
(cont'd)

LIST OF FIGURES
(cont'd)

LIST OF SYMBOLS

a = water depth below river surface

a_o = water depth below horizontal datum

a_m = water depth below mean water level

a_r = hydraulic radius

A = cross-sectional area

b = width of river at surface (storage width)

b_s = mean width of river section (stream width)

C = Chézy friction coefficient

d = water depth below sea surface

D = mean water depth below sea surface in center of rectangle

f = Coriolis parameter, $2\,\Omega\,\sin\phi$

g = gravitational acceleration

h = surface height above horizontal datum

$\hat{h}$ = amplitude of first harmonic of river surface height

H , H^+ , H^- = complex tide height amplitudes

H_m , H'_m = instantaneous finite-difference values of tide height above horizontal datum at ends of river sections. The prime denotes upper time level $t+\tau$

$H_{m,n}$, $H'_{m,n}$, $H''_{m,n}$ = instantaneous finite-difference values of tide height above horizontal datum at grid point m,n. The primes denote intermediate and upper time levels $t+(\tau/2)$ and $t+\tau$

i = $\sqrt{-1}$

k = complex propagation factor

k = friction coefficient, g/C^2

ℓ = section length in river scheme

L = complex transfer coefficient

L = wavelength

m_1 = Lorentz's number, $8/(3\pi)$

M = complex transfer coefficient

N = complex transfer coefficient

O = complex transfer coefficient

q = instantaneous flow rate through a cross-section

$\hat{q}$ = amplitude of first harmonic of flow rate

Q , Q^+ , Q^- = complex flow rate amplitudes

Q_m , Q'_m = instantaneous finite-difference values of flow rate at ends of river sections. The prime denotes upper time level $t+\tau$. Q is positive in direction of increasing x

t = time

T = period of first harmonic

u = current positive in direction of increasing x, except in Chapter X

$U_{m,n}$, $U'_{m,n}$, $U''_{m,n}$ = instantaneous finite-difference values of current in the x-direction at grid point m,n. The primes denote intermediate and upper time levels $t+(\tau/2)$ and $t+\tau$

v = current in sea, positive in direction of increasing y

$V_{m,n}$, $V'_{m,n}$, $V''_{m,n}$ = instantaneous finite-difference values of current in the y-direction at grid point m,n. The primes denote intermediate and upper time levels $t+(\tau/2)$ and $t+\tau$

x = distance along river

x, y = rectangular coordinates, counterclockwise in the horizontal plane

z = vertical coordinate, positive upwards

β = wave frequency, $2\pi/T$

$(\Delta x)_m$ = section length in river scheme

$(\Delta x)_m$ = spacing between grid lines $(m-1)$ and $(m+1)$

$(\Delta y)_n$ = spacing between grid lines $(n-1)$ and $(n+1)$

λ = eigenvalue

δ = wave number, $2\pi/L$

τ = time step

ϕ = northerly latitude

ω = angular frequency of first harmonic, $2\pi/T$

Ω = angular frequency of earth's rotation

CHAPTER I

INTRODUCTION

It has been possible for some sixty years or more to make use of numerical tidal models in order to compute the propagation of tides in inlets and semi-enclosed seas. The first phase of the development was one which was dominated by the use of the equations of motion and continuity in a form such that the time dependency was removed. Although this restricted the user to solutions that were represented by the first few terms of a harmonic series, it provided the investigator, armed only with a desk calculator, the means of obtaining an insight into the tidal behavior of one-dimensional river networks.

The second phase of the development of numerical tidal models occurred with the advent of digital computers: the investigator was freed from the restraints of over-simplified equations and series solutions, and the direct solution of the nonlinear equations of motion and continuity in one or two dimensions became possible. Arbitrary boundary conditions could be specified as a function of time, and the distribution of heights and flow rates (or currents) could be obtained at discrete time steps.

In order to extend the predictive capability of models to cover a wide range of problems, considerable efforts have been made recently by various workers to increase the performance and flexibility of one- and two-dimensional numerical tidal models. The performance of the

1

models has been improved mostly by the careful selection of finite-difference schemes, and guide lines as to the effect of choice of time step and grid-spacing on error-wave propagation have been determined. Attention has been paid to the requirement of flexibility with the goal of providing the investigator with a range of models to suit his requirements. Examples of possibilities now available to the modeller are: ease of application as regards schematization and reprogramming, the inclusion of sloping or flooding boundaries, the choice of coordinate system, the approximation of tidal bores, the inclusion of storm surges, and the study of diffusion.

On considering the above, it was felt that an area needing attention was that of schematization; in particular it seems that the modeller is too restricted as to the positioning of computation points when using two-dimensional models. Although this problem may be alleviated to a certain extent by an appropriate choice of coordinate system, a large amount of flexibility is sacrificed. Furthermore, on the one hand the modeller may wish to increase the density of computation points in certain areas of interest within the model, and on the other hand he may wish to decrease the density of computation points in less interesting regions in order to lessen computer core storage requirements, and to decrease computer time. This is usually not practical with conventional coordinate systems.

The main objective of this investigation is then to present an alternative solution; a two-dimensional grid scheme with unequal spacing. The user is restricted to an orthogonal grid constructed from vertical and horizontal lines; other than this he can choose the spacing between

the lines as he wishes, although he must always consider the possibility
of distortion of the computed tidal wave due to choice of time step
and grid spacing and furthermore the user may be limited by the require-
ment that violent increases in grid-spacing should be avoided.

It is felt appropriate here to present the layout of the chapters
that follow. Pertinent background to the proposed scheme is contained
in Chapters II and III. Two of the most important types of variable
section-length one-dimensional methods, the harmonic method and a
sophisticated implicit method, are covered in detail and are applied in
turn to the same estuary network. The reasons for the selection of
these particular methods is of importance. The harmonic method was
developed by Lorentz (1926) for the study of the proposed enclosure
of the Zuiderzee. The method assumes that the solution for the heights
and flow rates can be obtained in the form of a single sinusoid. The
method was later extended to include a steady river-flow term (Mazure,
1937) and further to include additional harmonics (Dronkers, 1947).
Stability problems are totally absent due to the removal of the time-
dependency. Despite the criticism of Harleman and Lee (1969, p. 5) that
the programming of methods such as the harmonic method represents a step
backwards on account of the use of linearized equations, it is felt that
the method is still of considerable interest. The use of models extends
beyond that of accurate prediction -- a suitably designed model can aid
in gaining an insight into the relationship between the variables of the
system being studied (an example of this is given in Chapter X). The
analogy between river networks and electrical transmission lines also

may be helpful. Furthermore the harmonic method was designed for hand
computation, and thus can be used when a computer is not available.
As no detailed references in English are available except that of
Dronkers (1964), who concentrates mainly on the theory of what might
be called the multiple harmonic method, it is felt that a useful purpose
will be served by a detailed description.

The implicit method described in Chapter III is the so-called
third implicit method of Dronkers (1969). As it is the extension of
this method into two dimensions that forms the basis of the proposed
two-dimensional model with unequal grid-spacing, it is felt that a
full description of the method is mandatory. Unfortunately in his
1969 publication Dronkers gave only the briefest mention of the additions
necessary for the solution of problems involving networks. The so-called
down-river recursion formulae are presented in an overly compact form,
and only one paragraph is devoted to networks. For this reason particu-
lar attention has been devoted to a full presentation of the method as
needed for the solution of river network problems.

The description of the proposed scheme is presented in Chapter IV.
The concept of extending the method described in Chapter III to that of
applying pairs of equations alternately to rows and columns arose as
a combination of the one-dimensional implicit method and of the
alternating-direction method of carrying out implicit computations in
two dimensions. Besides mention of previous two-dimensional methods
that compare to a certain degree with the proposed unequal grid-spacing
method, Chapter IV includes descriptions of the grid scheme and the

finite-difference forms of the equations of motion and continuity, and of the arrangement in time and space of the computation points required by each pair of finite-difference equations. Compact versions of the finite-difference equations in forms suitable for solution by the double sweep method are given in Chapter V. Although the elements of the method of solution were described in Chapter III, the method is covered in detail in Chapter V for the sake of completeness.

It was decided that a description of programming and analysis considerations as applied to numerical tidal modelling should be included in Chapter VI. Although most experienced modellers will doubtless have their own approach to the problem of organizing the programs, the chapter may perhaps be of interest to anyone entering the field.

Chapters VII, VIII, and IX are concerned with three series of tests to which the proposed scheme was subjected. The first two series are based on the application of the model to areas for which solutions of the tidal regime are available (the Irish Sea and a 'rectangular' North Sea). The tests were conducted to compare the model results with these previous results, to determine the effect of unequal grid-spacing, and to investigate the effect of time step, depth, grid-spacing, and friction on stability. The third and last series of tests was to apply the model to the relatively unstudied region of Cook Inlet for which results were required. Owing to its size and complexity the region is such that the investigation could not have been conveniently undertaken without the unequal grid-spacing scheme. The results were compared with tidal constants obtained from the United States Coast and Geodetic

Survey. It is felt that this application constitutes a realistic test of the model.

The results of the three series of tests were in close agreement with the previously calculated or observed values of other investigators. Because the tests on the Irish Sea and Cook Inlet were performed with realistic schematizations it was felt that it would be a pity not to make additional use of the data produced. Some time was spent in devising meaningful ways of presenting in condensed form the great quantity of data that is generated by finite-difference models. In particular it was decided that the information could best be presented via perspective views of the sea surface, and via plots of current vectors along with contours of tide height for any desired time step. To this end 35 mm films were produced using a cathode ray tube graphic output device at the National Center for Atmospheric Research. Chapter X contains representative frames from these films for each lunar hour of the M_2 tidal cycle. To increase the information content, the two types of output, perspective and plan view, were rephotographed side-by-side, as this could not be done during the computation for reasons of resolution. It is hoped that the resulting pictures of the Irish Sea will make a useful contribution to the literature on the Irish Sea. The pictures of Cook Inlet may also be of use to those concerned with shipping, oil-well operations, and future investigations.

CHAPTER II

HYDRAULIC CALCULATIONS USING THE HARMONIC METHOD

Introduction

The harmonic method, developed during preliminary studies on the closure of the Zuiderzee (Lorentz, 1926), was the first of the hydraulic computation methods that permitted the inclusion of sections of different lengths. It will be discussed in some detail because of this, and also because it is currently being used and is amenable to hand computation. For more detailed information on the harmonic method the reader is referred to Dronkers and Schönfeld (1955) and to Dronkers (1964).

Simplification of the Equations of Motion and Continuity

The form in which the equations of motion and continuity are used is as follows (Dronkers, 1964):

$$\frac{\partial h}{\partial x} + \frac{1}{gA}\frac{\partial q}{\partial t} + \frac{q|q|}{C^2 A^2 a_r} = 0 \tag{2.1}$$

and

$$\frac{\partial q}{\partial x} + b\frac{\partial h}{\partial t} = 0 \quad . \tag{2.2}$$

h is the height of the water surface above some horizontal datum, q is the flow rate in the x-direction, and b is the width of the

channel at the water surface. A is the cross-sectional area, a_r is the hydraulic radius (cross-sectional area divided by wetted perimeter), C is the Chézy friction coefficient, and g is the gravitational acceleration. In this simplified description of the harmonic method, both flow rate and tide height will be represented by one harmonic only, of angular frequency ω. Furthermore, the steady-state flow rate and the change of mean water level with distance will be taken as zero, thus,

$$q = \hat{q} \cos(\omega t - \alpha) \tag{2.3}$$

$$h = h_0 + h_1 = 0 + \hat{h} \cos(\omega t - \beta) \quad . \tag{2.4a,b}$$

The object of the harmonic method is to arrive at a set of equations from which the time-dependence has been removed. Once this has been achieved, there will be no need of a form of solution (as is usually the case) involving repeated time steps.

The first step is to linearize equation (2.1). The approach of Lorentz (1926) was to ensure that $C^2 A^2 a$ total energy lost in the form of friction over a full tidal cycle should be the same in the nonlinear and linearized friction terms. Thus at any instant of time, the work per unit mass done against friction in the nonlinear and linearized forms during time δt is
$C^2 A^2 a$

$$\frac{g \, q|q|}{C^2 A^2 a_r} \, \delta x \quad \text{and} \quad \frac{g \, kq}{C^2 A^2 a_r} \, \delta x \quad , \tag{2.5a,b}$$

where k is the constant to be determined, and $\delta x = (q/A)\delta t$. Thus, over

a complete tidal cycle of period T we have

$$\int_0^T \frac{g\,q|q|}{C^2 A^2 a_r} \frac{q}{A}\,dt = \int_0^T \frac{g\,kq}{C^2 A^2 a_r} \frac{q}{A}\,dt \quad . \tag{2.6}$$

Substituting equation (2.3) into equation (2.6):

$$\int_0^T \frac{g[\hat{q}\cos(\omega t)]^2 |\hat{q}\cos(\omega t)|}{C^2 A^3 a_r}\,dt = \int_0^T \frac{g\,k[\hat{q}\cos(\omega t)]^2}{C^2 A^3 a_r}\,dt \quad , \tag{2.7}$$

or

$$k = \frac{\hat{q}\displaystyle\int_0^T \cos^2(\omega t)|\cos(\omega t)|\,dt}{\displaystyle\int_0^T \cos^2(\omega t)\,dt} \quad . \tag{2.8}$$

Finally,

$$k = \frac{\hat{q}\left[\dfrac{\sin(\omega t)}{\omega} - \dfrac{\sin^3(\omega t)}{3\omega}\right]_0^{T/4}}{\left[\dfrac{t}{2} + \dfrac{\sin(\omega t)\cos(\omega t)}{2\omega}\right]_0^{T/4}} \quad , \tag{2.9}$$

or

$$k = \frac{8}{3\pi}\hat{q} = m_1\hat{q} \quad . \tag{2.10a,b}$$

The numerical quantity $8/(3\pi)$, which is equal to 0.8488 , is sometimes called Lorentz's number.

Thus equation (2.1) becomes

$$\frac{\partial h}{\partial x} + \frac{1}{gA} \frac{\partial q}{\partial t} + \frac{m_1 \hat{q} q}{C^2 A^2 a_r} = 0 \quad . \tag{2.11}$$

The second step is to include, in simple form, the effect of the variation of the cross-sectional area and hydraulic radius with tide height. To achieve this, mean values will be used along with time-independent corrections. The development of these two terms follows closely that of Stroband (1970a).

Referring to Figure 2.1, the following new quantities are introduced:

    a = total water depth

    a_o = depth of bottom below datum

    a_m = depth of bottom below mean water level

    b_s = mean stream width .

The quantity $1/(gA)$ in equation (2.11) is found as follows:

$$M = \frac{1}{gA} = \frac{1}{g \, b_s a} = \frac{1}{g \, b_s (a_m + h_1)} \quad ,$$

or

$$M = \frac{\left[1 + \dfrac{h_1}{a_m} \right]^{-1}}{g \, b_s a_m} \quad .$$

Expanding the quantity in the brackets,

$$M = \frac{1}{g \, b_s a_m} \left\{ 1 - \frac{h_1}{a_m} + \frac{h_1^2}{a_m^2} - \, \ldots \, \right\} \quad ,$$
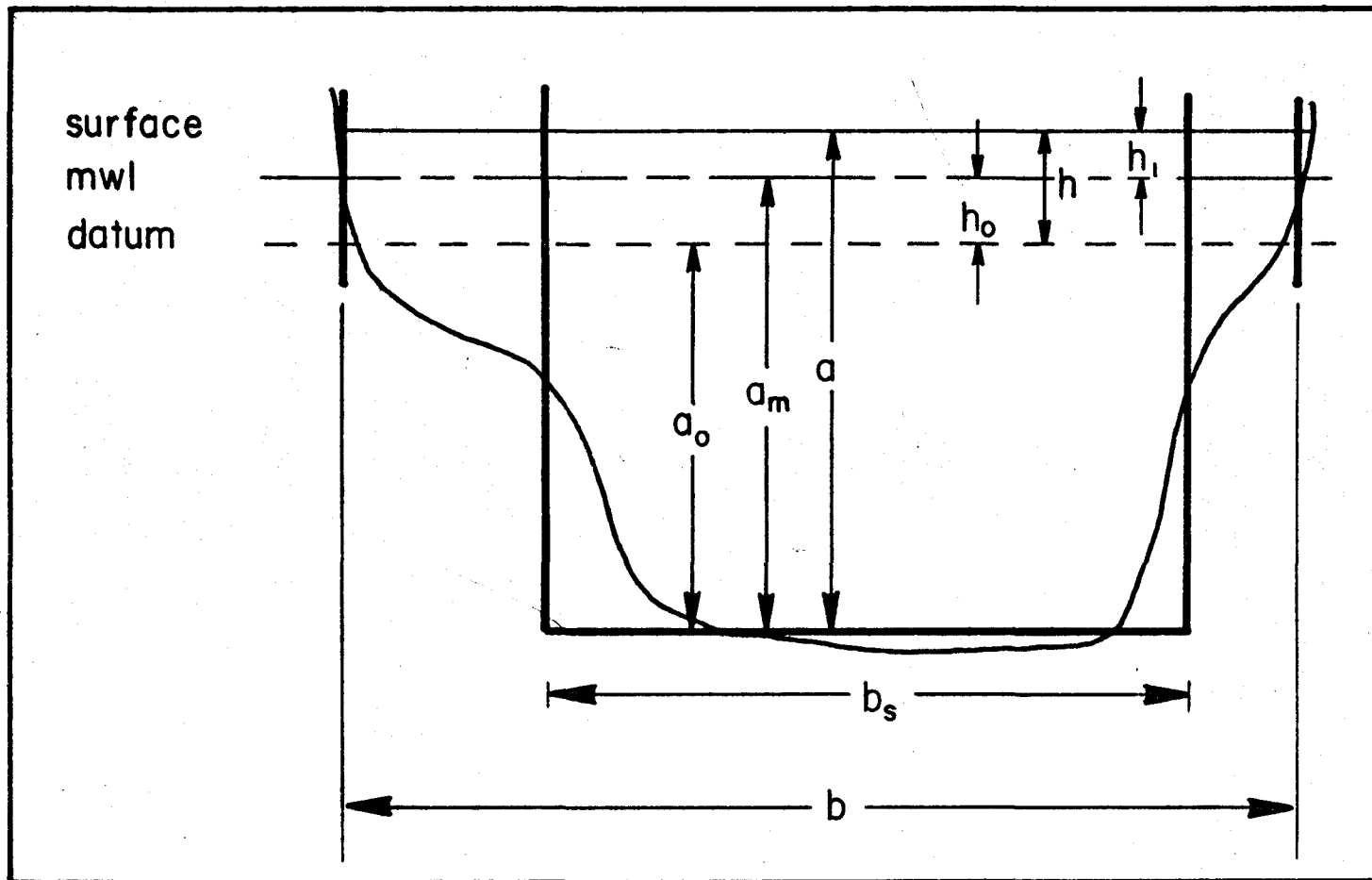
Figure 2.1. Location of dimensions referred to in Chapters 2 and 3.

or

$$M = \frac{1}{g\,b_s a_m} \left\{ 1 + \frac{(\hat{h})^2}{2a_m^2} - \frac{\hat{h}}{a_m}\cos(\omega t - \beta) + \frac{(\hat{h})^2}{2a_m^2}\cos 2(\omega t - \beta) + \dots \right\}. \tag{2.12}$$

On retaining only the time-independent part of equation (2.12).

$$M = \frac{\bar{N}_o}{g\,A_m}, \tag{2.13}$$

where

$$A_m = b_s a_m, \quad \bar{N}_o = 1 + \frac{(\hat{h})^2}{2a_m^2}, \tag{2.14a,b}$$

A_m being the mean cross-sectional area of the section.

The quantity $1/(C^2 A^2 a_r)$ in equation (2.11) is found as follows.

$$W = \frac{1}{C^2 A^2 a_r} = \frac{1}{C^2 b_s^2 a^3 \dfrac{a_r}{a}} = \frac{1}{C^2 b_s^2 \dfrac{a_r}{a} a_m^3 \left[1 + \dfrac{h_1}{a_m}\right]^3},$$

or

$$W = \frac{\left[1 + \dfrac{h_1}{a_m}\right]^{-3}}{C_m^2 b_s^2 \dfrac{a_{rm}}{a_m} a_m^3} = \frac{\left[1 + \dfrac{h_1}{a_m}\right]^{-3}}{(C^2 A^2 a_r)_m},$$

where C_m and a_{rm} are respectively the mean friction coefficient and the mean hydraulic radius.

On expanding,

$$W = \frac{1}{(C^2 A^2 a_r)_m} \left\{ 1 - 3 \frac{h_1}{a_m} + 6 \left(\frac{h_1}{a_m} \right)^2 - \ldots \right\},$$

or

$$W = \frac{1}{(C^2 A^2 a_r)_m} \left\{ 1 + \frac{3(\hat{h})^2}{a_m^2} - \frac{3\hat{h}}{a_m} \cos(\omega t - \beta) + \frac{3(\hat{h})^2}{a_m^2} \cos 2(\omega t - \beta) - \ldots \right\}.$$

$$(2.15).$$

The subscript 'm' indicates that a mean value of the quantity in brackets is to be used. Again, retaining only the time independent part of equation (2.15),

$$W = \frac{1}{(C^2 A^2 a_r)_m} \left(1 + \frac{3(\hat{h})^2}{a_m^2} \right) . \qquad (2.16)$$

Finally, for convenience, we put

$$R = m_1 \hat{q} W = \frac{m_1 \hat{q} N_o}{(C^2 A^2 a_r)_m} \qquad (2.17a)$$

where

$$N_o = 1 + \frac{3(\hat{h})^2}{a_m^2} , \qquad (2.17b)$$

so that equation (2.11) becomes

$$\frac{\partial h}{\partial x} + M \frac{\partial q}{\partial t} + R q = 0 . \qquad (2.18)$$

Again,

$$\frac{\partial q}{\partial x} + b \frac{\partial h}{\partial t} = 0 . \qquad (2.2)$$

Derivation of Time-Independent Equations of Motion and Continuity

First, equations (2.3) and (2.4b) are put into complex form:

$$q = \frac{Q^+}{2} \exp(i\omega t) + \frac{Q^-}{2} \exp(-i\omega t) \ , \tag{2.19}$$

and

$$h = \frac{H^+}{2} \exp(i\omega t) + \frac{H^-}{2} \exp(-i\omega t) \ , \tag{2.20}$$

where

$$Q^+ = \hat{q} \exp(-i\alpha); \quad Q^- = \hat{q} \exp(i\alpha) \tag{2.21a,b}$$

and

$$H^+ = \hat{h} \exp(-i\beta); \quad H^- = \hat{h} \exp(i\beta) \ . \tag{2.22a,b}$$

Substituting equations (2.19) and (2.20) into equations (2.18) and (2.2), upon equating terms containing $\exp(i\omega t)$ one obtains:

$$\frac{dH^+}{dx} + (i\omega M + R)Q^+ = 0 \tag{2.23}$$

and

$$\frac{dQ^+}{dx} + i\omega b \ H^+ = 0 \ . \tag{2.24}$$

Combining equations (2.23) and (2.24),

$$\frac{d_2 H^+}{dx^2} - k^2 H^+ = 0 \ , \tag{2.25}$$

where

$$k^2 = -\omega^2 bM + i\omega bR \ . \tag{2.26}$$

Assuming a solution to equation (2.25) of the form

$$H^+(x) = A \exp(kx) + B \exp(-kx) \tag{2.27}$$

so that

$$H^+(0) = A + B \, , \qquad (2.28)$$

one arrives at

$$H(x) = L\,H(0) + M\,Q(0) \qquad (2.29)$$

and

$$Q(x) = N\,H(0) + 0\,Q(0) \, , \qquad (2.30)$$

(where the '+' superscript has been dropped for convenience), and

$$L = \cosh(kx) \qquad (2.31)$$

$$M = \frac{ik}{\omega b}\,\sinh(kx) \qquad (2.32)$$

$$N = -\frac{i\omega b}{k}\,\sinh(kx) \qquad (2.33)$$

$$0 = \cosh(kx). \qquad (2.34)$$

It should be noted that $(L0 - MN) = 1$

Also, as a reminder,

$$H = \hat{h}\,\exp(-i\beta); \qquad Q = \hat{q}\,\exp(-i\alpha) \qquad (2.35a,b)$$

so that

$$\hat{h} = \sqrt{H_r^2 + H_i^2} \, ; \qquad \tan\beta = -\frac{H_i}{H_r} \qquad (2.36a,b)$$

and

$$\hat{q} = \sqrt{Q_r^2 + Q_i^2} \, ; \qquad \tan\alpha = -\frac{Q_i}{Q_r} \, , \qquad (2.37a,b)$$

where the suffixes r and i denote respectively real and imaginary parts.

The significance of equations (2.29) and (2.30) is that given a section of length ℓ , once one has estimated $\hat{h}$ and $\hat{q}$ in the center of the section and calculated the complex quantities L , M , N , and O , the complex values of height and flow rate at $x=\ell$ may be found in terms of those at $x=0$.

The Development of Recursion Formulae for a River Branch

To calculate the tides in a river branch, the branch must first be divided into a number of sections, and the mean stream width, cross-sectional area, hydraulic radius, and Chézy coefficient determined for each. A distinct advantage of the harmonic method is that the sections need not be of equal length, and so may be chosen as is most convenient. At the start of each iteration values for $\hat{h}_m$ and $\hat{q}_m$ are selected for the center of each section and L_m , M_m , N_m and O_m are then calculated for each of the M-1 sections (see Figure 2.2). An example of the calculation of L_m , M_m , N_m and O_m' is given in Appendix I.

The next step in the procedure is to express H_m and Q_m in terms of H_M and Q_M (the height and flow rate at the right-hand end of the branch) -- both of which are assumed for the moment to be unknown. The necessary recursion formulae are developed using the repeated application of equations (2.29) and (2.30). Thus for section M-1

$$H_{M-1} = L_{M-1}H_M + M_{M-1}Q_M \tag{2.38}$$

$$Q_{M-1} = N_{M-1}H_M + O_{M-1}Q_M , \tag{2.39}$$
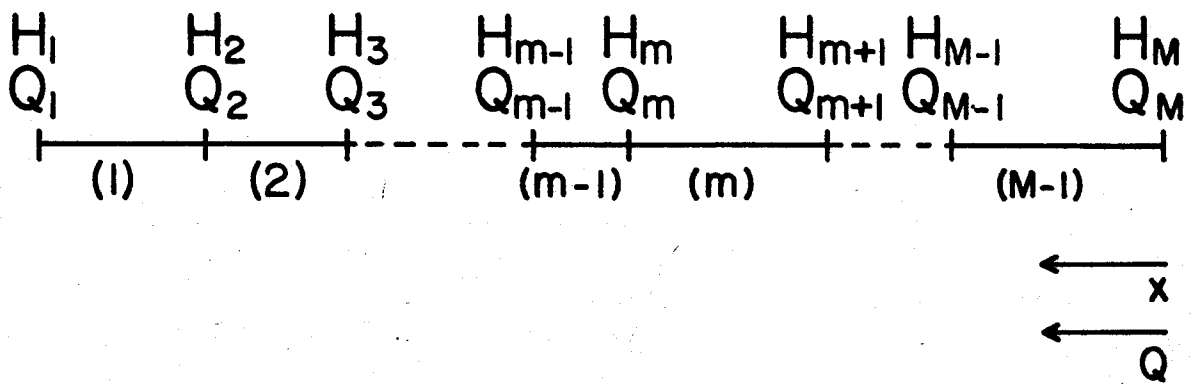
Figure 2.2. Location of quantities for the Harmonic Method.

and for section M-2

$$H_{M-2} = \left(L_{M-2} L_{M-1} + M_{M-2} N_{M-1} \right) H_M + \left(L_{M-2} M_{M-1} + M_{M-2} O_{M-1} \right) Q_M$$

(2.40)

$$Q_{M-2} = \left(N_{M-2} L_{M-1} + O_{M-2} N_{M-1} \right) H_M + \left(N_{M-2} M_{M-1} + O_{M-2} O_{M-1} \right) Q_M.$$

(2.41)

In general,

$$H_m = L'_m H_M + M'_m Q_M$$

(2.42)

$$Q_m = N'_m H_M + O'_m Q_M$$

(2.43)

for m = M-1, M-2, ..., 2, 1,

where

$$L'_{M-1} = L_{M-1} \; ; \quad M'_{M-1} = M_{M-1} \; ; \quad N'_{M-1} = N_{M-1} \; ; \quad O'_{M-1} = O_{M-1} \quad ,$$

and

$$L'_{m-1} = L_{m-1} L'_m + M_{m-1} N'_m$$

(2.44)

$$M'_{m-1} = L_{m-1} M'_m + M_{m-1} O'_m$$

(2.45)

$$N'_{m-1} = N_{m-1} L'_m + O_{m-1} N'_m$$

(2.46)

$$O'_{m-1} = N_{m-1} M'_m + O_{m-1} O'_m$$

(2.47)

for m = M-1, M-2, ..., 2.

Of interest is the fact that, if $(LO - MN) = 1$, then we also have $(L'O' - M'N') = 1$. Equations (2.44) through (2.47) are used to calculate L'_m , M'_m , N'_m , and O'_m for each section in turn. Equations (2.42) and (2.43), with m=1, give

$$H_1 = L'_1 H_M + M'_1 Q_M$$

(2.48)

$$Q_1 = N_1' \, H_M + O_1' \, Q_M \; . \tag{2.49}$$

For the case of a river without branch-points, two of the four complex values H_1 , Q_1 , H_M and Q_M must be given as boundary conditions. This allows the other two values to be calculated from equations (2.48) and (2.49). When H_M and Q_M have been determined, equations (2.42) and (2.43) are used to calculate all the remaining unknown H_m and Q_m . New values of $\hat{q}_m$ and $\hat{h}_m$ for the center of each section are computed from the values Q_{m+1} and Q_m , H_{m+1} and H_m , and are then compared with the values selected at the start of the iteration. A fresh estimate is then made, and another iteration performed. The process is continued until the difference between consecutive values of $\hat{h}_m$ and $\hat{q}_m$ reaches an acceptable level.

Calculation of Heights and Flow Rates for the Case of Two or More River Branches

The calculation of the tides for a river network such as that shown in Figure 2.3 presents no particular difficulties as long as the assumptions mentioned earlier are adhered to.

In general, two unknowns, H and Q , will occur at the left and the right of each branch j -- thus there are 24 unknown branch-point values in the above example. If ℓ and r (left and right) are used as subscripts, and superscripts 1, 2, ..., 6 are used to indicate branches 1, 2, ..., 6, the unknowns are of the form H_ℓ^1 , Q_ℓ^1 , H_r^1 , Q_r^1 , H_ℓ^2 , Q_ℓ^2 ....., H_ℓ^6 , Q_ℓ^6 , H_r^6 , Q_r^6 . The method of solution is to apply the
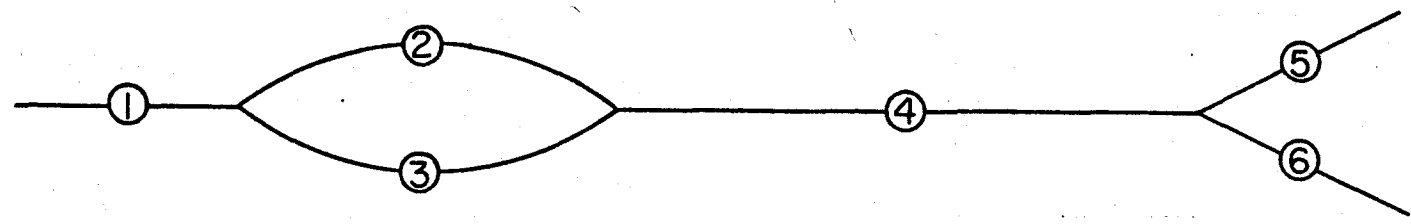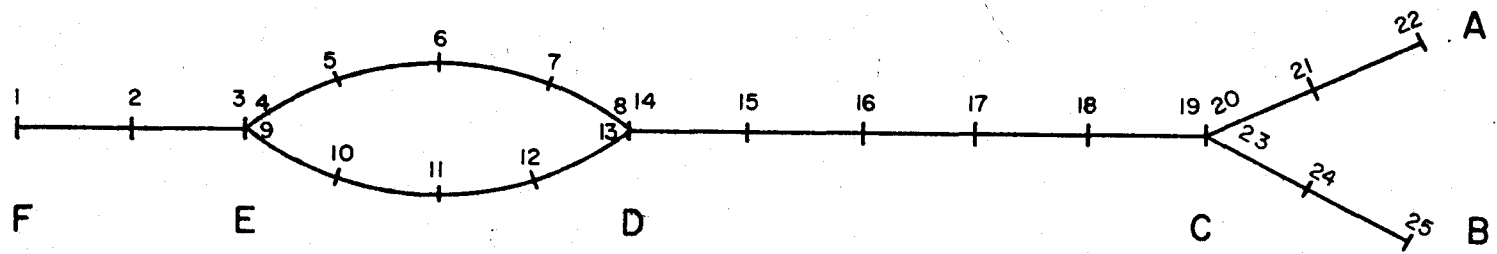
Figure 2.3. River System showing computation points and branch numbers

recursion formulae, equations (2.44) through (2.47), to each of the 6 branches in turn so as to produce 6 pairs of equations of the type

$$H_\ell^j = L_\ell'^j H_r^j + M_\ell'^j Q_r^j \tag{2.50}$$

$$Q_\ell^j = N_\ell'^j H_r^j + O_\ell'^j Q_r^j \tag{2.51}$$

$$\text{for } j = 1, 2, \ldots, 6.$$

Then, to apply the boundary conditions, the tide heights are put equal at points C, D, and E, giving

$$H_r^1 = H_\ell^2 = H_\ell^3 = H_E, \tag{2.52a,b}$$

$$H_r^2 = H_r^3 = H_\ell^4 = H_D, \tag{2.53a,b}$$

$$H_r^4 = H_\ell^5 = H_\ell^6 = H_C. \tag{2.54a,b}$$

Next, conservation of mass is applied at branch-points C, D, and E. The step requires first that equations (2.50) and (2.51) (for j=1, 2, 3, and 4) be rearranged so that Q_ℓ^j and Q_r^j are each expressed in terms of H_ℓ^j and H_r^j. Thus

$$Q_r^j = \left[\frac{1}{M_\ell'^j} \right] H_\ell^j + \left[-\frac{L_\ell'^j}{M_\ell'^j} \right] H_r^j \tag{2.55}$$

and

$$Q_\ell^j = \left[\frac{O_\ell'^j}{M_\ell'^j} \right] H_\ell^j + \left[N_\ell'^j - \frac{O_\ell'^j L_\ell'^j}{M_\ell'^j} \right] H_r^j \quad , \tag{2.56a}$$

or

$$Q_\ell^j = \left[\frac{O_\ell'^j}{M_\ell'^j} \right] H_\ell^j + \left[-\frac{1}{M_\ell'^j} \right] H_r^j \tag{2.56b}$$

$$\text{for } j = 1, 2, 3, 4.$$

For branches 5 and 6 (with flow rates of zero at the right-hand ends), it is convenient to calculate

$$Q_\ell^j = \frac{N_\ell^{'j}}{L_\ell^{'j}} H_\ell^j \qquad (2.57)$$

for j=5, 6.

Then finally one forms the equations

$$Q_r^1 = Q_\ell^2 + Q_\ell^3 , \qquad (2.58)$$

$$Q_r^2 + Q_r^3 = Q_\ell^4 , \qquad (2.59)$$

$$Q_r^4 = Q_\ell^5 + Q_\ell^6 . \qquad (2.60)$$

At this point we have 12 + 6 + 3 = 21 equations and 24 unknowns. The remaining 3 equations are obtained from the boundary conditions at points A, B, and F. For example, one might have

$$Q_r^5 = Q_r^6 = 0 \qquad (2.61a,b)$$

and

$$H_\ell^1 = \hat{h} + i.0 , \qquad (2.62)$$

i.e. the flow rate is zero at points A and B, and the tide height is specified at point F as having zero phase. The set of (complex) algebraic equations is then solved to give the 24 unknowns, and then the values H_r^j, Q_r^j at the right of each branch enable H_m^j and Q_m^j to be calculated for each j by the use of equations (2.42) and (2.43). The iteration process is then repeated as desired. The process is shown in Appendix II.

HYDRAULIC CALCULATIONS USING THE ONE-DIMENSIONAL
IMPLICIT METHOD

Introduction

The method discussed here, the third implicit method of Dronkers (1969), is of particular interest in that it is unconditionally stable, and is well suited for use in complicated situations. It allows the use of sections of different lengths, and presents no difficulties at branch-points other than the fact that a set of simultaneous linear algebraic equations must be solved at each time step. The derivation of the equations of motion and continuity in forms suitable for use with the method will not be covered in detail here as it has been adequately described elsewhere (Dronkers, 1969). As the extension of this method into two dimensions forms the basis of the proposed unequal spacing scheme, it is considered necessary to present the method in detail -- all the omitted steps in Dronkers' 1969 paper being shown. Furthermore the latter paper gave only the shortest of descriptions as to the application of his implicit method to river branch systems. This matter is also dealt with in full in the following pages.

In terms of the current u , the equations of continuity and motion as used here are

$$\frac{\partial(Au)}{\partial x} = - b \frac{\partial h}{\partial t} \qquad (3.1)$$

$$\frac{\partial h}{\partial x} = - \frac{1}{g} \frac{\partial u}{\partial t} - \frac{u}{g} \frac{\partial u}{\partial x} - \frac{u|u|}{C^2(a_o + h)} \quad , \qquad (3.2)$$

where the variables are as defined earlier. In terms of the flow rate q , equation (3.1) is written

$$\frac{\partial q}{\partial x} = - b \frac{\partial h}{\partial t} \quad, \tag{3.3}$$

while equation (3.2) can be approximated by

$$\frac{\partial h}{\partial x} = - \frac{1}{gA} \frac{\partial q}{\partial t} - \frac{(b_s + b)}{gA^2} \frac{q}{b} \frac{\partial q}{\partial x} - \frac{q|q|}{C^2 A^2 (a_o + h)} \quad, \tag{3.4}$$

where b_s is the stream width, that is, $A = b_s (a_o + h)$.

The river branch is divided into M-1 sections of convenient length, each of length $(\Delta x)_m$ (see Figure 3.1). Height and flow rate are evaluated at the ends of each section. In the finite-difference form of equations (3.3) and (3.4) two time levels are used. Space derivatives are evaluated at the upper time level (indicated by primed superscripts) and time derivatives are evaluated from differences between the spatial averages at the two levels. For section m, the equations, in implicit finite-difference form, are

$$\frac{Q'_{m+1} - Q'_m}{(\Delta x)_m} = - b_m \left(\frac{\frac{H'_{m+1} + H'_m}{2} - \frac{H_{m+1} + H_m}{2}}{\tau} \right) \tag{3.5}$$

and

$$\frac{H'_{m+1} - H'_m}{(\Delta x)_m} = - \frac{1}{gA_m} \left(\frac{\frac{Q'_{m+1} + Q'_m}{2} - \frac{Q_{m+1} + Q_m}{2}}{\tau} \right)$$

$$- \frac{(b_{sm} + b_m)}{gA_m^2 b_m} \left(\frac{Q_{m+1} + Q_m}{2} \right) \left(\frac{Q'_{m+1} - Q'_m}{(\Delta x)_m} \right)$$

$$- \frac{\left(\frac{Q'_{m+1} + Q'_m}{2} \right) \left| \frac{Q_{m+1} + Q_m}{2} \right|}{C_m^2 A_m^2 (a_o + H)_m} \quad, \tag{3.6}$$
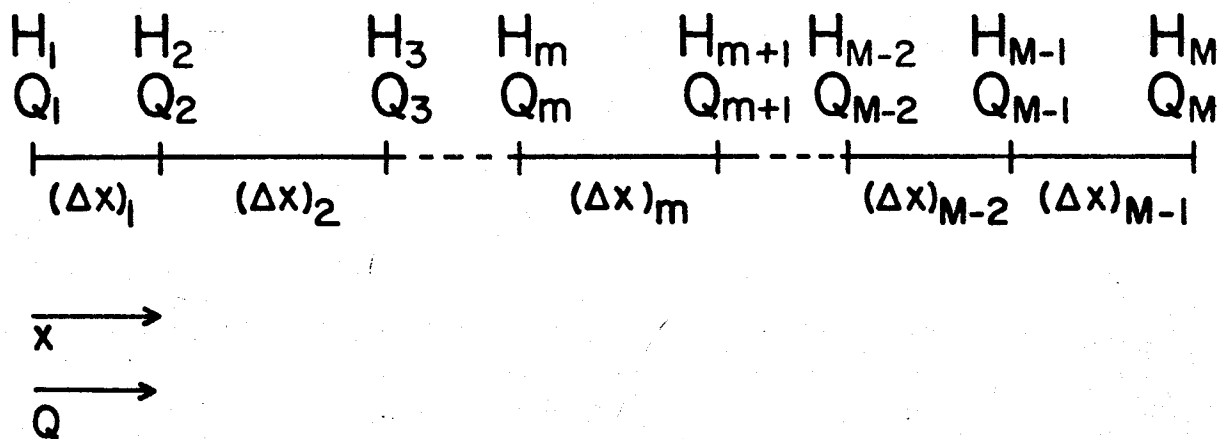
Figure 3.1. Location of quantities for the Implicit Method.

$$m=1, 2, \ldots, M-1,$$

where $(a_o + H)_m = a_{om} + \dfrac{H_{m+1} + H_m}{2}$, and τ is the time step.

A stability analysis (performed in Appendix III) shows that the above finite-difference scheme is unconditionally stable.

Equations (3.5) and (3.6) are handled more conveniently in the form

$$\nu_m \left(H'_{m+1} + H'_m \right) + Q'_{m+1} - Q'_m = \xi_m \tag{3.7}$$

and

$$H'_{m+1} - H'_m + \eta_m Q'_{m+1} + \theta_m Q'_m = \mu_m , \tag{3.8}$$

$$m=1, 2, \ldots, M-1.$$

ν_m , ξ_m , η_m , θ_m , and μ_m may be found by comparison (see Appendix IV) to be

$$\nu_m = \frac{(\Delta x)_m \, b_m}{2 \, \tau} \tag{3.9a}$$

$$\xi_m = \frac{(\Delta x)_m \, b_m \, (H_{m+1} + H_m)}{2 \, \tau} \tag{3.9b}$$

$$\eta_m = \frac{(\Delta x)_m}{2 \, \tau \, g A_m} + \frac{\left(b_{sm} + b_m \right)\left(Q_{m+1} + Q_m \right)}{2 g A_m^2 \, b_m} + \frac{(\Delta x)_m \left| Q_{m+1} + Q_m \right|}{4 \, C_m^2 \, A_m^2 \, a_m} \tag{3.9c}$$

$$\theta_m = \frac{(\Delta x)_m}{2 \, \tau \, g A_m} - \frac{\left(b_{sm} + b_m \right)\left(Q_{m+1} + Q_m \right)}{2 g A_m^2 \, b_m} + \frac{(\Delta x)_m \left| Q_{m+1} + Q_m \right|}{4 \, C_m^2 \, A_m^2 \, a_m} \tag{3.9d}$$

$$\mu_m = \frac{(\Delta x)_m \left(Q_{m+1} + Q_m \right)}{2 \, \tau \, g A_m} \tag{3.9e}$$

Equations (3.7) and (3.8) cannot be immediately evaluated as they each contain more than one unknown. To solve the equations one uses the so-called double sweep method which is based on the fact that the matrix for equations (3.7) and (3.8) may be reduced to one that is tridiagonal. The first and last rows of the matrix each contain one nonzero value located respectively in the first and last columns, and for the remaining rows all but the three elements centered on the diagonal are zero.

Up-river Recursion Formulae

Putting m=1 in equation (3.8)

$$Q_1' = - q_1 H_2' - t_1 Q_2' + s_1 + b_1 H_1' \ , \tag{3.10}$$

where

$$q_1 = \frac{1}{\theta_1} \ ; \ t_1 = \frac{\eta_1}{\theta_1} \ ; \ s_1 = \frac{\mu_1}{\theta_1} \ ; \ b_1 = \frac{1}{\theta_1} \ . \tag{3.11a,b,c,d}$$

Putting m=1 into equation (3.7) and substituting from equation (3.10)

$$H_2' = - p_2 Q_2' + r_2 + a_2 H_1' \ , \tag{3.12}$$

where

$$p_2 = \frac{1 + t_1}{\nu_1 + q_1} \ ; \ r_2 = \frac{\xi_1 + s_1}{\nu_1 + q_1} \ ; \ a_2 = \frac{b_1 - \nu_1}{\nu_1 + q_1} \ . \tag{3.13a,b,c}$$

Putting m=2 into equation (3.8) and substituting from equation (3.12)

$$Q_2' = - q_2 H_3' - t_2 Q_3' + s_2 + b_2 H_1' \ , \tag{3.14}$$

where

$$q_2 = \frac{1}{\theta_2 + p_2} \; ; \quad t_2 = \frac{\eta_2}{\theta_2 + p_2} \; ; \qquad (3.15a,b)$$

$$s_2 = \frac{\mu_2 + r_2}{\theta_2 + p_2} \; ; \quad b_2 = \frac{a_2}{\theta_2 + p_2} \; . \qquad (3.15c,d)$$

Putting m=2 into equation (3.7) and substituting from equations (3.12) and (3.14)

$$H'_3 = - p_3 Q'_3 + r_3 + a_3 H'_1 \; , \qquad (3.16)$$

where

$$\sigma_2 = 1 + \nu_2 p_2 \; ; \qquad p_3 = \frac{\sigma_2 t_2 + 1}{\sigma_2 q_2 + \nu_2} \; ; \qquad (3.17a,b)$$

$$r_3 = \frac{\xi_2 + \sigma_2 s_2 - \nu_2 r_2}{\sigma_2 q_2 + \nu_2} \; ; \quad a_3 = \frac{\sigma_2 b_2 - \nu_2 a_2}{\sigma_2 q_2 + \nu_2} \; . \qquad (3.17c,d)$$

In general, the up-river recursion formulae are

$$Q'_{m-1} = - q_{m-1} H'_m - t_{m-1} Q'_m + s_{m-1} + b_{m-1} H'_1 \qquad (3.18)$$

$$H'_m = - p_m Q'_m + r_m + a_m H'_1 \; , \qquad (3.19)$$

$$\text{for } m=2, 3, \ldots, M,$$

and

$$p_1 = 0 \; ; \quad r_1 = 0 \; ; \quad a_1 = 1 \; , \qquad (3.20a,b,c)$$

$$q_{m-1} = \frac{1}{p_{m-1} + \theta_{m-1}} \; ; \qquad t_{m-1} = \frac{\eta_{m-1}}{p_{m-1} + \theta_{m-1}} \; ; \qquad (3.20d,e)$$

$$s_{m-1} = \frac{r_{m-1} + \mu_{m-1}}{p_{m-1} + \theta_{m-1}} \; ; \qquad b_{m-1} = \frac{a_{m-1}}{p_{m-1} + \theta_{m-1}} \; ; \qquad (3.20f,g)$$

$$\sigma_{m-1} = 1 + \nu_{m-1} p_{m-1} \; ; \tag{3.20h}$$

$$p_m = \frac{\sigma_{m-1} \, t_{m-1} + 1}{\sigma_{m-1} \, q_{m-1} + \nu_{m-1}} \; ; \tag{3.20i}$$

$$r_m = \frac{\xi_{m-1} + \sigma_{m-1} \, s_{m-1} - \nu_{m-1} \, r_{m-1}}{\sigma_{m-1} \, q_{m-1} + \nu_{m-1}} \; ; \tag{3.20j}$$

$$a_m = \frac{\sigma_{m-1} \, b_{m-1} - \nu_{m-1} \, a_{m-1}}{\sigma_{m-1} \, q_{m-1} + \nu_{m-1}} \; , \tag{3.20k}$$

for m=2, 3, ..., M.

In particular, putting m=M into equation (3.19)

$$H'_M = - p_M Q'_M + r_M + a_M H'_1 \; , \tag{3.21}$$

so, in effect, we now have

$$H'_r = - p_M Q'_r + r_M + a_M H'_\ell \; , \tag{3.22}$$

where ℓ = left and r = right.

If H'_ℓ and Q'_r are available as boundary conditions, then H'_r can at once be found, and the remaining unknowns Q'_{M-1} , H'_{M-1} , ..., Q'_1 can be obtained using equations (3.18) and (3.19) and the values (stored during the computation) from equations (3.20a) to (3.20k). If, however, the estuary consists of a number of branch points, more equations are necessary to permit the solutions of the heights and flow rates at the branch points.

Down-River Recursion Formulae

The second equation is formed by a process similar to the previous upwards sweep. This time the flow rate at the right-hand end of the section is eliminated. Equation (3.8), for m=M-1 gives

$$Q'_M = - q^*_M H'_{M-1} - t^*_M Q'_{M-1} + s^*_M + b^*_M H'_M \quad , \tag{3.23}$$

where

$$q^*_M = \frac{-1}{n_{M-1}} \; ; \quad t^*_M = \frac{\theta_{M-1}}{n_{M-1}} \; ; \quad s^*_M = \frac{\mu_{M-1}}{n_{M-1}} \; ; \quad b^*_M = \frac{-1}{n_{M-1}} \quad . \tag{3.24a,b,c,d}$$

Putting m=M-1 into equation (3.7) and substituting from equation (3.23) gives

$$H'_{M-1} = - p^*_{M-1} Q'_{M-1} + r^*_{M-1} + a^*_{M-1} H'_M \quad , \tag{3.25}$$

where

$$p^*_{M-1} = \frac{1 + t^*_M}{q^*_M - \nu_{M-1}} \; ; \qquad r^*_{M-1} = \frac{s^*_M - \xi_{M-1}}{q^*_M - \nu_{M-1}} \; ; \tag{3.26a,b}$$

$$a^*_{M-1} = \frac{\nu_{M-1} + b^*_M}{q^*_M - \nu_{M-1}} \quad . \tag{3.26c}$$

Putting m=M-2 into equation (3.8) and substituting from equation (3.25) gives

$$Q'_{M-1} = - q^*_{M-1} H'_{M-2} - t^*_{M-1} Q'_{M-2} + s^*_{M-1} + b^*_{M-1} H'_M \quad , \tag{3.27}$$

where

$$q^*_{M-1} = \frac{-1}{n_{M-2} - p^*_{M-1}} \; ; \qquad t^*_{M-1} = \frac{\theta_{M-2}}{n_{M-2} - p^*_{M-1}} \; ; \tag{3.28a,b}$$

$$s^*_{M-1} = \frac{\mu_{M-2} - r^*_{M-1}}{n_{M-2} - p^*_{M-1}} \quad ; \qquad b^*_{M-1} = \frac{-a^*_{M-1}}{n_{M-2} - p^*_{M-1}} \quad . \tag{3.28c,d}$$

Putting m=M-2 into equation (3.7) and substituting from equations (3.25) and (3.27) gives

$$H'_{M-2} = -p^*_{M-2} Q'_{M-2} + r^*_{M-2} + a^*_{M-2} H'_M , \tag{3.29}$$

where

$$p^*_{M-2} = \frac{1 + t^*_{M-1} \sigma^*_{M-1}}{q^*_{M-1} \sigma^*_{M-1} - \nu_{M-2}} \quad ; \tag{3.30a}$$

$$r^*_{M-2} = \frac{s^*_{M-1} \sigma^*_{M-1} - \xi_{M-2} + \nu_{M-2} r^*_{M-1}}{q^*_{M-1} \sigma^*_{M-1} - \nu_{M-2}} \quad ; \tag{3.30b}$$

$$a^*_{M-2} = \frac{\nu_{M-2} a^*_{M-1} + b^*_{M-1} \sigma^*_{M-1}}{q^*_{M-1} \sigma^*_{M-1} - \nu_{M-2}} , \tag{3.30c}$$

and

$$\sigma^*_{M-1} = 1 - p^*_{M-1} \nu_{M-2} \quad . \tag{3.30d}$$

In general, the down-river recursion formulae are

$$Q'_m = -q^*_m H'_{m-1} - t^*_m Q'_{m-1} + s^*_m + b^*_m H'_M \tag{3.31}$$

$$H'_{m-1} = -p^*_{m-1} Q'_{m-1} + r^*_{m-1} + a^*_{m-1} H'_M , \tag{3.32}$$

$$\text{both for m=M, M-1, ..., 2,}$$

where

$$p^*_M = 0 ; \quad r^*_M = 0 ; \quad a^*_M = 1 , \tag{3.33a,b,c}$$

and

$$q_m^* = \frac{1}{p_m^* - \eta_{m-1}} \quad ; \quad t_m^* = \frac{-\theta_{m-1}}{p_m^* - \eta_{m-1}} \quad ; \qquad (3.33d,e)$$

$$s_m^* = \frac{r_m^* - \mu_{m-1}}{p_m^* - \eta_{m-1}} \quad ; \quad b_m^* = \frac{a_m^*}{p_m^* - \eta_{m-1}} \quad ; \qquad (3.33f,g)$$

$$\sigma_m^* = 1 - \nu_{m-1} \, p_m^* \, ; \qquad (3.33h)$$

$$p_{m-1}^* = \frac{\sigma_m^* \, t_m^* + 1}{\sigma_m^* \, q_m^* - \nu_{m-1}} \quad ; \qquad (3.33i)$$

$$r_{m-1}^* = \frac{-\xi_{m-1} + \sigma_m^* \, s_m^* + \nu_{m-1} \, r_m^*}{\sigma_m^* \, q_m^* - \nu_{m-1}} \quad ; \qquad (3.33j)$$

$$a_{m-1}^* = \frac{\sigma_m^* \, b_m^* + \nu_{m-1} \, a_m^*}{\sigma_m^* \, q_m^* - \nu_{m-1}} \quad , \qquad (3.33k)$$

for m=M, M-1, ..., 2.

In particular, putting m=2 in equation (3.32)

$$H_1' = - p_1^* \, Q_1' + r_1^* + a_1^* \, H_M' \, , \qquad (3.34)$$

i.e.

$$H_\ell' = - p_1^* \, Q_\ell' + r_1^* + a_1^* \, H_r' \, . \qquad (3.35)$$

Two equations, (3.21) and (3.34), are now available for each river branch. The application of the hydraulic form of Kirchoff's laws to the branch points in conjunction with the boundary conditions (a value of

H or Q for every branch termination) provides the extra equations necessary for the solution of H and Q at the ends of each branch. Equations (3.18) and (3.19), or (3.31) and (3.32) permit the remaining H and Q to be determined.

As an example, the solution of the network shown in Figure 2.3 will be discussed. The application of mass continuity at the three branch points leads to (superscripts now referring to branch number)

$$Q_r^1 = Q_\ell^2 + Q_\ell^3 \tag{3.36}$$

$$Q_r^2 + Q_r^3 = Q_\ell^4 \tag{3.37}$$

$$Q_r^4 = Q_\ell^5 + Q_\ell^6 \quad . \tag{3.38}$$

Putting the tide heights equal at the branch points, one has

$$H_r^1 = H_\ell^2 = H_\ell^3 = H_E \quad , \tag{3.39a,b,c}$$

$$H_r^2 = H_r^3 = H_\ell^4 = H_D \quad , \tag{3.40a,b,c}$$

$$H_r^4 = H_\ell^5 = H_\ell^6 = H_C \quad . \tag{3.41a,b,c}$$

To make use of equations (3.36), (3.37) and (3.38), it is convenient to rewrite equations (3.21) and (3.34) in the form

$$Q_r^j = \alpha_1^j H_\ell^j + \beta_1^j H_r^j + \gamma_1^j \tag{3.42}$$

and

$$Q_\ell^j = \alpha_2^j H_\ell^j + \beta_2^j H_r^j + \gamma_2^j \quad . \tag{3.43}$$

Putting $H_\ell^1 = H_F$, $H_r^5 = H_A$, and $H_r^6 = H_B$, on applying equations (3.42) and (3.43) to equations (3.36), (3.37) and (3.38), one obtains three

linear equations of the form

$$C_1 \, H_E + C_2 \, H_F + C_3 \, H_D + C_4 = 0 \qquad (3.44)$$

$$C_5 \, H_D + C_6 + C_7 \, H_E + C_8 \, H_C = 0 \qquad (3.45)$$

$$C_9 \, H_C + C_{10} + C_{11} \, H_D + C_{12} \, H_A + C_{13} \, H_B = 0 \; . \qquad (3.46)$$

Applying as boundary conditions at points A and B a flow rate of

zero, the application of equation (3.43) to branches 5 and 6 gives

$$C_{14} \, H_A + C_{15} + C_{16} \, H_C = 0 \qquad (3.47)$$

$$C_{17} \, H_B + C_{18} + C_{19} \, H_C = 0 \; . \qquad (3.48)$$

The tide height H_F is specified as the third boundary condition.

Thus we now have 5 equations with 5 unknowns, so that H_A , H_B ,

..., H_E may be found. The flow rates at the right-hand ends of all

the branches may then be found via equation (3.42) and thus the remain-

ing H_m and Q_m can be calculated for each branch using equations (3.31)

and (3.32). The application of the above is shown in full in Appendix V.

Using such an approach, the solution of the branch point heights

and flow rates may be performed by hand once and for all, and the result

placed within the computer program. It is necessary to point out that,

as demonstrated in Appendix III, although the method is unconditionally

stable, the use of a time step considerably greater than $\left(\dfrac{(\Delta x)_m}{\sqrt{g \, (a_o + h)}_m} \right)_{min}$

will result in stable but increasingly incorrect

results when the number of sections per physical wavelength is less than,

say, 20. For this reason Figures 3.2 a,b,and c have been computed from

$\Delta t = \Delta x / \sqrt{ga}$ as a rough guide line to the selection of the time step

when given section length and depth.
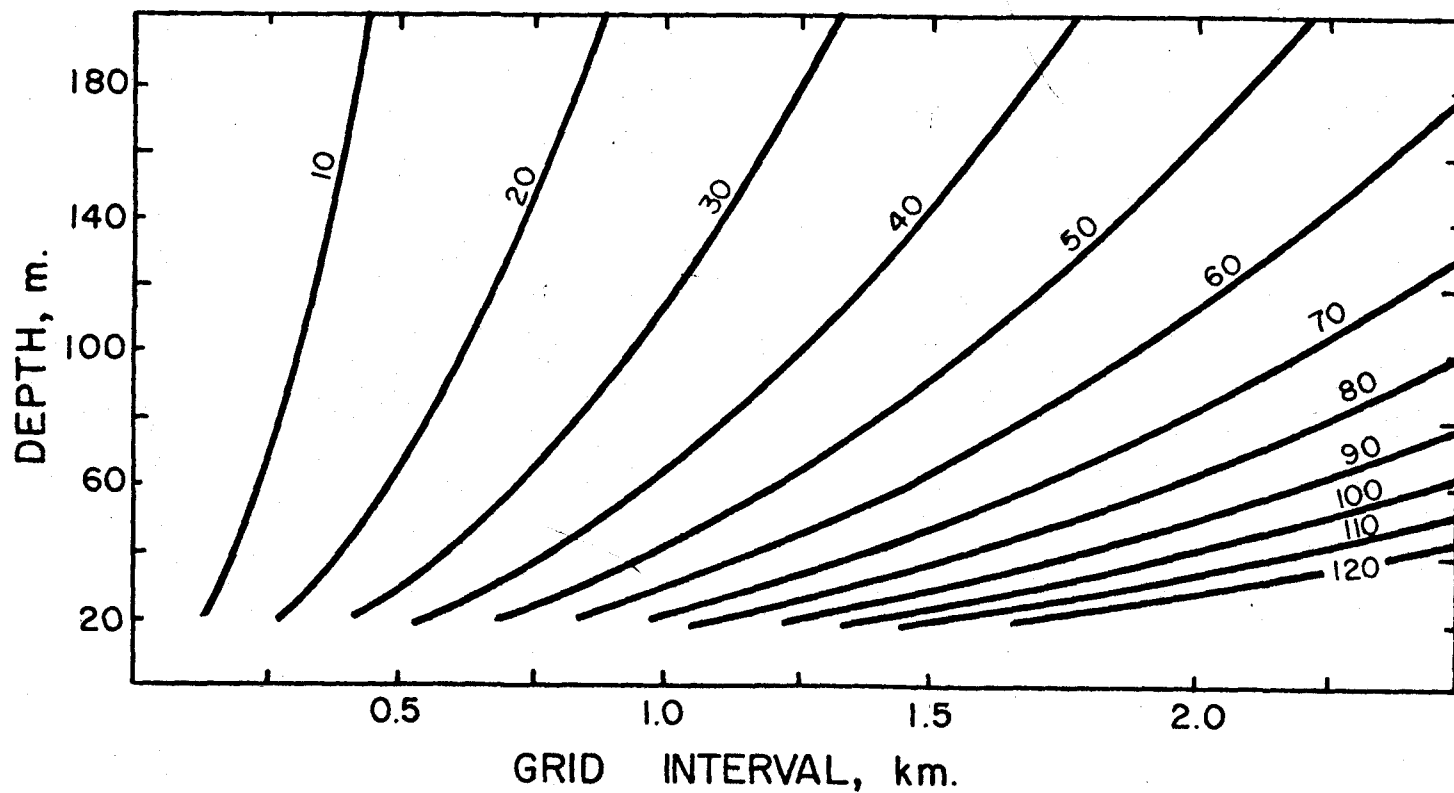
Figure 3.2a. Time step in seconds vs depth and grid interval.
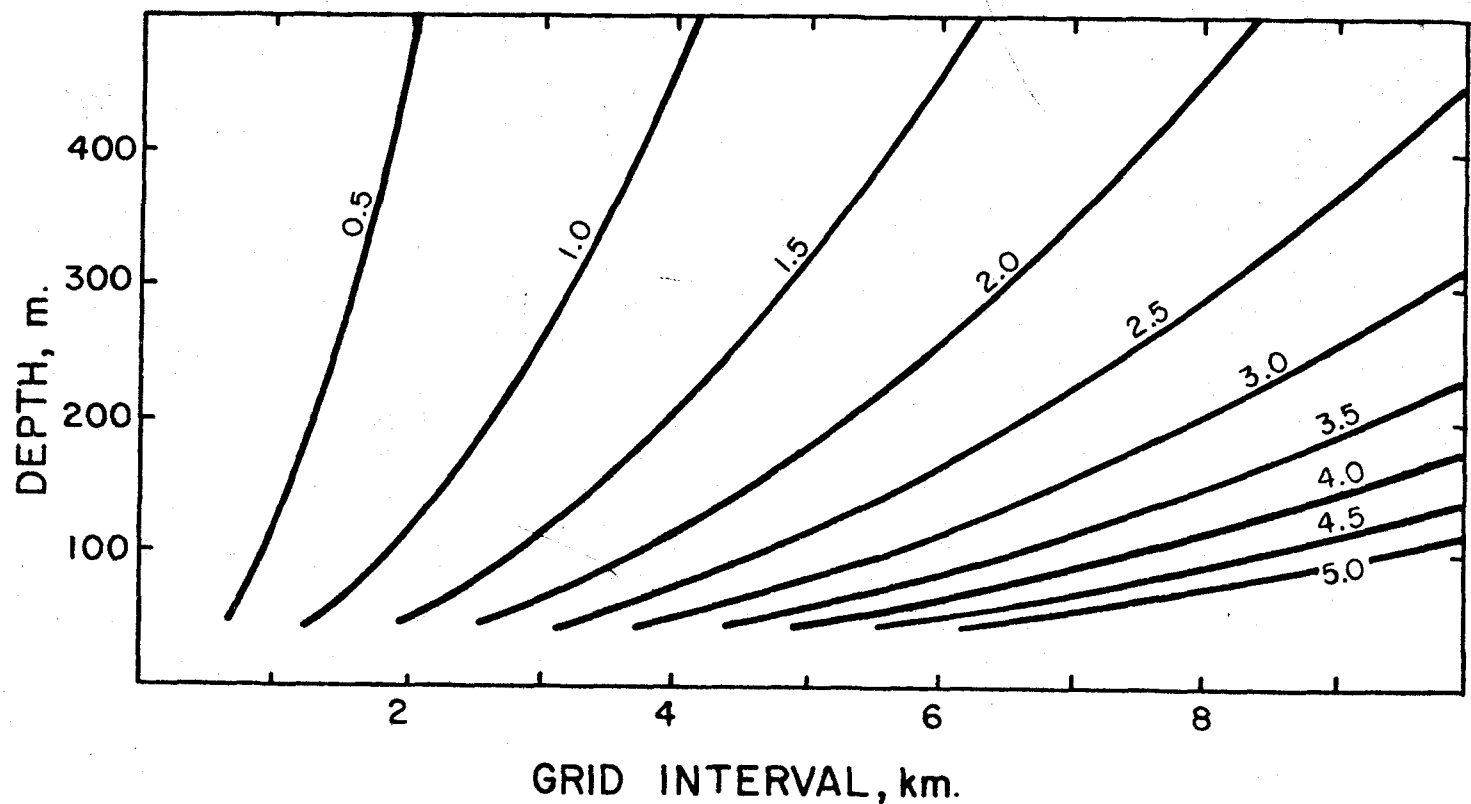
Figure 3.2b. Time step in minutes vs depth and grid interval.
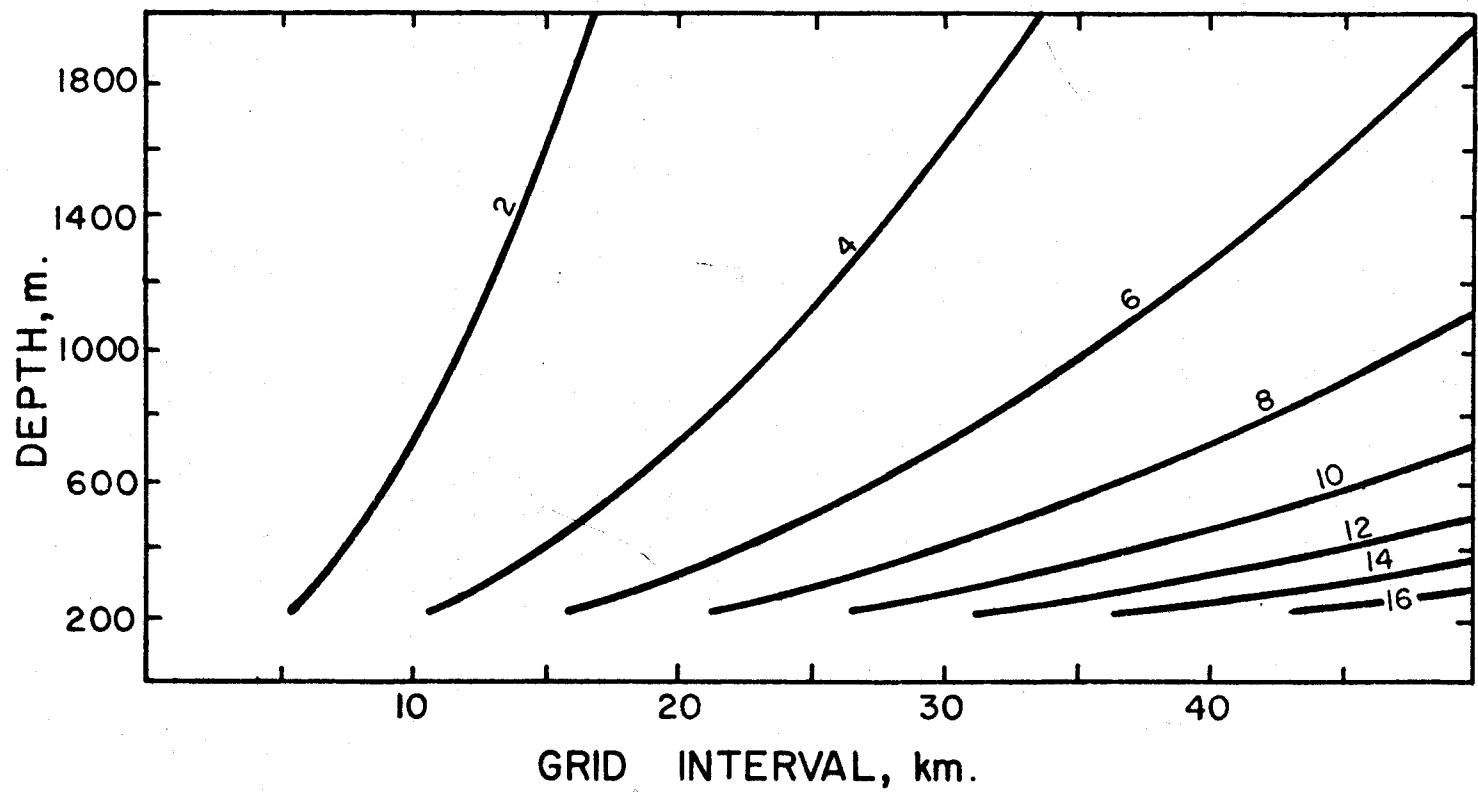
Figure 3.2c. Time step in minutes vs depth and grid interval.

37

CHAPTER IV

A TWO-DIMENSIONAL MODEL WITH UNEQUAL GRID-SPACING

Introduction

The development of two-dimensional numerical tidal models has become sufficiently advanced so that users are now offered an extensive range of options. There are available a variety of explicit finite-difference initial-value models, amongst which is the widely used model of Hansen (1961). Other explicit models are available that offer numerous boundary configurations (Heaps, 1969) or ease of applications (Matthews & Mungall, 1970). Models that can handle flooding boundaries have been devised; Reid and Bodine's model (1968) assumes vertical boundaries while Sielecki and Wurtele's model (1970) permits the inclusion of sloping boundaries. Alternating-direction implicit models of considerable sophistication have been described by Leendertse (1967) and Dronkers (1969), and a more recent publication of Leendertse's (1970) discusses a model that includes both flooding boundaries and diffusion. A fully implicit model (in which the simultaneous algebraic equations are solved by relaxation) was developed by Uusitalo (1960).

One of the next steps in the development of numerical tidal models should be that of giving the user more control over the positioning of the points at which heights and currents are calculated.

Although an ideal goal might be that of permitting the user to locate
the computation points wherever he desires, a more realistic goal is
that of being able to vary the spacing or orientation of the grid
lines on which the computation points lie. Finite-difference models
with "quasi-variable grid-spacing" have been devised in the past,
however their variability is essentially the result of the coordinate
system used. Amongst them are those based on polar coordinates
(Hyacinthe and Kravtchenko, 1967), spherical polar coordinates
(Heaps, 1969), and orthogonal curvilinear coordinates (mentioned
by Parkinson (1970)). These are shown in Table 4.1. The possibility
of a model with unequal grid-spacing in a rectangular cartesian
coordinate system seems to have received surprisingly little attention,
and in fact the only model known to the author is that of Grace (1932),
which is a boundary-value tidal model (i.e. one from which the time
dependence has been removed). A grid system and computation method is
discussed here that offers some interesting possibilities in the field
of unequal grid-spacing.

Grid Configuration

Consider a rectangular grid of M x N lines numbered respectively
m=1, 3, 5, ..., 2M-1 (parallel to the y-axis) and n=1, 3, 5, ...,
2N-1 (parallel to the x-axis) as shown in Figure 4.1. If $(\Delta x)_m$ and
$(\Delta y)_n$ represent the separation between lines m-1 and m+1, and lines
n-1 and n+1, in the limit one would like to have the option of
specifying M+N-2 different separations. Several important benefits

Author and Year	Coordinate System	Model Type	$u\frac{\partial u}{\partial x}$	τ surface	τ bottom	fV	unequal grid-spacing
Hyacinthe and Kravtchenko (1967)	polar	explicit	no	no	yes	yes	no
Heaps (1969)	spherical polar	explicit	no	yes	yes	yes	no
Parkinson (1970)	curvilinear orthogonal	explicit ?	no?	no	yes	yes	no
Grace (1932)	rectangular cartesian	harmonic	no	no	no	yes	yes

Table 4.1. Comparison between models based on coordinate systems other than a rectangular cartesian system with constant grid-spacing.
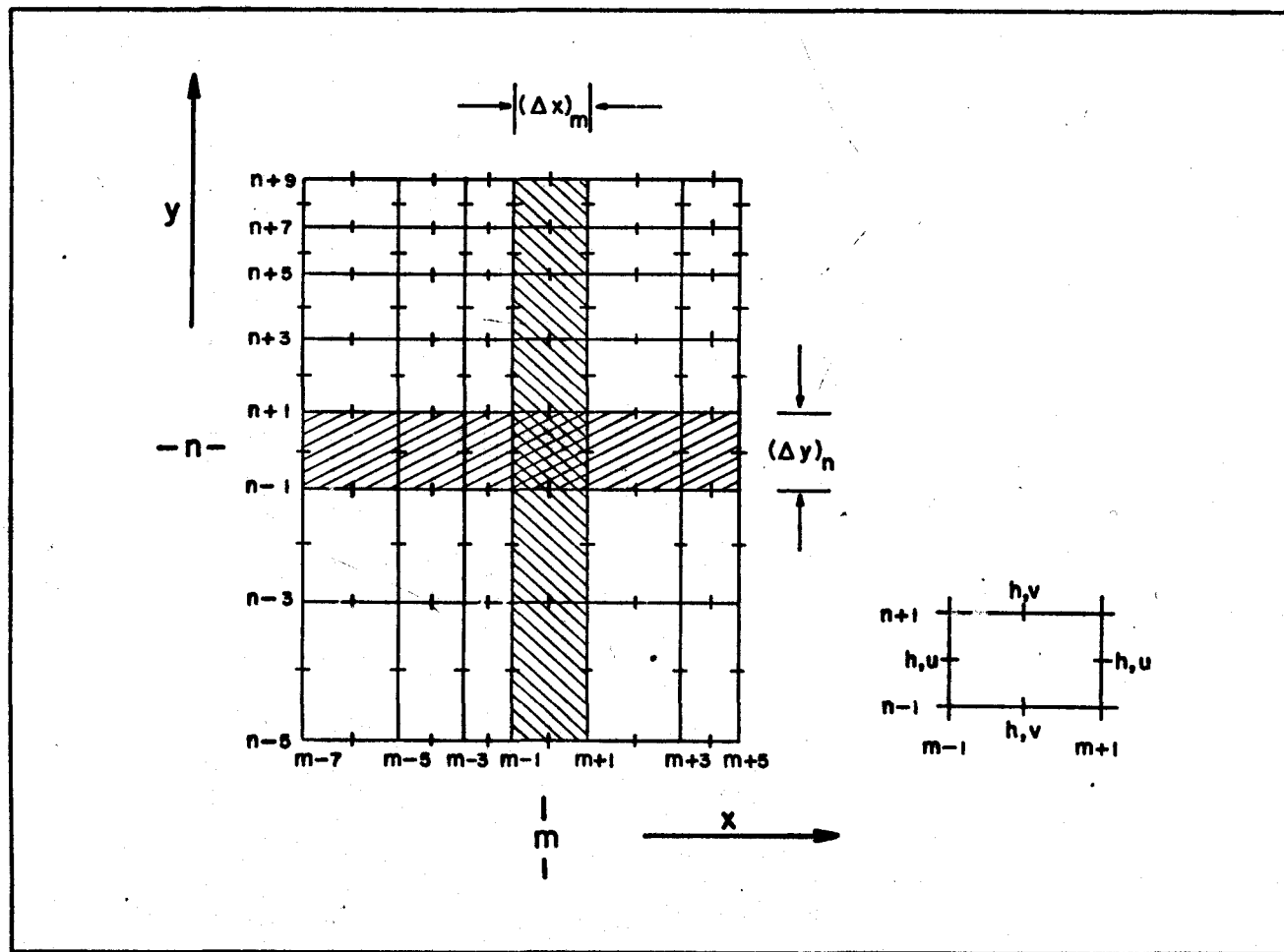
Figure 4.1. Grid scheme for 2-Dimensional Implicit Method.

result from such a scheme, the most significant of them being the
possibility of concentrating computation points in areas of interest
or in areas of rapidly varying topography, or conversely the possibility
of conserving core storage and computer time by decreasing the density
of computation points in areas of lesser interest. The usual situation
of having to suffer the increase of computation time and storage
requirements associated with a choice of grid spacing dictated by
the area of interest (barrage location, estuary head, etc.) no longer
holds. Furthermore, a better coastline fit can be obtained and one
can arrange for most of the locations for which data exist to coincide
with computation points. The main objection that existed in the past
to this approach was that non-centered spatial differences were required.
This objection is overcome, except for convective acceleration terms,
by using an extension of the one-dimensional third implicit method
described in Chapter III.

The Equations of Motion and Continuity

The equations of motion and continuity as used throughout the
remainder of this work are given by equations (4.1), (4.2), and (4.3).
They are considered to be in the most abbreviated form permissible
(Dronkers, 1964).

$$\frac{\partial u}{\partial t} = fv - g\frac{\partial h}{\partial x} - g\frac{(u^2 + v^2)^{1/2}u}{C^2(a_o + h)} \qquad (4.1)$$

$$\frac{\partial v}{\partial t} = - fu - g\frac{\partial h}{\partial y} - g\frac{(u^2 + v^2)^{1/2}v}{C^2(a_o + h)} \qquad (4.2)$$

$$\frac{\partial h}{\partial t} = - \frac{\partial u \, (a_o + h)}{\partial x} - \frac{\partial v \, (a_o + h)}{\partial y} \, . \qquad (4.3)$$

The sense of rotation of the x and y axes is counterclockwise in the horizontal plane, and u and v are the vertically averaged velocity components in the x and y directions respectively. The total depth d equals $(a_o + h)$ where a_o is the water depth below some convenient horizontal datum and h is the instantaneous height of the surface above the datum. C is the Chézy friction coefficient and f is the Coriolis parameter ($f = 2\omega \sin\phi$, where ω is the angular velocity of the earth's rotation and ϕ is the latitude).

Location of Computation Points

The location of the computation points on the proposed grid is shown in Figure 4.1. The current components u and v are evaluated at U- and V-points lying midway between the points of intersection of the lines: the U-points being located along vertical lines and the V-points along horizontal lines. The tide height h is evaluated both at U-points and at V-points, the discrete value being called H. Similarly a_o and C (both usually taken as being constant with time) are also evaluated at both U-points and at V-points, and are specified as input data. Initial values for U , V , and H must be provided at time t=0. These are usually set equal to zero or to values taken from the end of the previous computer run.

Computation Scheme

The finite-difference scheme requires four computation steps for a complete cycle. During this interval one advances by two time steps,

each of duration $\tau/2$. The finite-difference equations are written in implicit form and are solved by means of an alternating-direction double sweep technique. Spatial derivatives are evaluated from the difference between values at the upper time level and apply to hypothetical values in the center of the rectangle. The scheme is thus implicity centered (using the word 'implicit' in its conventional meaning). Time derivatives are constructed from the difference between mean values at the upper and lower time levels. Thus if the superscript notation of Dronkers (1969) is adhered to (i.e. a single prime referring to time level $t + \tau/2$, and a double prime to time level $t + \tau$), the evaluation of $\partial u/\partial t$ is written

$$\frac{\partial u}{\partial t} = \frac{\bar{U}'_n - \bar{U}_n}{\tau/2} , \tag{4.4}$$

where the notation

$$\bar{U}_n = \frac{U_{m+1,n} + U_{m-1,n}}{2} \tag{4.5}$$

has been used for brevity. Similar equations result for $\bar{U}'_n$, $\bar{V}_n$, $\bar{V}'_n$, etc. The evaluation of $\partial h/\partial t$ is more complicated and varies with the computation step.

First Computation Step (Along Rows): Time t to Time $t + \tau/2$

During the first of the four computation steps only those values of U , V , and H at times t and $t + \tau/2$ are used. Equations (4.1) and (4.3) are applied to each rectangle of center m,n along row n to result in the simultaneous calculation of $U'_{m,n}$ and $H'_{m,n}$ (m = ML, ML+2, ...,

MR-2, MR, where ML and MR define the left and right-hand ends of the row). This is then repeated for each of the remaining rows or parts of rows. $\partial h/\partial t$ is evaluated by taking as the average height in the center of the rectangle at time t the quantity $(\bar{H}_m + \bar{H}_n)/2$, and at time $t + \tau/2$ the quantity $\bar{H}'_n$.

Thus

$$\frac{\partial h}{\partial t} = \frac{\bar{H}'_n - \dfrac{\bar{H}_m + \bar{H}_n}{2}}{\tau/2} \ . \tag{4.6}$$

If we use the additional shorthand notations

$$C = \left(C_{m+1,n} + C_{m-1,n} + C_{m,n+1} + C_{m,n-1} \right)/4 \tag{4.7}$$

and

$$D = \left(d_{m+1,n} + d_{m-1,n} + d_{m,n+1} + d_{m,n-1} \right)/4 \ , \tag{4.8}$$

(where updated d-values are used as they become available), equations (4.1) and (4.3) may be written in finite-difference form as

$$\frac{\bar{U}'_n - \bar{U}_n}{\tau/2} = f\bar{V}_m - g\frac{\left(H'_{m+1,n} - H'_{m-1,n}\right)}{(\Delta x)_m} - R_1 \ \bar{U}'_n \cdot \frac{2}{\tau} \tag{4.9}$$

and

$$\frac{\bar{H}'_n - \dfrac{\bar{H}_m + \bar{H}_n}{2}}{\tau/2} = - \frac{\left(U'_{m+1,n} \ d_{m+1,n} - U'_{m-1,n} \ d_{m-1,n}\right)}{(\Delta x)_m}$$

$$- \frac{\left(V_{m,n+1} \ d_{m,n+1} - V_{m,n-1} \ d_{m,n-1}\right)}{(\Delta y)_n} \ , \tag{4.10}$$

where

$$R_1 = \frac{g\left[\left(\bar{U}_n\right)^2 + \left(\bar{V}_m\right)^2\right]^{1/2}}{(C)^2 \ D} \cdot \frac{\tau}{2} \ . \tag{4.11}$$

The location of the U- , V- , and H-values used during the first set of computations is shown in Figure 4.2. Unknown quantities have been underlined.

Second Computation Set (up Columns): Time t to Time t + τ/2

Equations (4.2) and (4.3) are applied to each rectangle of center m,n up column m in order to obtain $V'_{m,n}$ and $H'_{m,n}$ (n=NB, NB+2, ..., NT, where NB and NT define the bottom and top of the column). $\partial h/\partial t$ is evaluated by taking as the average height in the center of the rectangle at time t the quantity $(\bar{H}_m + \bar{H}_n)/2$, and at time t + τ/2 the quantity $(\bar{H}'_m + \bar{H}'_n)/2$. Thus

$$\frac{\partial h}{\partial t} = \frac{\left(\bar{H}'_m + \bar{H}'_n - \bar{H}_m - \bar{H}_n\right)/2}{\tau/2} \quad . \tag{4.12}$$

The finite-difference equations are

$$\frac{\bar{V}'_m - \bar{V}_m}{\tau/2} = - f\bar{U}'_n - g\frac{\left(H'_{m,n+1} - H'_{m,n-1}\right)}{(\Delta y)_n} - R_2 \; \bar{V}'_m \cdot \frac{2}{\tau} \tag{4.13}$$

and

$$\frac{\left(\bar{H}'_m + \bar{H}'_n - \bar{H}_m - \bar{H}_n\right)/2}{\tau/2} = - \frac{\left(U'_{m+1,n} \; d'_{m+1,n} - U'_{m-1,n} \; d'_{m-1,n}\right)}{(\Delta x)_m}$$

$$- \frac{\left(V'_{m,n+1} \; d_{m,n+1} - V'_{m,n-1} \; d_{m,n-1}\right)}{(\Delta y)_n} \tag{4.14}$$

where

$$R_2 = \frac{g\left[(\bar{U}'_n)^2 + (\bar{V}_m)^2\right]^{1/2}}{(C)^2 \; D} \cdot \frac{\tau}{2} \quad . \tag{4.15}$$
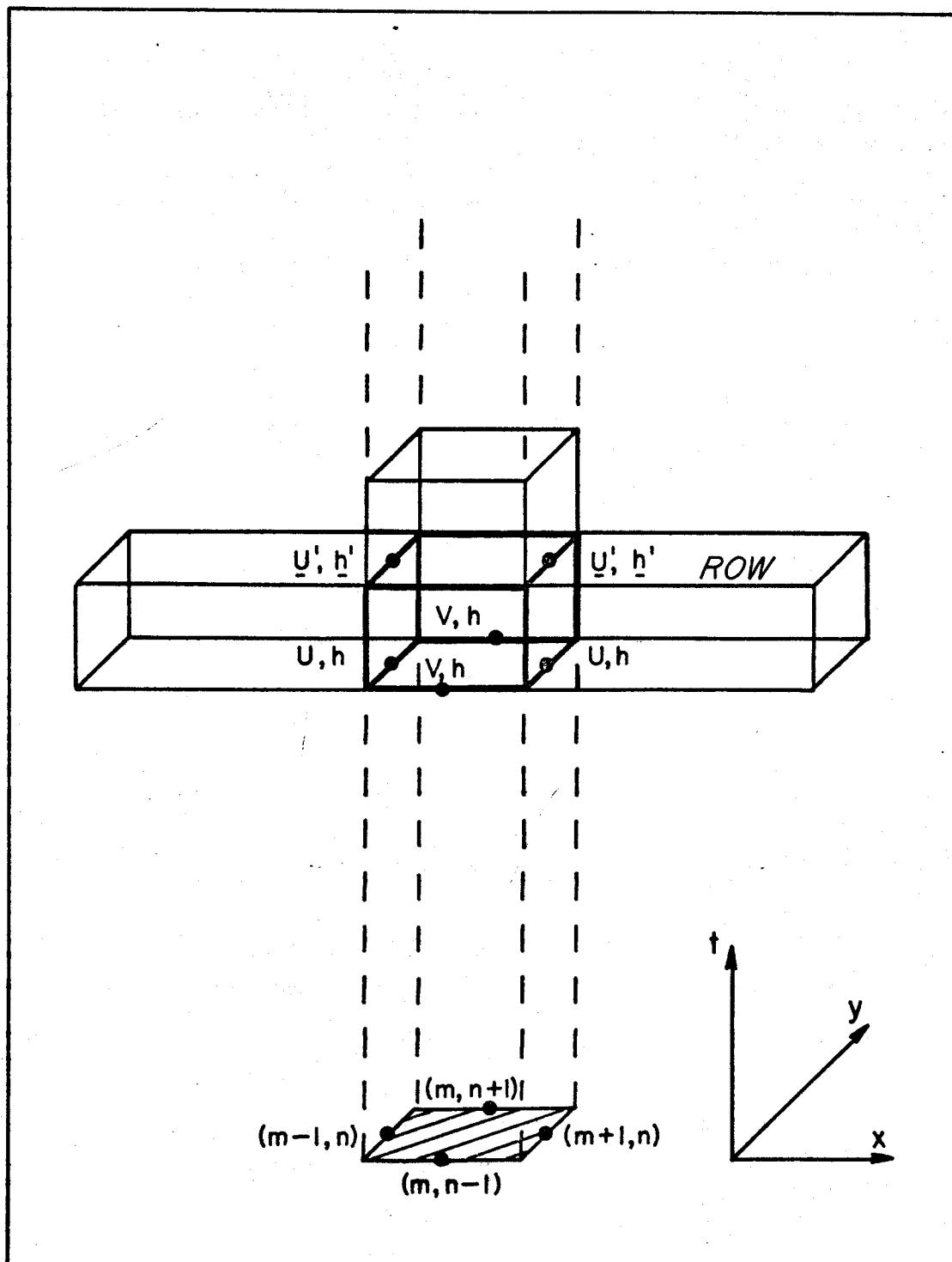
Figure 4.2.　Location of quantities used during the first set of computations.

The location of the U- , V- , and H-values used during the second set of computations is shown in Figure 4.3. Underlined quantities again denote unknown terms. In equation (4.15), D must be altered to include the updated depths $d'_{m+1,n}$ and $d'_{m-1,n}$.

Third Computation Set: Time $t + \tau/2$ to Time $t + \tau$

The third computation set is similar to the first in that one has available a full set of known values of U' , V' , and H' at the lower time level. To preserve the symmetry of the computation scheme, the third computation set is performed up columns, instead of along rows as was done in the first computation set.

The finite-difference forms of equations (4.2) and (4.3) are

$$\frac{\bar{V}''_m - \bar{V}'_m}{\tau/2} = - f\bar{U}'_n - g\frac{\left(H''_{m,n+1} - H''_{m,n-1}\right)}{(\Delta y)_n} - R_3 \bar{V}''_m \cdot \frac{2}{\tau} \qquad (4.16)$$

and

$$\frac{\bar{H}''_m - \frac{\bar{H}'_m + \bar{H}'_n}{2}}{\tau/2} = - \frac{\left(U'_{m+1,n}\, d'_{m+1,n} - U'_{m-1,n}\, d'_{m-1,n}\right)}{(\Delta x)_m}$$

$$- \frac{\left(V''_{m,n+1}\, d'_{m,n+1} - V''_{m,n-1}\, d'_{m,n-1}\right)}{(\Delta y)_n} \ , \qquad (4.17)$$

where

$$R_3 = \frac{g\left[(\bar{U}'_n)^2 + (\bar{V}'_m)^2\right]^{1/2}}{(C)^2 D} \cdot \frac{\tau}{2} \ . \qquad (4.18)$$
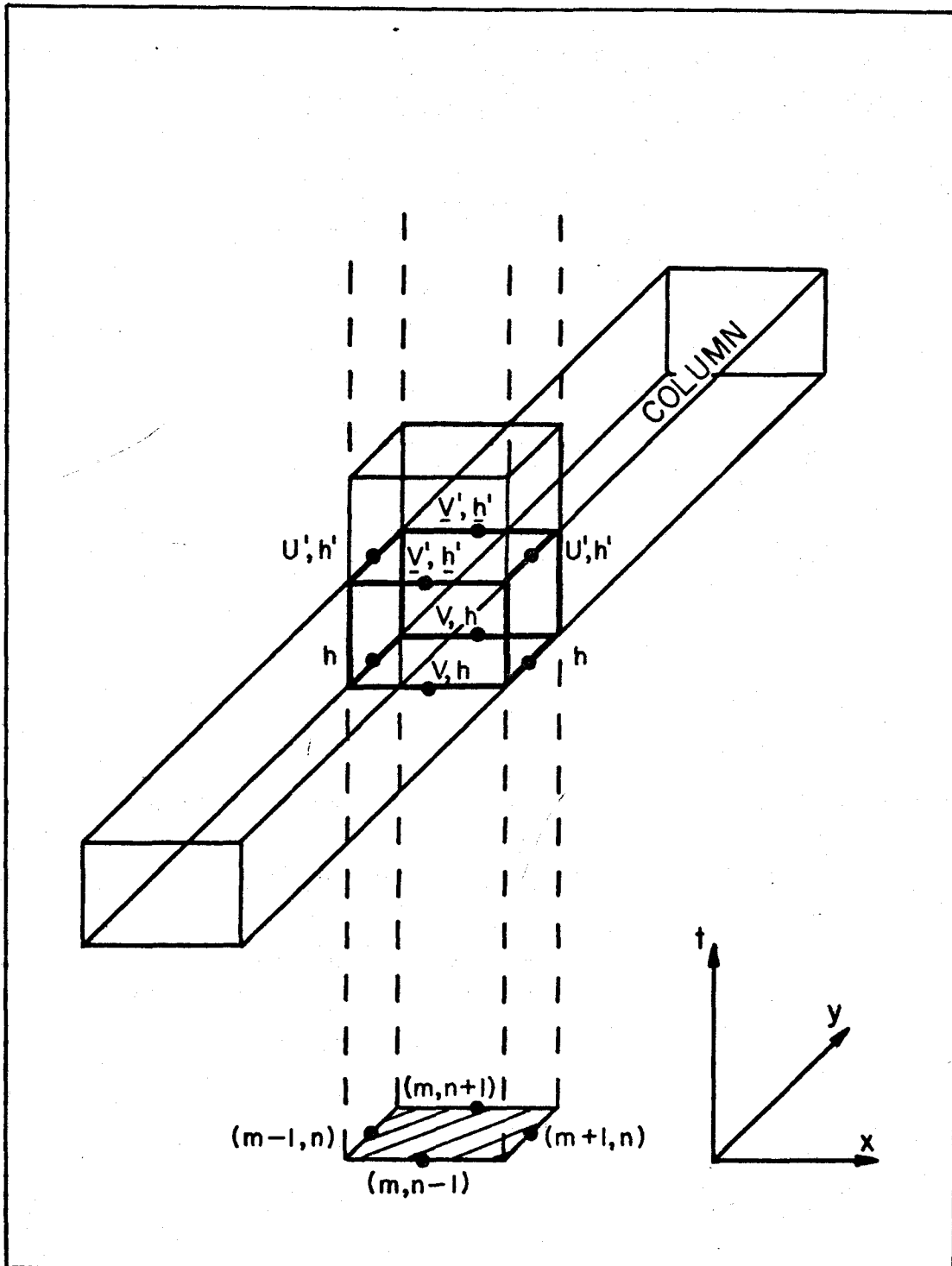
Figure 4.3.   Location of quantities used during the second
set of computations.

The location of the U- , V- , and H-values used during the third set of computations is shown in Figure 4.4. Underlined quantities again denote unknown terms. In equation (4.18), D is further altered to include $d'_{m,n+1}$ and $d'_{m,n-1}$.

Fourth Computation Set: Time $t + \tau/2$ to Time $t + \tau$

The last computation set is performed along rows. The finite-difference forms of equations (4.1) and (4.3) are

$$\frac{\bar{U}''_n - \bar{U}'_n}{\tau/2} = f\bar{V}''_m - g\frac{\left(H''_{m+1,n} - H''_{m-1,n}\right)}{(\Delta x)_m} - R_4 \; \bar{U}''_n \cdot \frac{2}{\tau} \qquad (4.19)$$

and

$$\frac{\left(\bar{H}''_m + \bar{H}''_n - \bar{H}'_m - \bar{H}'_n\right)/2}{\tau/2} = -\frac{\left(U''_{m+1,n} \; d'_{m+1,n} - U''_{m-1,n} \; d'_{m-1,n}\right)}{(\Delta x)_m}$$

$$-\frac{\left(V''_{m,n+1} \; d''_{m,n+1} - V''_{m,n-1} \; d''_{m,n-1}\right)}{(\Delta y)_n} \; ,$$

$$\qquad (4.20)$$

where

$$R_4 = \frac{g\left[(\bar{U}'_n)^2 + (\bar{V}''_m)^2\right]^{1/2}}{(C)^2 \; D} \cdot \frac{\tau}{2} \; . \qquad (4.21)$$

The location of the U- , V- , and H-values used during the fourth set of computations is shown in Figure 4.5. Underlined quantities again denote unknown terms. In equation (4.21), D is altered yet again to include $d''_{m,n+1}$ and $d''_{m,n-1}$.
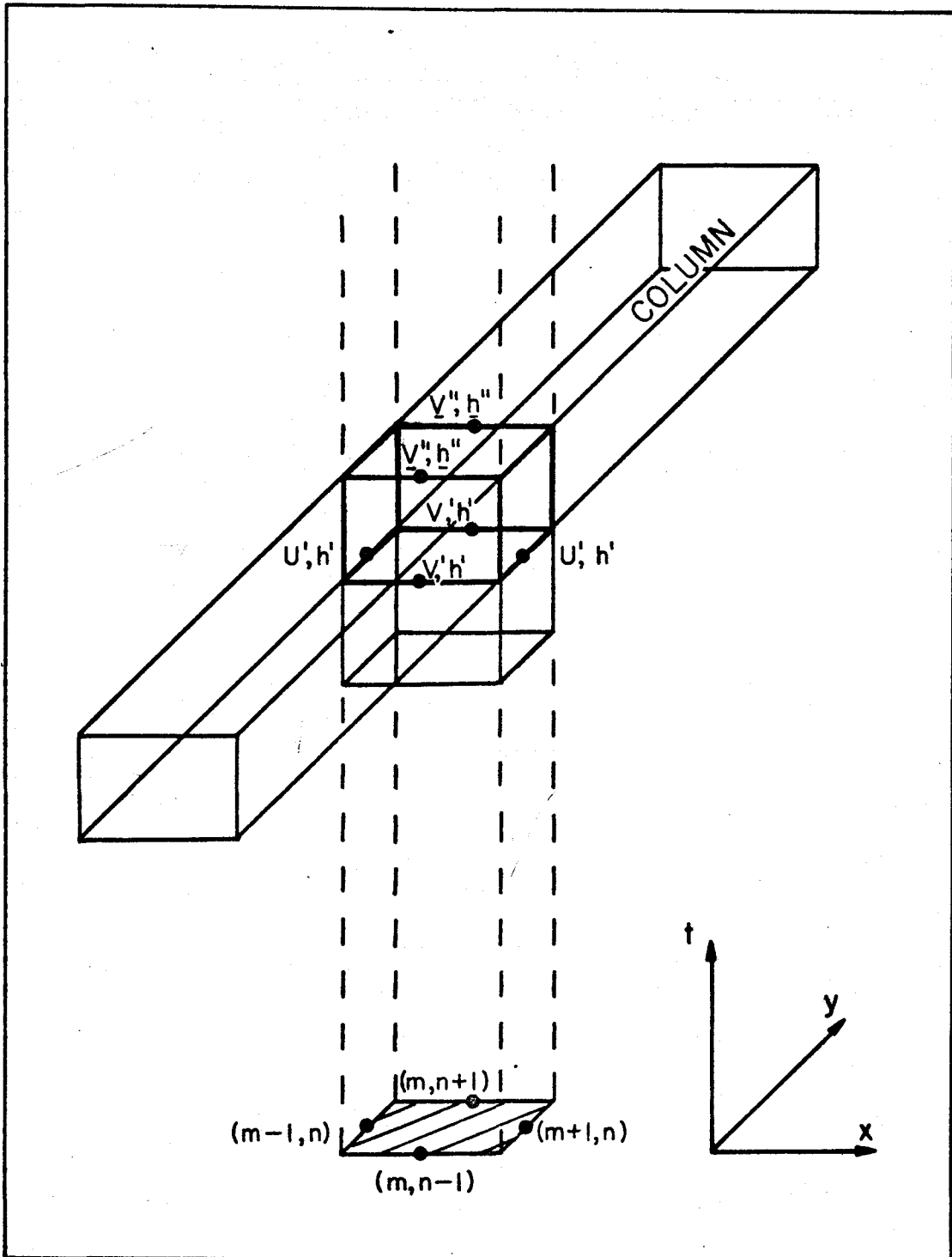
Figure 4.4.   Location of quantities used during the third set
of computations.
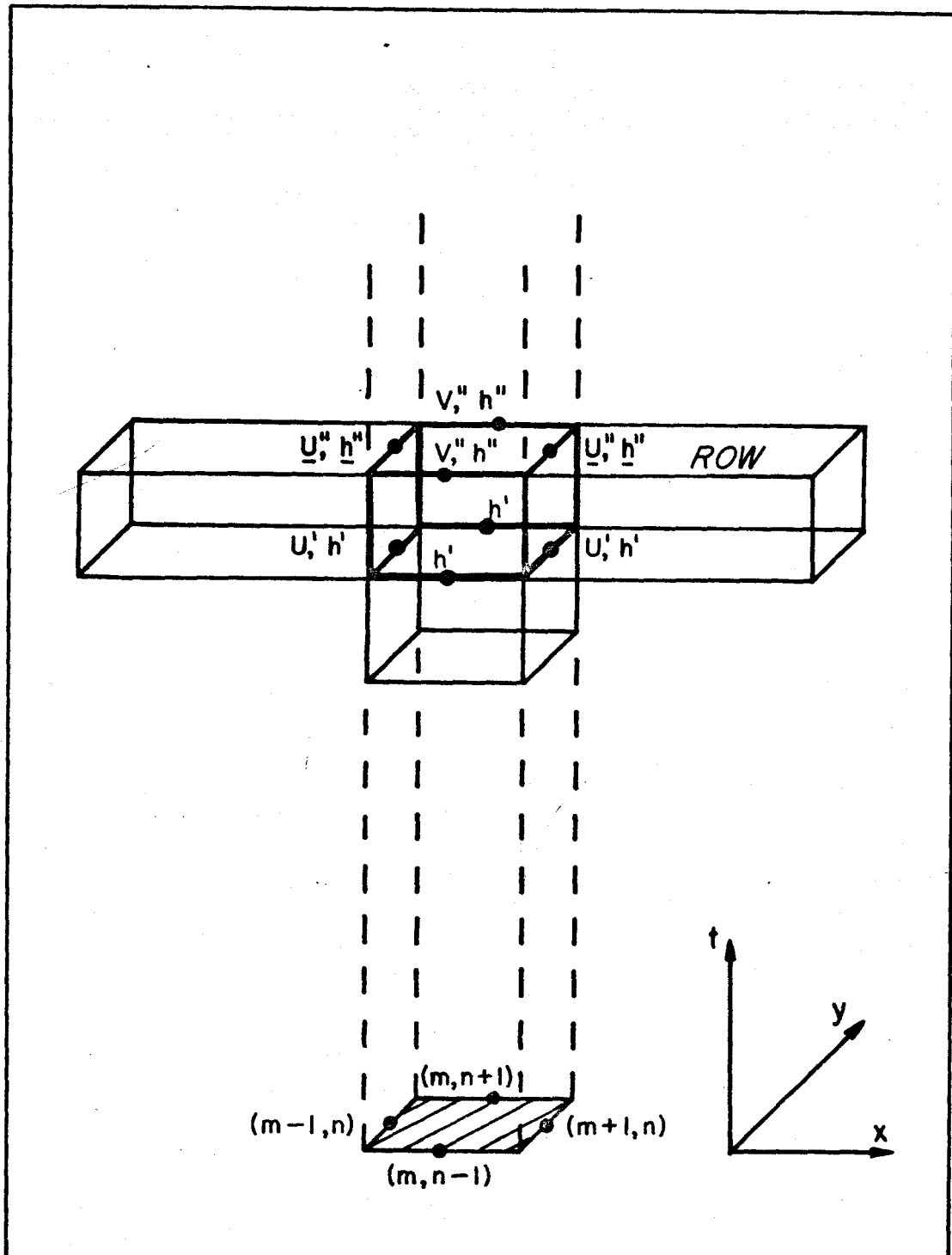
Figure 4.5. Location of quantities used during the fourth set of computations.

CHAPTER V

THE FINITE-DIFFERENCE EQUATIONS AND
THEIR SOLUTION

Introduction

This chapter covers the reduction of the finite-difference

equations to convenient forms and their solution. The chapter

is included here for reasons of continuity and can be skipped by

those readers not immediately interested in the rearrangement

and solution of the finite-difference equations. The process

is similar to that described in Chapter 3 in connection with

the one-dimensional implicit method, and is again an application

of the double sweep method of J. J. Dronkers (1969).

First Computation Set

Equations (4.9) and (4.10) may be rewritten in the form

$$U'_{m+1,n} + U'_{m-1,n} + \alpha_m H'_{m+1,n} - \alpha_m H'_{m-1,n} = \beta_m \tag{5.1}$$

$$H'_{m+1,n} + H'_{m-1,n} + \gamma_m U'_{m+1,n} + \delta_m U'_{m-1,n} = \epsilon_m \tag{5.2}$$

for m=ML+1, ML+3, ..., MR-1.

α_m, β_m, ..., ϵ_m involve input parameters and values of U, V, and

H calculated at time t. They may be shown by comparison (see

Appendix VI) to be

$$\alpha_m = \frac{g\tau}{(\Delta x)_m (1 + R_1)} \quad ; \tag{5.3a}$$

$$\beta_m = \frac{(U_{m+1,n} + U_{m-1,n})}{1 + R_1} + \frac{(V_{m,n+1} + V_{m,n-1})\tau f}{2(1 + R_1)} \quad ; \tag{5.3b}$$

$$\gamma_m = \frac{\tau \, d_{m+1,n}}{(\Delta x)_m} \quad ; \quad \delta_m = -\frac{\tau \, d_{m-1,n}}{(\Delta x)_m} \quad ; \tag{5.3c,d}$$

$$\epsilon_m = -\frac{\tau(V_{m,n+1} \, d_{m,n+1} - V_{m,n-1} \, d_{m,n-1})}{(\Delta y)_n}$$

$$+ \frac{(H_{m,n+1} + H_{m,n-1})}{2} + \frac{(H_{m+1,n} + H_{m-1,n})}{2} ; \tag{5.3e}$$

$$R_1 = \frac{g\tau\left[(U_{m+1,n} + U_{m-1,n})^2 + (V_{m,n+1} + V_{m,n-1})^2\right]^{1/2}}{4 \, C_{m,n}^2 \, D_{m,n}} . \tag{5.3f}$$

Knowing the boundary values H'_{ML} or U'_{ML} at the left-hand end of the row, and H'_{MR} or U'_{MR} at the right-hand end of the row, the double sweep method may again be used to solve equations (5.1) and (5.2). As the method is applicable (with minor variations) to all four computation steps, its description will be kept until the end of the chapter.

Second Computation Set

Equations (4.13) and (4.14) are rewritten in the form

$$V'_{m,n+1} + V'_{m,n-1} + \alpha_n H'_{m,n+1} - \alpha_n H'_{m,n-1} = \beta_n \tag{5.4}$$

$$H'_{m,n+1} + H'_{m,n-1} + \gamma_n V'_{m,n+1} + \delta_n V'_{m,n-1} = \epsilon_n \tag{5.5}$$

for n=NB+1, NB+3, ..., NT-1.

α_n , β_n , ..., ϵ_n are again found by comparison (see Appendix VI), and are

$$\alpha_n = \frac{g\tau}{(\Delta y)_n (1 + R_2)} \; ; \tag{5.6a}$$

$$\beta_n = \frac{(V_{m,n+1} + V_{m,n-1})}{1 + R_2} - \frac{(U'_{m+1,n} + U'_{m-1,n})\tau f}{2(1 + R_2)} \; ; \tag{5.6b}$$

$$\gamma_n = \frac{2\tau \, d_{m,n+1}}{(\Delta y)_n} \; ; \quad \delta_n = - \frac{2\tau \, d_{m,n-1}}{(\Delta y)_n} \; ; \tag{5.6c,d}$$

$$\epsilon_n = - \frac{2\tau(U'_{m+1,n} \, d'_{m+1,n} - U'_{m-1,n} \, d'_{m-1,n})}{(\Delta x)_m} \tag{5.6e}$$

$$+ \, H_{m,n+1} + H_{m,n-1} + H_{m+1,n} + H_{m-1,n} - H'_{m+1,n} - H'_{m-1,n} \; ;$$

$$R_2 = \frac{g\tau \left[(U'_{m+1,n} + U'_{m-1,n})^2 + (V_{m,n+1} + V_{m,n-1})^2\right]^{1/2}}{4 \, C^2_{m,n} \, D_{m,n}} \; . \tag{5.6f}$$

To solve equations (5.4) and (5.5) one needs values H'_{NB} or V'_{NB} , and H'_{NT} or V'_{NT}. The result is that all the U' , V' , and H' are now known at time $t + \tau/2$.

Third Computation Set

Equations (4.16) and (4.17) are rewritten as

$$V''_{m,n+1} + V''_{m,n-1} + \alpha_n H''_{m,n+1} - \alpha_n H''_{m,n-1} = \beta_n \tag{5.7}$$

$$H''_{m,n+1} + H''_{m,n-1} + \gamma_n V''_{m,n+1} + \delta_n V''_{m,n-1} = \epsilon_n \tag{5.8}$$

$$\text{for } n = NB+1, \; NB+3, \; ...., \; NT-1.$$

For the third computation set, α_n , β_n , ..., ϵ_n are (see Appendix VI)

$$\alpha_n = \frac{g\tau}{(\Delta y)_n(1+R_3)} \quad ; \qquad \qquad (5.9a)$$

$$\beta_n = \frac{(V'_{m,n+1} + V'_{m,n-1})}{1 + R_3} - \frac{(U'_{m+1,n} + U'_{m-1,n})\tau f}{2(1 + R_3)} \quad ; \qquad (5.9b)$$

$$\gamma_n = \frac{\tau \, d'_{m,n+1}}{(\Delta y)_n} \quad ; \qquad \delta_n = - \frac{\tau \, d'_{m,n-1}}{(\Delta y)_n} \quad ; \qquad (5.9c,d)$$

$$\epsilon_n = - \frac{\tau \left(U'_{m+1,n} \, d'_{m+1,n} - U'_{m-1,n} \, d'_{m-1,n}\right)}{(\Delta x)_m}$$

$$+ \frac{(H'_{m,n+1} + H'_{m,n-1})}{2} - \frac{(H'_{m+1,n} \, H'_{m-1,n})}{2} \quad ; \qquad (5.9e)$$

$$R_3 = \frac{g\tau \left[\left(U'_{m+1,n} + U'_{m-1,n}\right)^2 + \left(V'_{m,n+1} + V'_{m,n-1}\right)^2\right]^{1/2}}{4 \, C^2_{m,n} \, D_{m,n}} \quad . \quad (5.9f)$$

To solve equations (5.7) and (5.8) one needs H''_{NB} or V''_{NB} , and H''_{NT} or V''_{NT} .

Fourth Computation Set

Equations (4.19) and (4.20) are rewritten in the form (see Appendix VI)

$$U''_{m+1,n} + U''_{m-1,n} + \alpha_m H''_{m+1,n} - \alpha_m H''_{m-1,n} = \beta_m \qquad (5.10)$$

$$H''_{m+1,n} + H''_{m-1,n} + \gamma_m U''_{m+1,n} + \delta_m U''_{m-1,n} = \epsilon_m \qquad (5.11)$$

where

$$\alpha_m = \frac{g\tau}{(\Delta x)_m(1+R_4)} \quad ; \qquad \qquad (5.12a)$$

$$\beta_m = \frac{\left(U'_{m+1,n} + U'_{m-1,n}\right)}{1 + R_4} + \frac{\left(V''_{m,n+1} + V''_{m,n-1}\right)\tau f}{2\left(1 + R_4\right)} \quad ; \tag{5.12b}$$

$$\gamma_m = \frac{2\tau \, d'_{m+1,n}}{(\Delta x)_m} \quad ; \qquad \delta_m = -\frac{2\tau \, d'_{m-1,n}}{(\Delta x)_m} \quad ; \tag{5.12c,d}$$

$$\epsilon_m = -\frac{2\tau\left(V''_{m,n+1} \, d''_{m,n+1} - V''_{m,n-1} \, d''_{m,n-1}\right)}{(\Delta y)_n}$$

$$+ \, H'_{m,n+1} + H'_{m,n-1} + H'_{m+1,n} + H'_{m-1,n} - H''_{m,n+1} - H''_{m,n-1} \quad ;$$

$$\tag{5.12e}$$

$$R_4 = \frac{g\tau\left[\left(U'_{m+1,n} + U'_{m-1,n}\right)^2 + \left(V''_{m,n+1} + V''_{m,n-1}\right)^2\right]^{1/2}}{4 \, C^2_{m,n} \, D_{m,n}} \quad . \tag{5.12f}$$

Finally, to solve equations (5.10) and (5.11), one needs the boundary conditions, H''_{ML} or U''_{ML} , and H''_{MR} or U''_{MR} .

Solution of the Finite-Difference Equations by the Double Sweep Method

The four sets of finite-difference equations to be solved, of which equations (5.1) and (5.2) are an example, may all be solved by the double sweep method. Although only equations (5.1) and (5.2) will be considered here, it should be realized that with minor changes the method applies equally to equations (5.4) and (5.5), (5.7) and (5.8), and (5.10) and (5.11). For convenience, equations (5.1) and (5.2) will be rewritten with a single subscript.

In general (noting that the subscripts of α , β , $\ldots$, ϵ have been shifted)

$$U'_{m+2} + U'_m + \alpha_m H'_{m+2} - \alpha_m H'_m = \beta_m \tag{5.13}$$

$$H'_{m+2} + H'_m + \gamma_m U'_{m+2} + \delta_m U'_m = \epsilon_m \tag{5.14}$$

$$\text{for } m = ML, \ ML+2, \ \ldots, \ MR-2.$$

Starting at the left-hand side of the row, putting m=ML, we have

$$H'_{ML+2} + H'_{ML} + \gamma_{ML} U'_{ML+2} + \delta_{ML} U'_{ML} = \epsilon_{ML} \tag{5.15}$$

$$U'_{ML+2} + U'_{ML} + \alpha_{ML} H'_{ML+2} - \alpha_{ML} H'_{ML} = \beta_{ML} . \tag{5.16}$$

The form taken by the recursion formulae depends on whether current or height is specified at the left-hand end of the row.

Case 1, H'_{ML} known

From equation (5.15)

$$U'_{ML} = A_{ML} + B_{ML} H'_{ML+2} + C_{ML} U'_{ML+2} , \tag{5.17}$$

where

$$A_{ML} = \frac{\epsilon_{ML} - H'_{ML}}{\delta_{ML}} ; \quad B_{ML} = \frac{-1}{\delta_{ML}} ; \quad C_{ML} = \frac{-\gamma_{ML}}{\delta_{ML}} . \tag{5.18a,b,c}$$

Substituting equation (5.17) into equation (5.16) and rearranging,

$$H'_{ML+2} = D_{ML+2} U'_{ML+2} + E_{ML+2} , \tag{5.19}$$

where

$$D_{ML+2} = -\frac{1 + C_{ML}}{B_{ML} + \alpha_{ML}} ; \quad E_{ML+2} = \frac{\beta_{ML} - A_{ML} + \alpha_{ML} H'_{ML}}{B_{ML} + \alpha_{ML}} . \tag{5.20a,b}$$

Putting m=ML+2 into equations (5.13) and (5.14).

$$H'_{ML+4} + H'_{ML+2} + \gamma_{ML+2} U'_{ML+4} + \delta_{ML+2} U'_{ML+2} = \epsilon_{ML+2} \tag{5.21}$$

$$U'_{ML+4} + U'_{ML+2} + \alpha_{ML+2} H'_{ML+4} - \alpha_{ML+2} H'_{ML+2} = \beta_{ML+2} . \tag{5.22}$$

Substituting equation (5.19) into equation (5.21) and rearranging,

$$U'_{ML+2} = A_{ML+2} + B_{ML+2} \, H'_{ML+4} + C_{ML+2} \, U'_{ML+4} \quad , \tag{5.23}$$

where

$$A_{ML+2} = \frac{\epsilon_{ML+2} - E_{ML+2}}{\delta_{ML+2} + D_{ML+2}} \quad ; \qquad B_{ML+2} = \frac{-1}{\delta_{ML+2} + D_{ML+2}} \quad ; \tag{5.24a,b}$$

$$C_{ML+2} = \frac{-\gamma_{ML+2}}{\delta_{ML+2} + D_{ML+2}} \quad . \tag{5.24c}$$

Substituting equations (5.19) and (5.23) into equation (5.22) and rearranging,

$$H'_{ML+4} = D_{ML+4} \, U'_{ML+4} + E_{ML+4} \quad , \tag{5.25}$$

where

$$D_{ML+4} = - \frac{1 + C_{ML+2} \left(1 - \alpha_{ML+2} \, D_{ML+2} \right)}{B_{ML+2} \left(1 - \alpha_{ML+2} \, D_{ML+2} \right) + \alpha_{ML+2}} \quad ; \tag{5.26a}$$

$$E_{ML+4} = \frac{\beta_{ML+2} - A_{ML+2} \left(1 - \alpha_{ML+2} \, D_{ML+2} \right) + \alpha_{ML+2} \, E_{ML+2}}{B_{ML+2} \left(1 - \alpha_{ML+2} \, D_{ML+2} \right) + \alpha_{ML+2}} \quad . \tag{5.26b}$$

In general,

$$U'_m = A_m + B_m \, H'_{m+2} + C_m \, U'_{m+2} \tag{5.27}$$

$$H'_{m+2} = D_{m+2} \, U'_{m+2} + E_{m+2} \tag{5.28}$$

$$\text{for } m = ML, \; ML+2, \; \ldots, \; MR-2,$$

and

$$A_m = \frac{\epsilon_m - E_m}{\delta_m + D_m} \; ; \qquad B_m = \frac{-1}{\delta_m + D_m} \; ; \qquad C_m = \frac{-\gamma_m}{\delta_m + D_m} \; ; \tag{5.29a,b,c}$$

$$\sigma_m = 1 - \alpha_m D_m \quad ; \qquad\qquad\qquad\qquad\qquad\qquad (5.29d)$$

$$D_{m+2} = -\frac{1 + C_m \sigma_m}{B_m \sigma_m + \alpha_m} \quad ; \quad E_{m+2} = \frac{\beta_m - A_m \sigma_m + \alpha_m E_m}{B_m \sigma_m + \alpha_m} \quad . \qquad (5.29e,f)$$

$$\text{for } m = ML, ML+2, \ldots, MR-2,$$

and where

$$D_{ML} = 0.0 \text{ and } E_{ML} = H'_{ML} \quad . \qquad\qquad\qquad (5.29g,h)$$

The calculation sequence is to evaluate $(\alpha_m , \ldots, \epsilon_m , A_m ,$ $B_m , C_m , \sigma_m , D_{m+2} , E_{m+2})$ for $m = ML, ML+2, \ldots, MR-2$, and to store the values $A_m , \ldots, E_{m+2}$. This part of the calculation is called the upward sweep. If current U'_{MR} is specified at the right-hand end of the row, equations (5.27) and (5.28) may be used to evaluate $H'_{MR} , U'_{MR-2} , H'_{MR-2} , \ldots, U'_{ML}$ in descending order. This is the downward sweep part of the calculation. If height H'_{MR} is specified at the right-hand end of the row, U'_{MR} must first be obtained via

$$U'_{MR} = \left(H'_{MR} - E_{MR} \right) / D_{MR} \qquad\qquad\qquad (5.30)$$

and the downward sweep applied as before.

Case 2, U'_{ML} known

From equation (5.16)

$$H'_{ML} = P_{ML} + Q_{ML} U'_{ML+2} + R_{ML} H'_{ML+2} \quad , \qquad\qquad (5.31)$$

where

$$P_{ML} = \frac{U'_{ML} - \beta_{ML}}{\alpha_{ML}} \quad ; \qquad Q_{ML} = \frac{1}{\alpha_{ML}} \quad ; \qquad R_{ML} = 1 \quad . \qquad (5.32a,b,c)$$

Substituting equation (5.31) into equation (5.15) and rearranging,

$$U'_{ML+2} = S_{ML+2} \, H'_{ML+2} + T_{ML+2} \, , \tag{5.33}$$

where

$$S_{ML+2} = - \frac{1 + R_{ML}}{\gamma_{ML} + Q_{ML}} \; ; \quad T_{ML+2} = \frac{\epsilon_{ML} - \delta_{ML} \, U'_{ML} - P_{ML}}{\gamma_{ML} + Q_{ML}} \, . \tag{5.34a,b}$$

Substituting equation (5.33) into equation (5.22) and rearranging

$$H'_{ML+2} = P_{ML+2} + Q_{ML+2} \, U'_{ML+4} + R_{ML+2} \, H'_{ML+4} \, , \tag{5.35}$$

where

$$P_{ML+2} = \frac{T_{ML+2} - \beta_{ML+2}}{\alpha_{ML+2} - S_{ML+2}} \; ; \quad Q_{ML+2} = \frac{1}{\alpha_{ML+2} - S_{ML+2}} \; ; \tag{5.36a,b}$$

$$R_{ML+2} = \frac{\alpha_{ML+2}}{\alpha_{ML+2} - S_{ML+2}} \, . \tag{5.36c}$$

Substituting equations (5.33) and (5.35) into equation (5.21), and
rearranging,

$$U'_{ML+4} = S_{ML+4} \, H'_{ML+4} + T_{ML+4} \, , \tag{5.37}$$

where

$$S_{ML+4} = - \frac{1 + R_{ML+2} \left(1 + \delta_{ML+2} \, S_{ML+2} \right)}{\gamma_{ML+2} + Q_{ML+2} \left(1 + \delta_{ML+2} \, S_{ML+2} \right)} \; ; \tag{5.38a}$$

$$T_{ML+4} = \frac{\epsilon_{ML+2} - \delta_{ML+2} \, T_{ML+2} - P_{ML+2} \left(1 + \delta_{ML+2} \, S_{ML+2} \right)}{\gamma_{ML+2} + Q_{ML+2} \left(1 + \delta_{ML+2} \, S_{ML+2} \right)} \, . \tag{5.38b}$$

In general,

$$H'_m = P_m + Q_m \, U'_{m+2} + R_m \, H'_{m+2} \tag{5.39}$$

$$U'_{m+2} = S_{m+2} \, H'_{m+2} + T_{m+2} \qquad\qquad (5.40)$$

$$\text{for } m = ML, \; ML+2, \; \dots, \; MR-2,$$

and

$$P_m = \frac{T_m - \beta_m}{\alpha_m - S_m} \; ; \quad Q_m = \frac{1}{\alpha_m - S_m} \; ; \quad R_m = \frac{\alpha_m}{\alpha_m - S_m} \; ; \qquad (5.41a,b,c)$$

$$\rho_m = 1 + \delta_m \, S_m \; ; \qquad\qquad (5.41d)$$

$$S_{m+2} = -\frac{1 + R_m \, \rho_m}{\gamma_m + Q_m \, \rho_m} \; ; \quad T_{m+2} = \frac{\varepsilon_m - \delta_m \, T_m - P_m \, \rho_m}{\gamma_m + Q_m \, \rho_m} \; . \qquad (5.41e,f)$$

$$\text{for } m = ML, \; ML+2, \; \dots, \; MR-2,$$

and where

$$S_{ML} = 0.0 \quad \text{and} \quad T_{ML} = U'_{ML} \; . \qquad\qquad (5.41g,h)$$

Having calculated $(\alpha_m, \; \dots, \; \varepsilon_m, \; P_m, \; Q_m, \; R_m, \; \rho_m, \; S_{m+2}, \; T_{m+2})$ for $m = ML, \; ML+2, \; \dots, \; MR-2$, one completes the upward sweep. If height H'_{MR} is specified at the right-hand end of the row, equations (5.39) and (5.40) are used to evaluate $U'_{MR}, \; H'_{MR-2}, \; U'_{MR-2}, \; H'_{MR-4}, \; \dots,$ H'_{ML} in descending order. If current U'_{MR} is specified at the right-hand end of the row, H'_{MR} is found from

$$H'_{MR} = \left(U'_{MR} - T_{MR} \right) / S_{MR} \; , \qquad\qquad (5.42)$$

and the downward sweep again applied as before.

CHAPTER VI

PROGRAMMING CONSIDERATIONS

Introduction

The form of the program is necessarily of great importance in the application of numerical tidal models. Computer time and core storage limitations almost always exist, so that the early consideration of these problems will pay dividends when one actually comes to apply the program to complicated situations. The discussion of the means by which computer time may be saved will be directed more towards the efficient use of each computer run than towards a discussion of programming techniques (such as saving time by reducing the number of multiplications). The computer language is assumed to be FORTRAN, however, most of the comments will have their counterpart in other languages.

Reduction of Core Storage Requirements

There are two main approaches by which core storage requirements may be reduced: those which involve splitting up the original full-length program into smaller segments, and those involving the optimization of the storage arrays. The discussion that follows is based on the tripartite-nature of numerical tidal models: an initial phase in which data on the inlet dimensions are read from cards and then assembled in arrays, a phase during which boundary values are supplied

and calculations are made at every time step throughout several tidal cycles, and finally an output phase in which tide heights and currents are analyzed and the results printed.

An obvious approach to the problem of splitting up the original program is to make several separate programs. These may then be run successively, with each producing an output tape of relevant values as needed by the next program. This approach is not particularly more expensive in terms of computer time but it does mean that more time will elapse before the several jobs are run. In some ways this is not a disadvantage for it gives the user time to reflect upon the progress of the calculations, something often lacking when people make use of sophisticated programs. A second approach to the problem is the use of overlays (IBM, 1970, p.43).

The overlay technique consists of splitting the original program into subroutines, collectively called 'phases', which are then stored on a peripheral device (such as a disk) until needed. When a phase is copied from disk to core, it is placed starting at some fixed location and erases the phase previously there (thus 'overlaying' the previous subroutine). Since the copying process from a disk usually involves mechanical movement, it is advisable to form the phases so as to avoid too many transfers. For example, it would not be good practice to have to call a phase from the disk at every time step. A natural selection is to have as the first phase the input part of the program. The second phase could be the part of the program that assigns and performs the calculations throughout the program, and the third phase would then be output and analysis.

When considering the optimization of the core storage taken up by matrices or arrays, one can, as a start, make use of the FORTRAN IV option of variable-length words. In particular, the use of the "INTEGER*2" specification permits the storage of integers up to the value of 32,767 (assuming that the normal word length is 32 bits). Depths and friction values may be stored in this fashion, as can certain other quantities. A more important possibility is the interleaving of two (or more) quantities into one array, bearing in mind the slight inconvenience caused during programming by, say, the storage of the quantity $H(M,N)$ in location $U(M,N+1)$. By the use of "EQUIVALENCE" statements, one can write $H(M,N+1)$ instead of $U(M,N+1)$. The method of interleaving, if possible at all, will of course depend on the grid layout used.

When using the numerical scheme discussed in Chapter IV it will be found that three large arrays are required as shown in Table 6.1.

Array	Equivalenced Values	Purpose
1	U, V, H	Heights and currents at lower time level
2	UU, VV, HH	Heights and currents at upper time level
3	A, C	Water depths and Chézy friction coefficients

Table 6.1. Major arrays used by the two-dimensional implicit program.

Flexibility Requirements

It is usually to the advantage of the originator of the program, and to that of future users, that the program be made as flexible as possible. The foremost and most time consuming task of importance is that of designing the program to be applicable to different boundary configurations with the minimum amount of reprogramming. The implementation of this needs careful consideration, as the resulting approach will be used many times throughout the program. If it is permitted by the method being used to solve the hydrodynamic equations, it is convenient to divide up the computations into those performed along rows, and those performed up columns. (This is usually the case if two-dimensional relaxation methods are not involved.) The two most useful methods are a representation of the boundaries by integers located in a large array like a map, and the storage of the integer coordinates of the end points of computational rows or columns, along with an integer denoting the nature of the boundary.

The first of these two methods, described by Matthews and Mungall (1970), is somewhat wasteful of core storage and computer time but has the great advantage that the boundaries may easily be adjusted during the computation, of use when flooding boundaries are present. Briefly, the method consists of using a two-dimensional integer array which acts as a map for the boundaries. The integer '1' is used to denote the transition from land to sea (or vice versa). The integer '2' is used whenever the model terminates at a boundary where the tide height must be specified as a function of time. During the course of the program

the array is scanned row by row and column by column, calculations and boundary conditions then being applied accordingly.

The second method, developed by Leendertse (1967), is very economical in computer time and storage (but is not so simple to use when flooding boundaries have to be considered). Two arrays are used to describe, respectively, the location and type of horizontal and vertical boundaries. Taking as an example the array LIMX(IX,J) that describes vertical boundaries, we have J ranging through the values 1, 2, and 3, and IX between 1 and the number of vertical boundaries. The M and N integer coordinates of the boundary are contained in LIMX(IX,1) and LIMX(IX,2), while the type of boundary (a '1' for one at which current is specified, and a '3' for one at which height is specified) is contained in LIMX(IX,3). When this array is scanned in pairs (IX=1,2; 3,4; etc.) it will provide the start and end locations of the computational row, and an indication of the numerical scheme necessary to deal with the boundary conditions.

Flexibility should also be aimed at in the control of input/output operations. The first of these is that of the use of a tape containing the values of height and current at the end of each cycle. This tape may be used to restart the job economically on a fresh computer run, or to limit the loss of data to part of a single tidal cycle should an unscheduled program termination occur. In either case the program must be modified so as to construct or read the tape. Other examples of output options needing to be programmed are the printing of sample values of tide height at every time step, current and height values

at the start and end of the computations, and (occasionally) the field of heights and currents at every time step during the last tidal cycle. Finally there is the requirement for boundary conditions to be specified at every time step.

The best way to meet these requirements is to have two short subroutines that are modified or rewritten by the user: a boundary value subroutine and a master subroutine that deals with all non-standard input/outputs (tape reading and writing, etc.). A diagram showing the way in which the writer's program was set up, taking the above into account, is shown in Figure 6.1. It will be noticed that the analysis-phase of the job is left for a later computer run. The reason for this is mentioned later.

Documentation

Both for reasons of documentation and of error detection, it is most desirable to have as full a record as possible of all input values. Thus every data card read should be printed, along with a description of the variable (e.g. latitude in degrees, time step in minutes, etc.). When quantities such as depths are read row by row from cards, each card should be printed as well as a full summary in the form of a two-dimensional array. Initial and final values of tide height and current should also be printed for future reference. A final precaution that may be taken, as mentioned in the previous section, is to prepare and save a tape containing the values of tide height and current from the very last time step. With the above
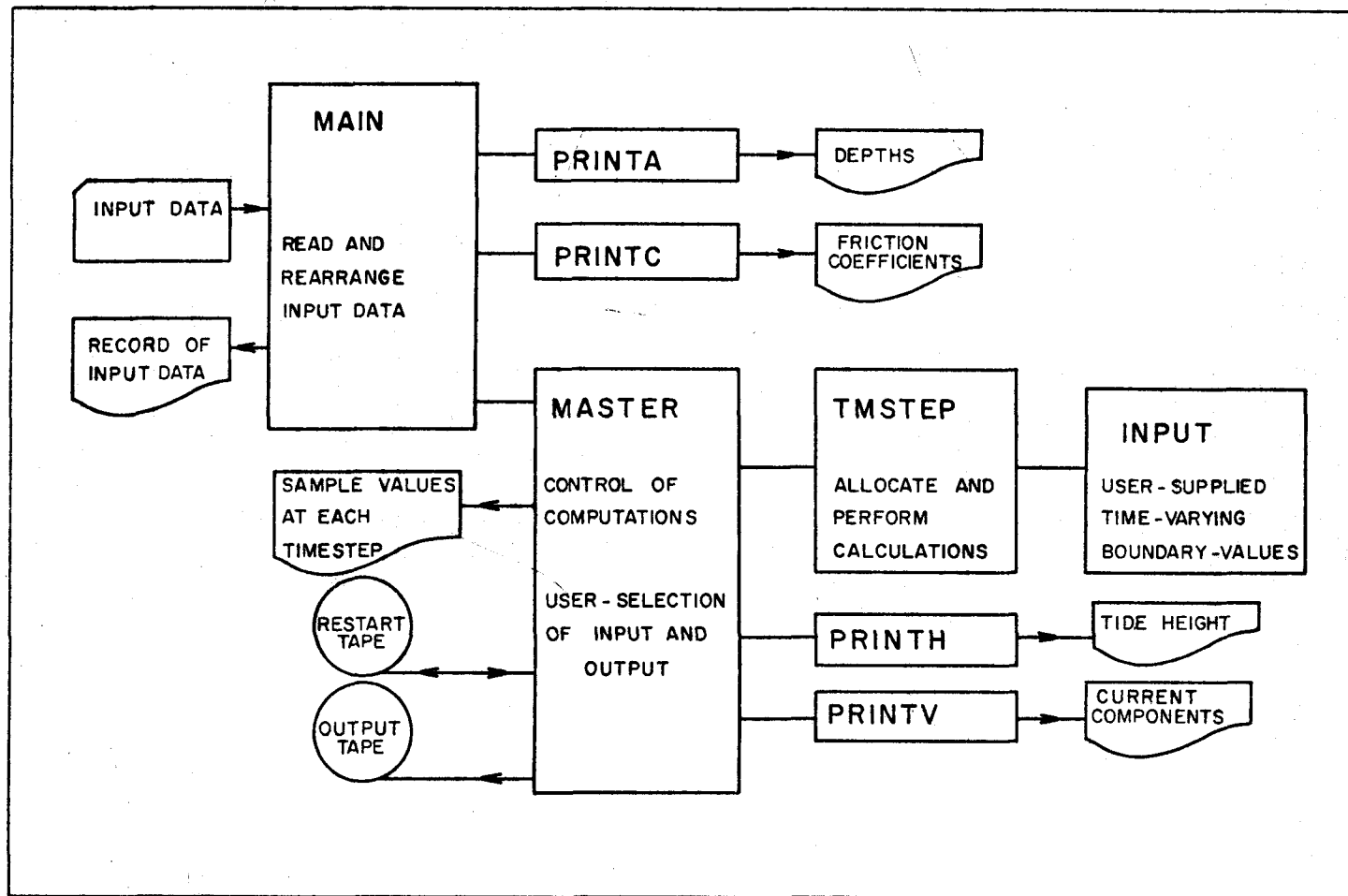
Figure 6.1. Arrangement of tidal computation program.

information no trouble should be experienced in rerunning a particular test at some later date, or in preparing a report summarizing a series of tests.

Analysis and Presentation of Tide Heights and Currents

In order to extract the maximum possible information from a given run, it is desirable to produce and retain a tape containing every value of height and current calculated during the last tidal cycle. This tape may then be analyzed by standard programs or can be used for any other purpose at a later date. The cost of the tape and the time spent in producing it will almost invariably be less than the cost of rerunning the whole job.

1. Tide height analysis

The first standard analysis program will probably be that of a Fourier analysis of the tide heights. Once the amplitude and phase corresponding to the lowest harmonic are available for every grid rectangle, simple investigations as to the height distribution (for example) at any instant may be made without having to scan the original tape; the information has been 'compressed'. This may similarly be done for the currents, since the raw data for these are also available on the original output tape.

The Fourier analysis process can be time consuming if one requires the maximum number of harmonics possible. As this equals the quantity (number of complete time steps per tidal cycle)/2, often an unrealistically large number, it is usual to limit the process to only a few

harmonics. By suitable programming it is possible to restrict the number of passes of the tape to one per harmonic.

The data from the last cycle is in the form h_1 , h_2 , ..., h_N (N being the number of time steps per tidal cycle), where $h = (H''_{m+1,n} + H''_{m-1,n} + H''_{m,n+1} + H''_{m,n-1})/4.0$. The record is assumed to be of length 2π, so that the data are located at points $1.2\pi/N$, $2.2\pi/N$, ..., $N.2\pi/N$. (Note that the first data point is not at time $t = 0$.)

In this case we have (adapted from Schureman (1958));

$$S_p = \frac{2}{N} \sum_{i=1}^{N} h_i \sin(ip \frac{2\pi}{N}) \qquad (6.1)$$

$$C_p = \frac{2}{N} \sum_{i=1}^{N} h_i \cos(ip \frac{2\pi}{N}) \qquad (6.2)$$

$$A_o = \frac{1}{N} \sum_{i=1}^{N} h_i \qquad . \qquad (6.3)$$

Also

$$(A_p)^2 = (C_p)^2 + (S_p)^2 \qquad (6.4)$$

$$\sin \xi_p = S_p/A_p \qquad (6.5)$$

$$\cos \xi_p = C_p/A_p \qquad (6.6)$$

and finally (remembering that t has period 2π),

$$f(t) = A_o + \sum_{p=1}^{\frac{N}{2} - 1} A_p \cos(pt - \xi_p) \qquad (6.7)$$

The procedure is thus to calculate $\sin(ip\,2\pi/N)$ and $\cos(ip\,2\pi/N)$ at the end of each time step, to calculate the mean values of tide height at the center of each rectangle, and to keep a running sum as indicated by equations (6.1), (6.2), and (6.3). Finally, at the end of the cycle, the sums are multiplied by 1/N or 2/N as necessary, and the amplitudes and phases are determined via equations (6.4), (6.5), and (6.6). If the mean value and first harmonic only are required, as often is the case in tidal studies, one needs to store 3 values for each item being analyzed. As there are 4 positions available per rectangle (keeping to the original subscripts), three major arrays are required. Because (when currents are also analyzed) this takes about the same amount of storage as that required during the main part of the program, it is convenient to separate the analysis phase from the first two phases mentioned earlier.

2. Current analysis

Average current components are first calculated for the center of each rectangle; thus

$$U''_n = \frac{U''_{m+1,n} + U''_{m-1,n}}{2}$$

$$V''_m = \frac{V''_{m,n+1} + V''_{m,n-1}}{2} .$$

These values are then analyzed for the desired Fourier components as were the heights (there will probably be sufficient core for heights and currents to be analyzed during the same pass of the tape). The

automatic analysis provides a mean value, a phase, and an amplitude for each current component.

Of more practical interest than the above are the components of the current ellipse. The dimensions of the semi-major and semi-minor axes and their orientations provide information as to the magnitude and direction of the maximum and minimum currents. These are obtained as follows.

Neglecting mean values for the moment (as they only produce a shift of the center of the ellipse), one has

$$u(t) = U \cos(\omega t - \theta)$$

$$v(t) = V \cos(\omega t - \phi)$$

where U, θ, V, and φ came from the Fourier analysis.
Denoting the magnitude of the current vector by S ,

$$S^2 = U^2 \cos^2(\omega t - \theta) + V^2 \cos^2(\omega t - \phi)$$

For a maximum or minimum, $\frac{dS}{dt} = 0$. ie

$$2\omega U^2 \cos(\omega t - \theta) \sin(\omega t - \theta) + 2\omega V^2 \cos(\omega t - \phi) \sin(\omega t - \phi) = 0$$

or

$$U^2 \sin 2(\omega t - \theta) + V^2 \sin 2(\omega t - \phi) = 0.$$

Thus

$$\sin 2\omega t \cos 2\theta - \cos 2\omega t \sin 2\theta = -\frac{V^2}{U^2} \sin 2\omega t \cos 2\phi + \frac{V^2}{U^2} \cos 2\omega t \sin 2\phi$$

or

$$\text{Tan } 2\omega t = \frac{\sin 2\theta + \frac{V^2}{U^2} \sin 2\phi}{\cos 2\theta + \frac{V^2}{U^2} \cos 2\phi} .$$

Thus two values, 90° apart, can be found for ωt . The establish-
ment of the value of ωt corresponding to one of the maxima of S (for
convenience, the one associated with the maximum northwards value), the
values of the semi-major and semi-minor axes, and the determination of
the sense of rotation of the current vector is merely a matter of pro-
gramming.

It has been found convenient to terminate the analysis program at
the end of the current ellipse calculations. The following is given
as an example of how one might proceed from this point, although
it is realized that each user will have his own requirements.

At the end of the analysis program the following quantities are
both summarized on the printer and written on tape:

HEIGHT ⎫ ⎧ mean value
U-CURRENT ⎬ ⎨ amplitude of 1st harmonic
V-CURRENT ⎭ ⎩ phase of 1st harmonic
                             (9 values in all).

                    ⎧ semi-major axis
CURRENT ELLIPSE   ⎨ semi-minor axis
                    ⎩ time of maximum northwards current.

These 12 values may conveniently be stored in three arrays.

Eight programs were written to make use of the above information.
They all make use of an off-line plotter (which could be replaced by
a display terminal). With the exception of the last program the plotter
automatically draws the inlet boundary, and very little work has to be
done by the user. A list of the programs follows.

1.   Corange and cotidal lines.

2.   Contours of equal maximum current.

3. Phase of maximum current
    (user-participation needed in complex cases).

4. Ellipse axes.   .

5. Ellipses, sense of rotation, current vector at $t=0$.

6. Current vectors at any instant.

7. Tide height at any instant.

8. 3-dimensional perspective view of sea surface at
    any instant.

CHAPTER VII

APPLICATION OF THE MODEL TO THE IRISH SEA

Introduction

It was felt that the first comprehensive test should be an application of the model to a real situation, with the model being run under the most favorable conditions possible. The area chosen for the test was the Irish Sea on account of the attention that it has received in the literature. Amongst the basic references on the Irish Sea tides are the papers of Taylor (1919), Defant (1920), Doodson and Corkan (1932), and Doodson, Rossiter and Corkan (1954). Taylor's classic paper deals with the propagation and absorption of energy and Defant's is one of the first applications of a one-dimensional model. Doodson and Corkan made use of vertical and horizontal tide amplitudes and phases along various sections crossing the sea to obtain a corange and cotidal chart (published also as part of Admiralty Chart No. 301), while Doodson, Rossiter and Corkan obtained similar results by a relaxation method based on tidal values along solid boundaries.

Constant grid-spacing was chosen for the Irish Sea test so that the errors developed would not be attributable to the effects of variable grid-spacing. Using a grid-spacing of 7.5 nm, it was possible to make use of the grid (and thus the depths) used by Doodson, Rossiter and Corkan (1954), as in both schemes depths are specified

midway between the sides of the squares. Besides greatly reducing the labor involved, this enables a more meaningful comparison of results.

The tests made included investigations of the effect of changing the time step, friction coefficient, and boundary values. The results compared so favorably with those of Doodson and Corkan (1932) that the original program was extended to produce information as to the nature of the current associated with the M_2 tide in the Irish Sea.

Description of the Irish Sea

The Irish Sea is bounded by portions of the coastlines of Eire, Northern Ireland, Scotland, England, and Wales (see Admiralty Chart No. 1824a, and Figure 7.1.). Its center can be taken as 53.5°N , 4.5°W , and the sea has a north-south length of about 180 nm and a greatest width of 100 nm. Connections with the Atlantic are via St. George's Channel in the south (40 nm wide) and North Channel in the north (20 nm wide). The Isle of Man is located in the center of the northern part of the Irish Sea, and appears to exert considerable influence on the currents of the region. The Irish Sea is generally shallow, with a maximum depth of 149 f (272 m) in the North Channel, and 87 f (159 m) in the main part of the sea (between Dublin and Holyhead). Shipping is extensive in the region, with Dublin and Liverpool as the major ports.

The tides of the region are fairly complex (see Bowden (1955) for an excellent description of the region). There is a degenerate amphidromic point on the coast of Eire near Arklow, and the greatest
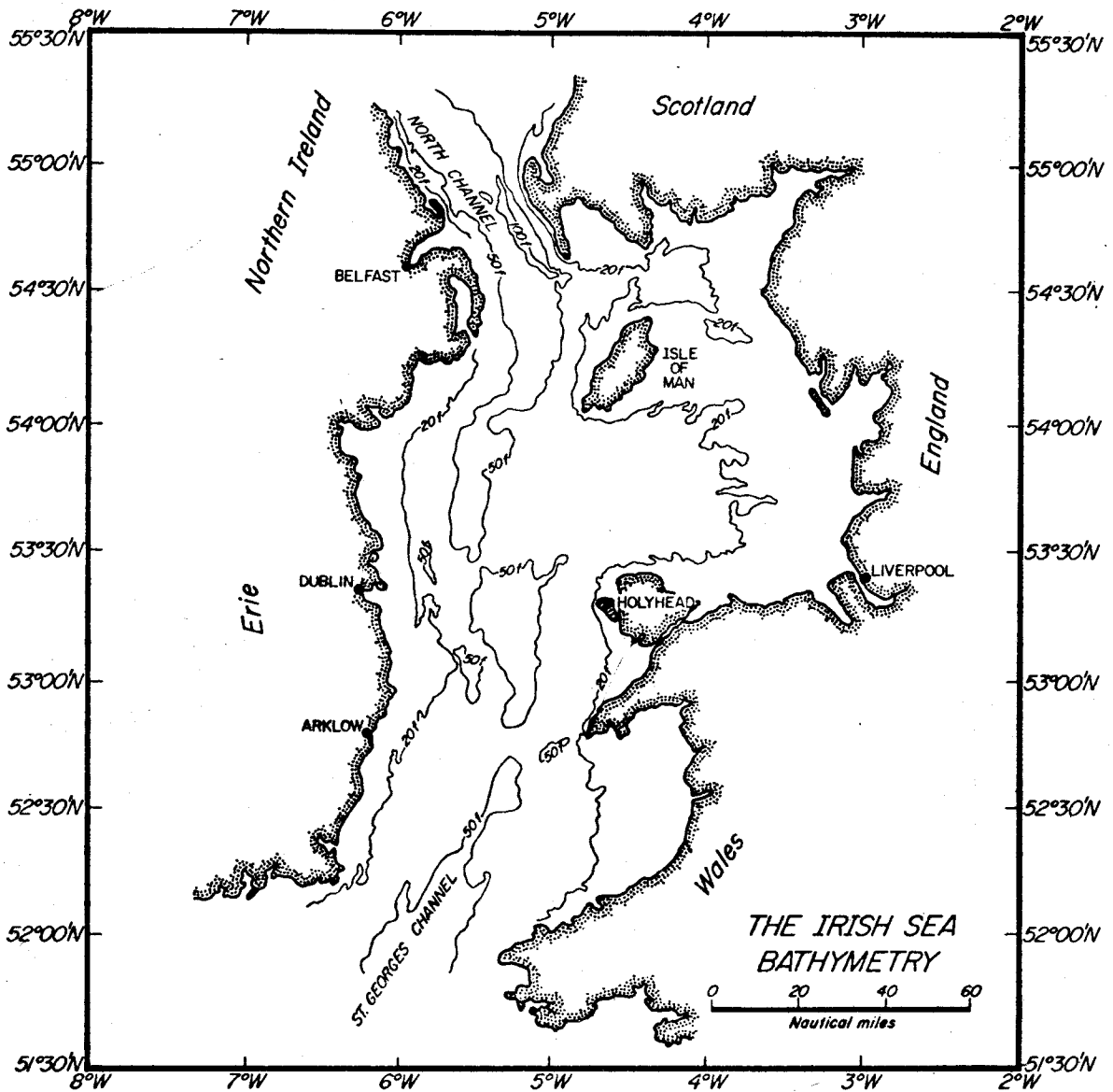
Figure 7.1. Bathymetry of the Irish Sea.

tidal range occurs in the region of Liverpool (the M_2 tidal amplitudes being about 40 cm and 300 cm respectively). The surface currents of the region are shown in the Irish Sea Pocket Tidal Stream Atlas (British Admiralty, 1962), and during spring tides they can attain over 200 cm/sec. The sea 'fills' from both entrances essentially simultaneously, with the tidal streams flowing towards Liverpool on either side of the Isle of Man. The region bounded by lines running west and southwest from the Isle of Man and by the coast of Eire is one of small currents at all stages of the tide (the maximum value being of the order of 50 cm/sec).

Grid selection and boundary values

The first step in selecting a suitable grid outline was to recreate the grid network of Doodson, Rossiter and Corkan (1954). As Admiralty Chart No. 1824a is based on a Mercator projection it was necessary to allow for the 'spreading' of lines of constant spacing running in northerly directions. Having found that their grid network was based on the line of 4°40'W longitude (J. R. Rossiter, personal communication), this line was established on the chart. Then, starting with the line of 53°20' N latitude, using the part of the latitude scale level with that line, points were marked off at distances of 7.5 nm to the left and right of the line of 4°40'W longitude. This was repeated every 30 nm north and south of the line of 53°20'N latitude, always using the correct scale for that latitude. The points were then joined up, forming a series of diverging lines. The remaining

horizontal lines were then drawn at 7.5 nm intervals, and finally
the grid outline shown in Figure 7.2 was selected as the best compromise
between good coastline fit and similarity to the sloping outline of
Doodson, Rossiter and Corkan (1954).

For all but one of the computer runs, the input values for St.
George's Channel were determined from the cotidal and corange chart in
Doodson and Corkan. The relevant points were located on the chart, and
the range and phase then found by interpolation. As there was not
sufficient information on the diagram for values to be obtained for
North Channel, the necessary values were obtained from an unpublished
cotidal and corange chart (Laska, 1965) based on all the available
harmonic constants, with the general shape of the lines coming from
Doodson and Corkan's work. For the last computer run, a test was
made as to the sensitivity of the results to the use of boundary
values were obtained by using the M_2 amplitudes and phases of the
three most convenient tide stations. These consisted, in the north,
of Larne, Port Patrick and Port Avogie; in the south, of Waterford,
Wexford, and Fishguard.

The amplitudes and phases at the input points were obtained as
follows: the triangle having the three tide stations at its apexes
was drawn, and points were located along each side at convenient
values. Corresponding points were joined, forming equidistant, parallel
lines. A first-order surface of amplitude or phase for that part of
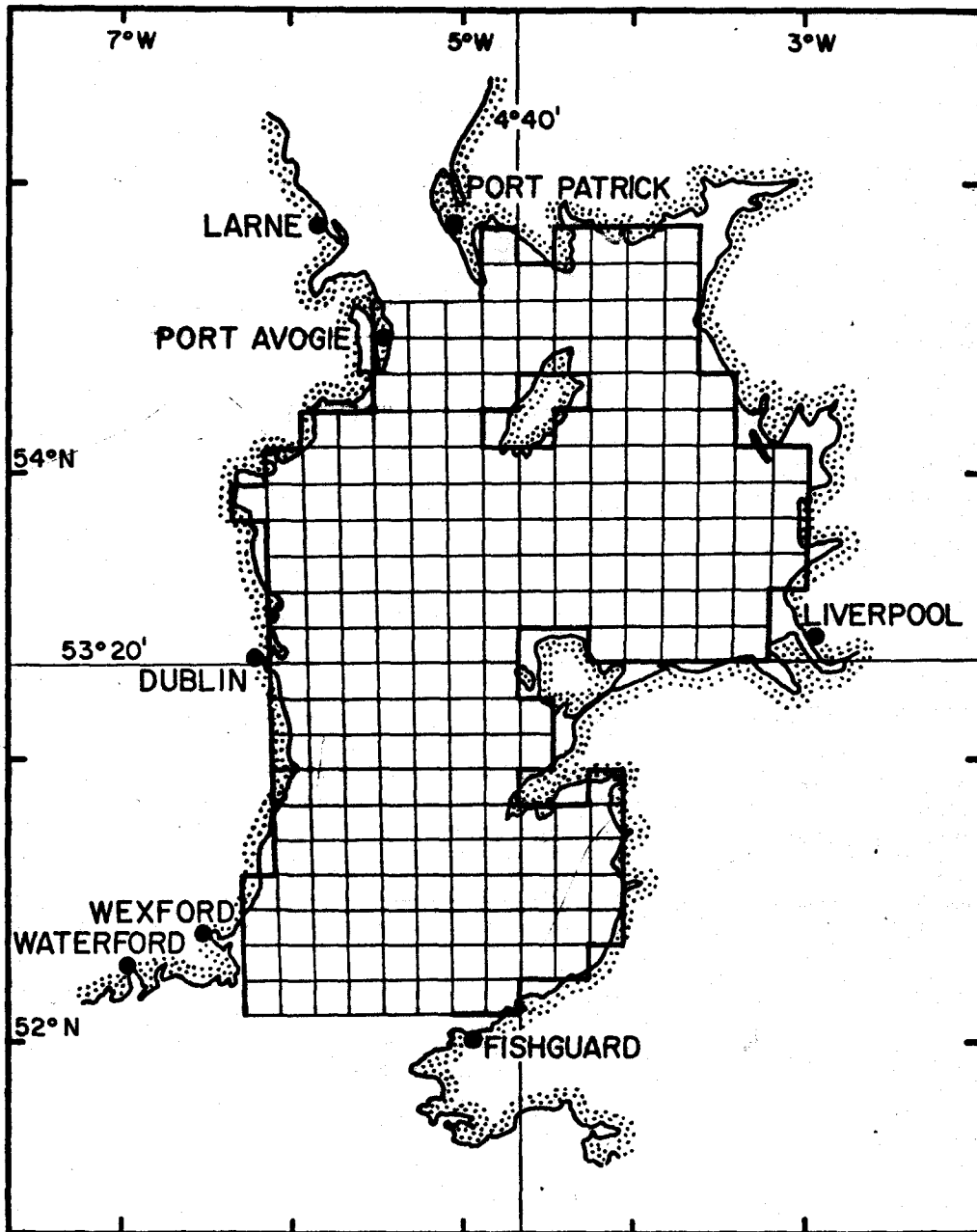the sea was thus constructed. The triangles are shown in Figures 7.3

Figure 7.2. Grid used for the Irish Sea tests.

and 7.4. The values found from the corange and cotidal diagrams, and from the triangles, may be seen in Table 7.1, and in Figures 7.5 and 7.6. The effect of the difference between the two sets of input values is discussed later.

North Channel

	Amplitude, cms.		Phase, degrees	
	Charts	Constitutents	Charts	Constituents
West	147	138	325	318.2
	156	152	328	319.4
East	170	166	330	320.6

St. George's Channel

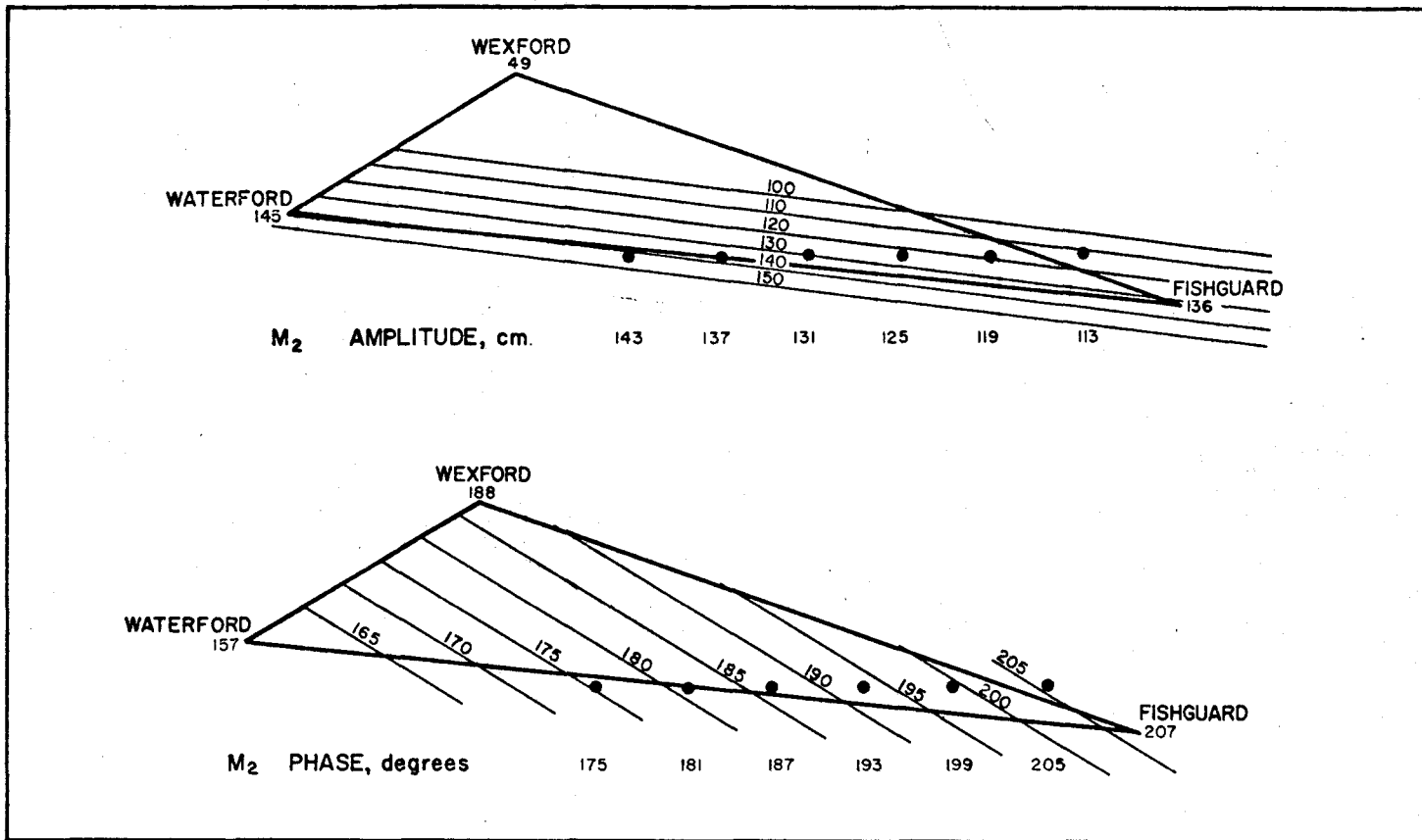|	Amplitude, cms.		Phase, degrees	
	Charts	Constituents	Charts	Constituents
West	112	143	180	175
	108	137	190	181
	108	131	196.5	187
	109	125	198	193
	112	119	202	199
East	120	113	204	205

Table 7.1. Amplitudes and Phases for Input Points.

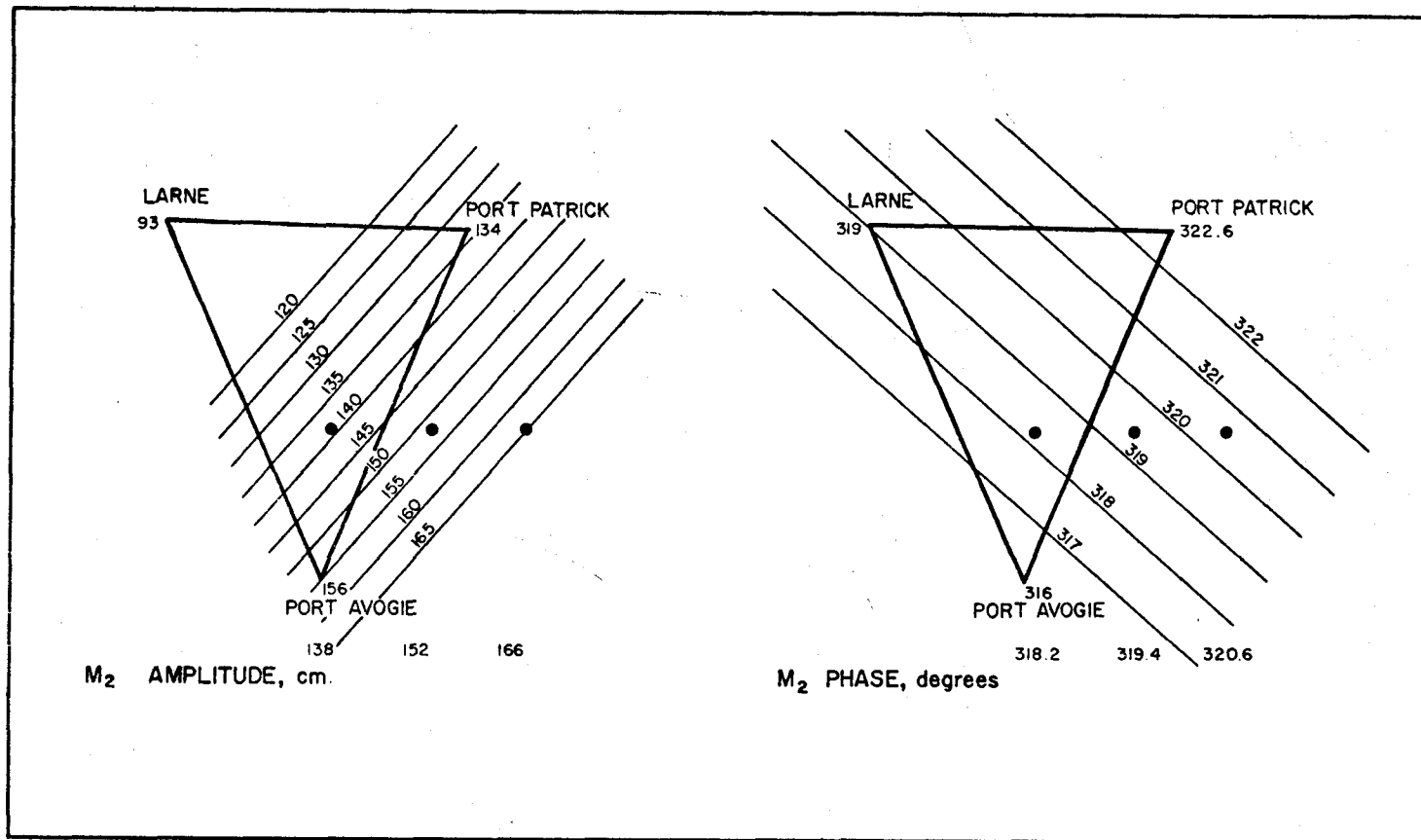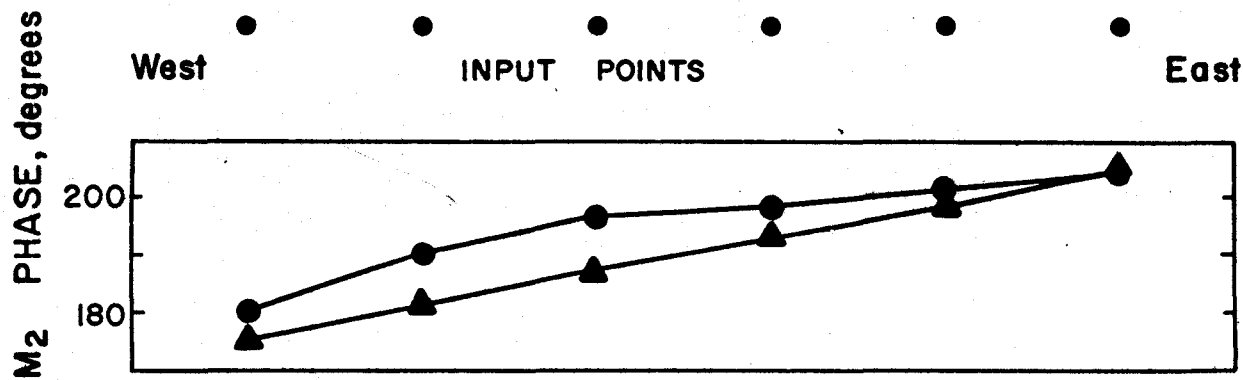Figure 7.3. Construction used to obtain tidal data for St. Georges Channel.

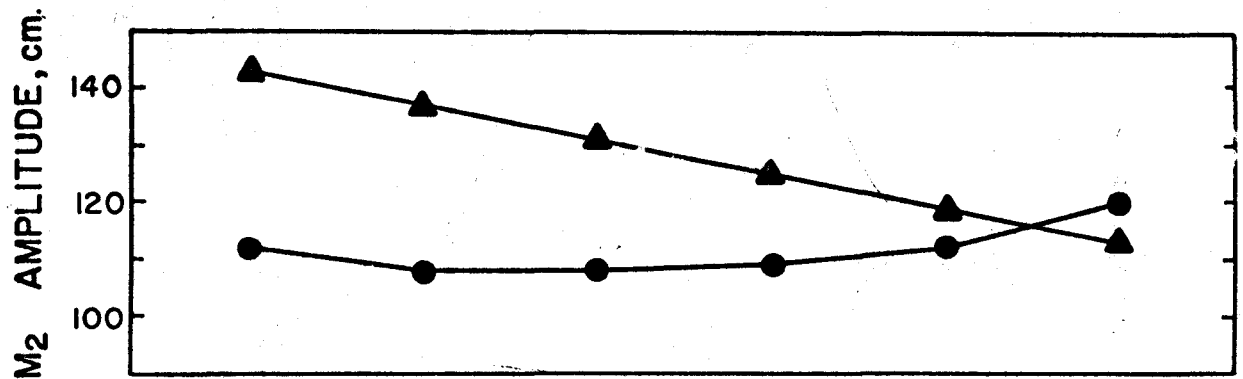Figure 7.4.   Construction used to obtain tidal data for
North Channel.
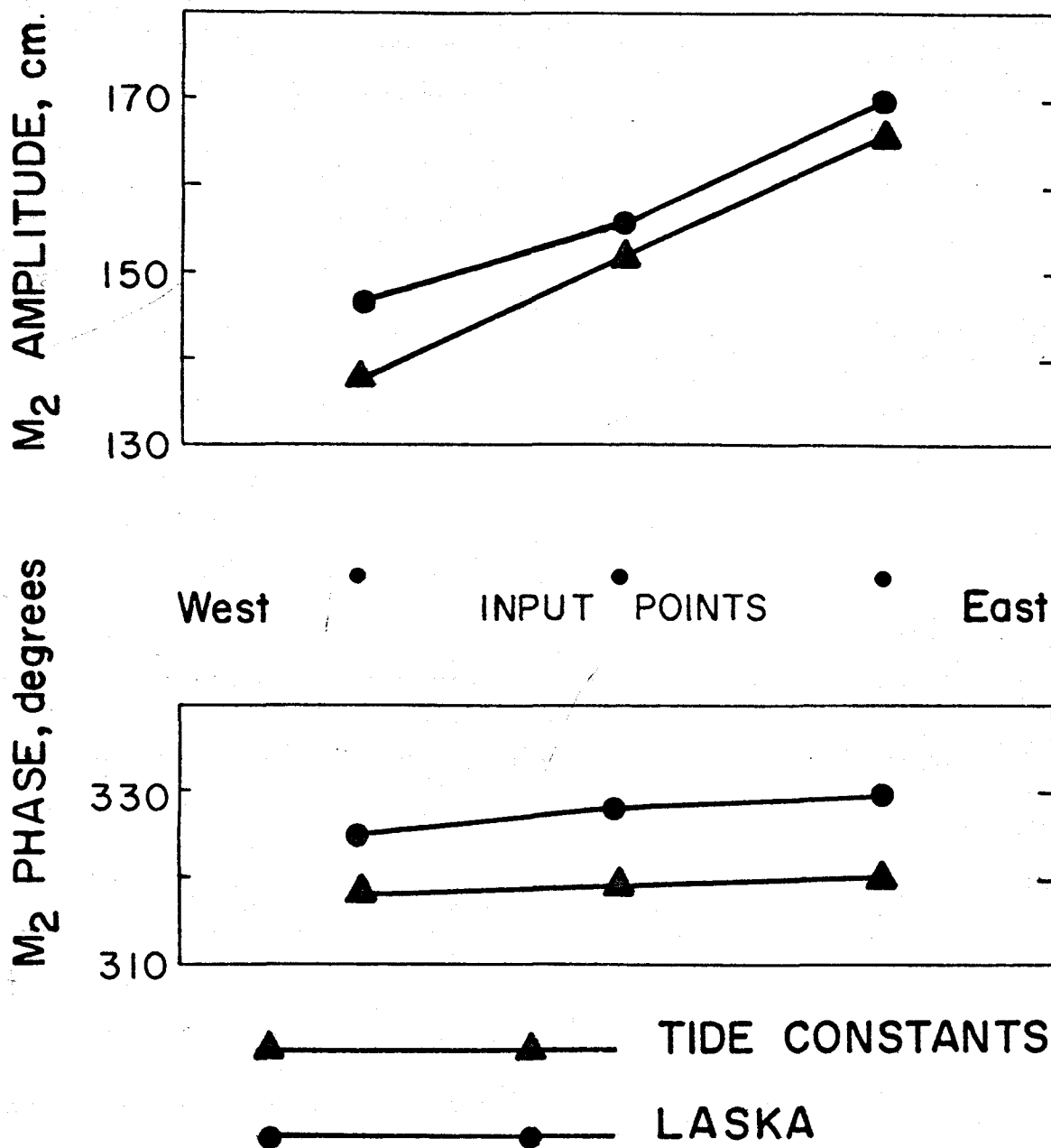
Figure 7.5. Tidal data for St. Georges Channel.

Figure 7.6.   Tidal data for North Channel.

Description and Results of the Tests

The tests to which the model was subjected were of three types: time step variation, friction variation, and boundary condition variation. A list of the tests is shown in Table 7.2. The standard to which the various corange and cotidal diagrams may be compared is shown in Figure 7.7. In this figure are shown the corange and cotidal lines for the Irish Sea as obtained by Doodson and Corkan (1932) along with the grid outline of the present model.

Test Number	Time Step min.	C $m^{1/2}$ sec^{-1}	$k(=g/C^2)$ dimensionless	Source of Boundary Condition
1	5.175	70.0	0.0020	charts
2	10.350	70.0	0.0020	charts
3	20.700	70.0	0.0020	charts
4	41.400	70.0	0.0020	charts
5	62.100	70.0	0.0020	charts
6	10.350	55.0	0.0032	charts
7	10.350	1000.0	∿0.0000	charts
8	10.350	70.0	0.0020	Tidal Constants

Table 7.2. List of tests performed on the Irish Sea Model.

Based on the one-dimensional implicit method error wave propagation analysis of Appendix II, a rough guide line for the model is that $(\tau \sqrt{gh}/\Delta x)$ should be less than 1.0 . As the greatest schematized depth in the central region of the modelled region is of the order of 120 m, one arrives at a suggested value for τ of the order of 400 sec. It was decided that a longer time step than this could probably be tolerated since the above is only a guide and not, as in the case of
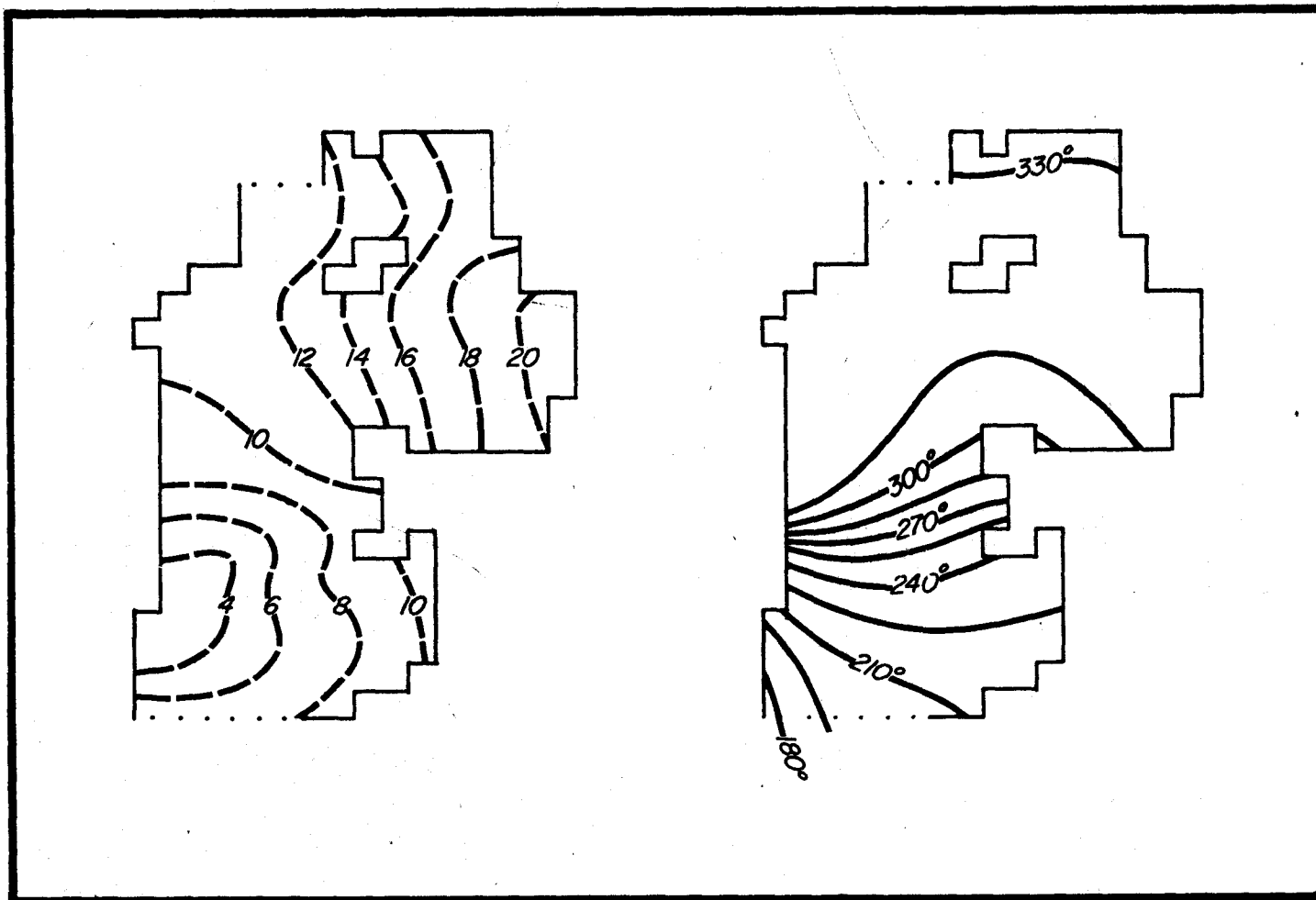
Figure 7.7. M_2 corange lines (in feet) and cophase lines from Doodson and Corkan (1932) superimposed on the Irish Sea grid.

explicit models, a fixed requirement. Thus the shortest time step used in the tests was that associated with 144 time intervals per tidal period (12.42 hours): a value for τ of 310.5 sec.

Test No. 1 was continued for a total of seven cycles before the computations reached a 'quasi steady-state'. During this particular test each cycle required some 10 minutes of computer time on an IBM 360/65, so that the test was rather costly. It was observed that there were no signs whatsoever of instability either in the form of diverging calculations or in the form of high frequency error waves. The output of the last cycle was then analyzed for the first harmonic, and the resulting corange and cophase lines were computed and plotted. Similar tests were run using the time steps listed in Table 7.2. It was noted that as the time step was increased the model achieved a 'quasi steady-state' in fewer cycles: test No. 5 required only 3 cycles. The result of test Nos. 1 through 4 can be seen in Figure 7.8. A comparison between Figure 7.7 (the standard) and Figure 7.8 reveals an excellent agreement for the case of $\tau=10.35$ min. For this particular time step the main points of disagreement are in the shape of the corange lines opposite Wales, and in the northeastern part of the Irish Sea. The former situation is traceable to one of the computation lines used by Doodson and Corkan (1932). It is possible that the sudden perturbation in their corange lines is not entirely realistic, and until deep sea tide gauges become available, the resolution of this difference of opinion will be difficult.

Some general features that can be seen in Figure 7.8 are as follows. As the time step increases the amphidromic region appears
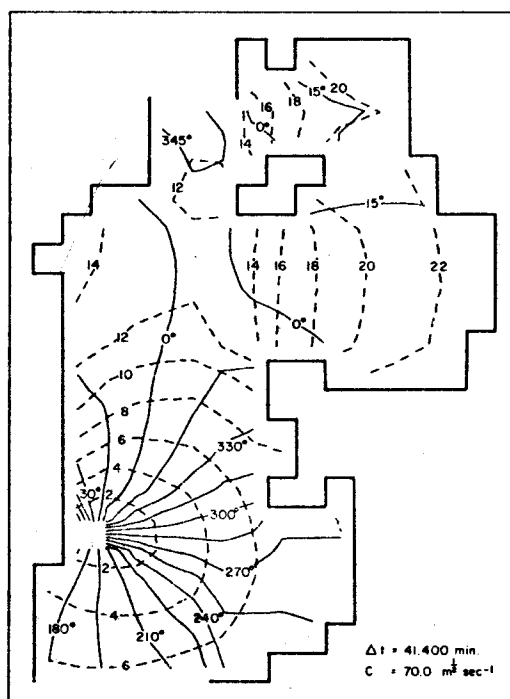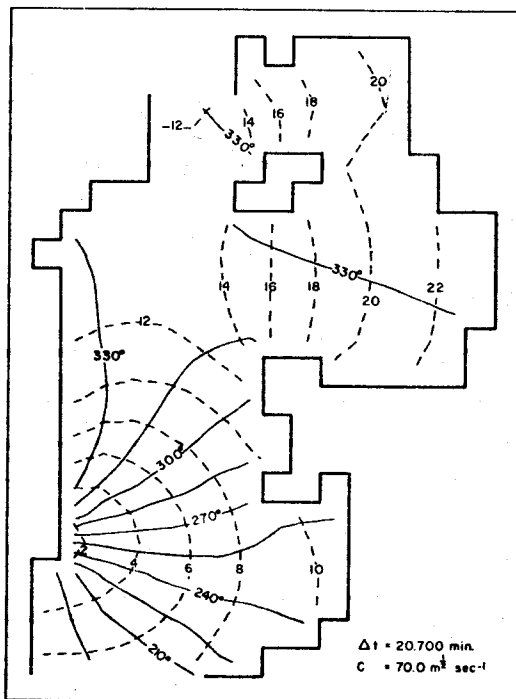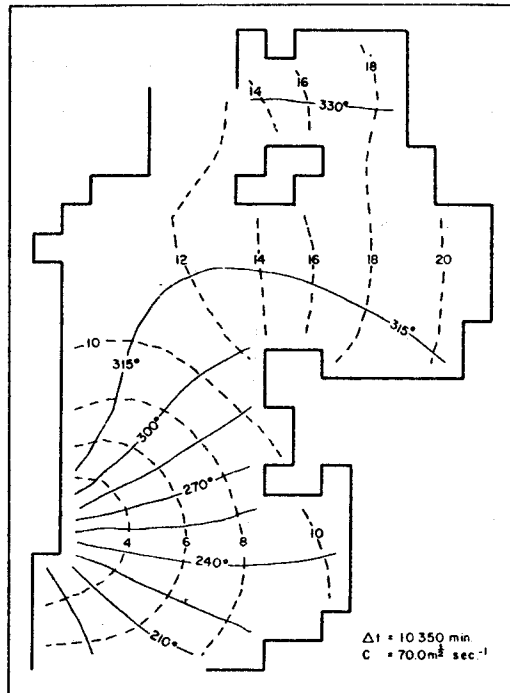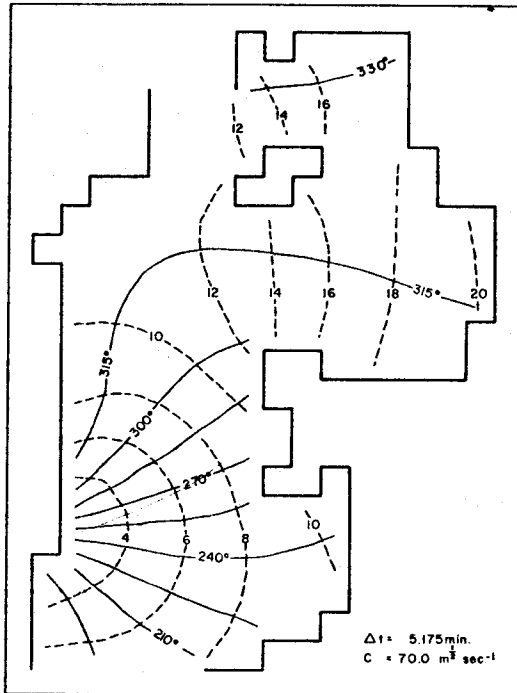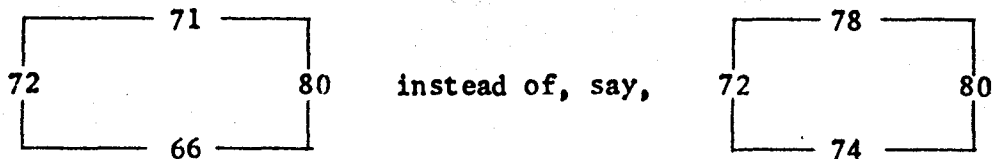
Figure 7.8. Comparison of results for different time step intervals. The corange lines are in feet.

off the coast of Eire, and associated with this is an increase of tidal range in the northeastern part of the sea. The increase in tidal range is the opposite of what would be expected from the graph of amplitude distortion in Figure III.1, and so may be associated with some resonance phenomena. A clockwise rotation of the cophase lines occurs with increasing time step, so that the phase near Liverpool goes from ~315° to ~10°. The actual changes are somewhat academic as a time step of 20.7 min or greater is clearly too large if one's goal is accurate results. However, it is important to note that a great saving in computer time can result if a long time step is used for the first run on a new area. After three or four cycles at, say, a time step of about 1 hour, one can then change to a suitably small time step. Evidence for this can be seen from satisfactory results of the run with time step of 41.40 min (see Figure 7.8).

During the first set of tests a feature of importance concerning the mode of breakdown of the model (due to large time steps) was noticed. One of the disadvantages of implicit models is that, in the absence of comparisons made during the computations, the user does not usually receive any warning (such as instability) as to the fact that the long time step he has chosen is producing poor results. The feature that was noticed was that there tends to be a loss of coherency between the heights calculated along rows and the heights calculated along columns. This manifests itself in at least two forms: the field

of heights tends to assume a 'bumpy' appearance, and heights on
the vertical sides of rectangles are not consistent with those on
the horizontal sides, eg.

```
   ┌──── 71 ────┐                      ┌──── 78 ────┐
72 │            │ 80    instead of, say, 72 │        │ 80
   └──── 66 ────┘                      └──── 74 ────┘
```

A breakdown of this nature is readily observable if the height field
is occasionally printed, and an internal check can readily be
programmed. An example of a height field containing such values
(from test 5 at t=0) is shown in Figure 7.9.

The second set of tests, involving test Nos. 2, 6, and 7, was
run partly to see if the model would tend to become unstable as the
friction was reduced and partly to see what is the part played by
friction in the 'tuning' of the Irish Sea model, which is the usual
way in which a model is adjusted to coincide with reality. The
comparison between the results of the three runs is shown in Figure
7.10. The first observation is, of course, that instability did not
result from the removal of friction. The second observation is
that the calculated ranges increase with decrease of friction, as
one would expect. The power of the method of tuning the model by
altering the friction values is readily observed.

The third set of tests, involving test Nos. 2 and 8 was run
as a matter of interest to see what would happen if one only had
available the tidal constituents for locations along the coastline,
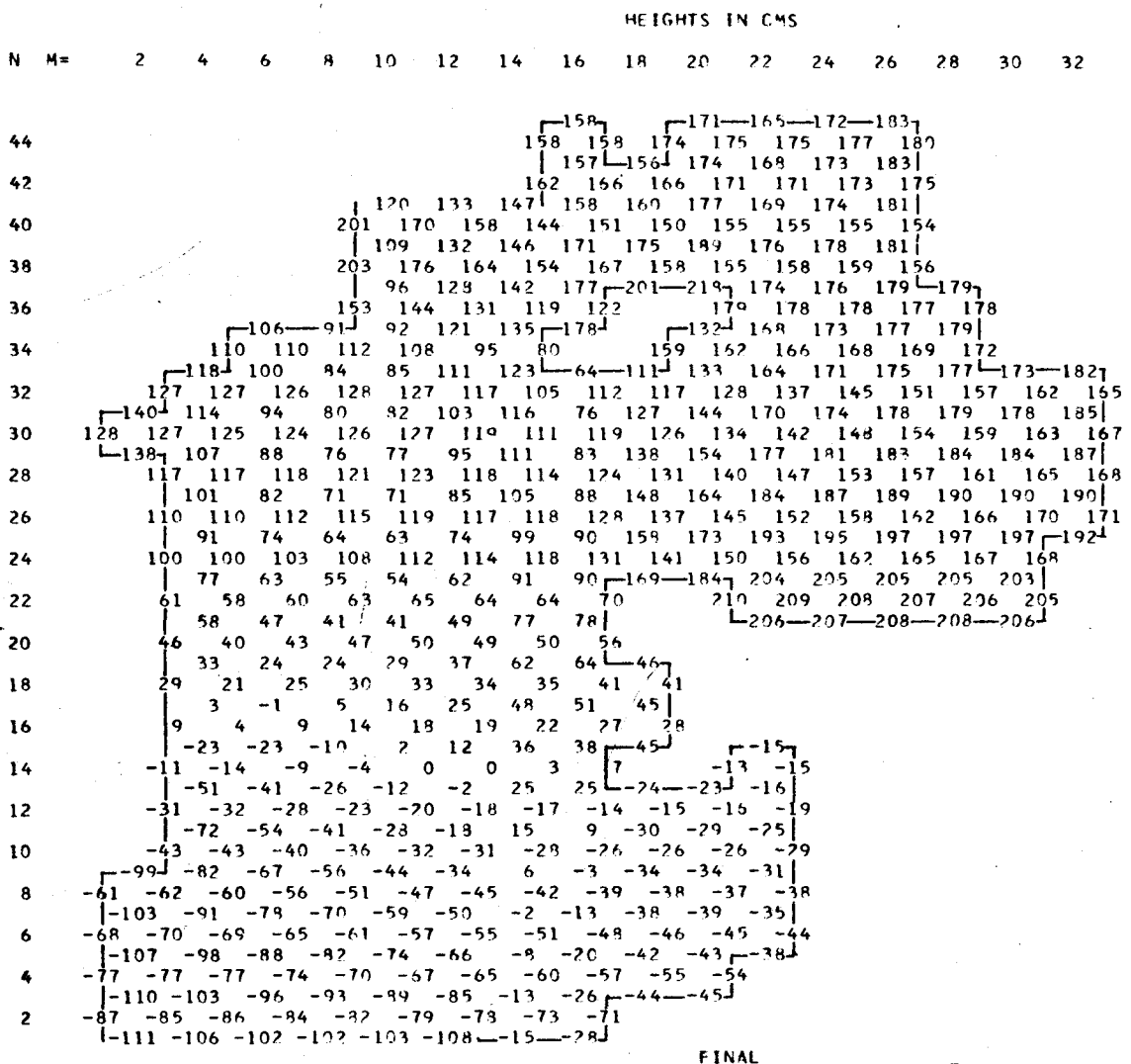ie. if there wee no access to corange and cotidal maps. Because

HEIGHTS IN CMS

N	M=	2	4	6	8	10	12	14	16	18	20	22	24	26	28	30	32

```
                                              ┌─158┐      ┌─171──165──172──183┐
44                                            158  158  174  175  175  177  180
                                              │ 157└─156┘ 174  168  173  183│
42                                            162  166  166  171  171  173  175
                                    ┌ 120  133  147│ 158  160  177  169  174  181│
40                              201  170  158  144  151  150  155  155  155  154
                                │ 109  132  146  171  175  189  176  178  181│
38                              203  176  164  154  167  158  155  158  159  156
                                │  96  129  142  177┌─201──219┐ 174  176  179└─179┐
36                        153  144  131  119  122      179  178  178  177  178
                  ┌─106──91┘  92  121  135┌─178┘     ┌─132┘ 168  173  177  179│
34                110  110  112  108   95   80        159  162  166  168  169  172
          ┌─118┘ 100   94   85  111  123└─64──111┘ 133  164  171  175  177└─173──182┐
32        127  127  126  128  127  117  105  112  117  128  137  145  151  157  162  165
    ┌─140┘ 114   94   80   82  103  116   76  127  144  170  174  178  179  178  185│
30  128  127  125  124  126  127  119  111  119  126  134  142  148  154  159  163  167
    └─138┐ 107   88   76   77   95  111   83  138  154  177  181  183  184  184  187│
28  117  117  118  121  123  118  114  124  131  140  147  153  157  161  165  168
    │ 101   82   71   71   85  105   88  148  164  184  187  189  190  190  190│
26  110  110  112  115  119  117  118  128  137  145  152  158  162  166  170  171
    │  91   74   64   63   74   99   90  159  173  193  195  197  197  197┌─192┘
24  100  100  103  108  112  114  118  131  141  150  156  162  165  167  168
    │  77   63   55   54   62   91   90┌─169──184┐ 204  205  205  205  203│
22   61   58   60   63   65   64   64   70      210  209  208  207  206  205
    │  58   47   41   41   49   77   78│         └─206──207──208──208──206┘
20   46   40   43   47   50   49   50   56
    │  33   24   24   29   37   62   64└─46┐
18   29   21   25   30   33   34   35   41   41
    │   3   -1    5   16   25   48   51   45│
16   9    4    9   14   18   19   22   27   28
    │ -23  -23  -10    2   12   36   38└─45┐      ┌─15┐
14  -11  -14   -9   -4    0    0    3   │ 7      -13  -15
    │ -51  -41  -26  -12   -2   25   25└─24──23┘ -16│
12  -31  -32  -28  -23  -20  -18  -17  -14  -15  -16  -19
    │ -72  -54  -41  -28  -19   15    9  -30  -29  -25│
10  -43  -43  -40  -36  -32  -31  -28  -26  -26  -26  -29
  ┌─99┘ -82  -67  -56  -44  -34    6   -3  -34  -34  -31│
 8  -61  -62  -60  -56  -51  -47  -45  -42  -39  -38  -37  -38
    │-103  -91  -78  -70  -59  -50   -2  -13  -38  -39  -35│
 6  -68  -70  -69  -65  -61  -57  -55  -51  -48  -46  -45  -44
    │-107  -98  -88  -82  -74  -66   -8  -20  -42  -43┌─38┘
 4  -77  -77  -77  -74  -70  -67  -65  -60  -57  -55  -54
    │-110 -103  -96  -93  -89  -85  -13  -26┌─44──45┘
 2  -87  -85  -86  -84  -82  -79  -73  -73  -71
    │-111 -106 -102 -102 -103 -108──15──28┘
```

FINAL

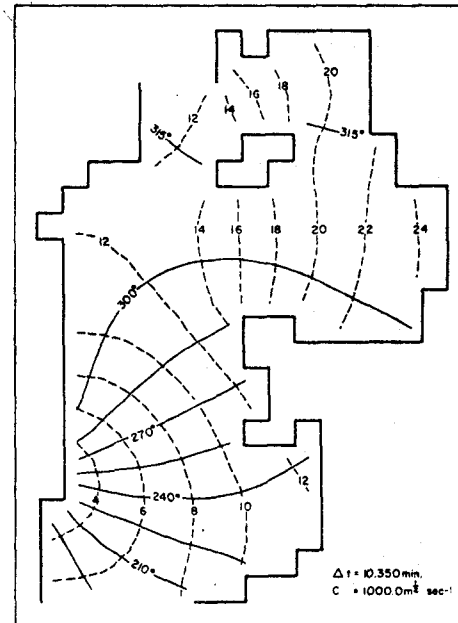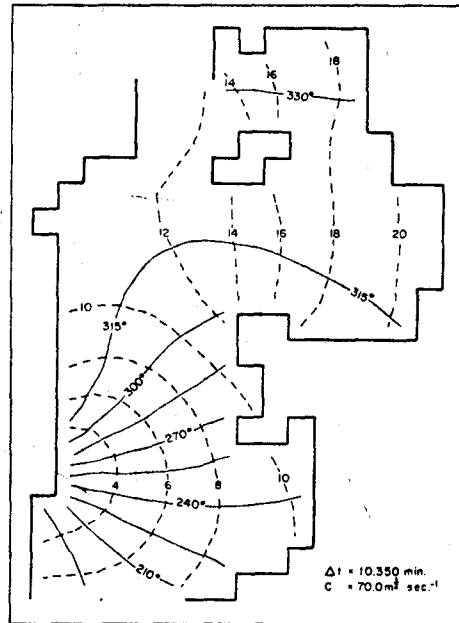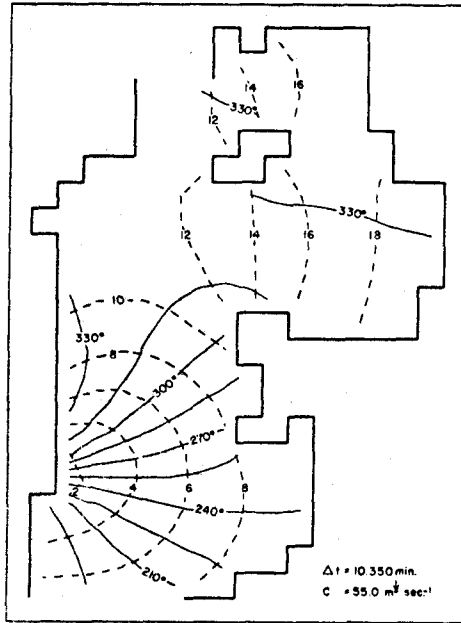**Figure 7.9.** Example of height field showing loss of coherency between rows and columns.

Figure 7.10. Comparison of results for different friction values. The corange lines are in feet.

the former is the more usual case the results are of practical interest. As can be seen in Figure 7.11 the difference between the corange lines in either case is small; significant changes only occuring between the two sets of cotidal lines. The latter difference is mostly the result of the phase of the tide used in the northern entrance.

As a conclusion to the series of tests which were based on the application of the model to the Irish Sea, it is felt that the following points have been established:

1) The model is unconditionally stable with or without friction

2) A rough criterion for reasonably accurate results is $(\tau \sqrt{gh} \gtrsim \Delta x)$

3) A running check as to the deterioration of the computations may be accomplished via an inspection of the height field
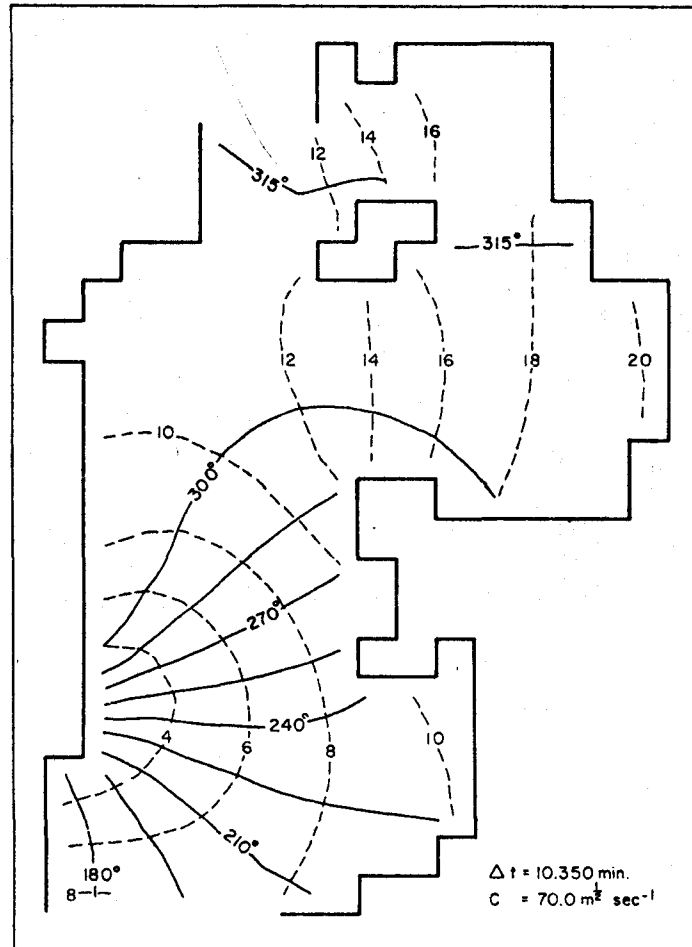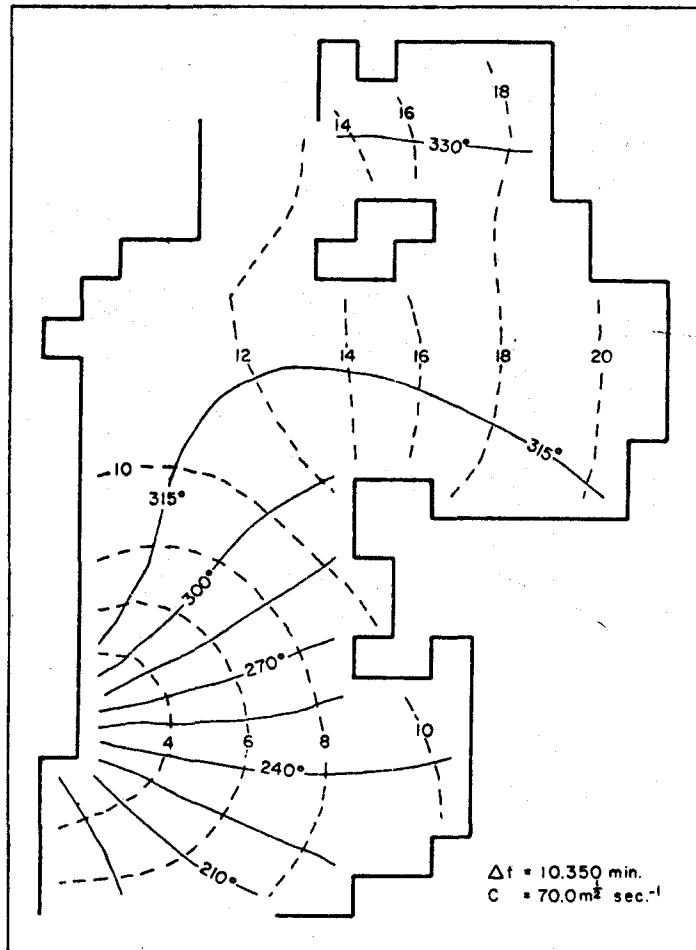
Figure 7.11. Comparison of results for different boundary conditions. On the left using values obtained from corange and cophase charts; on the right using values from linear interpolation between coastal stations. The corange lines are in feet.

CHAPTER VIII

APPLICATION OF THE MODEL TO A RECTANGULAR NORTH SEA

Test Description

The second test of consequence was one chosen to show the differences that result in the solution when identical regions are schematized using grids of equal or unequal spacing. It was decided that the region should be simple in shape, yet should possess suitably complicated tidal characteristics. Preferably the situation should also correspond to one for which a numerical solution had already been achieved (since there appear to be no two-dimensional analytical solutions that include realistic square-law friction).

The most suitable example found was that of a 'rectangular' North Sea of constant depth 50 m, with one open boundary along its northern side. Brettschneider (1967b) applied the numerical method of Hansen (1961) to this schematization taking the dimensions of the idealized sea to be 555 x 758.5 km. The results of his calculations (see Figure 8.1) show two distinct amphidromic regions, in good accordance with reality.

In this test identical friction and coriolis parameters were used, and M_2 tide data for 6 points along the open boundary were adapted from Table II.2 of Brettschneider (1967a). The distributions of amplitude and phase with distance are shown in Figure 8.2. It
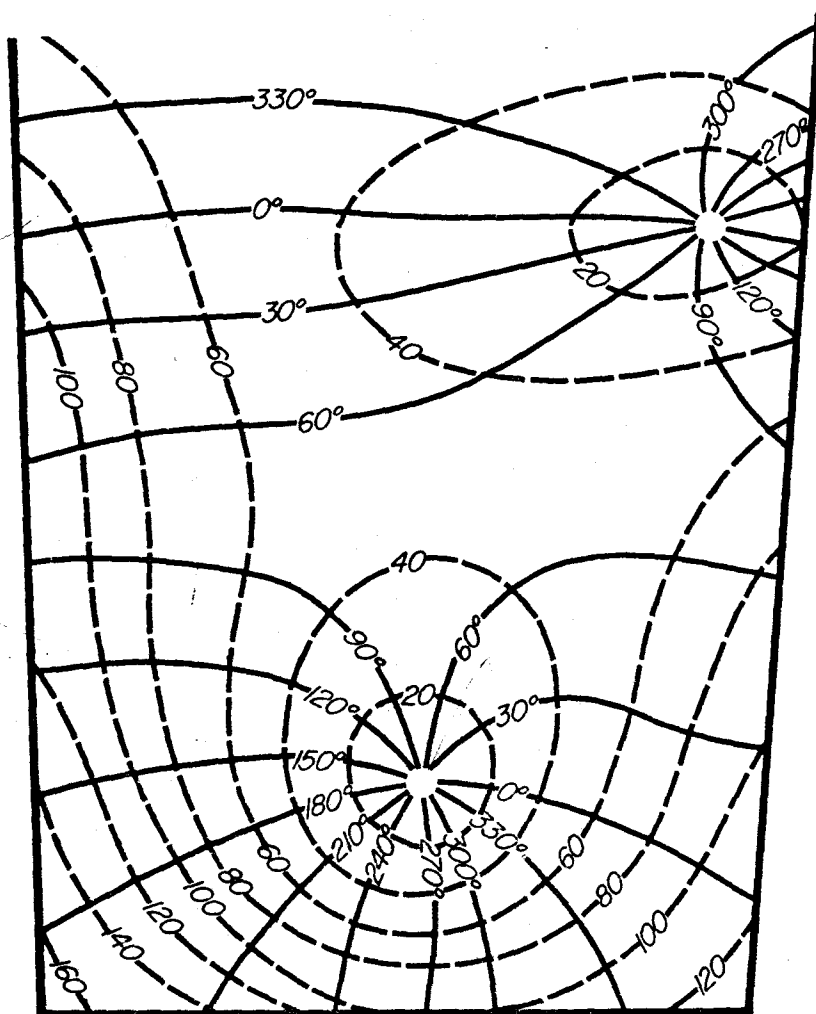
Figure 8.1. M_2 coamplitude lines (in cm) and cophase lines from
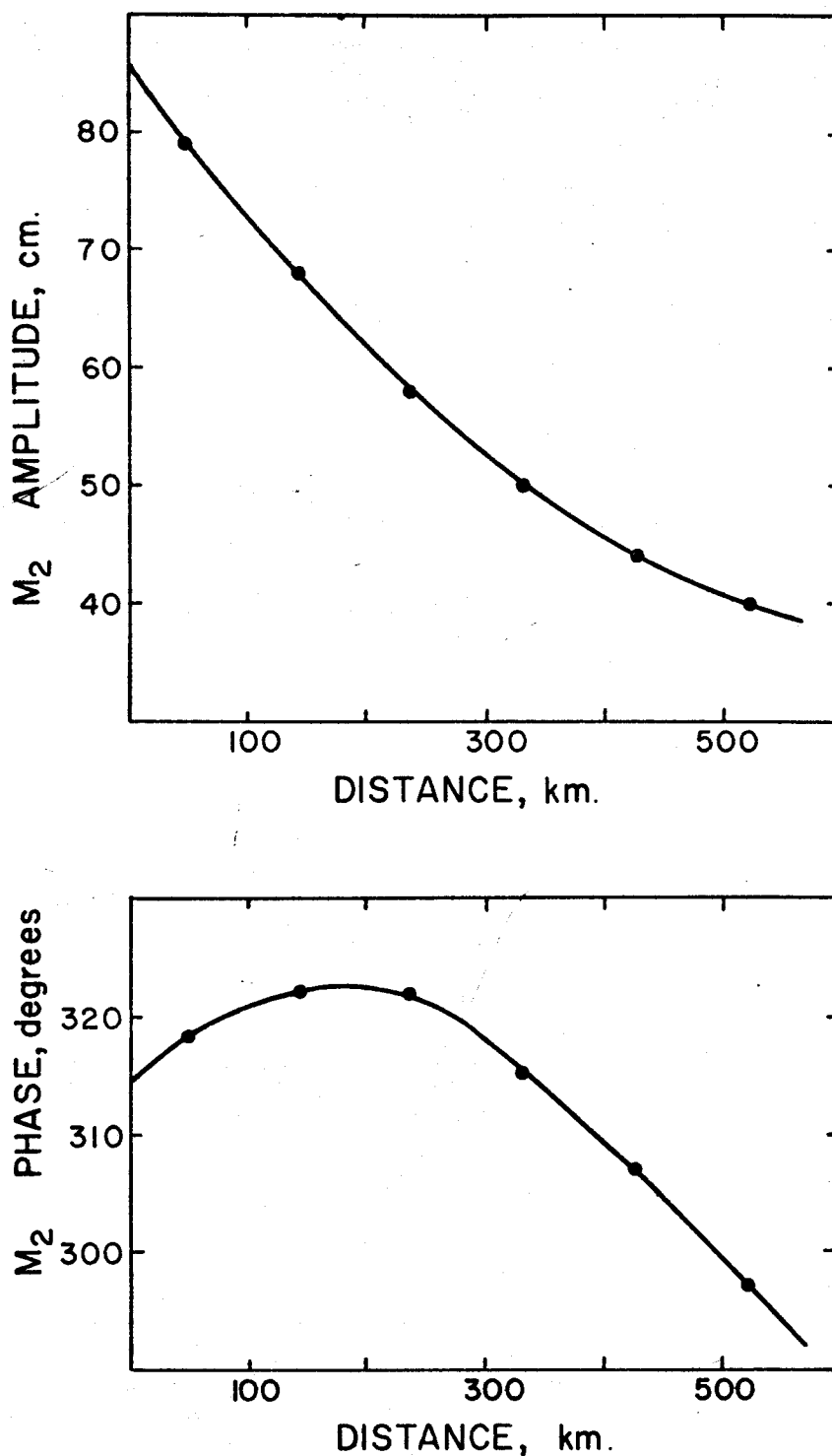Brettschneider (1967a) for a 'rectangular' North Sea.

Figure 8.2. Tidal data for open end of North Sea (Brettschneider, 1967b).

will be seen that there is some disagreement between Figures 8.1 and 8.2 as to the amplitudes along the northern boundary of the model, and unfortunately it did not prove possible to resolve this problem from the limited descriptions available in Brettschneider's two articles.

On account of the numerical scheme of Hansen, it was not possible to match the dimensions of Brettschneider's North Sea using a grid of constant spacing. This is because Hansen's method is bounded in this application by height points in the north and current points in the south, but by current points in the east and west of the model. The first of the two grids used was composed of squares of side $(\Delta x) = (\Delta y) = 95$ km. The best fit resulted thus in 6 x 8 squares and a region of dimension 570 x 760 km. It is felt that the differences in width and length between the original and test grid (2.7% and 0.2% respectively) will cause only minor differences between the results.

The second grid, with the same overall dimensions, was limited to 10 x 10 rectangles, the grid lines being positioned so as to obtain a greater density of computation points in the two amphidromic regions. The grid-spacings varied between 40 and 125 km. The two grid schemes used are shown side-by-side in Figure 8.3. Input data for the 10 input points along the northern side of the sea were interpolated from the curves shown in Figure 8.2.

In order to conserve computer time a time step of 20.7 minutes (36 intervals per 12.42 - hour tidal period) was used in both tests.
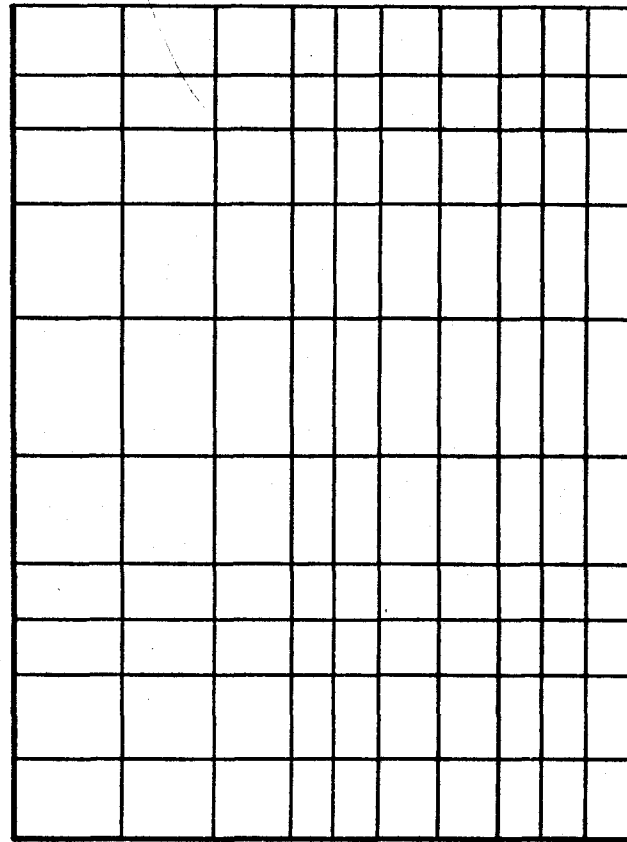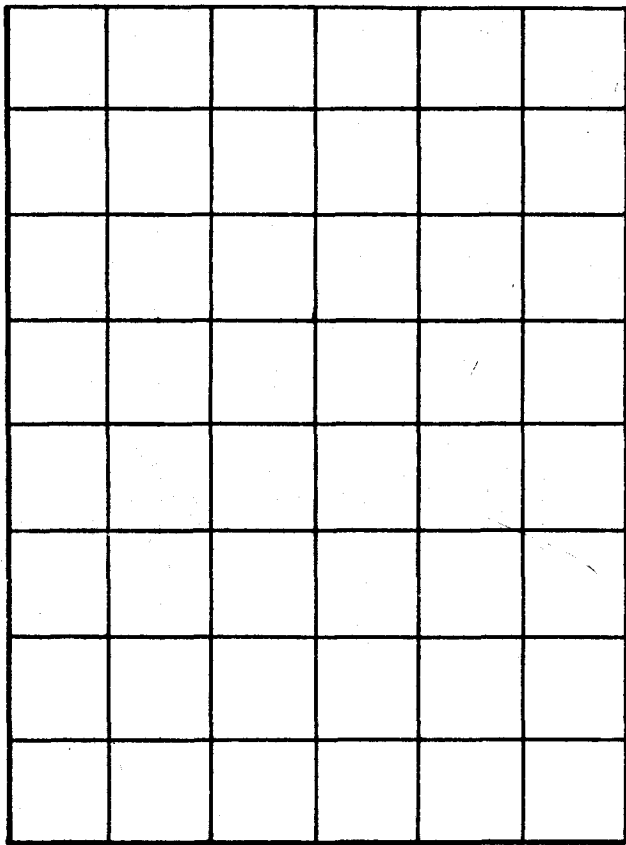
Figure 8.3.   The two grids used in the tests on the North Sea.

This was sufficiently small so that the quantity $\tau\sqrt{gh}$ was always less than the minimum grid interval. It was found that the model required some 6 cycles before it converged to a periodic solution, although small changes were still observable after 8 cycles. An example of the process of convergence (starting from a field of zero current and zero tide height) is shown in Figure 8.4 for the unequal grid-spacing test, the heights being taken from the V-point lying on the southern (solid) boundary of the bottom-left rectangle.

The results of the constant and unequal grid spacing tests (amplitude and phase of the first harmonic) are shown in Figure 8.5. It is apparent that the results are both in reasonable agreement with those of Brettschneider (Figure 8.1.). The main difference is in the position of the corange lines along the open northern boundary. This has been commented on earlier. The slight differences between the boundary conditions do not seem to have influenced values within the model to any great extent. Of greater consequence are the differences between the two tests themselves. It is seen that the chief difference lies in the position of the 40 cm amplitude curves, however, the greatest amplitude on a line between the amphidromes in each case is about 46 cm, so the difference is felt to be of no serious consequence.

Thus it appears that, in this test of the model, the effect of changing the grid-spacing makes very little difference between the solutions. It is realized that this one test can scarcely be considered as a conclusive test, however it is definitely encouraging. The best test for the model would be to repeat the above type of test using hydrographic data for a well-surveyed estuary for which concurrent
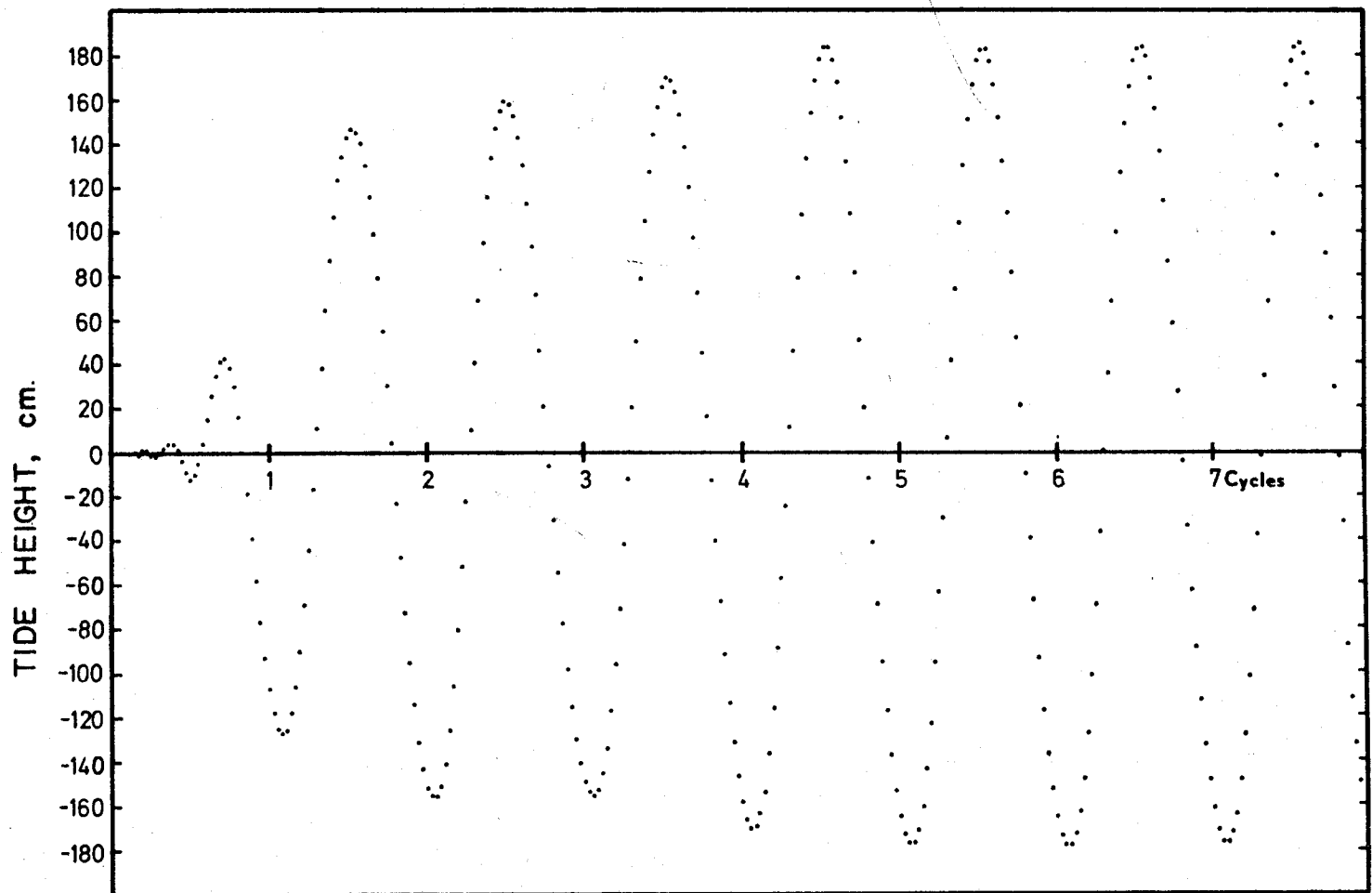
Figure 8.4.   Convergence of tide heights during the unequal grid-spacing test (see text for location).
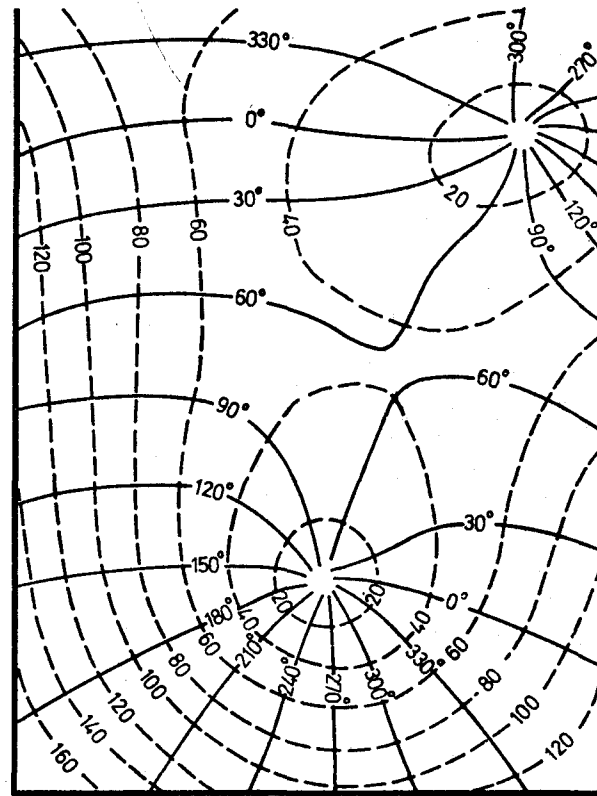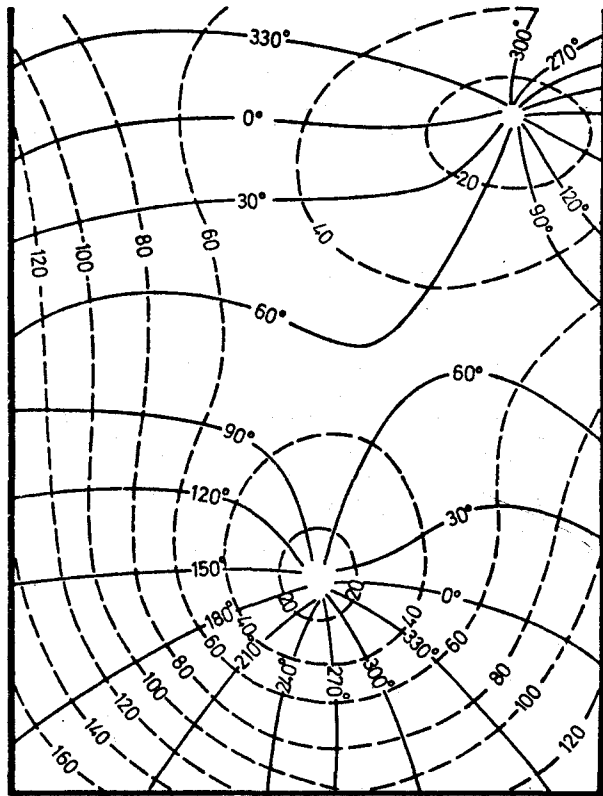
Figure 8.5. Comparison of results (grid with constant spacing on the left).

tide-gauge and current-meter data are available. Although an investigation of this magnitude could probably be undertaken with the cooperation of a suitable governmental agency, it is felt that such an undertaking should be deferred until such a time as the model is tested and improved to the point that less sophisticated tests can no longer be tolerated. It was felt that the most practical test of the model at this stage of the development should be the application of the model to a situation which made it obligatory to use the unequal grid-spacing feature. The model would then be 'tuned' via the friction coefficient until some tidal constituent in the region of the model most distant from the open boundary agreed fairly well with reality, and then the remaining calculated values would be compared with those predicted from measurements.

CHAPTER IX

APPLICATION OF THE MODEL TO COOK INLET, ALASKA

Introduction

The results of the first two series of tests demonstrated that the model is capable of producing accurate results which are not affected by the unequal grid-spacing. It was felt that the third and last of the series of tests should be one in which the model was applied to a complex area. During the tests the Chézy friction factor (considered constant over the whole inlet) would be adjusted until the amplitude at a point well within the inlet agreed fairly closely with the known value; then amplitudes and phases would be compared with the remaining known values obtained from Coast and Geodetic Survey measurements, and the behavior of the new model thus demonstrated. The area chosen, on account of the author's previous interest in the area and on account of the need for a predictive capability, is Cook Inlet, Alaska.

Description of the problem

Cook Inlet is located with its entrance on the coast of south-central Alaska, and is centered approximately on latitude 60°N and longitude 152°W. The inlet (see Figure 9.1) is some 190 nm in length and has a maximum width (at its entrance) of 48 nm. The tides of the region are complicated. The range of the tide at Anchorage, some 25
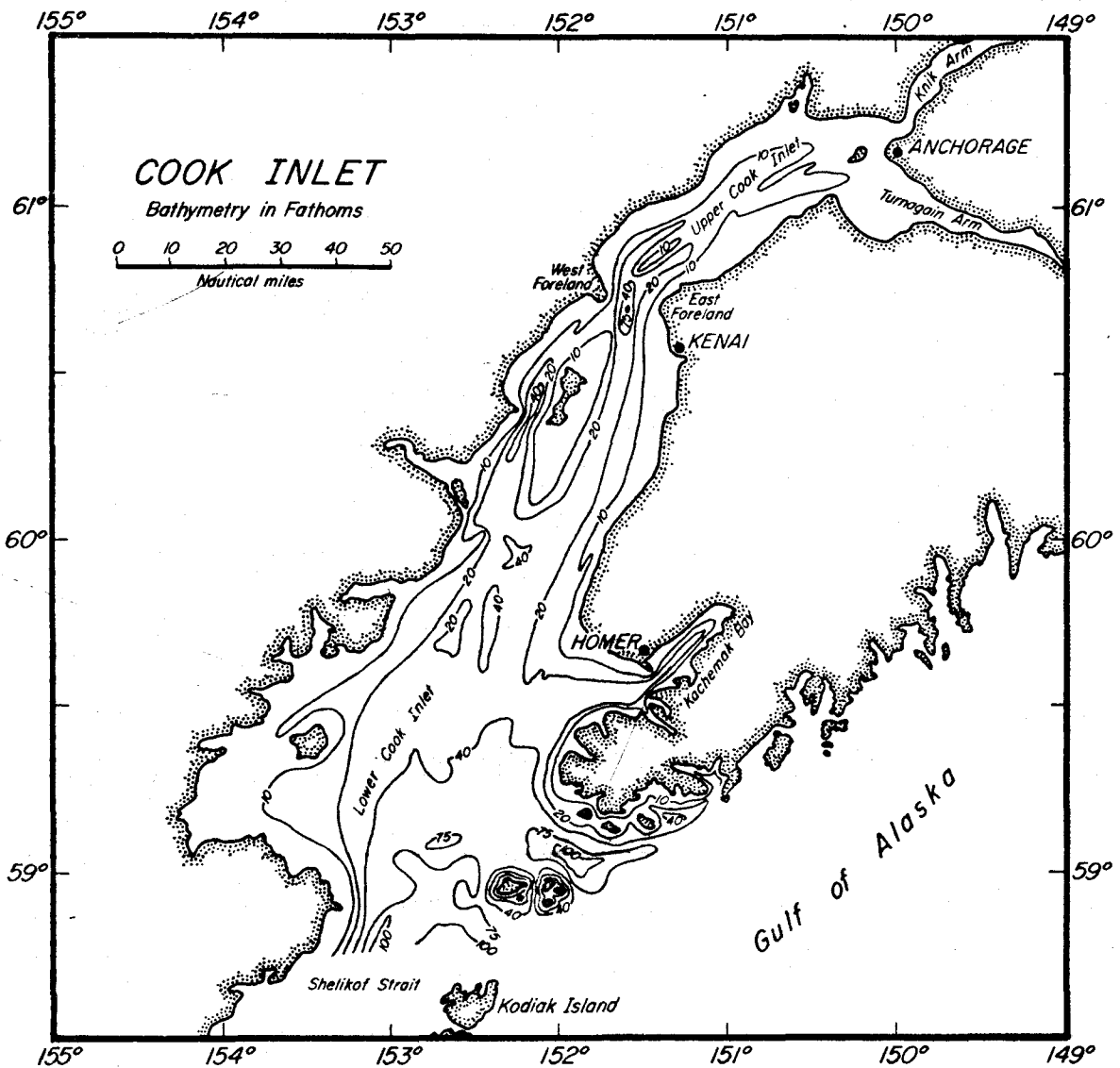
Figure 9.1.   Bathymetry of Cook Inlet, Alaska.

feet, is amongst the world's highest, and currents of over 6 knots can occur between the East and West Forelands. The tides are predominantly semi-diurnal, and between the entrance and Anchorage the M_2 tide component increases its amplitude by a factor of two and undergoes a change in phase of 140° (ie the time of the M_2 tide maximum differs by nearly 5 hours).

The greatest depth within the inlet, approximately 75 fathoms, occurs between the East and West Forelands, where the maximum currents appear to exist. Unfortunately this is also the location of a constriction where the inlet locally narrows to 9 nm. In order to schematize the inlet adequately in this region, it is felt that a grid-spacing of about 1.5 nm should be used. A brief inspection of Figure 9.1 indicates that a rectangular region of some 60 x 200 nm is necessary to contain Cook Inlet for the purpose of modelling. This in turn requires (at a constant grid-spacing of 1.5 nm) some 40 x 130 grid-intervals, or, in terms of core storage, some (8 x 40 x 130) $\approx$ 40,000 words for the storage of arrays alone (the quantity 8 provides for arrays of heights and current components at two time levels, and arrays for depths and Chézy friction factors). The value 40,000 exceeds by about 20% the total available memory of a 128K - 8 bit computer memory (which must contain, in addition to the arrays, the supervisor and the program). On account of this, the first investigation of Cook Inlet (Matthews and Mungall, 1972) had to be restricted to that part of the inlet north of Homer.

The first investigation was aimed at obtaining the approximate distribution of the range and phase of the tide representing mean-range conditions. The results agreed well with values obtained from the Coast

and Geodetic Survey, however it appeared that the model predicted maximum currents (4.2 knots) that were somewhat less than those reported. This was probably due mainly to the inadequate grid resolution between the Forelands, and partly to the lack of convective acceleration terms (the absence of which tend to smooth out spacial variations in the currents).

The application of the model to Cook Inlet

It is in the problem of Cook Inlet that the model first displays its unique advantage of making the best possible use of the available core storage. The grid scheme was selected so as to achieve adequate resolution in the region of the Forelands and in Upper Cook Inlet. The orientation of the grid (see Figure 9.2) was selected as a compromise between the following: the grid lines should be essentially parallel to the main axis of the inlet, and the grid should be such that the part of the inlet lying to the south of Homer could be 'partitioned off' into a region schematized by large grid rectangles. The grid scheme ultimately consisted of 26 x 44 grid intervals, which requires an approximate core storage allocation of (8 x 26 x 44) ≈ 9000 words. This is only 22% of the former requirement, and meant that there was sufficient room in the computer core for the supervisor, program, and arrays. Furthermore, a comparable savings in computer time would also result. With the smallest grid interval being 3 km (along with a depth of 140 m) the guide for selecting the time step came to 80 seconds.
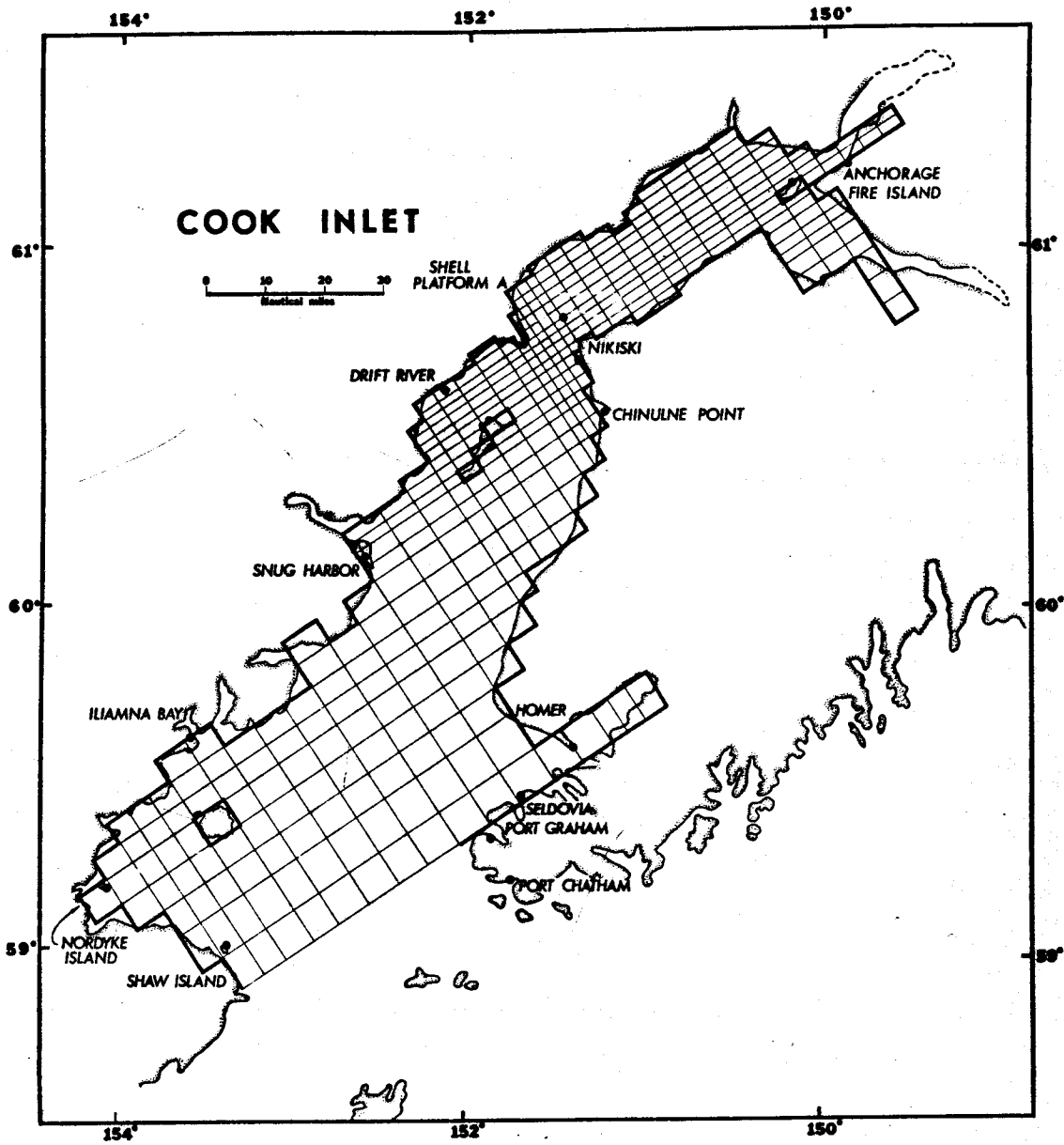
Figure 9.2.   Schematization of Cook Inlet, Alaska.

It was decided that the test should be run with the objective of calculating the M_2 tide distribution as this is the most important of the tidal constituents in the inlet. A summary of the available M_2 constants (obtained through the courtesy of the Coast and Geodetic Survey) is shown in Table 9.1 and in Figure 9.3. The epochs have been adjusted to 150°W for purposes of comparison. (The formula, $K_{150} = K_{local} + 2$ (west longitude - 150), where K is the phase lag, adapted from Schureman (1958, p. 77), was used.) Some difficulty was experienced in estimating the boundary conditions across the entrance owing to the awkward locations of the tide stations, however finally the phase was considered to be a constant 22°, while the amplitude increased linearly from 1.58 to 2.02 meters in the direction Shaw Island to Port Graham. The period of the input was that of the M_2 tide, 12.42 hours.

An initial test was run on the University of Alaska's IBM 360/40 using a time step of 12.42 minutes, some 9 times larger than the value suggested. As was suspected the model behaved poorly, as evidenced by loss of coherency between heights along rows and columns. The predicted amplitudes in the Anchorage area were too low by about 1.25 m. As each computational cycle required some 40 minutes of computer time, it was decided that future tests with a more suitable time step would have to be carried out elsewhere.

On being fortunate enough to receive permission to make use of the computing facilities of the National Center for Atmospheric Research, the tests were recommenced using a time step of approximately 112 seconds (400 intervals per period of 12.42 hours), this value being

Place	North Lat. ° '	West Long. ° '	K °	pΔL °	K^{150°} °	Amplitude ft.	Amplitude m
Anchorage	61 14	149 54	165.3	-0.20	165.1	11.07	3.37
Fire Island	61 10.4	150 12.2	157.9	+0.40	158.3	10.79	3.29
Shell Platform A	60 47.8	151 29.8	105.6	+3.00	108.6	7.51	2.29
Drift River	60 33.5	152 08.4	70.9	+4.26	75.2	7.38	2.25
Snug Harbor	60 06.2	152 34.0	50.6	+5.14	55.7	6.15	1.87
Nikiski	60 41.2	151 23.8	88.4	+2.80	91.2	7.82	2.38
Chinulne Point	60 30.7	151 17.5	76.9	+2.58	79.5	8.23	2.51
Homer	59 36	151 25	23.8	+2.84	26.6	7.50	2.29
Seldovia	59 26.4	151 43	20.8	+3.44	24.2	7.24	2.21
Port Graham	59 21	151 50	18.2	+3.66	21.9	6.76	2.06
Port Chatham	59 12.6	151 43.7	9.4	+3.46	12.9	5.61	1.71
Iliamna Bay	59 37	153 34	23.1	+7.12	30.2	5.70	1.74
Nordyke Island	59 10.7	154 05.2	19.1	+8.18	27.3	5.91	1.80
Shaw Island	59 00.1	153 22.8	19.0	+6.76	25.8	5.43	1.66

Table 9.1. M_2 components for Cook Inlet, Alaska.
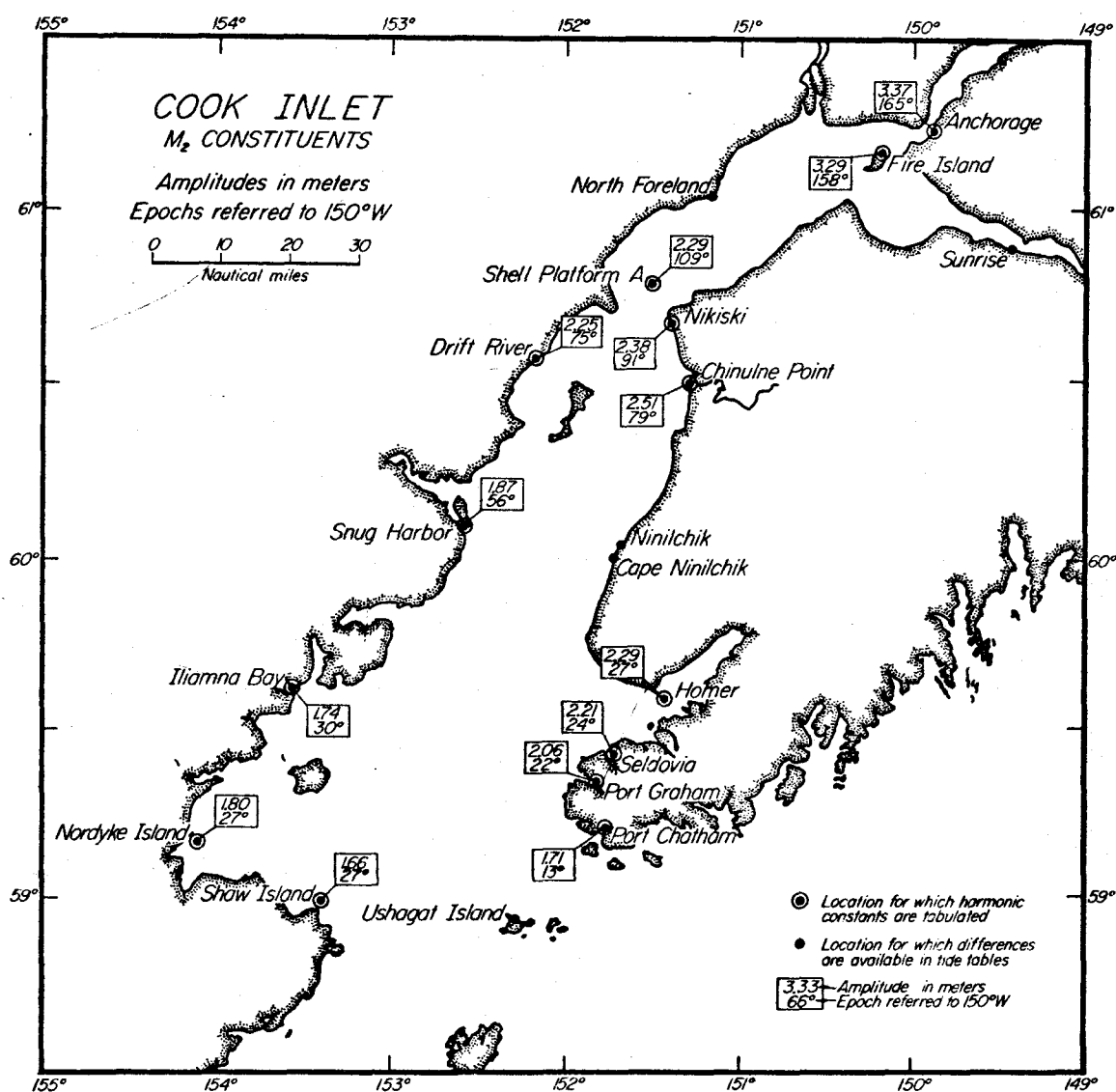
See text for explanation and
acknowledgements.

Figure 9.3.   M$_2$ constituents for Cook Inlet, Alaska.

sufficiently close to the guide value of 80 seconds. The computer time required per tidal cycle (on a CDC 7600) was about 40 seconds, which is to be compared with 140 minutes on the IBM 360/40, a decrease in computer time of a factor of 230.

The MASTER subprogram was slightly modified during these tests so as to put only 40 of the 400 fields of H , U , and V onto tape during the last tidal cycle. This was quite sufficient for the harmonic analysis program that followed. Three computer runs were made, using Chézy values of 80, 70, and 75 $m^{1/2}$ sec^{-1}, with the object of adjusting the amplitude of the tide predicted for Anchorage to that given by the Coast and Geodetic Survey (337 cm). The values obtained were, respectively, 350 cm, and 314 cm and 341 cm. Because the third value agreed within 4 cm it was not considered necessary to continue the tests. It is of interest to note that the phases at Anchorage in the three tests were, respectively, 171°, 170°, and 173°, so that changes in the Chézy value caused, in this inlet, little change in phase. The value given by the Coast and Geodetic Survey is 165°.

The distribution of the M_2 amplitudes and phases that are associated with the Chézy value of 75 $m^{1/2}$ sec^{-1} is shown in Figure 9.4, and a comparison between these values and Coast and Geodetic Survey values may be seen in Table 9.2. It will be seen that the orientation of the lines is essentially similar to that obtained by Matthews and Mungall (1972) and again shows the Kelvin-wave nature of the tide in Lower Cook Inlet. From Table 9.2 one sees that the differences between predicted and observed values are in most areas small; all but one of
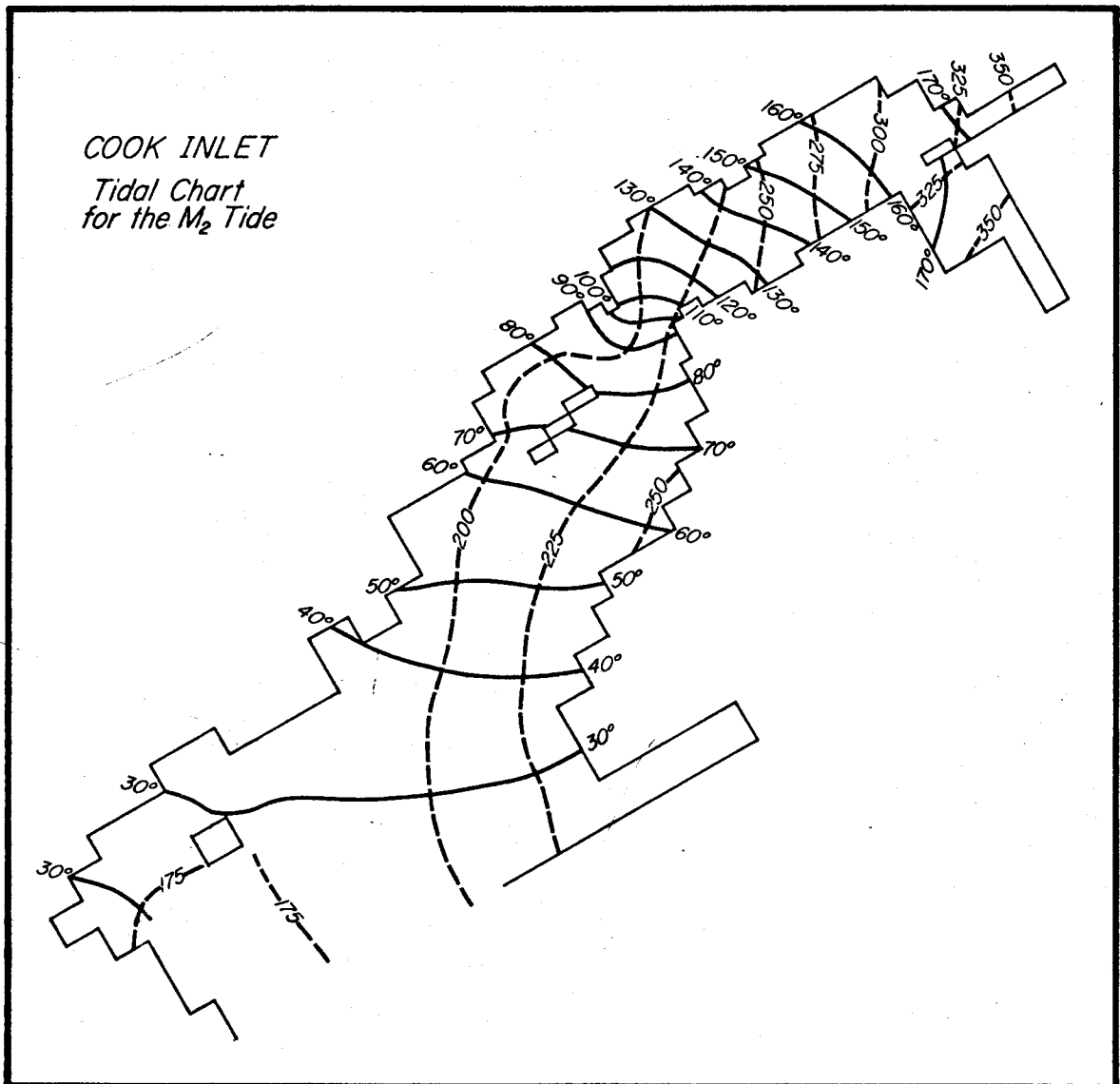
Figure 9.4. Computed M_2 coamplitude lines (in cm) and cophase lines for Cook Inlet, Alaska.

	M$_2$ Amplitude			M$_2$ Phase		
	Tide Constant	Predicted	Predicted-Observed	Tide Constant	Predicted	Predicted-Observed
Anchorage	337	341	+4	165	173	+8
Fire Island	329	317	-12	158	168	+10
Shell Platform A	229	214	-15	109	116	+7
Drift River	225	196	-29	75	77	+2
Snug Harbor	187	194	+7	56	54	-2
Nikiski	238	229	-9	91	89	-2
Chinulne Point	251	242	-9	79	77	-2
Homer	229	238	+9	27	27	0
Seldovia	221	232	+11	24	27	+3
Port Graham	206	214	+8	22	24	+2
Port Chatham		-			-	
Iliamna Bay	174	178	+4	30	30	0
Nordyke Island	180	180	0	27	31	+4
Shaw Island	166	165	-1	26	27	+1

Table 9.2 Comparison between test results and observed values supplied by the United States Coast and Geodetic Survey.

the amplitude differences are less than 16 cm (5% of the greatest amplitude in the inlet). The one predicted amplitude that appears to be seriously in error is that of 196 cm (at Drift River) versus an observed value of 225 cm. This difference, 29 cm, is about 8% of the maximum M_2 amplitude occurring within the inlet. The region in which Drift River is located is somewhat complex, and the error may be due to inadequacy of the schematization. The greatest difference between computed and predicted phases is 10 degrees. Equivalent values for the earlier Cook Inlet model (Matthews and Mungall, 1972) are a maximum height difference of 8% and a maximum phase difference of 13°.

It is felt that the agreement with the observed Coast and Geodetic Survey values is excellent considering the fact that no attempt was made to vary the Chézy values locally, the normal recourse of the modeller when adjustments have to be made. On this account the third series of tests indicate that the unequal grid-spacing method is capable of yielding good results under adverse conditions -- when no other available method could have conveniently done the job.

CHAPTER X

ADDITIONAL RESULTS OF INTEREST

Introduction

The main purpose of this investigation has been the development and testing of a two-dimensional tidal model with unequal grid-spacing, the successful or unsuccessful nature of the tests being determined via consideration of the corange and cophase diagrams that resulted from a harmonic analysis of the tide heights. As mentioned in Chapter VI the programs were set up so that both height and currents would be analyzed, so that in effect a considerable amount of information on the tidal behavior of the areas investigated remains as yet undisclosed. As a result of the visit made to the National Center for Atmospheric Research, 35 mm films were produced of perspective views of the sea surface, and of the current vector and tide height contours, both for every half (lunar) minute throughout a tidal cycle of 12.42 hours. This was done both for the Irish Sea and for Cook Inlet, as these areas had been realistically schematized. Representative frames are shown for both areas, the time interval between them being one lunar hour. The frames have been rephotographed side-by-side in order to indicate the tidal situation in the clearest fashion possible.

Brief description of the film-making process

Before commencing to describe the film-making process it is necessary to point out that it is essential to have the use of a

well maintained optical output device and 35-mm camera system; otherwise registration and jitter problems may produce very poor films. Centers that have the necessary output equipment are thus often not capable of producting high-quality films. A further consideration is that large amounts of computer time are necessary; the film of Cook Inlet (with a final running time of some 5 minutes) required on a CDC 7600 some 50 minutes (on an IBM 360/40 the equivalent time would be of the order of 190 hours). As mentioned later a reduction in time of a factor of 5 could have been achieved at the cost of increased photographic work and with a poorer image.

It was decided that the final film should consist of two cycles of perspective views (in monochrome) and three cycles of current vectors and height contours (in two colors). A reasonable duration of each cycle was considered to be 60 seconds (ie. 1440 frames at a speed of 24 frames/sec). The 2-color section of the film was such that the current vectors were blue, while the remainder (height contours, title, clock, etc.) were in yellow. Each complete frame of the final color film required 2 consecutive B&W 35-mm frames: the first frame contained the future blue lines, the second the future yellow lines. Thus the sequence on the computer is to select a starting time, to compute the height and currents for each grid point using the Fourier components, to compute the locations of the current vectors, and finally to photograph the cathode-ray tube and advance the film. In the next frame the outline of the inlet is drawn, descriptions are written, scales added, a

clock face is drawn to indicate the time, contours of height are drawn, contours are numbered, and the whole is photographed. The frame is then advanced, a new time selected, and the process is repeated throughout the tidal cycle (of 12 lunar hours). As 1440 intervals were required per cycle, the time interval in real time is 0.5 lunar minutes, and 2x1440 (ie. 2880) frames are required per cycle.

One has the option of making one cycle of film on the computer, and duplicating it twice to provide the 3 cycles, or to repeat the process twice over on the computer. On a very fast machine such as the CDC 7600, the recommendation of NCAR was to use the latter option (thus a total of 8640 frames were generated). It is considered good practice to provide a leading and trailing strip of film, and so an extra 50 blank frames were run off at each end.

The production of the 16-mm color film requires, among other things, the presence of a specialist and professional equipment. The first stage is to produce a 35-mm color film from the B&W original. The machine (in the case of a 2-color film) is set to advance the B&W film 2 frames at a time, while at the same time the color film advances by one frame. Thus the above film was produced by first using a blue filter and setting the first frame of the B&W film opposite the first frame of the color film. The machine was then set in motion with the mechanism advancing the frames as above. When this was completed, both films were rewound, a yellow filter was inserted, the second frame of the B&W film was set opposite the first frame of the previously exposed color film, and the process was again repeated. The net result was a

superimposed set of blue and yellow pictures. Finally the 35-mm color film was reduced to 16-mm size.

A simpler process was used to produce 2 cycles of monochromatic perspective views, each cycle consisting of 1440 frames of both B&W 35-mm film and final 16-mm film (yellow being used for clarity). Titles, acknowledgements, etc. were run off in B&W on the computer, this requiring about 15 seconds worth of film per sequence. Once the perspective program had been suitably modified (the 'Hidden Line' program was written by Tom Wright of NCAR), and the vector and contour programs written, the most time consuming task was the devising of a scheme to allocate contour numbers and to ensure that they moved in a smooth fashion. Unfortunately this was not too successfully carried out in the Cook Inlet film (owing to the awkward shape of the inlet and the variable grid-spacing) but was no problem in the Irish Sea film.

Features of the M_2 tide of the Irish Sea

The most important features are assembled together in the corange and cophase diagram that was calculated in test 2 of Chapter VII (with $k = 0.0020$). This is shown again in larger size in Figure 10.1. Another diagram of interest is Figure 10.2, which shows the distribution of current amplitude. Perhaps a better way in which to gain familiarity with the M_2 tide is to look at some of the frames from the film described earlier in this chapter. Frames have been selected at intervals of one lunar hour, and the perspective views are presented side-by-side with the current vector/tide height views (see
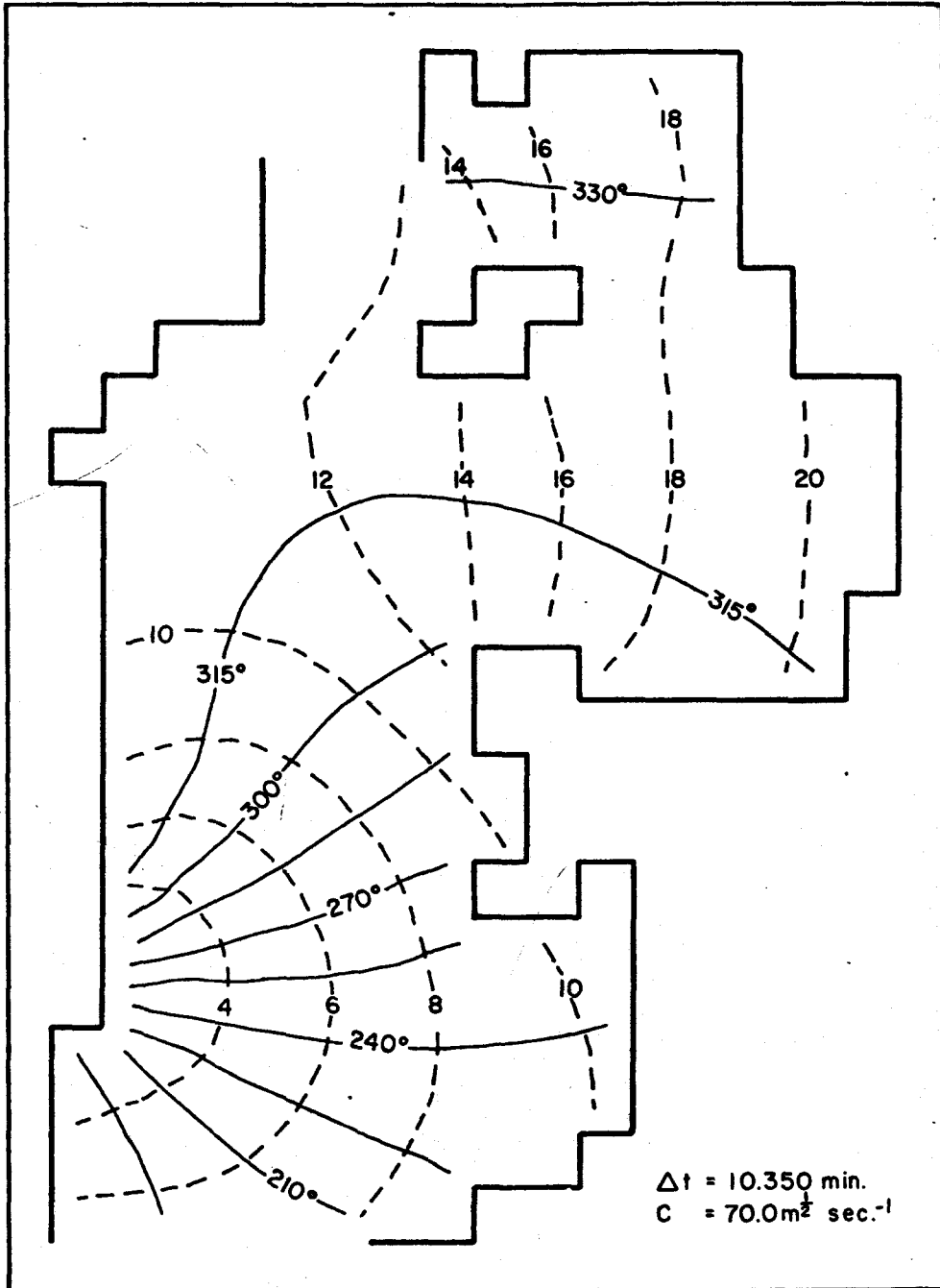
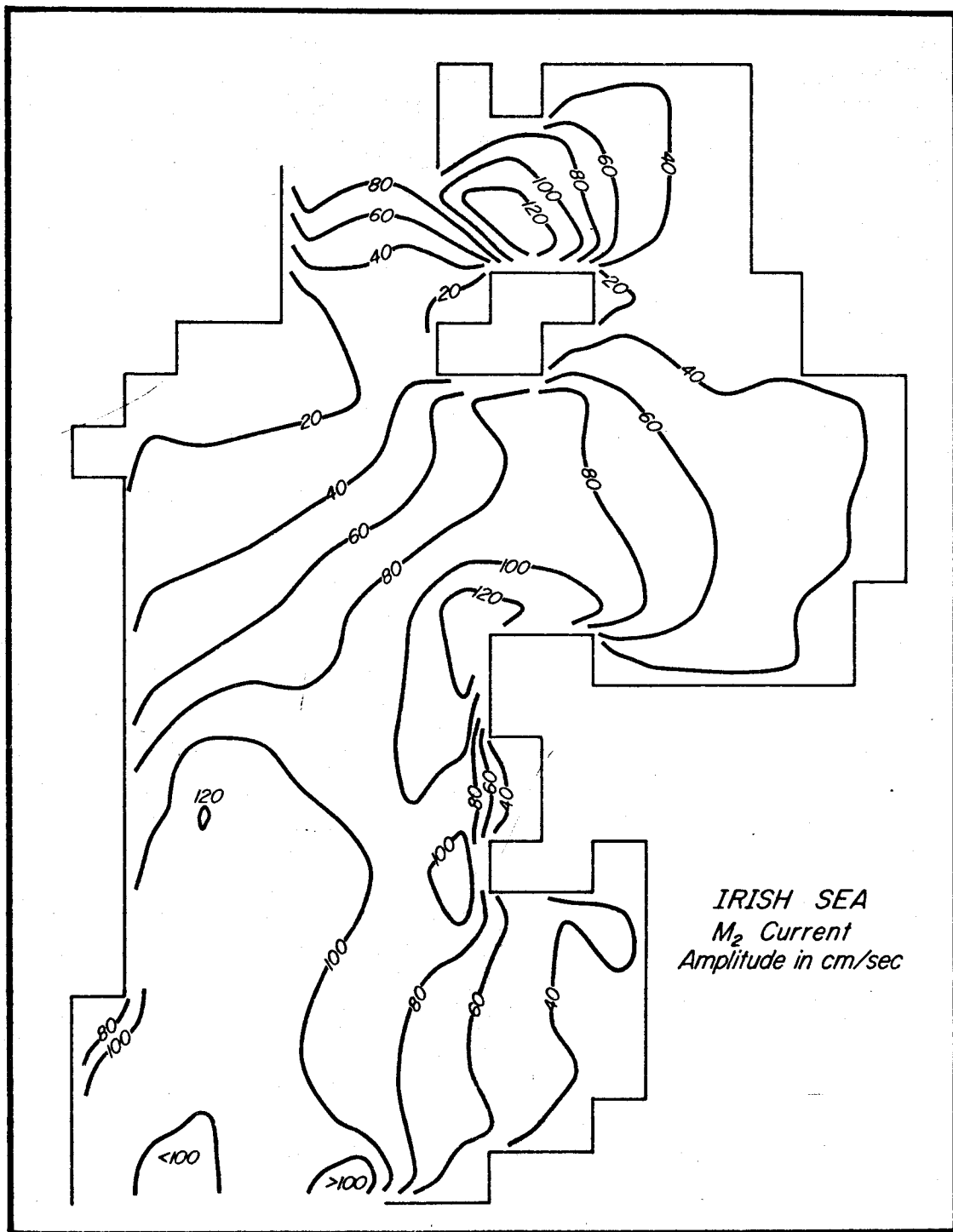Figure 10.1. Computed M_2 corange lines (in feet) and cophase lines for the Irish Sea.

Figure 10.2. Computed M_2 coamplitude lines (in cm/sec) for the currents of the Irish Sea.

Figure 10.3a. M$_2$ tide of the Irish Sea.

LUNAR HOURS
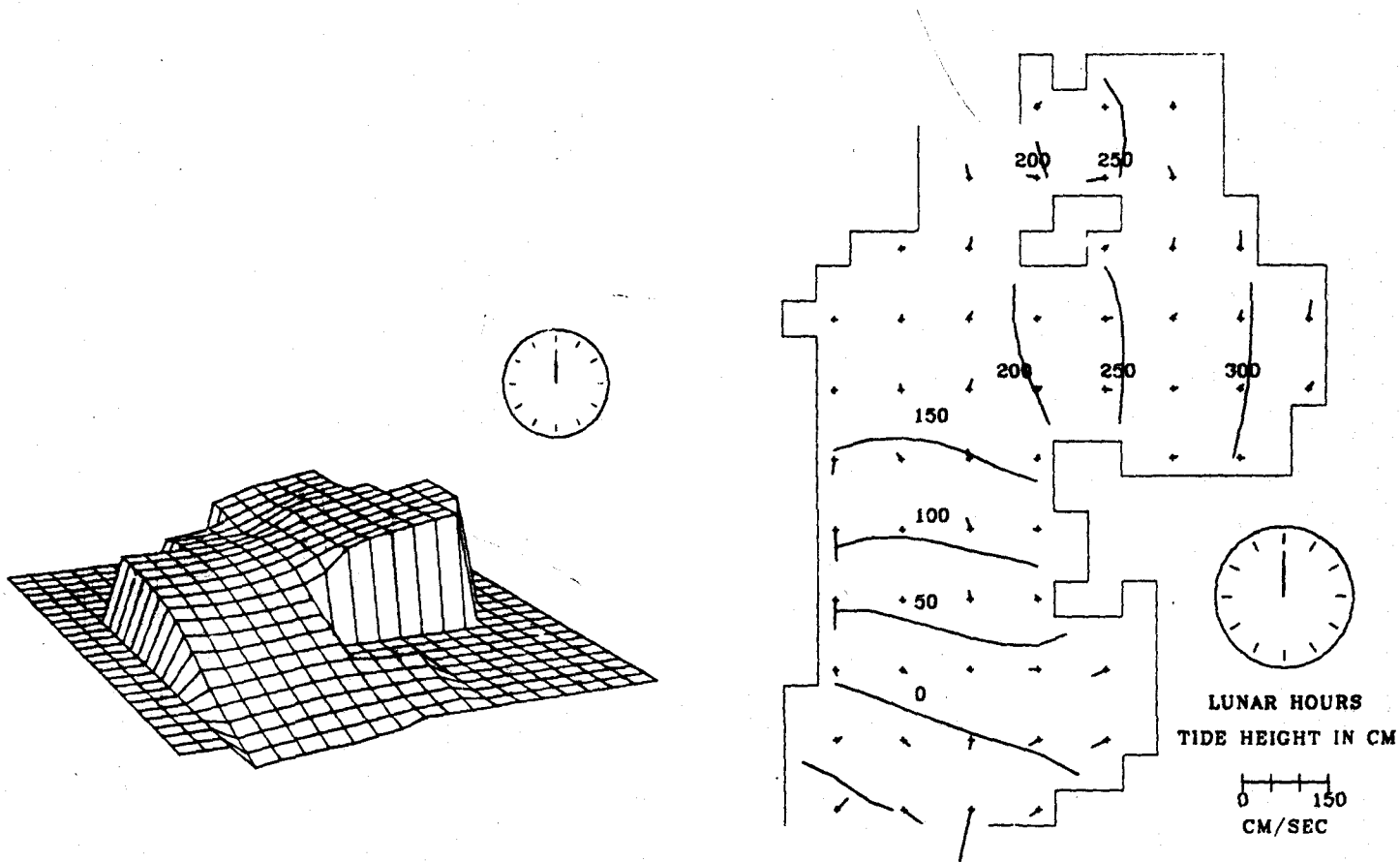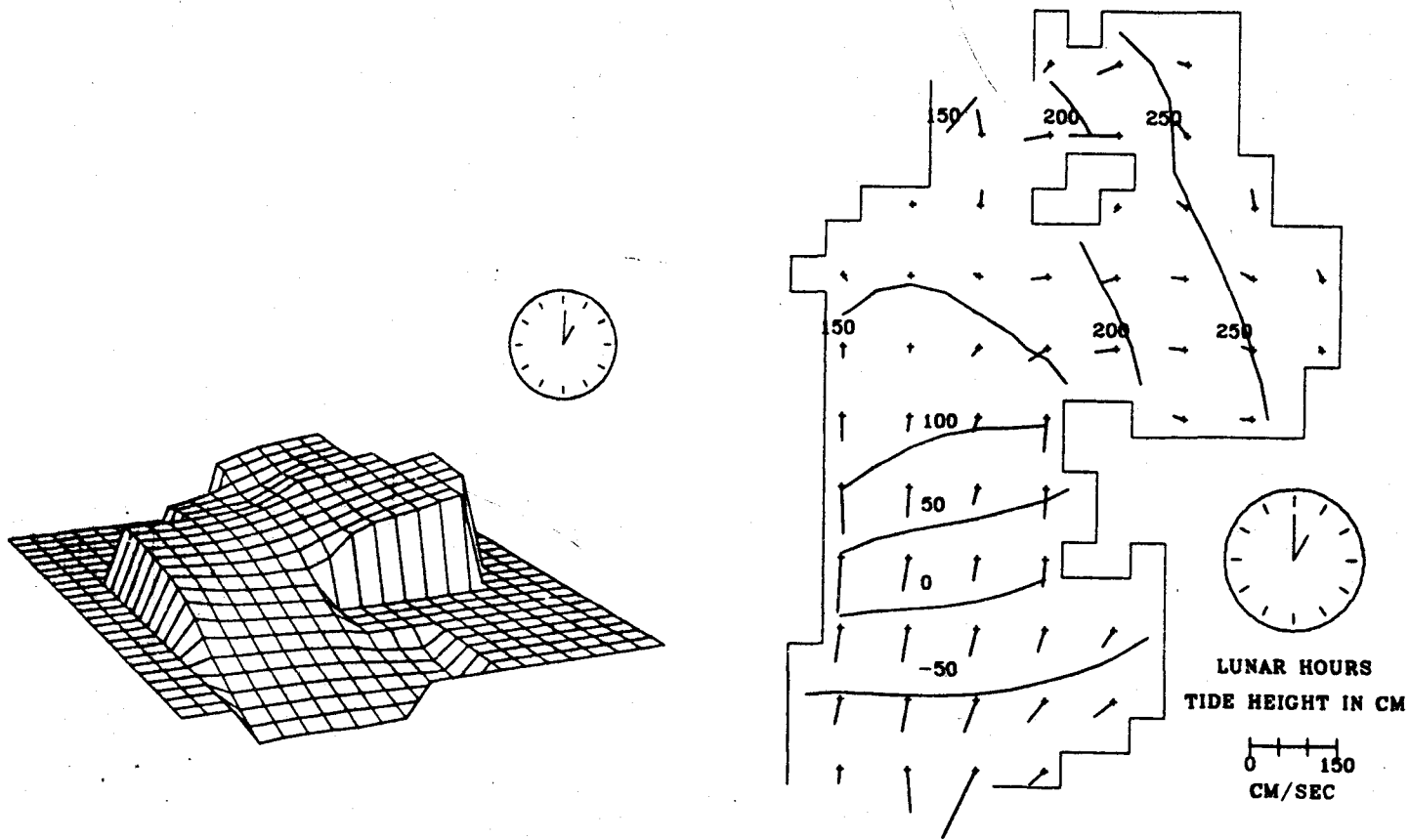TIDE HEIGHT IN CM

0   150
CM/SEC

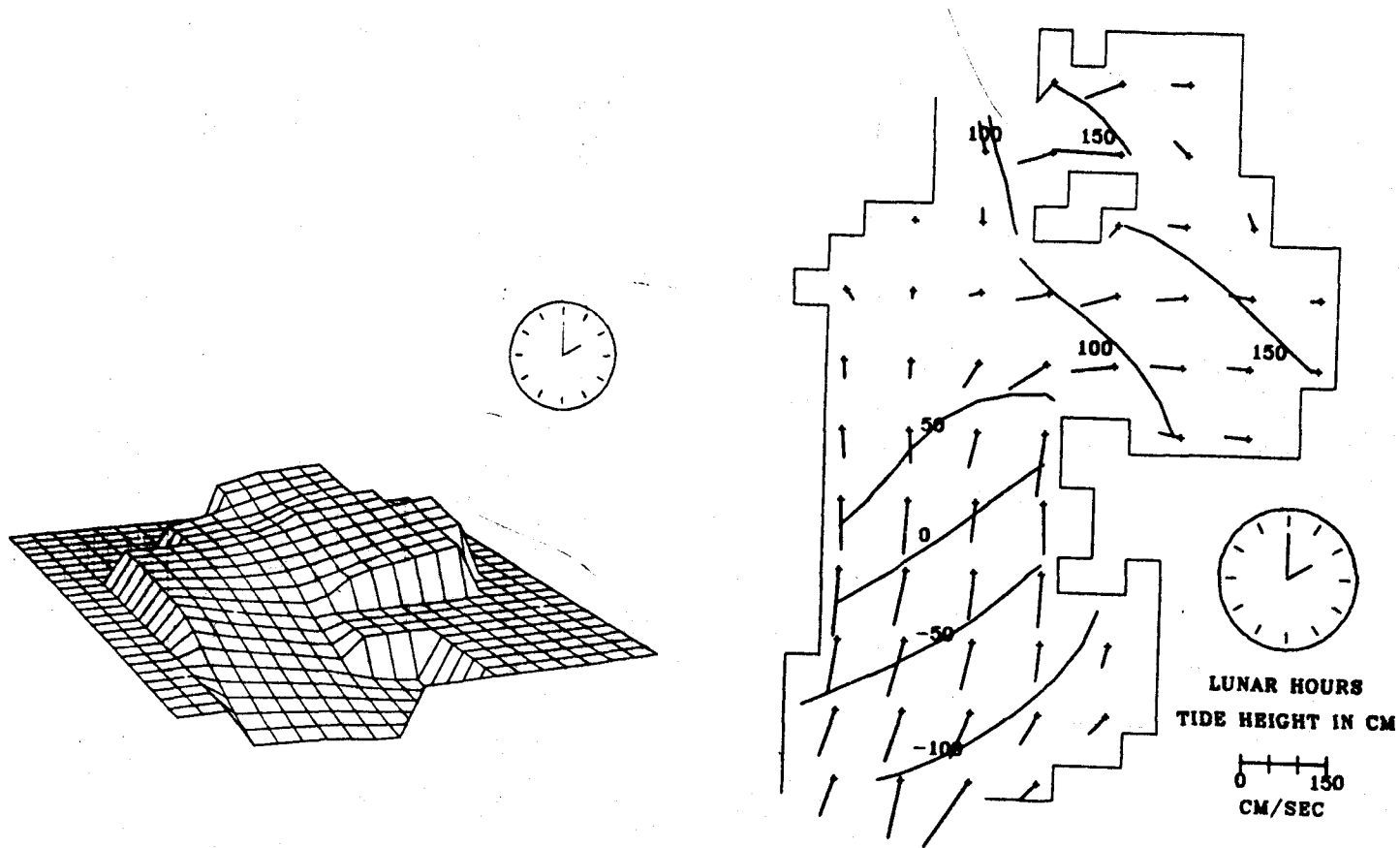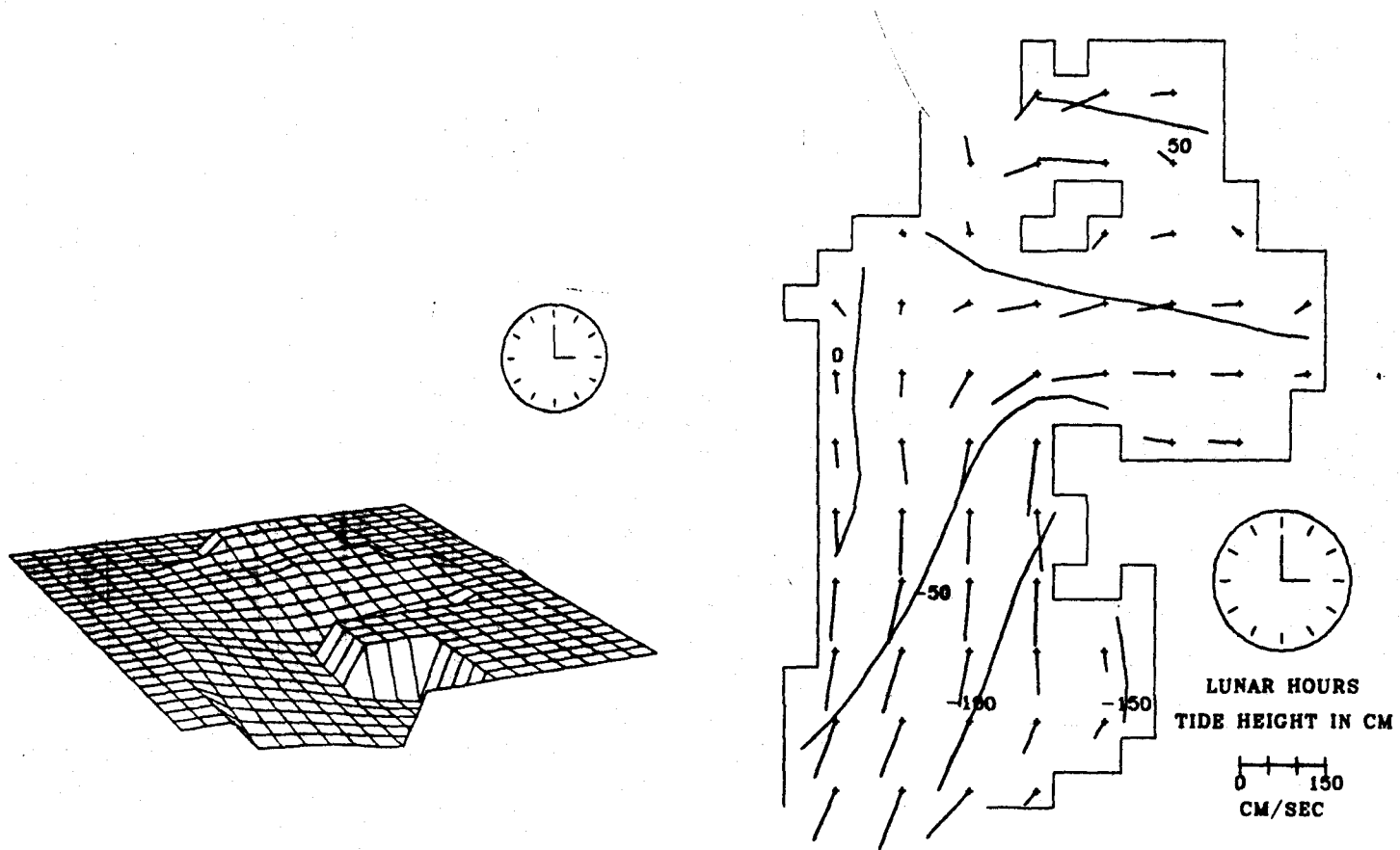Figure 10.3b. M_2 tide of the Irish Sea.

Figure 10.3c. M_2 tide of the Irish Sea.
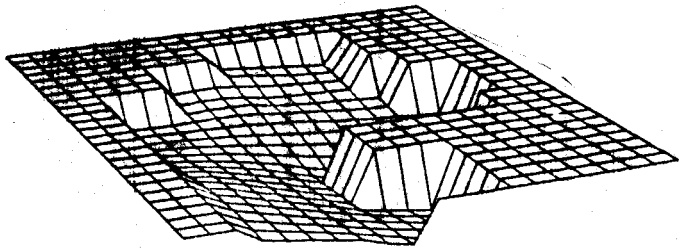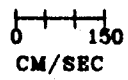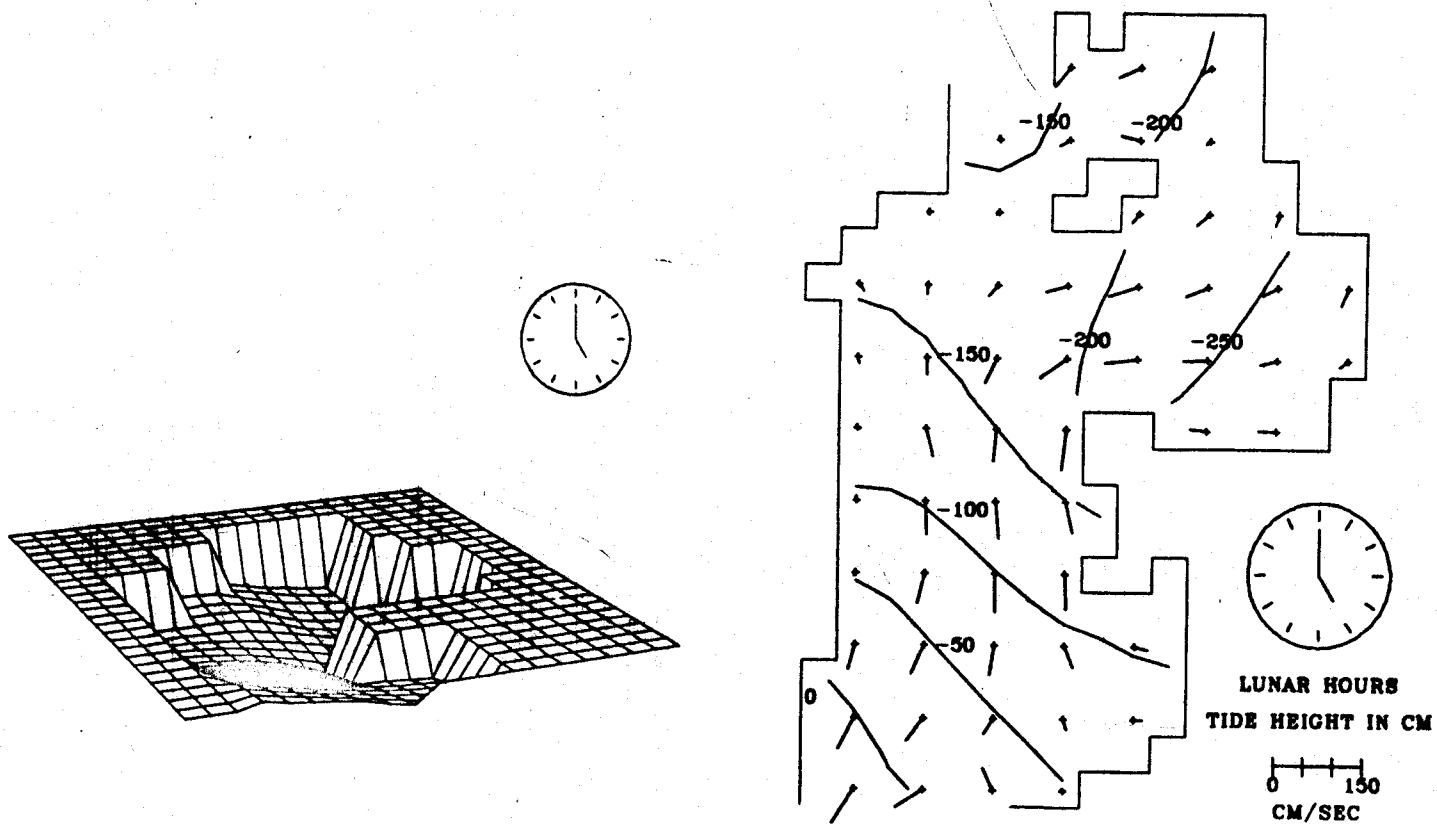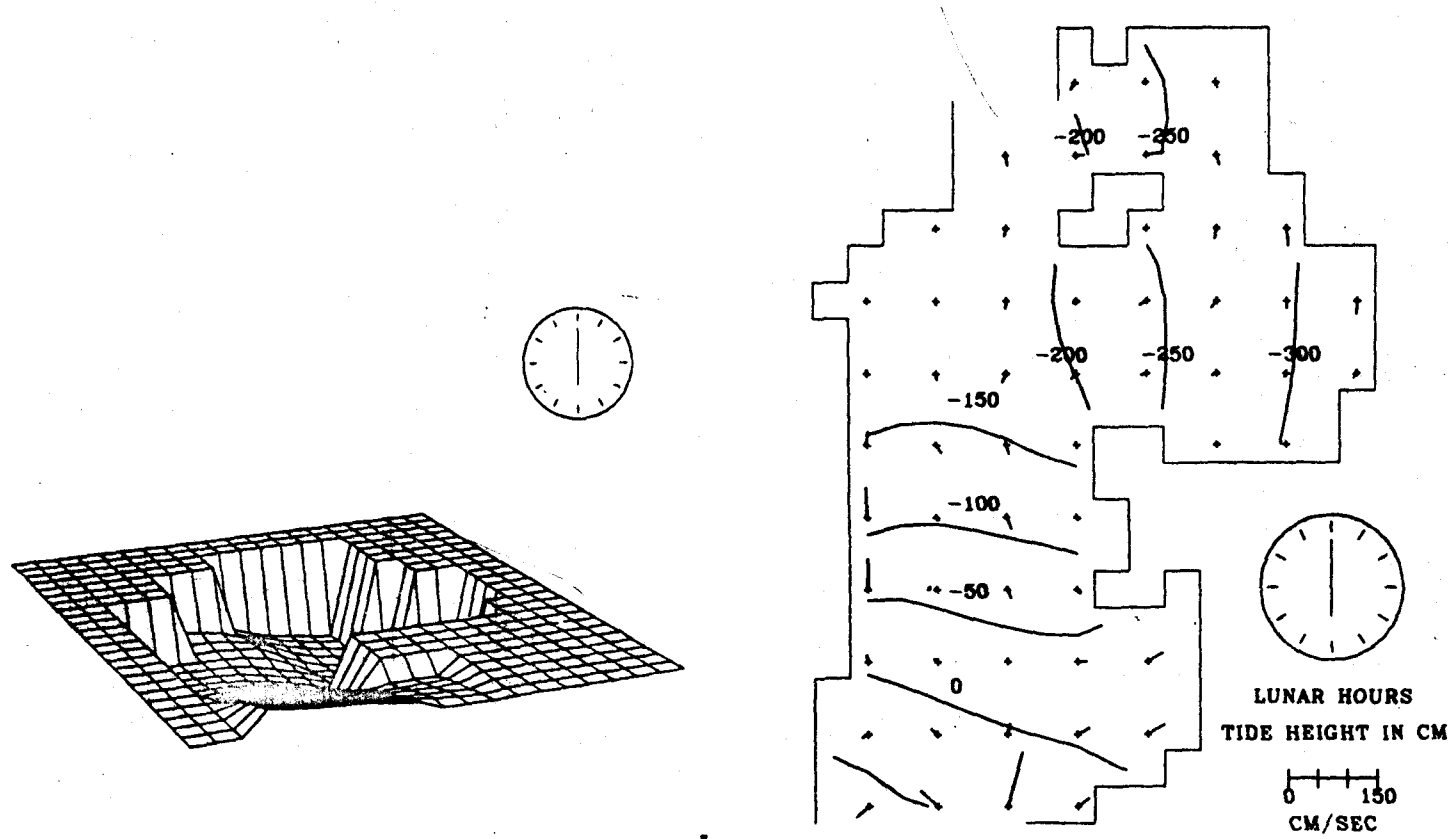
Figure 10.3d. M_2 tide of the Irish Sea.

Figure 10.3e.
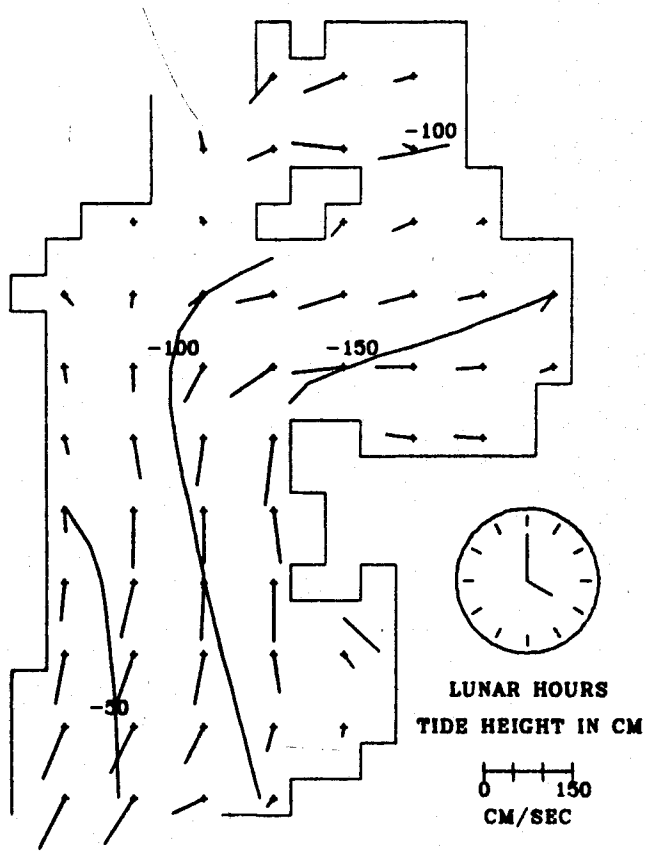
M$_2$ tide of the Irish Sea.

Figure 10.3f. M_2 tide of the Irish Sea.

LUNAR HOURS
TIDE HEIGHT IN CM
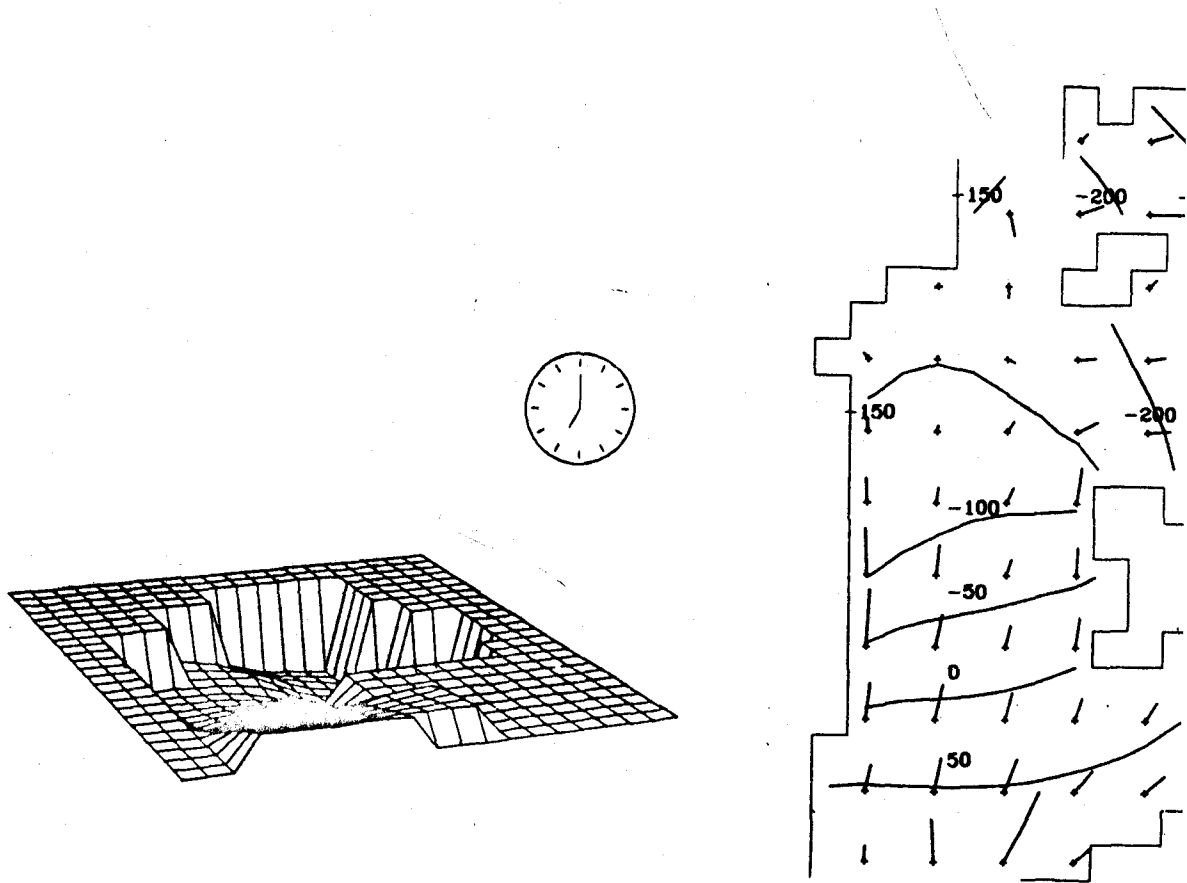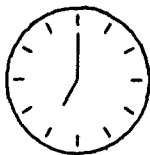
0   150
CM/SEC

Figure 10.3g. M_2 tide of the Irish Sea.

Figure 10.3h. M_2 tide of the Irish Sea.

-250

-250

LUNAR HOURS
TIDE HEIGHT IN CM

0	150

CM/SEC

Figure 10.3i.

LUNAR HOURS

TIDE HEIGHT IN CM

CM/SEC

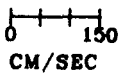M$_2$ tide of the Irish Sea.

Figure 10.3j. M_2 tide of the Irish Sea.

−50
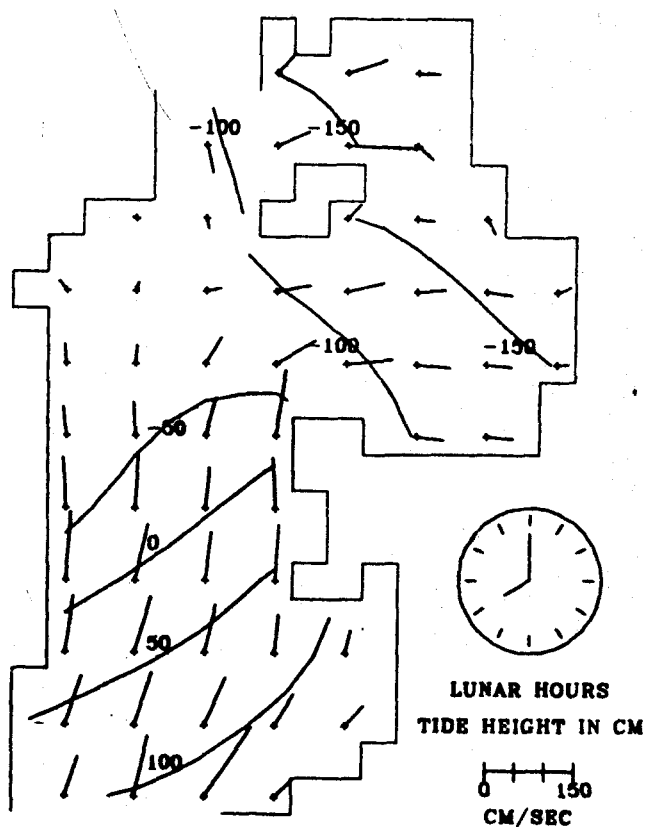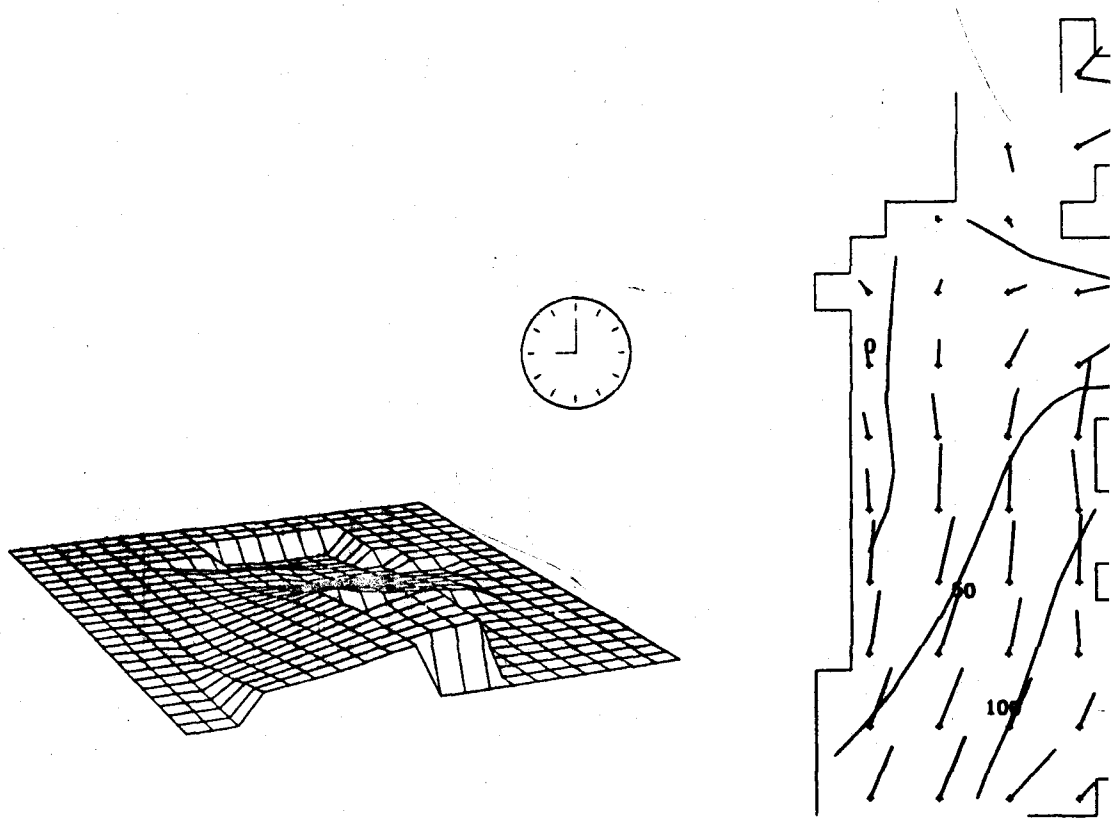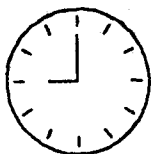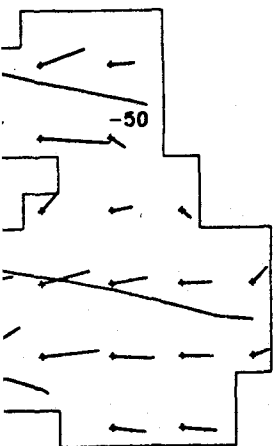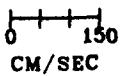
LUNAR HOURS
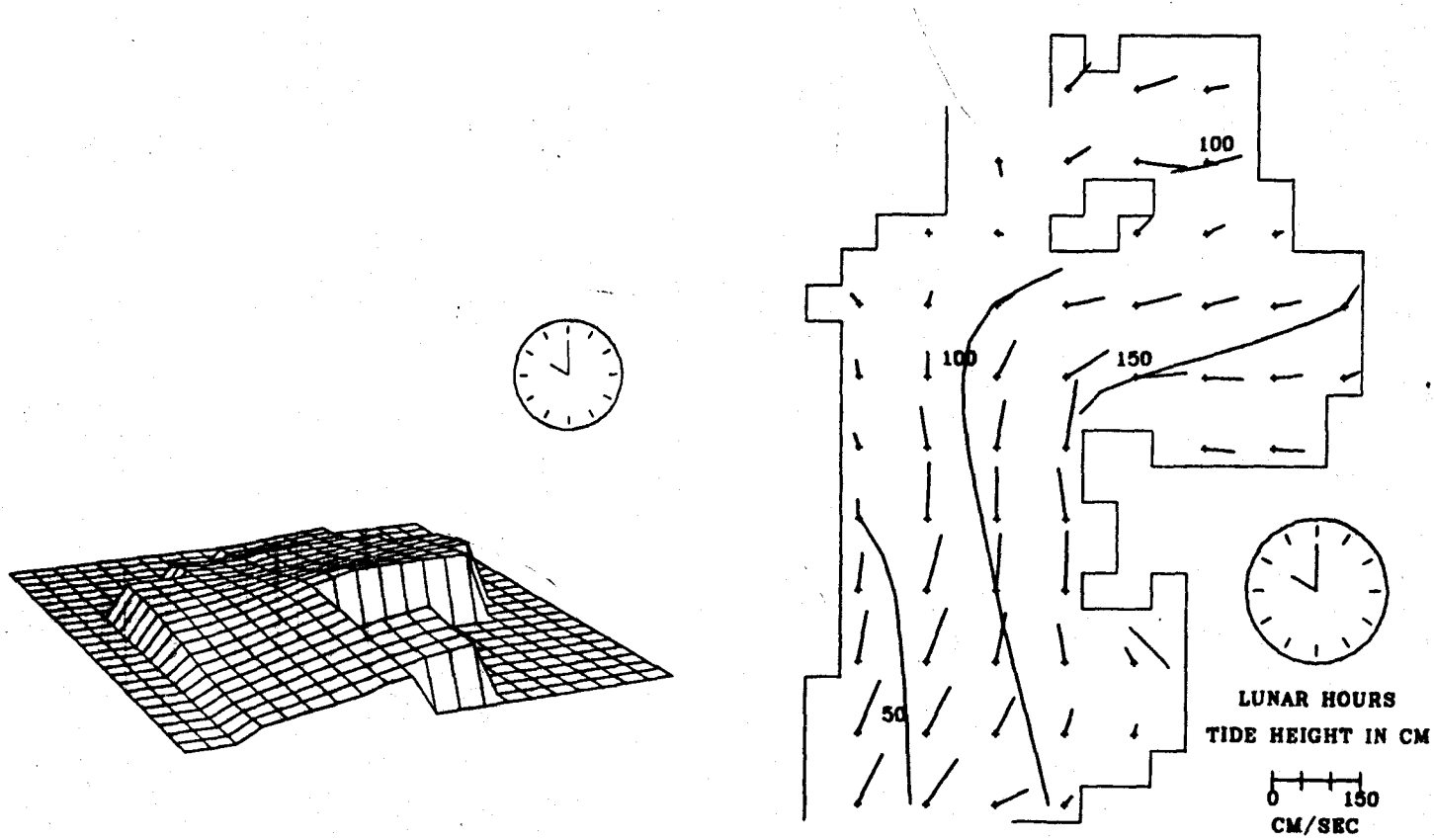TIDE HEIGHT IN CM

0   150
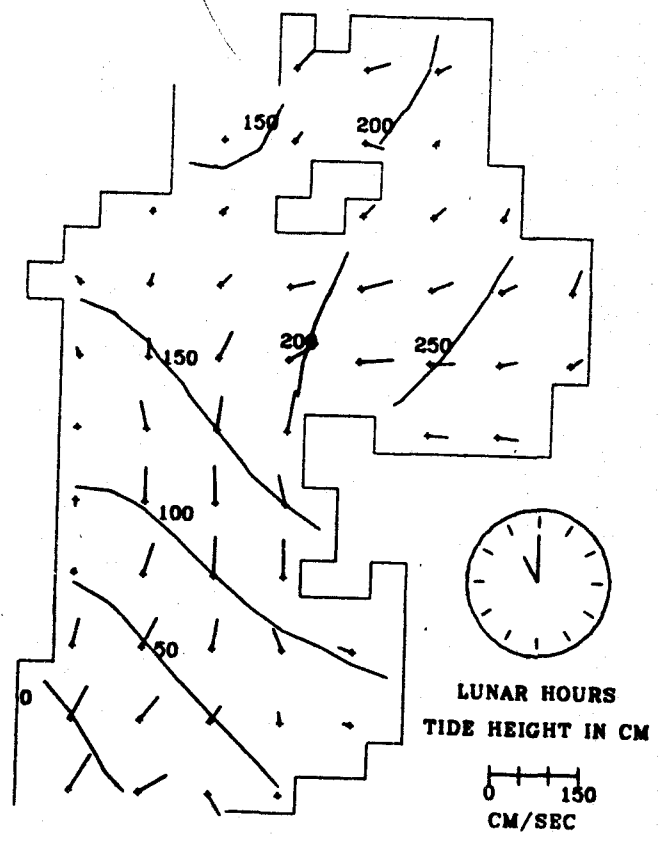CM/SEC

Figure 10.3k. M_2 tide of the Irish Sea.
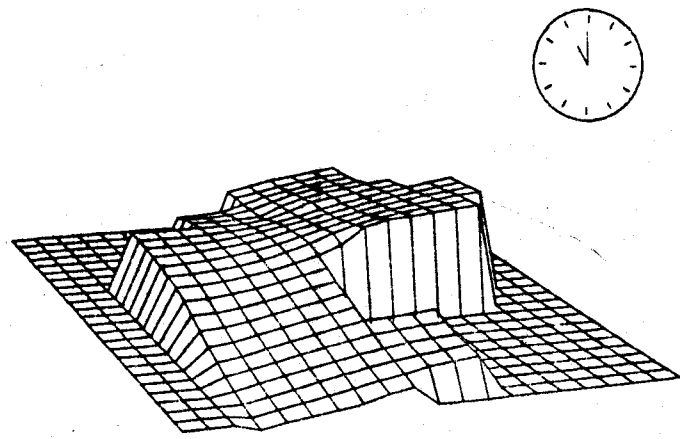
Figure 10.31.   M$_2$ tide of the Irish Sea.

Figures 10.3 a,b, ..., 1). The hands of the clock indicate the time in lunar hours after the occurence of the maximum M_2 tide at Liverpool. It is necessary to point out that during the computation of the perspective views, for reasons of clarity, the borders of the sea were 'straightened', the Isle of Man has been 'removed', and the northern entrance has been 'closed'. The observer is situated to the southwest of the southern entrance to the Irish Sea.

Among other things, the following features are evident (certain numerical values being used from the computer printout, and all times being in lunar hours):

There is a degenerate amphidromic point some 80 km north of the southern entrance in the region of Arklow. The amplitudes on the Irish and Welsh shore are respectively 30 cm and 160 cm.

High water at Liverpool (318 cm) occurs 4 hours after high water in the center of the southern entrance (100 cm), and 15 minutes before high water in the center of the northern entrance (166 cm).

For the most part, the maximum inward currents occur some 3 hours (± 30 minutes) before high water at Liverpool. In the center of the southern entrance the maximum inward (northward) current occurs about 1 hour after local high water, and in the center of the northern entrance the maximum inward (southward) current occurs about 3 hours 40 minutes before local high water.

According to the numerical computations, at the southern entrance maximum inward currents on the eastern side occur some 1 hour 40 minutes before those on the western side. In a similar fashion, at the northern entrance maximum inward currents on the western side occur about 1 hour before those on the eastern side.

Maximum currents are generally of the order of 100 cm/sec, with the highest currents occurring off the coast of northwest Wales (139 cm/sec) and north of the Isle of Man (131 cm/sec). An extensive region of currents of small amplitude exists to the west of the Isle of Man.

On an east-west line passing approximately through the amphidromic region, high water occurs essentially simultaneously (2 hours 30 minutes before high water at Liverpool). Along this line maximum currents occur 30 minutes before high water.

The sea surface along a line running up the center of the sea, from the southern entrance to Liverpool, is essentially horizontal 30 minutes after the times of maximum inward and outward currents (at about 2 hours 30 minutes before, and 3 hours 30 minutes after, high water at Liverpool). In the former case the surface along the central line is approximately 75 cm above mean sea level, and in the latter case it is 75 cm below mean sea level.

Explanation of the M_2 tide of the Irish Sea

Some of the features of the M_2 tide of the Irish Sea are so striking that it was thought it would be of interest to attempt an

explanation that would extend slightly beyond that of Proudman (1953). Proudman explained the position of the amphidromic region as being the consequence of two features: 1) the tendency of the tide to behave as if there were two channels from the entrances, each following the direction of the maximum inward current vectors (ie. passing on either side of the Isle of Man), and 2) the wavelength of a standing wave of period 12.42 solar hours in association with a mean depth of 60 m. Furthermore Proudman ascertained that friction is responsible both for the degeneration of the amphidromic point (shifting it from the center of the channel to beyond the coast of Eire), and for the difference between the time of high water at Arklow and Liverpool of some 3 hours and 30 minutes.

The description that follows is based, as was Proudman's, on the solution of the differential equations for the tides in an inlet of constant width and depth, closed at one end. The solution presented here however contains expressions that depend on the linearized friction term. Inevitably the process loses the incisive clarity of Proudman's compact explanation -- however it permits one to see in mathematical form the variation of height and current with time and distance along the center of the inlet. Furthermore a slight addition enables one to estimate the variation of the vertical tide amplitude and phase along both shores, thus describing more fully the M_2 tide of the region.

The approach is to return to the harmonic method described in Chapter II, and to consider the case of a single section having at

its right-hand end (at x=0) a zero flow rate and a specified tide. The effect of time-variation of cross-sectional area and hydraulic radius is neglected. The final results obtained are the same as those of Hunt (1964), although they are expressed in a different fashion and different conclusions are drawn.

Putting $Q(o)=0$ in equations (2.29) and (2.30), we have

$$H(x) = L \, H(o) \tag{10.1}$$

$$Q(x) = N \, H(o), \tag{10.2}$$

where, with the above simplifications (a now referring to mean depth),

$$L = \cosh(kx) \tag{10.3}$$

$$N = -\frac{i\omega b}{k} \sinh(kx) \tag{10.4}$$

$$k^2 = -\omega^2 bM + i\omega bR \tag{10.5}$$

$$M = \frac{1}{gA} \tag{10.6}$$

$$R = \frac{8}{3\pi} \frac{|\hat{q}|}{C^2 A^3 a}. \tag{10.7}$$

Using current ($u = Q/ba$) instead of Q, and putting $K = g/C^2$, we obtain, instead of equations (10.6) and (10.7), the following:

$$Mb = \frac{1}{ga} \tag{10.8}$$

$$Rb = \frac{f}{ga}, \tag{10.9}$$

where

$$f = \frac{8 \, K \, |\hat{u}|}{3\pi a}. \tag{10.10}$$

Putting $k = \beta + i\alpha$ in equation (10.5), where α and β are new variables corresponding to those used by Hunt (and thus should not be confused with their earlier use as phases), and using equations (10.5), (10.8) and (10.9), we obtain

$$\beta^2 = \frac{\omega\sqrt{\omega^2 + f^2} - \omega^2}{2ga} \qquad (10.11)$$

$$\alpha^2 = \frac{\omega\sqrt{\omega^2 + f^2} + \omega^2}{2ga} . \qquad (10.12)$$

Remembering that $\omega = 2\pi/(\text{Period})$, one usually finds that f is of the order of $\omega/5$ for the M_2 tide. This permits a convenient approximation to be found for α and β:

$$\beta \simeq \frac{f}{2\sqrt{ga}} \qquad (10.13)$$

$$\alpha \simeq \frac{\omega}{\sqrt{ga}} . \qquad (10.14)$$

A considerable amount of manipulation is required before the solution results:

$$h = h_0\left\{\cos^2(\alpha x) + \sinh^2(\beta x)\right\}^{1/2} \cos\left\{\omega t + \tan^{-1}(\tan\alpha x \, \tanh\beta x)\right\} \qquad (10.15)$$

$$u = U\left\{\sin^2(\alpha x) + \sinh^2(\beta x)\right\}^{1/2} \cos\left\{\omega t + \frac{\pi}{2} + \theta - \tan^{-1}(\tanh\beta x/\tan\alpha x)\right\} \qquad (10.16)$$

where

$$\theta = \tan^{-1}(\beta/\alpha) \qquad (10.17)$$

$$U = \frac{h_o\,\omega}{a\,\sqrt{(\alpha^2 + \beta^2)}} \quad , \tag{10.18}$$

and h_o is the amplitude of the tide at the closed end of the inlet. In equation (10.16) the current u is now the _inward_ (flood) current, ie. it is positive in the direction of decreasing x ; this facilitates the discussion that follows.

Having arrived at expressions similar to equations (10.15) and (10.16), Hunt goes on to make a simplification that is somewhat misleading for the purposes of this discussion; this is because Hunt was aiming his results at a discussion of the tides in the Thames, where throughout most of its length the current is $\pi/2$ radians out of phase with the height. This is not the case with the Irish Sea.

For the Irish Sea, using the following,

depth   a = 60 m

max average current $|\hat{u}|$ = 1.0 m sec^{-1}

friction   K = 0.0035

period   T = 12.42 hours

boundary height h_o = 3.0 m

we obtain

β = 1.005 x 10^{-4} m^{-1}

α = 5.879 x 10^{-4} m^{-1}

θ = 9.7 degrees

A preparatory inspection of equations (10.15) and (10.16), using the value (αx) = $\pi/2$ (which takes us near to but not exactly to, the

amphidromic region) results in the following observations: 1) the amplitude of the tide near the amphidromic region is non-zero and of the order of 85 cm, and 2) although a phase difference of over $\pi/2$ exists between the tide height constituent at the closed end and the amphidromic region, the corresponding difference in the phase of the current constituents is only 10 degrees.

Additional generalizations follow from the formula used by Taylor (1919) and Proudman (1953) in the investigation of the transport of energy in one tidal cycle through the southern entrance of the Irish Sea. The result, for any section, is

$$E = \frac{1}{2} g\rho T \int_A \hat{h} \, \hat{u} \, \cos(\delta) dA \qquad (10.19)$$

where δ is the lag of the maximum inward current ($\hat{u}$, normal to the section) over maximum tide height. One can at once see that, in order to make up for the energy lost to friction within the inlet, 1) the mean amplitude across any section other than the closed end cannot be zero, and 2) the angle δ on any section other than the closed end cannot be $\pi/2$, $3\pi/2$, etc.

Before the above solutions for the center of the channel are evaluated as a function of distance, the effect of coriolis force on the phase and amplitude of the tide height along the shores must be considered.

Assume the height and flood current along the inlet to be

$$h = \hat{h} \cos(\omega t - \phi) \qquad (10.20)$$

$$u = \hat{u} \cos(\omega t - \psi) \quad , \tag{10.21}$$

where $\hat{h}$, $\hat{u}$, ϕ, and ψ can be obtained at once from equations (10.15) and (10.16). Considering the change in sea level across the inlet that results from coriolis force to be

$$\Delta h = \frac{2\Omega \sin(\text{Latitude})}{g} b u \quad , \tag{10.22}$$

or

$$\Delta h = 2 A u \tag{10.23}$$

where

$$\Omega = 2\pi/24.0 \text{ hours}^{-1}$$

and

$$A = \frac{\Omega \sin(\text{Latitude}) b}{g} \quad , \tag{10.24}$$

we have for the tide on the sides of the inlet,

$$h \left\{ \begin{matrix} \text{left} \\ \text{right} \end{matrix} \right\} = \hat{h} \cos(\omega t - \phi) \begin{smallmatrix} - \\ + \end{smallmatrix} A \hat{u} \cos(\omega t - \psi) \quad . \tag{10.25a,b}$$

The time of maximum or minimum height is found by evaluating $dh/dt = 0$. The result may be expressed as

$$\omega t \left\{ \begin{matrix} \text{left} \\ \text{right} \end{matrix} \right\} = \tan^{-1} \left\{ \frac{\hat{h} \sin\phi \begin{smallmatrix} - \\ + \end{smallmatrix} A \hat{u} \sin\psi}{\hat{h} \cos\phi \begin{smallmatrix} - \\ + \end{smallmatrix} A \hat{u} \cos\psi} \right\} \quad . \tag{10.26a,b}$$

Making comments on the behavior of ωt for different situations is complicated by the number of variables in equations (10.26a,b), and it seems that each case will have to be separately investigated. The only obvious result is that, given the situation of the possibility of an amphidromic region, it will be degenerate (no point of zero

tide amplitude across the inlet) if $\hat{h} > A\hat{u}$. Finally one can substitute the value of (ωt) associated with the maximum back into equations (10.25a,b) to obtain the distribution of the tide height constituents with length.

Assuming a width of 100 km and a latitude of 53.5°N one obtains the constituent distribution with distance (0 km at Liverpool, ~300 km near the southern entrance) for the left-hand side (Eire), the center, and the right hand side of the Irish Sea (see Table 10.1). In addition to previously described features one should note how well this simple approach provides the main features of the two-dimensional results. This applies particularly to the low amplitudes on the left, and the considerable differences between the phases across the channel: those on the left are within 30° until the amphidromic region is approached, and those on the right change in a more linear fashion. The cosinusoidal rate of change along the center is roughly a mean between the values along the shore.

A final simple evaluation that can be made is to compute the energy E transported through the entrances. Using equation (10.19) and being careful to use the inward normal currents, and taking the section width as 13.89 km and the density ρ as 1.026, one arrives at the values shown in Tables 10.2 and 10.3. Thus over a complete tidal cycle, considering the M_2 tide, 346.3×10^3 Megawatt-hours are transmitted into the Irish Sea from the south, and 79.2×10^3 Megawatt-hours are transmitted out of the Irish Sea through the northern entrance. Thus the difference, divided by 12.42, represents the mean rate at which energy is absorbed by friction over a tidal cycle. This quantity

x	$\hat{h}_1$	$\hat{h}_c$	$\hat{h}_r$	ϕ_1	ϕ_c	ϕ_r	$\hat{u}$	ψ
km	cm	cm	cm	degrees	degrees	degrees	cm/sec	degrees
0	318	318	318	318.0	318.0	318.0	0	228.0
25	315	315	315	319.8	317.8	315.8	19	227.9
50	305	305	306	321.2	317.1	313.0	37	227.7
75	290	289	291	322.4	316.0	309.6	54	227.4
100	268	267	272	323.2	314.2	305.3	70	226.8
125	241	239	249	323.7	311.5	299.8	85	226.2
150	208	208	223	323.9	307.7	292.6	98	225.3
175	172	173	198	323.6	301.9	283.1	109	224.3
200	131	138	176	322.6	292.5	270.5	118	223.3
225	89	107	161	320.1	276.7	254.5	124	221.5
250	44	87	158	311.8	250.4	236.1	128	219.7
275	13	90	167	222.8	218.3	218.0	130	217.6
300	51	115	188	162.3	194.3	202.6	128	215.0

Table 10.1 Variation of constituents with distance from Liverpool.

Section	1	2	3	4	5	6	units
$\hat{h}$	98	99	99	102	109	117	cm
$\hat{u}$	104	88	88	105	107	120	cm/sec
ϕ	181	190	198	202	206	210	degrees
ψ_n	241	242	238	216	201	182	degrees
$\delta = \psi_n - \phi$	60	52	40	14	-5	-28	degrees
a	49	83	95	95	80	60	m
E/12.42	1.74	3.11	4.43	6.90	6.50	5.20	1000 Megawatts

Table 10.2. Distribution of various quantities along line of grid rectangles at southern entrance.

Section	1	2	3	units
$\hat{h}$	157	166	178	cm
$\hat{u}$	96	65	49	cm/sec
ϕ	323	326	329	degrees
ψ_n	18	34	51	degrees
ψ_s	198	214	231	degrees
$\delta = \psi_s - \phi$	-125	-112	-98	degrees
a	33	121	114	m
E/12.42	-1.99	-3.42	-0.97	1000 Megawatts

Table 10.3. Distribution of various quantities along line of rectangles at northern entrance.

comes to 21.5×10^3 Megawatts and is only one third of that predicted by Taylor (1919), although Taylor's value was for a spring tide.

To summarize the previous pieces of information, it is clear that most of the features of the Irish Sea can be explained by applying the effects of friction and coriolis force to the one-dimensional case of an inlet of constant width and depth. This can only be done after it has been ascertained that the tide behaves as a pair of channels divided by the Isle of Man. The tide in the southern channel behaves mostly as a wave, which, near the entrance has some features of a progressive wave travelling up the inlet, and near Liverpool behaves as a standing wave. It is not theoretically correct to regard the northern channel as one that terminates in a closed end, since it transmits energy out of the sea. If this transmission of energy is arbitrarily set to zero, then conditions in the northern channel are those of a pure standing wave.

Features of the M_2 tide of Cook Inlet, Alaska

The essential features of the M_2 tide of Cook Inlet were shown in the amplitude and cophase diagrams (Figure 9.4). Figures 10.4a and 10.4b contain additional information of interest, the former showing the distribution of the M_2 current amplitudes and the latter showing the lead of the maximum inward currents in lunar hours over the time of high tide at Anchorage. Hourly views of the sea surface and associated tide height contours and current vectors are shown in Figure 10.5a-1. Owing to the complexity of the region it is difficult
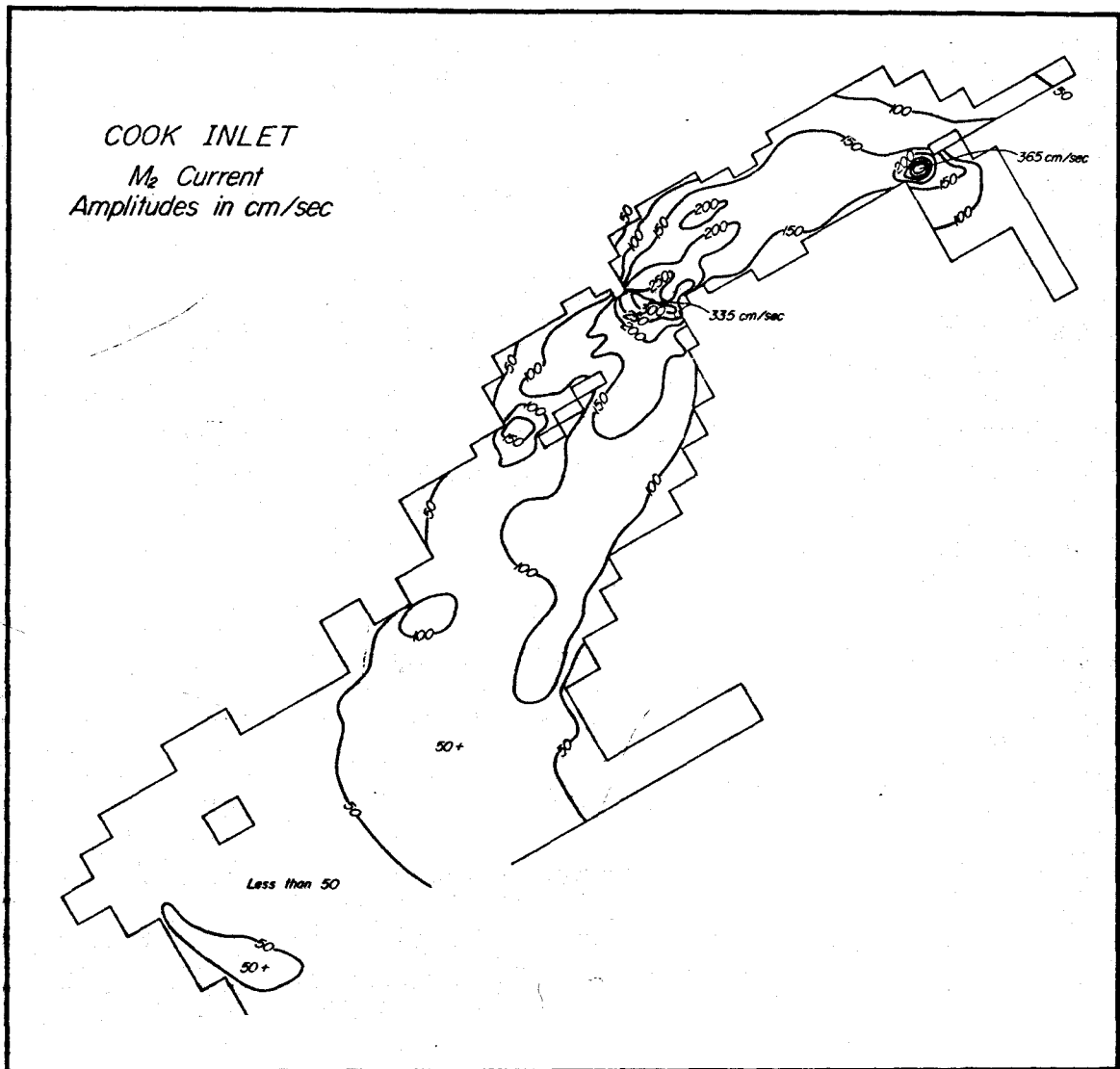
Figure 10.4a.   Computed M_2 coamplitude lines (in cm/sec) for the currents of Cook Inlet, Alaska.

COOK INLET

M_2 Current

Lead in lunar hours of
maximum inward current
over time of high water
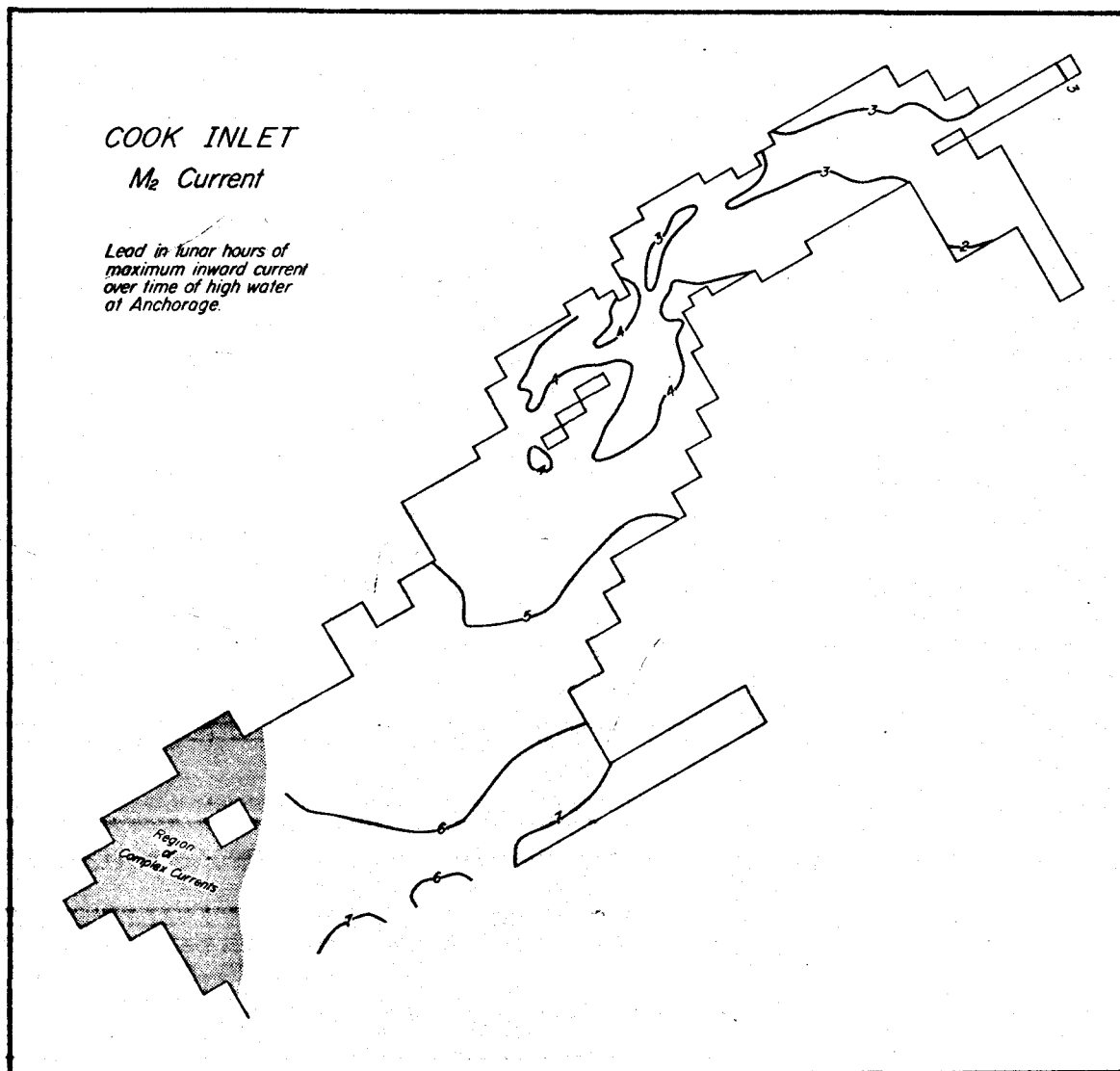at Anchorage.

Region
of
Complex Currents

Figure 10.4b.   Computed lead in lunar hours of the maximum inward
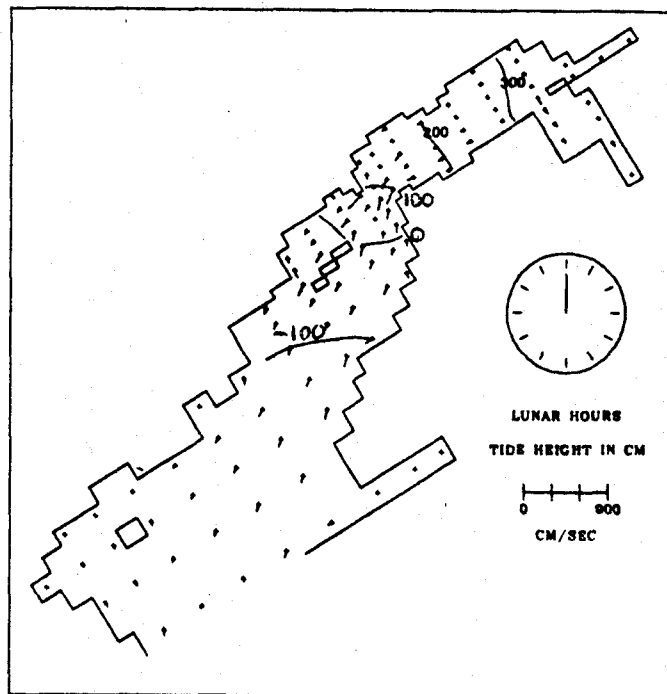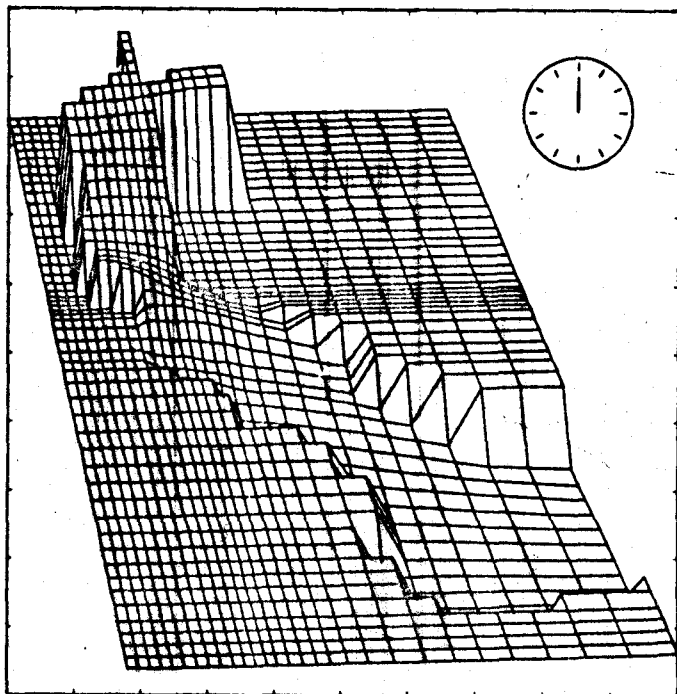M_2 current over the time of high water at Anchorage
for Cook Inlet, Alaska.

Figure 10.5a.   M$_2$ tide of Cook Inlet, Alaska

Figure 10.5b.   M$_2$ tide of Cook Inlet, Alaska.

Figure 10.5c.   M₂ tide of Cook Inlet, Alaska.

Figure 10.5d. M_2 tide of Cook Inlet, Alaska.

Figure 10.5e. M_2 tide of Cook Inlet, Alaska.

LUNAR HOURS

TIDE HEIGHT IN CM

CM/SEC

Figure 10.5f. M_2 tide of Cook Inlet, Alaska.
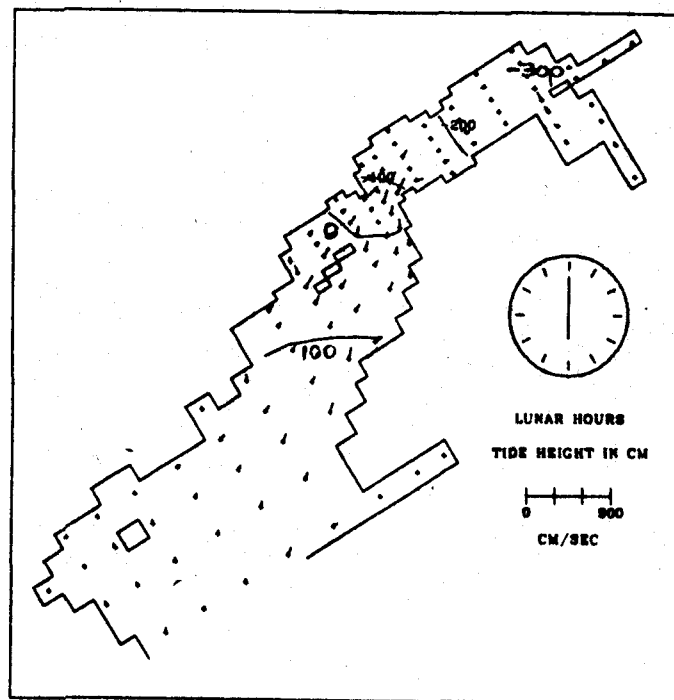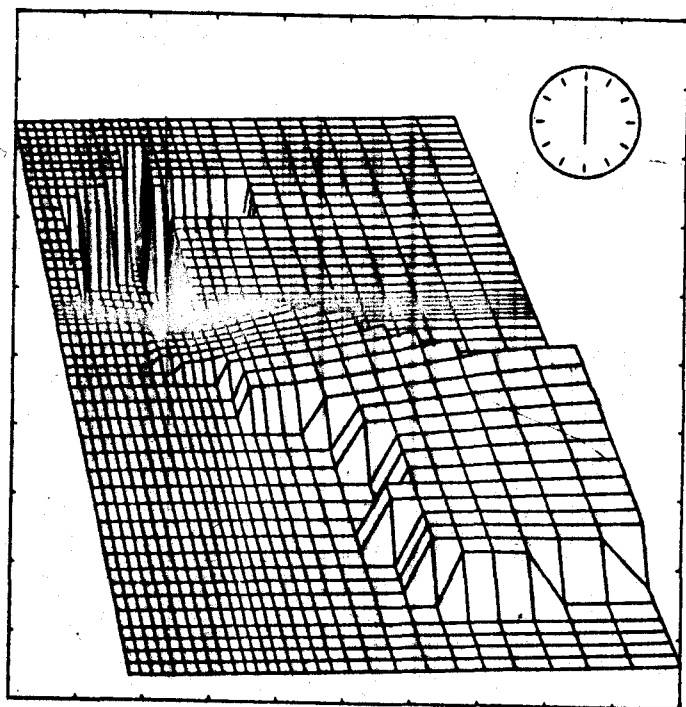
Figure 10.5g. M_2 tide of Cook Inlet, Alaska.
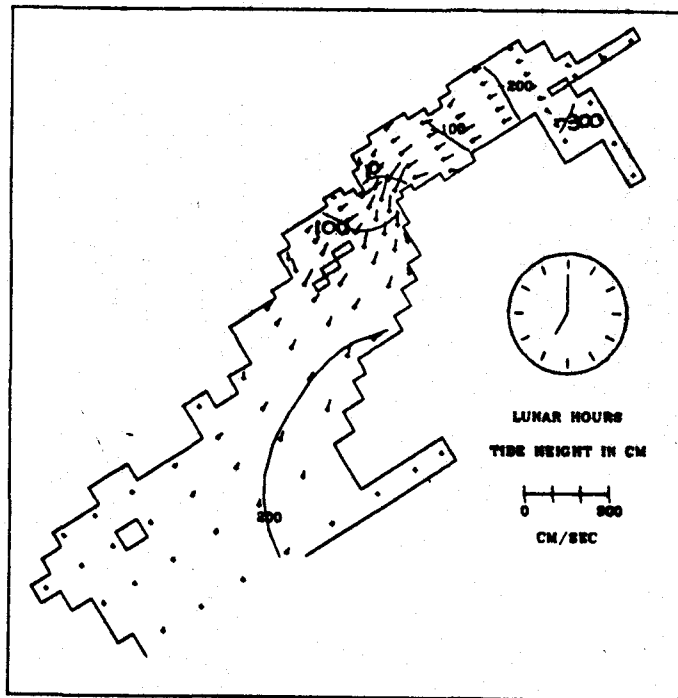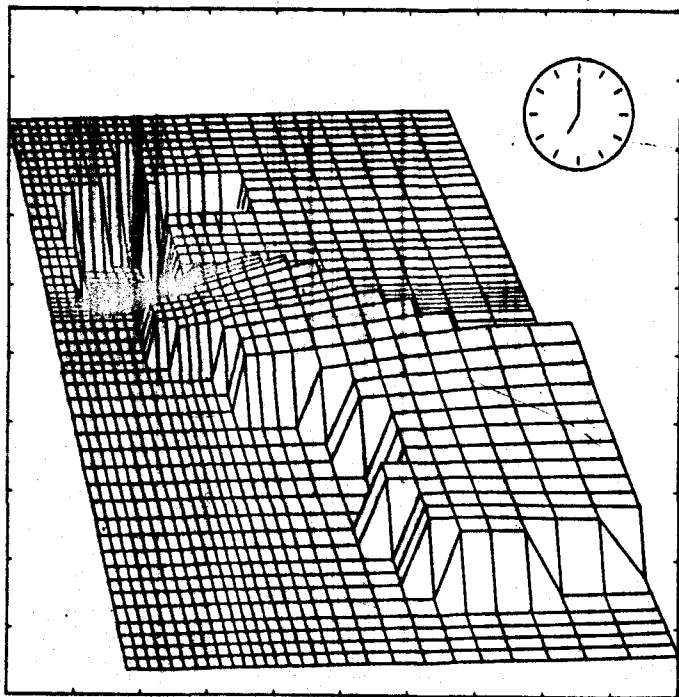
Figure 10.5h.   M$_2$ tide of Cook Inlet, Alaska.
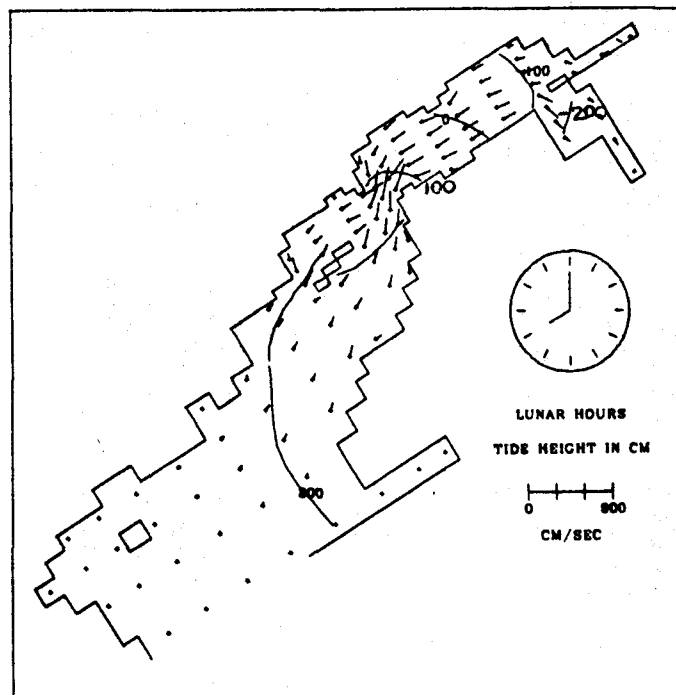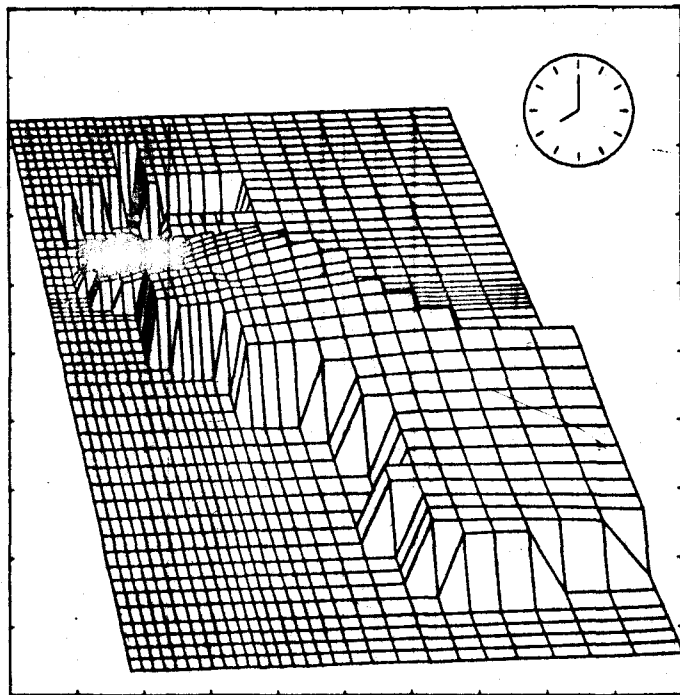
Figure 10.51.　M_2 tide of Cook Inlet, Alaska.
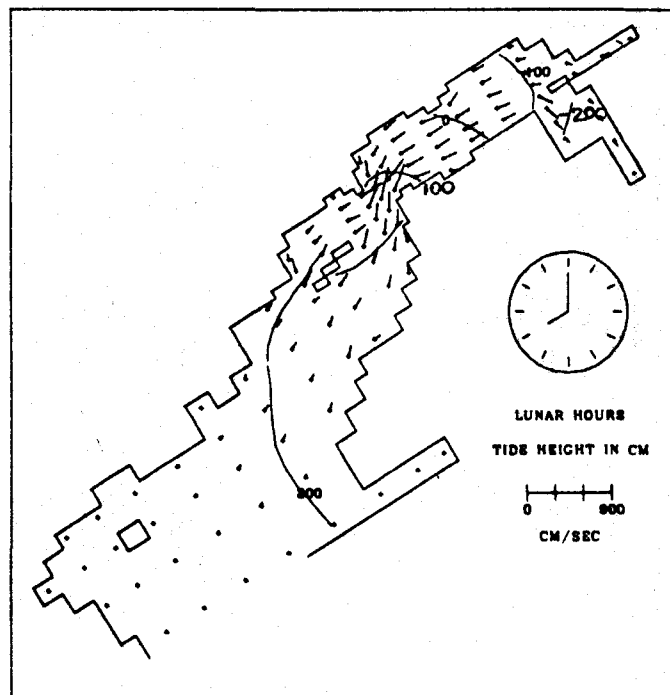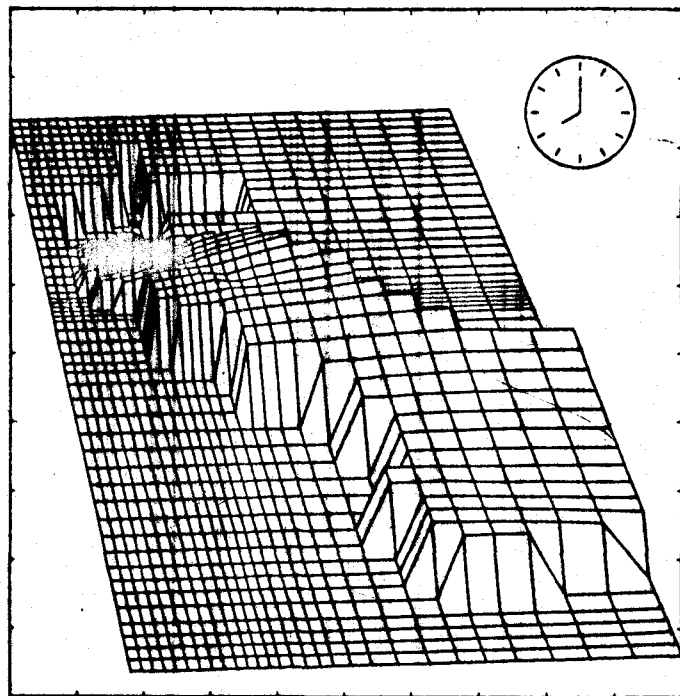
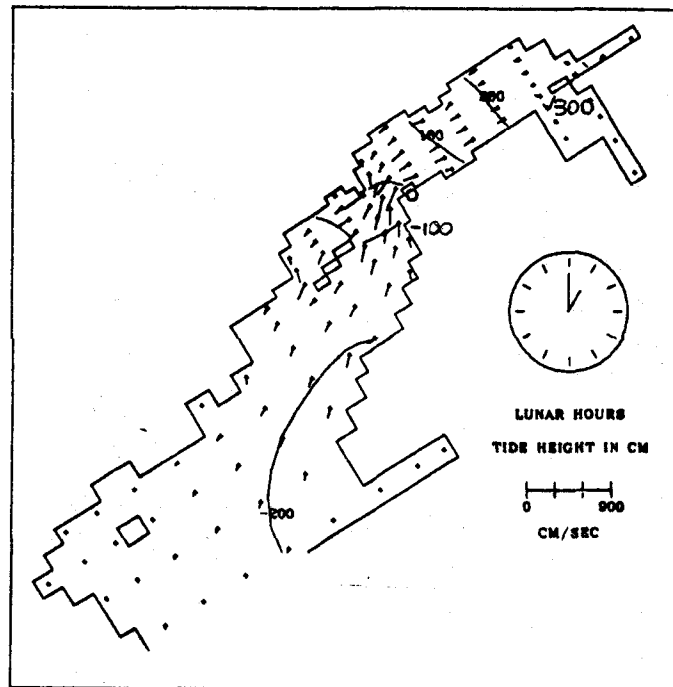Figure 10.51. M_2 tide of Cook Inlet, Alaska.
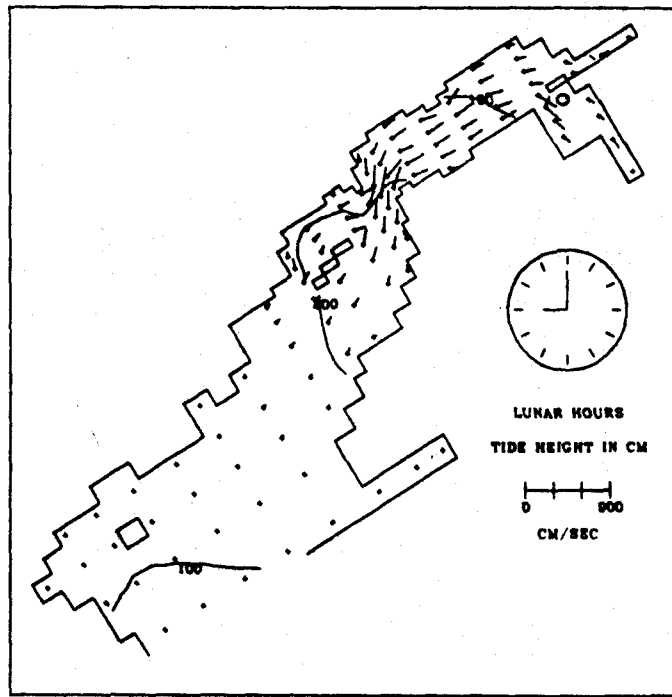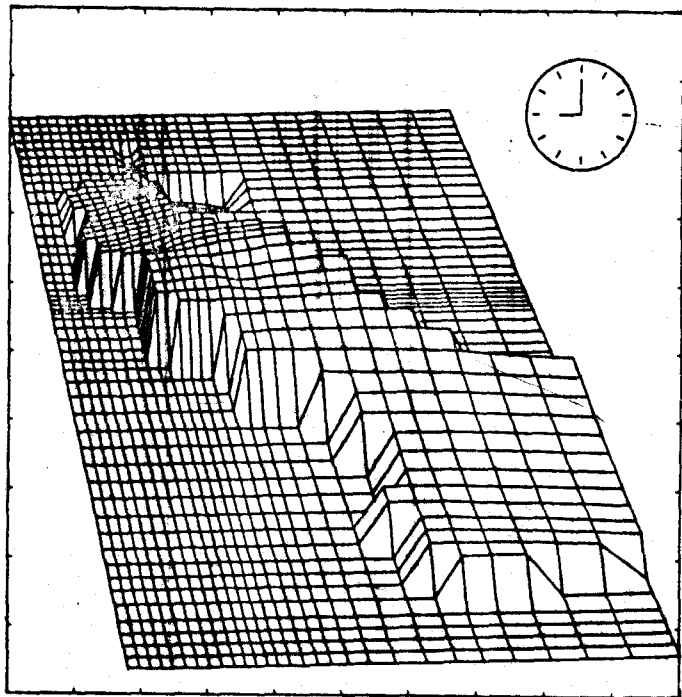
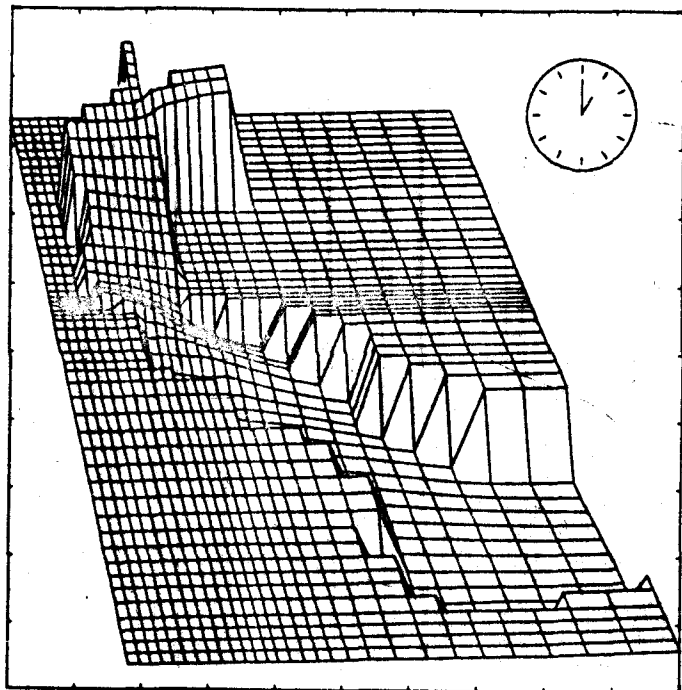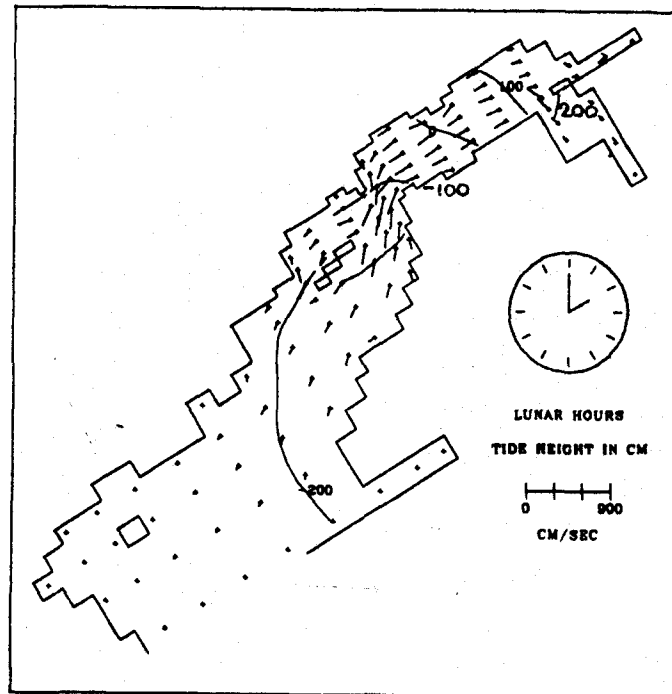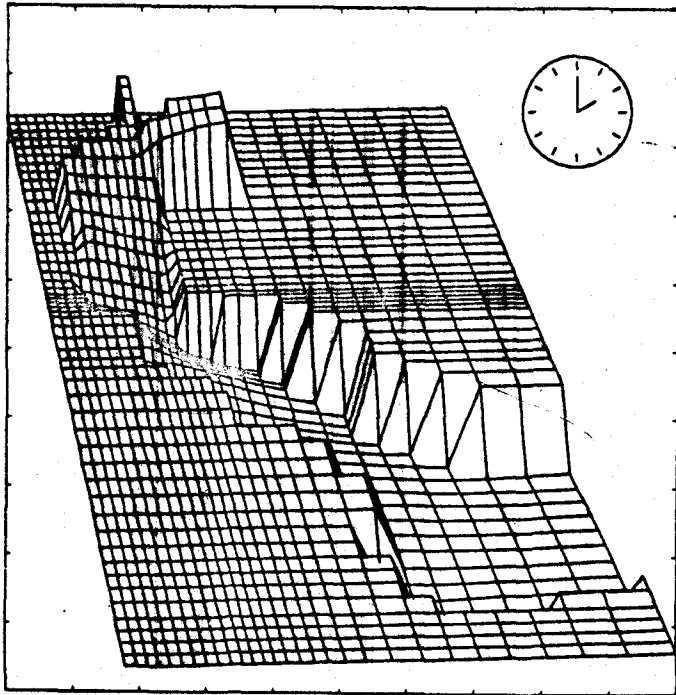Figure 10.5j.   M$_2$ tide of Cook Inlet, Alaska.

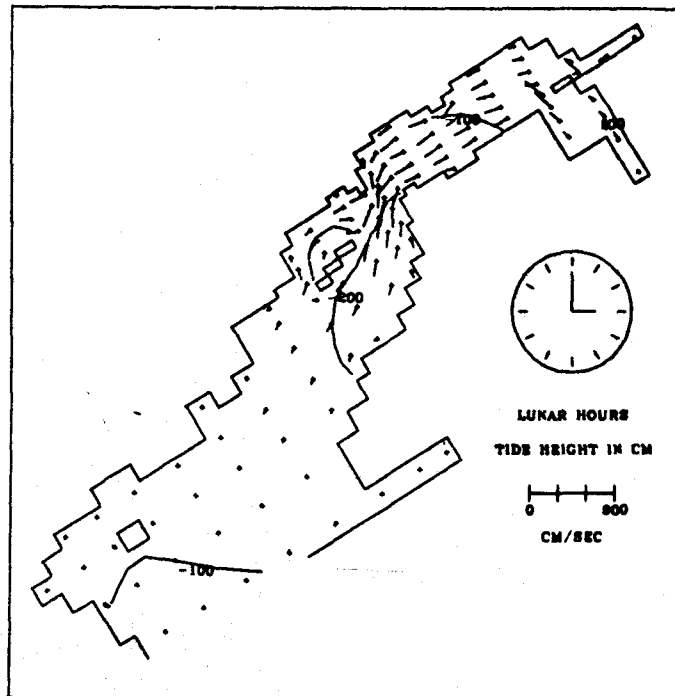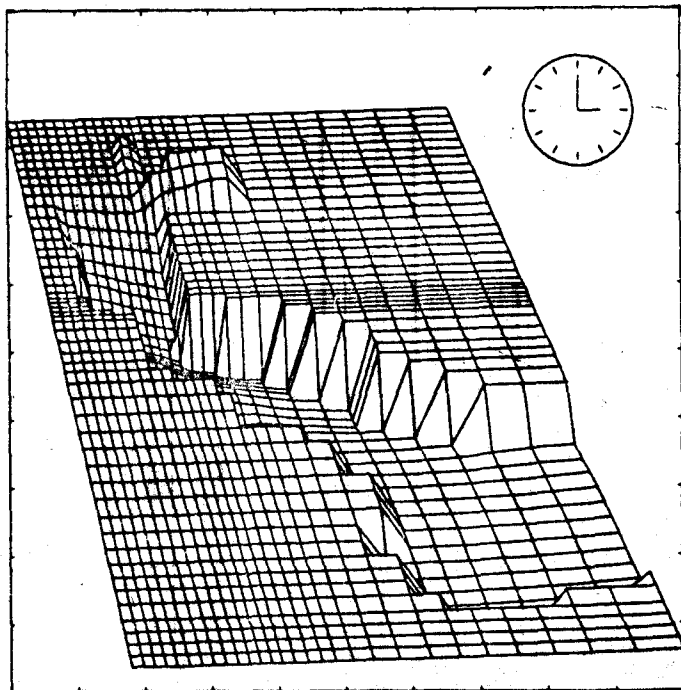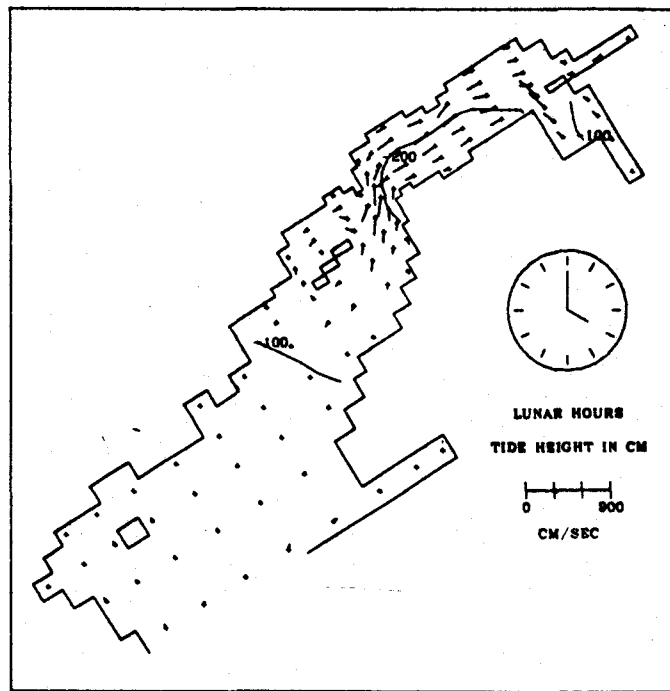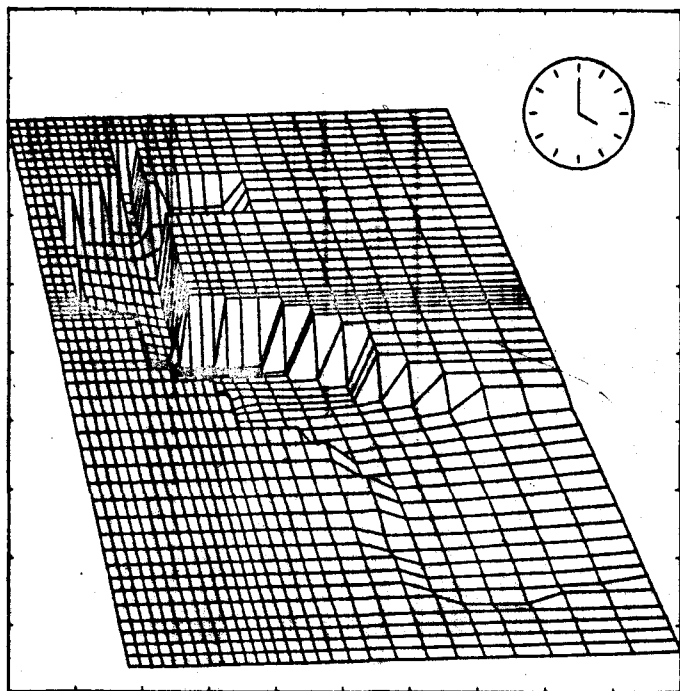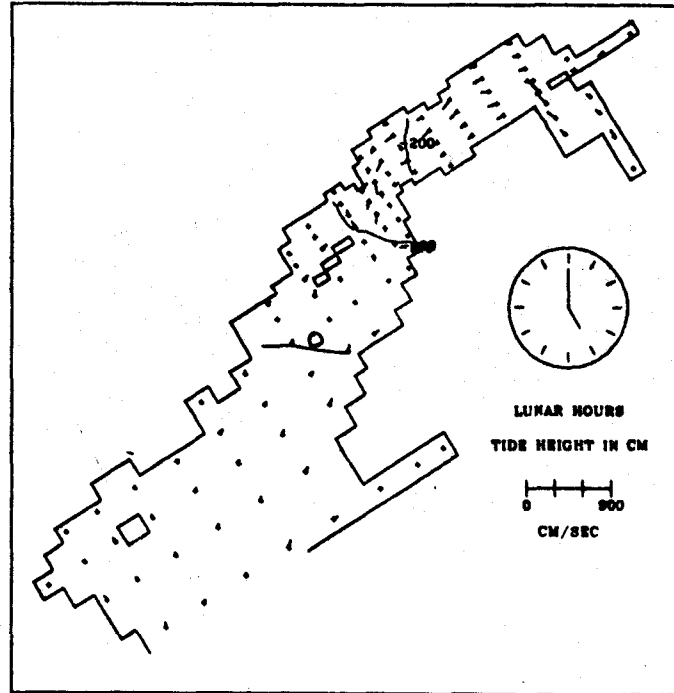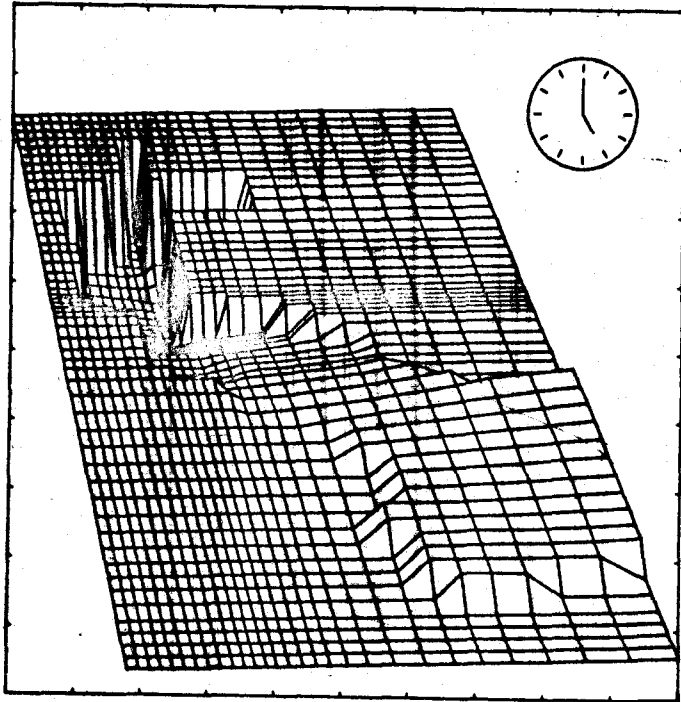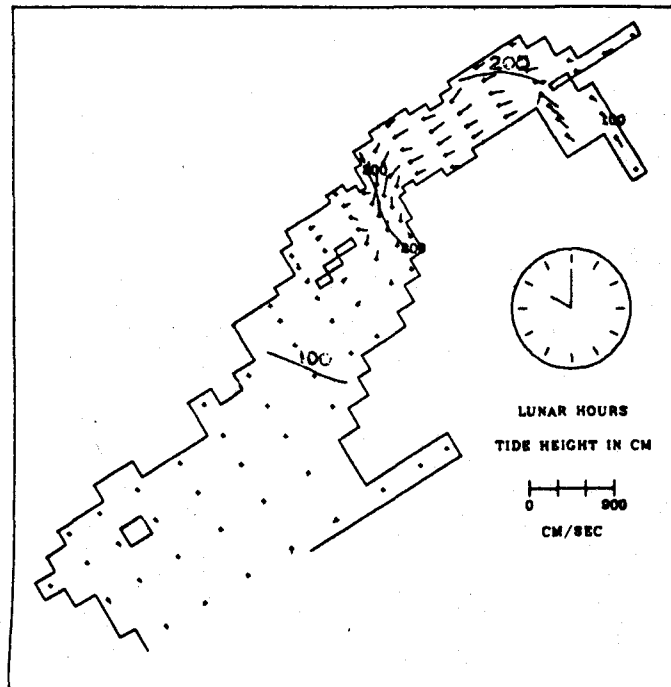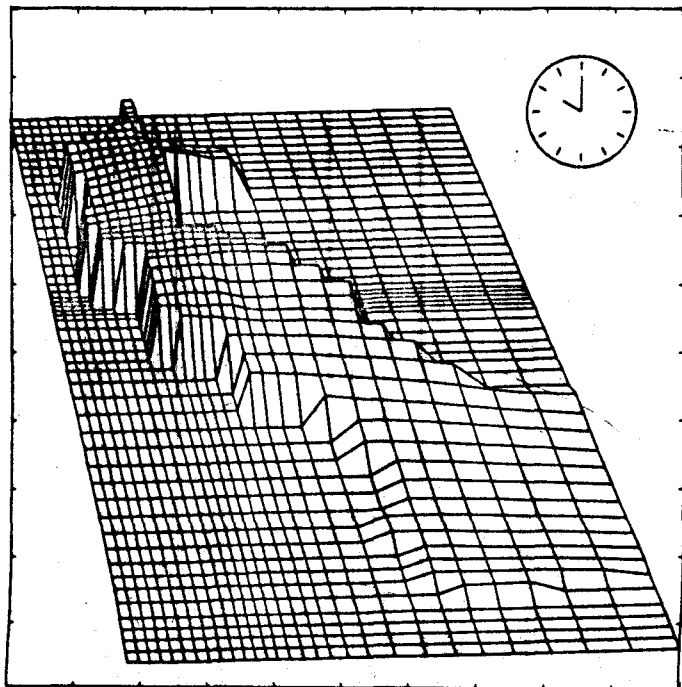Figure 10.5k.   M₂ tide of Cook Inlet, Alaska.
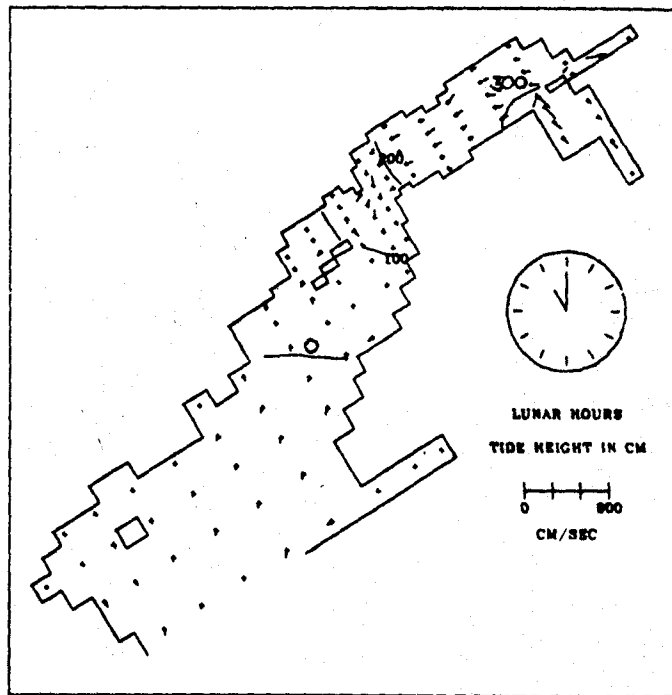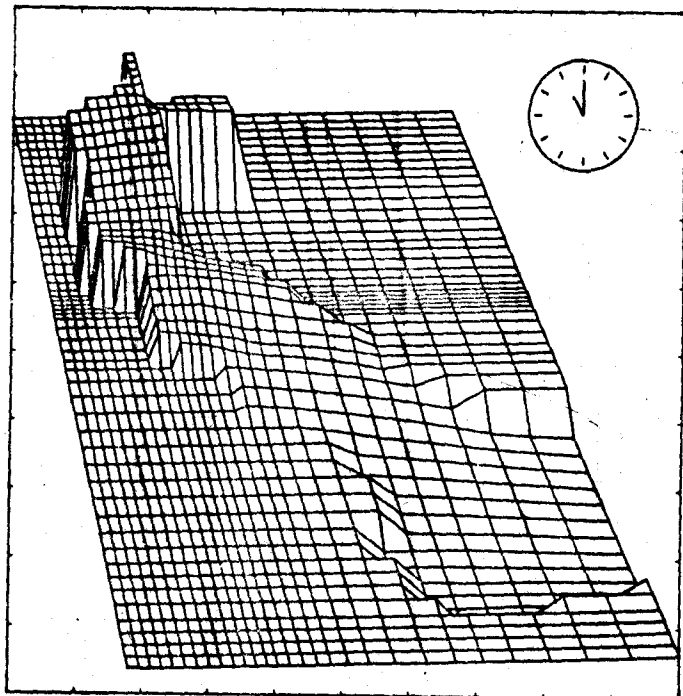
Figure 10.51.   M$_2$ tide of Cook Inlet, Alaska.

to make generalizations, however the following observations (all times in lunar hours) may be of interest.

The behavior of the tide in the lower part of Cook Inlet resembles that of a progressive Kelvin wave. There is no sign of amphidromicity on account of the large amplitudes along the center of the inlet. The approximate amplitudes across the entrance rise from 160 cm on the left to 200 cm on the right, while the corresponding values at Drift River and Chinulne Point are 200 cm and 240 cm respectively. Most of the amplification in the tidal range up the inlet takes place to the north of the Forelands.

High water at Anchorage (341 cm) occurs 5 hours after high water at the entrance (178 cm). High water between the Forelands (200 cm) occurs 2 hours 40 minutes after high water at the entrance, and thus 2 hours 20 minutes before high water at Anchorage.

The amplitude of the M_2 current varies widely throughout the region, making generalizations difficult. In the wide part of Cook Inlet near the entrance currents are of the order of 50 cm/sec. As the inlet narrows, currents fall essentially between 100 cm/sec and 200 cm/sec, with the region near the Forelands having currents between 200 cm/sec and 335 cm/sec. A second area of high currents is at the entrance to Turnagain Arm, where the predicted currents reach a maximum of 365 cm/sec. This value cannot be regarded as being particularly accurate on account of the coarse grid-spacing in this region.

In lower Cook Inlet, for the most part, maximum inward currents occur about 1 1/2 hours before local high water. In upper Cook Inlet they occur between 1 1/2 hours and 3 hours before local high water.

Relative to high water at Anchorage, the lead of the maximum inward currents are: 6 1/2 hours at the entrance, 3 hours 40 minutes between the Forelands, and 3 hours at Anchorage. There is much variability in the times of maximum current as can be seen in Figure 10.4b.

CHAPTER XI

CONCLUSIONS

The results of the three series of tests described in Chapters
VII, VIII, and IX indicate that the proposed implicit tidal model
with unequal grid-spacing is capable of producing good results
providing that the grid-spacing and time step are suitably selected.
The results of Chapters VIII and IX show that the technique behaves
well when used in the unequal grid-spacing mode.

It is felt that as far as the proposed method is concerned,
there are three items that need attention: a mathematical analysis
to investigate the error wave behavior of the model, the inclusion
of convective acceleration terms, and an extension of the model to
enable it to handle flooding boundaries. On the question of
extending the investigation of the tides in the Irish Sea and in
Cook Inlet, the most suitable course would seem to be that of running
the models for neap and spring tide conditions. This would provide
limiting values for such quantities as tide heights and currents, the
latter enabling one to construct tidal stream charts of practical use.

REFERENCES

BOWDEN, K. F.
>   1955. Physical oceanography of the Irish Sea. Fishery
>   Investigations II, 18(8). Her Majesty's Stationery
>   Office, London. 68 pp.

BRETTSCHNEIDER, GOTTFRIED
>   1967. Anwendung des hydrodynamisch-numerischen verfahrens
>   zur ermittlung der M_2-mitschwingungsgezeit der Nordsee.
>   Mitt. Inst. Meeres. Hamburg, 7.

BRETTSCHNEIDER, GOTTFRIED
>   1967. Modelluntersuchungen der gezeiten der Nordsee unter
>   anwendung des hydrodynamisch-numerischen verfahrens.
>   Mitt. Inst. Meeres. Hamburg, 8.

BRITISH ADMIRALTY
>   1962. Irish Sea pocket tidal stream atlas. N.P. 256. 16 pp.

DEFANT, ALBERT
>   1920. Untersuchungen uber die gezeitenerscheinungen in mittel-
>   und randmeren, in buchten und kanalen: Die gezeiten und
>   gezeitenstromungen im Irischen Kanal. Sber. Akad. Wiss.
>   Wien, IIa. 129: 253-308.

DOODSON, A. T., and R. H. CORKAN
>   1932. The principal constituent of the tides in the English and
>   Irish Channels. Phil. Trans. Roy. Soc. London, A231: 29-53.

DOODSON, A. T., J. R. ROSSITER, and R. H. CORKAN
>   1954. Tidal charts based on coastal data: Irish Sea. Proc. Roy.
>   Soc. Edinburgh, A64, part I: 90-111.

DRONKERS, J. J.
>   1947. Methoden van getijberekening. De Ingenieur, 59: 121-137.

DRONKERS, J. J.
>   1964. Tidal computations in rivers and coastal waters. North-
>   Holland Publishing Co., Amsterdam. 518 pp.

DRONKERS, J. J.
>   1969. Tidal computations for rivers, coastal areas, and seas.
>   J. Hydraul. Div., Am. Soc. Civ. Engrs., HY1(6341): 29-77.

DRONKERS, J. J., and J. C. SCHONFELD
>   1955. Tidal computations in shallow water. Proc. Sep. Am. Soc.
>   Civ. Eng., 81(714): 1-50.

GRACE, S. F.
1932. The principal diurnal constituent of tidal motion in the Gulf of Mexico. Monthly Notes Roy. Astr. Soc., Geophys. Supp., 3(2): 70-83.

HANSEN, WALTER
1956. Hydrodynamic methods applied to oceanographic problems. Proceedings of the Symposium on Mathematical-Hydrodynamical Methods of Physical Oceanography. Institut fur Meereskunde der Universitat Hamburg: 25-34.

HARLEMAN, D. R. F., and C. H. LEE
1969. The computation of tides and currents in estuaries and canals. Technical Bulletin No. 16, Committee on Tidal Hydraulics, Corps of Engineers, U. S. Army, Vicksburg, Mississippi. 143 pp.

HEAPS, N. S.
1969. A two-dimensional numerical sea model. Phil. Trans. Roy. Soc. London., A265: 93-137.

HUNT, J. N.
1964. Tidal oscillations in estuaries. Geophys. J. Roy. Astr. Soc. 8: 440-455.

HYACINTHE, J. -L., and J. KRAVTCHENKO
1967. Modèle mathématique des marées Littorales. Calcul numérique sur l'example de La Manche. La Houille Blanche, 6: 639-650.

I.B.M.
1970. IBM system/360 disk operating system Fortran IV programmer's guide. GC28-6397-2. 139 pp.

LASKA, MIECZYSLAW
1965. Chart of the M_2 tidal constituents of the Irish Sea. Unpublished, Institute of Coastal Oceanography and Tides, Birkenhead.

LEENDERTSE, J. J.
1967. Aspects of a computational model for long-period water-wave propagation. Rand Memorandum RM-5294-PR. 165 pp.

LEENDERTSE, J. J.
1970. A water-quality simulation model for well-mixed estuaries and coastal seas: Vol. 1: Principles of computation. Rand Memorandum RM-6230-RC 71 pp.

LORENTZ, H. A.
    1926. Verslag staatscommissie Zuiderzee, 1918-1926. Alg.
    Landsdrukkerij, The Hague.

MATTHEWS, J. B., and J. C. H. MUNGALL
    1970. A variable-boundary, two-dimensional tidal model. Nature,
    Lond., 226(5248): 835-836.

MATTHEWS, J. B., and J. C. H. MUNGALL
    1972. A numerical tidal model and its application to Cook
    Inlet, Alaska. J.M.R. 30(1): 27-38.

MAZURE, J. P.
    1937. De berekening van getijden en stormvloeden op beneden
    rivieren. Thesis, Delft.

PARKINSON, F. E.
    1970. Mathematical model of tidal regimes in the Bay of Fundy.
    International Conference on the Utilization of Tidal
    Power, May 24-29. 19 pp.

PROUDMAN, JOSEPH
    1953. Dynamical oceanography. J. Wiley, New York. 409 pp.

REID, R. O. and B. R. BODINE
    1968. Numerical model for storm surges in Galveston Bay. J. Wat.
    and Harb. Div. Am. Soc. Civ. Eng., 94(1): 33-57.

RICHTMYER, R. D., and K. W. MORTON
    1967. Difference methods for initial-value problems. 2nd. ed.
    Interscience, New York. 405 pp.

SCHUREMAN, PAUL
    1958. Manual of harmonic analysis and prediction of tides.
    Special Publication 98, U. S. Department of Commerce,
    Coast and Geodetic Survey. U. S. Government Printing
    Office, Washington. 317 pp.

SIELECKI, ANITA, and M. G. WURTELE
    1970. The numerical integration of the nonlinear shallow-water
    equations with sloping boundaries. J. Comp. Phys.,
    6: 219-236.

STROBAND, H. J.
    1970. The harmonic method. Unpublished manuscript, Rijkswater-
    staat Deltadienst, The Hague. 45 pp.

STROBAND, H. J.
    1970. Difference methods for one-dimensional tidal computations.
    Unpublished manuscript, Rijkswaterstaat Deltadienst, The
    Hague. 79 pp.

TAYLOR, G. I.
    1919.   Tidal friction in the Irish Sea.   Phil. Trans. Roy. Soc.
            London, A220: 1-33.

UUSITALO, SULO
    1960.   The numerical computation of wind effect on sea level
            elevations.   Tellus, 12: 427-435.

APPENDIX I

THE HARMONIC METHOD: CALCULATION OF L, M, N, AND O

In the interest of clarity, the method by which L, M, N, and O are calculated will be described, and an example given for section 9 (see Figure II.1 for location). It will be seen that the method may easily be set up for hand or computer calculation (Mazure, 1937). For hand computation, scale factors are necessary if the numbers are to be kept to reasonable values. Experience has shown that the following are suitable.

QUANTITY	UNITS
depth	1 m
hydraulic radius	1 m
section length	10000 m
width	1000 m
Chézy coefficient	100 $m^{1/2}$ sec^{-1}
g	1 m sec^{-2}
time	10000 sec
flow rate amplitude	1000 m^3 sec^{-1}
tide amplitude	1 m

Table I.1. Scale factors for the Harmonic Method

In general, the calculations should be made to 5 or more decimal places. If the calculations are performed by hand-calculator, the only difficulty encountered is the calculation of the quantity $k\ell$. The procedure for this is as follows. First one computes $R\ell$, $M\ell$, and $b\ell$, where R , M and b are as before, and ℓ is the section length (replacing x).
Then from equation (2.26)

$$k^2\ell^2 = (-\omega^2 bM + i\omega bR)\ell^2 \tag{I.1}$$

or

$$k^2\ell^2 = -\omega^2(M\ell)(b\ell) + i\omega(R\ell)(b\ell) . \tag{I.2}$$

Putting $k\ell = P + iQ$, $\tag{I.3}$

we have

$$k^2\ell^2 = P^2 - Q^2 + i2PQ \tag{I.4}$$

so that

$$P^2 - Q^2 = -\omega^2(M\ell)(b\ell) \tag{I.5}$$

and

$$2PQ = \omega(R\ell)(b\ell) . \tag{I.6}$$

From equation (I.6),

$$P = \frac{\omega(R\ell)(b\ell)}{2Q} . \tag{I.7}$$

Substituting equation (I.7) into equation (I.5) and rearranging,

$$Q^4 - \omega^2(M\ell)(b\ell)Q^2 - \frac{\omega^2(R\ell)^2(b\ell)^2}{4} = 0 . \tag{I.8}$$

Solving equation (I.8) for Q^2,

$$2Q^2 = \omega^2(M\ell)(b\ell) \pm \sqrt{\omega^4(M\ell)^2(b\ell)^2 + \omega^2(R\ell)^2(b\ell)^2} , \qquad (I.9)$$

where the positive square root is to be taken. From equation (I.9)

$$Q = \pm \sqrt{\frac{\omega^2(M\ell)(b\ell) + \sqrt{\omega^4(M\ell)^2(b\ell)^2 + \omega^2(R\ell)^2(b\ell)^2}}{2}} , \qquad (I.10)$$

and to repeat

$$P = \frac{\omega(R\ell)(b\ell)}{2Q} . \qquad (I.11)$$

$k\ell$ can be positive or negative, however, L , M , N , and O remain the same in either case. Thus, for convenience, the positive sign should be adopted in equation (I.10).

When L , M , N , and O have been calculated, the following should be verified:

$$(LO - MN) \approx 1 + i0 . \qquad (I.12)$$

In the example that follows, the M_2 tide is considered (ω, before scaling, equals 1.405×10^{-4}). Note that all values are scaled.

SECTION 9

(1)	Depth below mwl	a_m	35.4
(2)	Mean flow width	b_s	27.4
(3)	(1) (2)	A_m	969.96
(4)	Mean hydraulic radius	a_{rm}	35.4
(5)	Mean surface width	b	27.4
(6)	Section length	ℓ	1.5

(7)	Chézy coefficient	C_m	0.69
(8)	Mean flow rate amplitude	$\hat{q}_m$	1327.0
(9)	Mean tide amplitude	$\hat{h}_m$	2.41
(10)	$1 + 3(9)^2/(1)^2$	N_o	1.013904
(11)	$1 + (9)^2/2(1)^2$	$\bar{N}_o$	1.002317
(12)	$(7)^2(3)^2(4)$	$(C^2 A^2 a_r)_m$	15856540.0
(13)	$.85(6)(8)(10)/(12)$	$R\ell$	.0001082
(14)	$(6)(11)/9.81\ (3)$	$M\ell$	.0001580
(15)	$(5)(6)$	$b\ell$	41.10
(16)	$i\ 1.405\ (15)$	$i\omega b\ell$	$i\ 57.745489$
(17)	$1/(16)$	$1/i\omega b\ell$	$-i\ .017317$
(18)	$1.405(13)(15)$	U	.006247
(19)	$1.405^2(14)(15)$	V	.012819
(20)	$\sqrt{(18)^2 + (19)^2}$	X	.014261
(21)	$((19) + (20))/2$	Y	.013540
(22)	$\sqrt{(21)}$	Q	.116361
(23)	$(18)/2\ (22)$	P	.026844
(24)	$P + iQ$	$k\ell$	$.026844 + i\ .116361$
(25)	$(17)\ (24)$	$-ik/\omega b$	$.002015 - i\ .000465$
(26)	$1/(25)$	$i\omega b/k$	$471.183 + i\ 108.700$
(27)	$\cosh P$		1.000360
(28)	$\sinh P$		0.026847
(29)	$\cos Q$		0.993238
(30)	$\sin Q$		0.116099
(31)	$(27)(29) + i(28)(30)$	$\cosh(k\ell)$	$.993595 + i\ .003117$
(32)	$(28)(29) + i(27)(30)$	$\sinh(k\ell)$	$.026666 + i\ .116141$

(33)	(31)	L	.993595 + i .003117
(34)	-(25)(32)	M	-.000108 - i .000222
(35)	-(26)(32)	N	.060048 - i 57.622172
(36)	(31)	O	.993595 + i .003117
(37)	Check	LO-MN=1	1.00002 - i .00002

APPENDIX II

EXAMPLE OF BRANCH-POINT SOLUTION FOR
THE HARMONIC METHOD

In order to provide an illustration of the procedure necessary
for dealing with branch-point calculations, an example of the steps
required for a single iteration is shown in the following pages.
Reference should be made to the latter part of Chapter II. The scheme
used to refer to each section and its end points is shown in Figure
II.1. Detailed calculations are shown only for the branch consisting
of sections 8, 9, 10, and 11. The calculations were performed in double
precision (16-digit numbers) in order to reveal similarities between
certain numbers, these often being useful when checking hand calculations.
Note that, as in Appendix I, all values have been scaled except for the
final heights and flow rates. The distribution of the tide height
constituent is shown in Figure V.1 along with values obtained from the
one-dimensional implicit method.
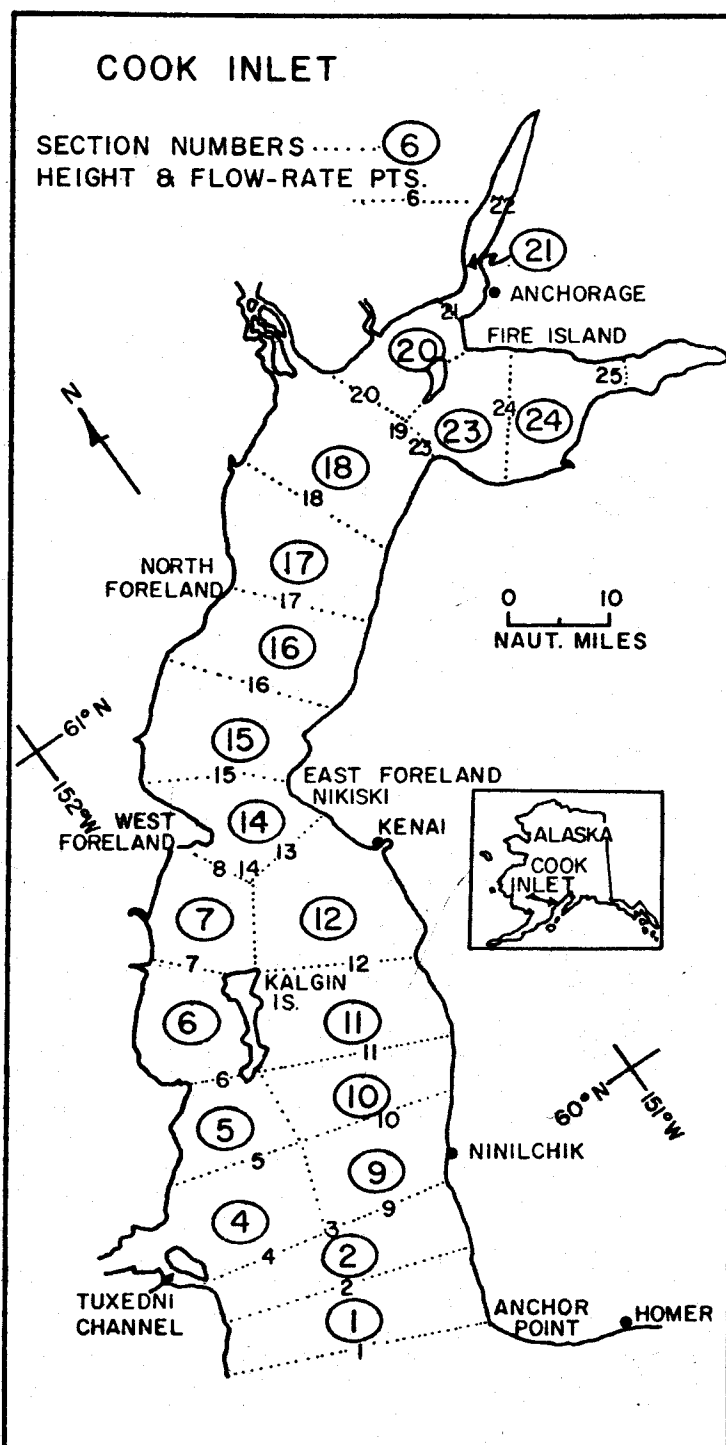
Figure II.1. Location of sections for Cook Inlet, Alaska.

AM	BM	ARM	B	L
40.8	50.0	40.8	50.0	1.66

L=(0.993201+J0.002638)
N=(0.102646-J116.350573)

AM	BM	ARM	B	L
42.7	52.0	42.7	54.0	1.30

L=(0.995861+J0.001298)
N=(0.042687-J98.494868)

AM	BM	ARM	B	L
36.0	25.4	36.0	26.0	1.68

L=(0.991917+J0.002553)
N=(0.052293-J61.204954)

AM	BM	ARM	B	L
36.4	15.8	36.4	16.2	1.60

L=(0.992734+J0.003237)
N=(0.039334-J36.329359)

```
   C           QM          HM
  0.67       2427.0       2.28

M=(-0.000045-J0.000116)
O=(0.993201+J0.002638)



   C           QM          HM
  0.68       2300.0       2.37

M=(-0.000026-J0.000084)
O=(0.995861+J0.001298)



   C           QM          HM
  0.69        826.0       2.44

M=(-0.000083-J0.000263)
O=(0.991917+J0.002553)



   C           QM          HM
  0.70        762.0       2.53

M=(-0.000177-J0.000399)
O=(0.992734+J0.003237)
```

AM	BM	ARM	B	L
31.5	15.5	31.5	17.0	2.10

L=(0.984523+J0.009251)
N=(0.154999-J49.899556)

AM	BM	ARM	B	L
19.8	16.7	19.8	18.2	2.00

L=(0.977575+J0.031612)
N=(0.540509-J50.760287)

AM	BM	ARM	B	L
35.4	27.4	35.4	27.4	1.50

L=(0.993595+J0.003117)
N=(0.060048-J57.622172)

AM	BM	ARM	B	L
29.6	32.4	29.6	32.5	1.45

L=(0.992813+J0.004181)
N=(0.092362-J66.051933)

```
   C           QM          HM
 0.67        686.0        2.62

M=(-0.000367-J0.000616)
O=(0.984523+J0.009251)



   C           QM          HM
 0.63        599.0        2.58

M=(-0.001227-J0.000880)          .
O=(0.977575+J0.031612)



   C           QM          HM
 .69         1327.        2.41

M=(-0.000108-J0.000222)
O=(0.993595+J0.003117)



   C           QM          HM
 .67         1230.        2.45

M=(-0.000126-J0.000217)
O=(0.992813+J0.004181)
```

AM	BM	ARM	B	L
26.1	32.0	26.1	32.5	1.7

$$L=(0.988645+J0.008090)$$
$$N=(0.209645-J77.332304)$$

AM	BM	ARM	B	L
25.0	25.8	25.0	26.1	2.3

$$L=(0.978374+J0.018802)$$
$$N=(0.530127-J83.733918)$$

AM	BM	ARM	B	L
33.0	17.8	33.0	18.1	2.00

$$L=(0.987562+J0.011903)$$
$$N=(0.202131-J50.650115)$$

AM	BM	ARM	B	L
29.5	25.0	29.5	27.1	1.70

$$L=(0.989275+J0.008508)$$
$$N=(0.183842-J64.496873)$$

```
  C            QM          HM
.66         1118.        2.48

M=(-0.000208-J0.000292)
O=(0.988645+J0.008090)


  C            QM          HM
.65         980.0        2.5

M=(-0.000443-J0.000512)
O=(0.978374+J0.018802)


  C            QM          HM
 0.68        1429.0       2.60

M=(-0.000466-J0.000489)
O=(0.987562+J0.011903)


  C            QM          HM
 0.67        1281.0       2.78

M=(-0.000262-J0.000331)
O=(0.989275+J0.008508)
```

AM	BM	ARM	B	L
24.6	27.1	24.6	27.9	1.60

L=(0.989139+J0.010596)
N=(0.221841-J62.492109)

AM	BM	ARM	B	L
21.7	26.1	21.7	27.4	1.80

L=(0.984040+J0.018068)
N=(0.418233-J68.926055)

AM	BM	ARM	B	L
21.9	22.7	21.9	26.9	2.15

L=(0.974506+J0.023934)
N=(0.650491-J80.567492)

AM	BM	ARM	B	L
13.8	11.8	13.8	14.8	1.9

L=(0.965572+J0.036579)
N=(0.483959-J39.055349)

```
   C           QM          HM
 0.65        1101.0        3.05

M=(-0.000337-J0.000346)
O=(0.989139+J0.010596)




   C           QM          HM
 0.63         887.0        3.25

M=(-0.000519-J0.000461)
O=(0.984040+J0.018068)




   C           QM          HM
 0.63         646.0        3.60

M=(-0.000584-J0.000627)
O=(0.974506+J0.023934)




   C           QM          HM
 0.59         118.0        4.0

M=(-0.001830-J0.001744)
O=(0.695572+J0.036579)
```

AM	BM	ARM	B	L
11.0	6.7	11.0	11.6	1.9

L=(0.938771+J0.064365)
N=(0.669877-J30.334546)

AM	BM	ARM	B	L
14.8	7.3	14.8	9.4	2.6

L=(0.935233+J0.153711)
N=(1.774229-J33.612474)

AM	BM	ARM	B	L
15.2	2.97	15.2	3.5	2.0

L=(0.967160+J0.063238)
N=(0.208220-J9.727995)

```
     C          QM          HM
    0.57        36.0        4.1

M=(-0.004071-J0.003960)
0=(0.938771+J0.064365)



     C          QM          HM
    0.60        211.0       4.0

M=(-0.008763-J0.003969)
0=(0.935233+J0.153711)



     C          QM          HM
    0.60        70.0        4.1

M=(-0.012719-J0.006780)
0=(0.967160+J0.063238)
```

CONNECTIONS ARE THEN PERFORMED FOR EACH BRANCH.
AS AN EXAMPLE, THAT FOR SECTIONS 9, 10, 11, AND 12 IS SHOWN.

$$H(12)=(\ 0.978374+J\ \ 0.018802)H(13) + (-0.000443-J0.000512)Q(13)$$
$$Q(12)=(\ 0.530127-J\ 83.733918)H(13) + (\ 0.978374+J0.018802)Q(13)$$

$$H(11)=(\ 0.942527+J\ \ 0.043735)H(13) + (-0.000631-J0.000800)Q(13)$$
$$Q(11)=(\ 2.860595-J158.434748)H(13) + (\ 0.927395+J0.060624)Q(13)$$

$$H(10)=(\ 0.900839+J\ \ 0.066701)H(13) + (-0.000727-J0.001006)Q(13)$$
$$Q(10)=(\ 6.478240-J219.535734)H(13) + (\ 0.867575+J0.105677)Q(13)$$

$$H(\ 9)=(\ 0.845507+J\ \ 0.091295)H(13) + (-0.000789-J0.001205)Q(13)$$
$$Q(\ 9)=(11.018584-J270.013819)H(13) + (\ 0.803693+J0.149530)Q(13)\ .$$

EXPRESSING FLOW-RATES IN TERMS OF HEIGHTS AT ENDS OF THE BRANCH,

$$Q(13)=(\ 374.523986-J\ 456.303557)H(13) + (-\ 380.251763+J\ 580.739059)H(9)$$
$$Q(\ 9)=(\ 380.251763-J\ 580.739059)H(13) + (-\ 392.443381+J\ 409.876653)H(9)\ .$$

LIKEWISE, FOR THE OTHER THREE BRANCHES WITH UNKNOWN END FLOW-RATES,

$$Q(\ 3)=(1580.424653-J4341.370194)H(3) + (-1578.541066+J4454.296038)H(1)$$
$$Q(\ 1)=(1578.541066-J4454.296038)H(3) + (-1576.927487+J4351.206277)H(1)$$

$$Q(\ 8)=(\ 221.138395-J\ 226.479673)H(8) + (-\ 231.871398+J\ 293.598699)H(4)$$
$$Q(\ 4)=(\ 231.871398-J\ 293.598699)H(8) + (-\ 246.994644+J\ 155.282498)H(4)$$

$$Q(19)=(\ 226.525950-J\ 117.201229)H(19) + (-\ 215.837216+J\ 291.808297)H(14)$$
$$Q(14)=(\ 215.837216-J\ 291.808293)H(19) + (-\ 231.245432+J\ 114.358970)H(14)$$

CONNECTIONS ARE THEN PERFORMED FOR EACH BRANCH.
AS AN EXAMPLE, THAT FOR SECTIONS 9, 10, 11, AND 12 IS SHOWN.

$$H(12)=(0.978374+J 0.018802)H(13) + (-0.000443-J0.000512)Q(13)$$
$$Q(12)=(0.530127-J 83.733918)H(13) + (0.978374+J0.018802)Q(13)$$

$$H(11)=(0.942527+J 0.043735)H(13) + (-0.000631-J0.000800)Q(13)$$
$$Q(11)=(2.860595-J158.434748)H(13) + (0.927395+J0.060624)Q(13)$$

$$H(10)=(0.900839+J 0.066701)H(13) + (-0.000727-J0.001006)Q(13)$$
$$Q(10)=(6.478240-J219.535734)H(13) + (0.867575+J0.105677)Q(13)$$

$$H(9)=(0.845507+J 0.091295)H(13) + (-0.000789-J0.001205)Q(13)$$
$$Q(9)=(11.018584-J270.013819)H(13) + (0.803693+J0.149530)Q(13) .$$

EXPRESSING FLOW-RATES IN TERMS OF HEIGHTS AT ENDS OF THE BRANCH,

$$Q(13)=(374.523986-J 456.303557)H(13) + (- 380.251763+J 580.739059)H(9)$$
$$Q(9)=(380.251763-J 580.739059)H(13) + (- 392.443381+J 409.876653)H(9) .$$

LIKEWISE, FOR THE OTHER THREE BRANCHES WITH UNKNOWN END FLOW-RATES,

$$Q(3)=(1580.424653-J4341.370194)H(3) + (-1578.541066+J4454.296038)H(1)$$
$$Q(1)=(1578.541066-J4454.296038)H(3) + (-1576.927487+J4351.206277)H(1)$$

$$Q(8)=(221.138395-J 226.479673)H(8) + (- 231.871398+J 293.598699)H(4)$$
$$Q(4)=(231.871398-J 293.598699)H(8) + (- 246.994644+J 155.282498)H(4)$$

$$Q(19)=(226.525950-J 117.201229)H(19) + (- 215.837216+J 291.808297)H(14)$$
$$Q(14)=(215.837216-J 291.808293)H(19) + (- 231.245432+J 114.358970)H(14) .$$

FOR THE TWO UPSTREAM BRANCHES (HAVING ZERO FLOW-RATES AT THE ENDS),

$$H(20)=(0.849959+J\ 0.150842)H(22) + (-0.005392-J0.0057281Q(22)$$
$$Q(20)=(4.724545-J65.898572)H(22) + (0.747468+J0.253577)Q(22)$$

$$H(23)=(0.854361+J\ 0.292228)H(25) + (-0.019078-J0.012689)Q(25)$$
$$Q(23)=(5.531588-J41.462381)H(25) + (0.644353+J0.623308)Q(25) .$$

SINCE Q(22)=0.0 ,

$$Q(20)=(-7.950508-J76.120456)H(20) .$$

SINCE Q(25)=0.0 ,

$$Q(23)=(-9.064412-J45.429861)H(23) .$$

REGROUPING THE ABOVE IN THE ORDER THAT THEY WILL BE NEEDED, AND PLACING
H(22)=H(A), H(25)=H(B), H(23)=H(19)=H(C), ETC,

$$Q(20)=(- 7.950508-J 76.120456)H(C)$$
$$Q(23)=(- 9.064412-J 45.429861)H(C)$$
$$Q(19)=(226.525950-J 117.201229)H(C) - (215.837216-J 291.8082971H(D)$$
$$Q(14)=(215.837216-J 291.808297)H(C) - (231.245432-J 114.358970)H(D)$$
$$Q(8)=(221.138395-J 226.479673)H(D) - (231.871398-J 293.598699)H(E)$$
$$Q(13)=(374.523986-J 456.303557)H(D) - (380.251763-J 580.739059)H(E)$$
$$Q(4)=(231.871398-J 293.598699)H(D) - (246.994644-J 155.282498)H(E)$$
$$Q(9)=(380.251763-J 580.739059)H(D) - (392.443381-J 409.876653)H(E)$$
$$Q(3)=(1580.424653-J4341.370194)H(E) - (1578.541066-J4454.296038)H(F) .$$

SOLUTION OF HEIGHTS AT BRANCH-POINTS .

AT JUNCTION C, Q(20) + Q(23) = Q(19) , SO THAT

$\qquad$ (-243.540869-J4.349088)H(C) = -(215.837216-J291.808297)H(D) ,

OR $\quad$ H(C) = (0.864574-J1.213630)H(D) .

AT JUNCTION D, $\quad$ Q(14) = Q(8) + Q(13) , SO THAT

(215.837216-J291.808297)H(C)=(826.907813-J797.142201)H(D)

$\qquad$ -(612.123161-J874.337757)H(E) ,

OR $\qquad$ (994.447813-J282.905986)H(D) = (612.123161-J874.337757)H(E) ,

SO THAT $\quad$ H(D) = (0.800850-J0.651389)H(E) .

AT JUNCTION E , Q(4) + Q(9) = Q(3) , SO THAT

(612.123161-J874.337757)H(D) - (2219.862679-J4906.529345)H(E)

$\qquad$ = -(1578.541066-J4454.296038)H(F) ,

OR $\qquad$ (2299.176745-J3807.584590)H(E) = (1578.541066-J4454.296038)H(F) ,

SO THAT FINALLY , H(E) = (1.040717-J0.213850)H(F) .

CALCULATION OF BRANCH-POINT HEIGHTS.

GIVEN H(F)=(2.25+J0.0), THEN

H(E)=(1.040717-J0.213850)(2.25   +J0.0   )=
H(D)=(0.800851-J0.651389)(2.341613-J0.481162)=
H(C)=(0.864574-J1.213630)(1.561861-J1.910640)=
H(B)=(1.047872-J0.358417)(-0.968465-J3.547409)=
H(A)=(1.140603-J0.202422)(-0.968465-J3.547409)=

IN TERMS OF AMPLITUDES AND PHASES, THE BRANCH-

    H(F)=2.25 M, 000 DEGREES
    H(E)=2.39 M, 012 DEGREES
    H(D)=2.47 M, 051 DEGREES
    H(C)=3.68 M, 105 DEGREES
    H(B)=4.07 M, 124 DEGREES
    H(A)=4.26 M, 115 DEGREES.

```
=(  2.341613-J0.481162)
=(  1.561861-J1.910640)
=(-0.968465-J3.547409)
=(-2.286277-J3.370115)
=(-1.822709-J3.850146) .
```

-POINT HEIGHTS ARE

CALCULATION OF FLOW-RATES AT UPSTREAM ENDS OF BRANCHES.

     Q(22)=0.0

     Q(25)=0.0

Q(19)= (226.525950-J 117.201229)(-0.968465-J3.547409)
        +(- 215.837216+J 291.808297)(1.561861-J1.910640)

   OR Q(19)=(- 414.710338+J 178.076117) .

Q(13)= (374.523986-J 456.303557)(1.561861-J1.910640)
        +(- 380.251763+J 580.739059)(2.341613-J0.481162)

   OR Q(13)=(- 897.850312+J 114.565921) .

Q(8)= (221.138395-J 226.479673)(1.561861-J1.910640)
        +(- 231.871398+J 293.598699)(2.341613-J0.481162)

   OR Q(8)=(- 489.018240+J 22.816782) .

Q(3)= (1580.424653-J4341.370194)(2.341613-J0.481162)
        +(-1578.541066+J4454.296038)(2.25   +J0.0   )

   OR Q(3)=(-1939.876592-J 904.083169) .

STARTING AT THE UPSTREAM END OF EACH BRANCH, HEIGHTS AND FLOW-RATES
   ARE THEN CALCULATED.

AGAIN, USING AS AN EXAMPLE THE BRANCH CONSISTING OF SECTIONS 9, 10, 11, AND 12,

H(12)= (0.978374+J 0.018802)(1.561861-J 1.910640)
     +(-0.000443-J 0.000512)(-897.850312+J114.565921)

          H(12)=(2.020111-J 1.430616)

Q(12)= (0.530127-J 83.733918)(1.561861-J 1.910640)
     +(0.978374+J 0.018802)(-897.850312+J114.565921)

          Q(12)=(-1039.744381-J 36.586503) .

H(11)= (0.942527+J 0.043735)(1.561861-J 1.910640)
     +(-0.000631-J 0.000800)(-897.850312+J114.565921)

          H(11)=(2.213943-J 1.086525)

Q(11)= (2.860595-J158.434748)(1.561861-J 1.910640)
     +(0.927395+J 0.060624)(-897.850312+J114.565921)

          Q(11)=(-1137.851176-J201.102162) .

H(10)= (0.900839+J 0.066701)(1.561861-J 1.910640)
     +(-0.000727-J 0.001006)(-897.850312+J114.565921)

          H(10)=(2.302301-J 0.797280)

Q(10)= (6.478240-J219.535734)(1.561861-J 1.910640)
     +(0.867575+J 0.105677)(-897.850312+J114.565921)

          Q(10)=(-1200.394678-J350.749537) .

H(9)= (0.845507+J 0.091295)(1.561861-J 1.910640)
    +(-0.000789-J 0.001205)(-897.850312+J114.565921)

        H(9)=(2.341613-J 0.481162)

Q(9)= (11.018584-J270.013819)(1.561861-J 1.910640)
    +(0.803693+J 0.149530)(-897.850312+J114.565921)

        Q(9)=(-1237.416257-J484.956199) .

IN TERMS OF AMPLITUDES AND PHASES, THE (UNSCALED) VALUES ARE
        H(13)=2.47 M, 051 DEGREES
        H(12)=2.48 M, 035 DEGREES
        H(11)=2.47 M, 026 DEGREES
        H(10)=2.44 M, 019 DEGREES
        H(9)=2.39 M, 012 DEGREES.

        Q(13)= 905130 CU M/SEC., 187 DEGREES
        Q(12)=1040390 CU M/SEC., 178 DEGREES
        Q(11)=1155490 CU M/SEC., 170 DEGREES
        Q(10)=1250590 CU M/SEC., 164 DEGREES
        Q(9)=1329050 CU M/SEC., 159 DEGREES.

APPENDIX III

ANALYSIS OF STABILITY AND WAVE-DEFORMATION
FOR THE ONE-DIMENSIONAL IMPLICIT METHOD

It is important to ascertain the conditions under which the one-dimensional implicit method will remain stable and relatively error-free. The approach used here follows closely that of Stroband (1970b) who used a method originally due to von Neumann (Richtmyer and Morton, 1967, p. 70). A useful addition to the method of von Neumann, as shown by Leendertse (1967), is that the deformation of a given wave may be calculated.

Von Neumann's approach is to assume that an error wave at any particular instant may be represented by a Fourier series. If the system being analysed is linear only one term each for height and flow rate need be considered. Thus, if L is the wave-length and T the period,

$$h = h^* \exp(i\sigma x) \exp(i\beta t) \qquad (III.1)$$

$$q = q^* \exp(i\sigma x) \exp(i\beta t) , \qquad (III.2)$$

where

$$\sigma = \frac{2\pi}{L} \text{ and } \beta = \frac{2\pi}{T} .$$

If equations (III.1) and (III.2) are substituted into the linearized versions of equations (3.3) and (3.4), the following important relation results:

$$\beta = \pm \sigma \sqrt{ga} \qquad (III.3)$$

or

$$L = \pm T\sqrt{ga} \quad . \tag{III.4}$$

When h and q exist only at discrete points in time and space, i.e.

$$x = m\Delta x \qquad\qquad m=0, 1, 2, 3, \ldots, \tag{III.5}$$

$$t = r\tau \qquad\qquad r=0, 1, 2, 3, \ldots, \tag{III.6}$$

then equations (III.1) and (III.2) may be rewritten as

$$H = H^* \exp(i\sigma m\Delta x) \cdot \lambda^r \tag{III.7}$$

$$Q = Q^* \exp(i\sigma m\Delta x) \cdot \lambda^r \quad , \tag{III.8}$$

and $\lambda = \exp(i\beta'\tau)$, where β' is the computed wave frequency.

Considering the equation of continuity (3.5) and the linear form of the equation of motion (3.6) of the implicit method, we have

$$\frac{b}{\tau}\left(\frac{H_{m+1}^{r+1} + H_{m}^{r+1}}{2} - \frac{H_{m+1}^{r} + H_{m}^{r}}{2}\right) + \frac{1}{\Delta x}\left(Q_{m+1}^{r+1} - Q_{m}^{r+1}\right) = 0 \tag{III.9}$$

$$\frac{1}{\tau}\left(\frac{Q_{m+1}^{r+1} + Q_{m}^{r+1}}{2} - \frac{Q_{m+1}^{r} + Q_{m}^{r}}{2}\right) + \frac{gA}{\Delta x}\left(H_{m+1}^{r+1} - H_{m}^{r+1}\right) = 0 \quad , \tag{III.10}$$

where A is the cross-sectional area, b the width (and hence A/b equals the depth, a). Substituting from equations (III.7) and (III.8), we obtain

$$\frac{b\Delta x}{\tau}(\lambda-1)\cos\frac{\sigma\Delta x}{2} + \frac{Q^*}{H^*} 2\lambda \, i \, \sin\frac{\sigma\Delta x}{2} = 0 \tag{III.11}$$

$$\frac{Q^*}{H^*}(\lambda-1)\cos\frac{\sigma\Delta x}{2} + \frac{gA\tau}{\Delta x} 2\lambda \, i \, \sin\frac{\sigma\Delta x}{2} = 0 \quad . \tag{III.12}$$

On eliminating Q^*/H^*,

$$\left(\frac{\lambda-1}{2\lambda}\right)^2 = \frac{-\tau^2}{\Delta x^2}\frac{gA}{b}\tan^2\frac{\sigma\Delta x}{2},$$
(III.13)

or

$$\lambda = \frac{1}{1 \pm 2\alpha\ i\ \tan\frac{\pi}{M}},$$
(III.14)

where

$$\alpha = \frac{\tau}{\Delta x}\sqrt{ga}$$
(III.15)

and

$$M = \frac{2\pi}{\sigma}\frac{1}{\Delta x} = \frac{L}{\Delta x},$$
(III.16)

so that M is the number of sections per physical wavelength. Furthermore there are M/α time intervals per period, so that the quantity M^2/α is proportional to the number of computations required for a given schematization and time step choice.

From equation (III.14),

$$\lambda_{1,2} = \frac{1 \pm i\ 2\alpha\ \tan\ \pi/M}{1 + 4\alpha^2\ \tan^2\ \pi/M}.$$
(III.17)

The von Neumann necessary condition for stability is that

$$|\lambda_{1,2}| \leq 1.$$
(III.18)

From equation (III.17),

$$|\lambda_{1,2}| = \frac{1}{\sqrt{1 + 4\alpha^2\ \tan^2\frac{\pi}{M}}},$$
(III.19)

which is always less than 1, thus the system is unconditionally stable.

To investigate the amplitude distortion occurring over one cycle, one raises $|\lambda|$ to the power M/α (this quantity being the number

of time intervals per period). We then have

$$|\lambda|^{M/\alpha} = \left[1 + 4\alpha^2 \tan^2 \frac{\pi}{M} \right]^{\frac{-M}{2\alpha}} , \tag{III.20}$$

or

$$|\lambda|^{M/\alpha} = \left[1 + \frac{4\tau^2 ga}{\Delta x^2} \tan^2 \frac{\pi \Delta x}{L} \right]^{-\frac{T}{2\pi}} .$$

To investigate the phase distortion that takes place over a physical wavelength one obtains the value β' (in the expression $\lambda = \exp(i\beta'\tau)$) from equation (III.17), so that β' is 2π times the actual wave frequency. To do this one needs the real part of β' , since the imaginary part contributes only to the amplitude distortion. Thus

$$\beta' = \frac{1}{\tau} \text{Re}(\beta'\tau) \tag{III.21}$$

$$= \frac{1}{\tau} \sin^{-1} \left(\frac{2\alpha \tan \pi/M}{1 + 4\alpha^2 \tan^2 \pi/M} \right) \tag{III.22}$$

$$= \frac{1}{\tau} \tan^{-1} \left(2\alpha \tan \frac{\pi}{M} \right) . \tag{III.23}$$

The phase lag or lead over a wavelength is found from the quantity $2\pi(\beta'/\beta -1)$:

$$\text{Phase lag or lead} = 2\pi \left(\frac{\tan^{-1} (2\alpha \tan \pi/M)}{\tau\beta} - 1 \right) \tag{III.24}$$

$$= 2\pi \left(\frac{\tan^{-1} (2\alpha \tan \pi/M)}{2\alpha \frac{\pi}{M}} - 1 \right) \tag{III.25}$$

or

$$= 2\pi \left(\frac{\tan^{-1} \left(2 \frac{\tau\sqrt{ga}}{\Delta x} \tan \frac{\pi \Delta x}{L} \right)}{\frac{2\pi\tau}{T}} \right)$$

since

$$\frac{\alpha}{M} = \frac{\tau\sqrt{ga}}{\Delta x} \cdot \frac{\Delta x}{L} = \frac{\tau\sqrt{ga}}{L} = \frac{\tau}{T} = \frac{\tau\beta}{2\pi} \quad .$$

Before the curves of amplitude and phase error can be drawn, it is necessary to inspect the behavior of each. The behavior of the amplitude error for certain combinations of α and M may easily be investigated. Considering equation (III.20):

$$|\lambda|^{M/\alpha} = \left[1 + 4\alpha^2 \tan^2 \frac{\pi}{M} \right]^{-\frac{M}{2\alpha}} \tag{III.20}$$

$$= 1 + \left(-\frac{M}{2\alpha} \right) 4\alpha^2 \tan^2 \frac{\pi}{M} + \frac{\left(+\frac{M}{2\alpha} \right)\left(+\frac{M}{2\alpha} + 1 \right)}{2} \left(4\alpha^2 \tan^2 \frac{\pi}{M} \right)^2 + \ldots$$

$$= 1 - 2M\alpha \tan^2 \frac{\pi}{M} + \frac{\left(M^2 + 2M\alpha \right)}{2.4\alpha^2} \cdot 16\alpha^4 \tan^4 \frac{\pi}{M} - \ldots$$

$$= 1 - 2M\alpha \tan^2 \frac{\pi}{M} + 2 \left(M^2 + 2M\alpha \right) \alpha^2 \tan^4 \frac{\pi}{M} - \ldots$$

$$\tag{III.26}$$

Case 1. $\alpha = 0$, $M > 2$.

$$|\lambda|^{M/\alpha} = 1 \quad .$$

Case 2. $\tau < T/2\pi^2$ and $M \gg 2$.

$$|\lambda|^{M/\alpha} = 1 - \frac{2\pi^2\alpha}{M} \text{ , and is always } > 0 \quad .$$

Case 3. $M=2$, $\alpha > 0$.

$$|\lambda|^{M/\alpha} = \left[1 + 4\alpha^2 \tan^2 \frac{\pi}{2} \right]^{-\frac{1}{\alpha}} = 0 \quad .$$

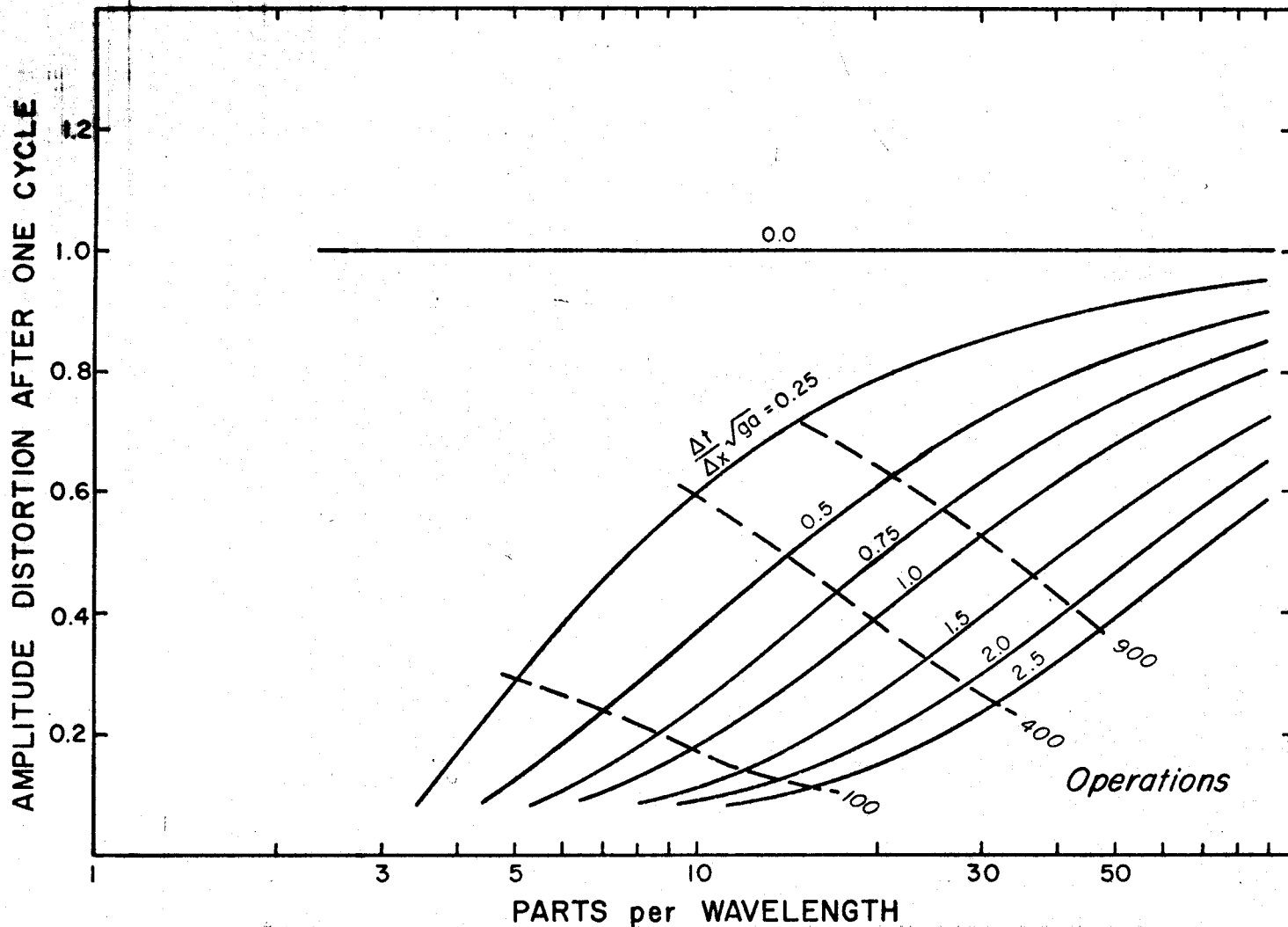The behavior of the amplitude error is shown in Figure III.1.

Figure III.1. Amplitude Distortion vs Parts per Wavelength.

It is also of interest to investigate the behavior of $\frac{\beta'}{\beta}$ for certain combinations of α and M. Considering equation (III.25), we have

$$\frac{\beta'}{\beta} = \frac{\tan^{-1}(2\alpha \tan \pi/M)}{2\alpha \ \pi/M} \ . \tag{III.27}$$

Case 1. $\alpha \to 0$, $M > 2$.

$$\frac{\beta'}{\beta} \to \frac{\tan \frac{\pi}{M}}{\frac{\pi}{M}} \qquad (ie. \ \frac{\beta'}{\beta} > 1) \ .$$

Case 2. $\alpha = 0.5$, $M > 2$.

$$\frac{\beta'}{\beta} \to \frac{\pi/M}{\pi/M} \qquad (ie. \ \frac{\beta'}{\beta} = 1) \ .$$

Case 3. $\frac{\alpha\pi}{M} < 0.5$, $M \gg 1$.

$$\frac{\beta'}{\beta} \to \frac{\tan^{-1}\left\{ 2\alpha\left[\left(\frac{\pi}{M}\right) + \frac{1}{3}\left(\frac{\pi}{M}\right)^3 + \dots \right] \right\}}{2\alpha \frac{\pi}{M}} \tag{III.28}$$

$$= \frac{2\alpha\left\{ \frac{\pi}{M} + \frac{1}{3}\left(\frac{\pi}{M}\right)^3 \right\}}{2\alpha \frac{\pi}{M}} - \frac{1}{3}\frac{\left\{ (2\alpha)^3 \ \frac{\pi}{M} + \frac{1}{3}\left(\frac{\pi}{M}\right)^3 \right\}^3}{2\alpha \frac{\pi}{M}} + \dots$$

$$= 1 + \frac{1}{3}\left(\frac{\pi}{M}\right)^2 \left(1 - 4\alpha^2\right) + \dots \tag{III.29}$$

ie. $\frac{\beta'}{\beta} > 1$ for $\alpha < 0.5$ and $M \gg 1$,

$\frac{\beta'}{\beta} = 1$ for $\alpha = 0.5$ and $M \gg 1$,

$\frac{\beta'}{\beta} < 1$ for $\alpha > 0.5$ and $M \gg 1$.

Case 4.   M=2.

As M decreases from ∞ to 4, from equation (III.27)

$\frac{\beta'}{\beta}$ ranges from $\frac{\tan^{-1}(0)}{\frac{\alpha\pi}{M}}$ to $\frac{\tan^{-1}(2\alpha)}{\frac{\alpha\pi}{2}}$.

As the value M=2 is approached, we have

$\frac{\beta'}{\beta} \to \frac{\tan^{-1} 2\alpha \tan\left(\frac{\pi}{2} - \epsilon\right)}{\alpha\pi}$, where ϵ is small.

Thus, for continuity of the arc tangent, at M=2 we get

$\frac{\beta'}{\beta} = \frac{\pi/2}{\alpha\pi} = \frac{1}{2\alpha}$.

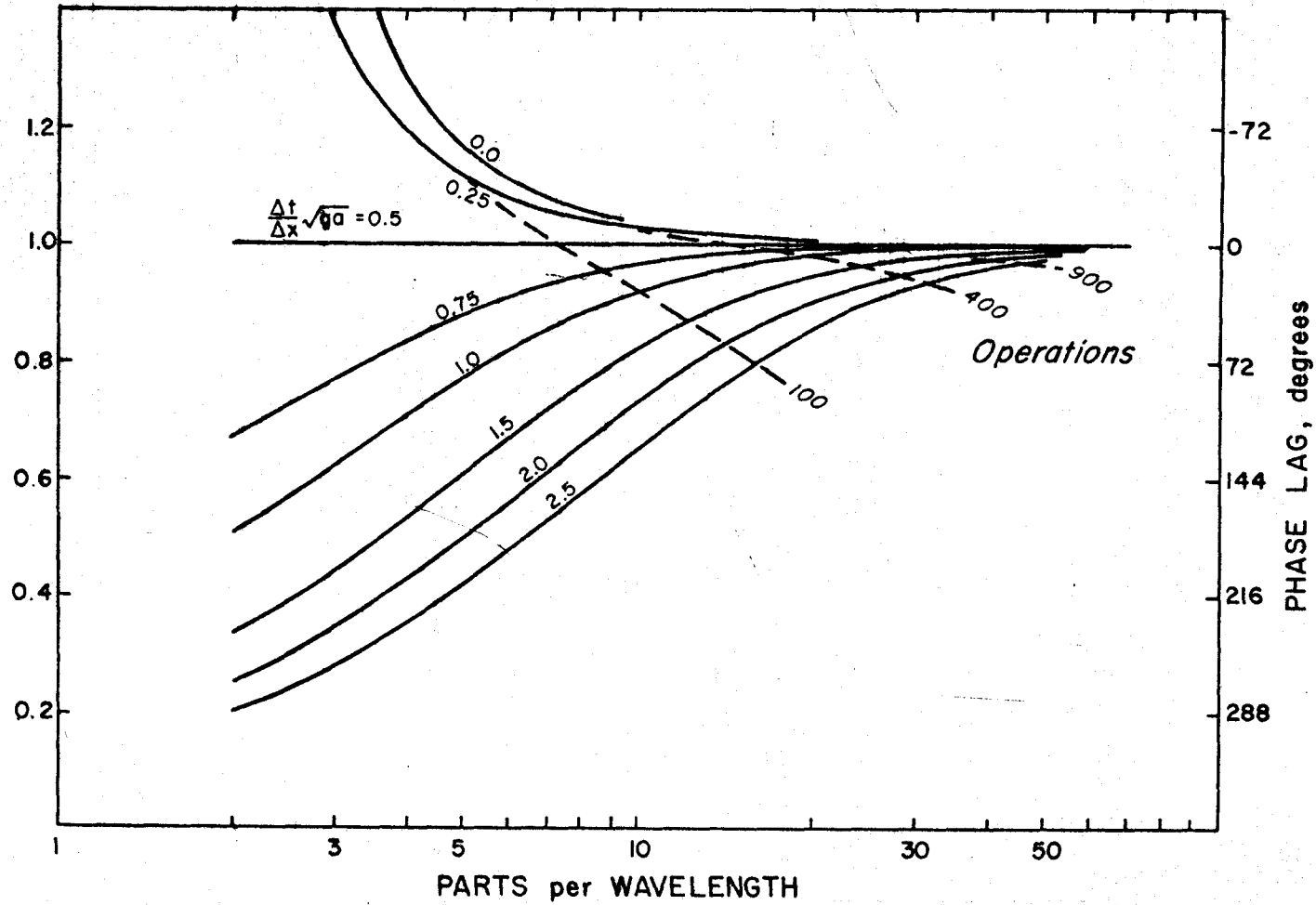The graph of $\frac{\beta'}{\beta}$ vs M for various values of α is shown in Figure III.2.

Figure III.2.   Phase Distortion vs Parts per Wavelength.

COMPACT FORM OF THE FINITE-DIFFERENCE EQUATIONS FOR
THE ONE-DIMENSIONAL IMPLICIT METHOD

Equation (3.5) is rewritten in the form

$$\frac{(\Delta x)_m \, b_m}{2\tau} \left(H'_{m+1} + H'_m \right) + \left(Q'_{m+1} - Q'_m \right) = \frac{(\Delta x)_m \, b_m \left(H_{m+1} + H_m \right)}{2\tau} \, ,$$

(IV.1)

so that equations (3.9a) and (3.9b) follow at once when equation (IV.1) is compared with equation (3.7).

Equation (3.6) is rewritten as

$$H'_{m+1} - H'_m = - \frac{(\Delta x)_m}{2\tau \, gA_m} \left(Q'_{m+1} + Q'_m - Q_{m+1} - Q_m \right)$$

$$- \frac{\left(b_{sm} + b_m \right)\left(Q_{m+1} + Q_m \right)}{2g \, A_m^2 \, b_m} \left(Q'_{m+1} - Q'_m \right)$$

$$- \frac{(\Delta x)_m \left| Q_{m+1} + Q_m \right|}{4 \, C_m^2 \, A_m^2 \, (a_o + h)_m} \left(Q'_{m+1} + Q'_m \right) .$$

(IV.2)

Equation (IV.2) is further condensed by writing it in the form

$$H'_{m+1} - H'_m = AC_m \left(Q'_{m+1} + Q'_m - Q_{m+1} - Q_m \right)$$

$$+ BRN_m \left(Q'_{m+1} - Q'_m \right) + FR_m \left(Q'_{m+1} + Q'_m \right) ,$$

(IV.3)

where

$$AC_m = \frac{-(\Delta x)_m}{2\tau \, gA_m}$$

(IV.4a)

$$BRN_m = \frac{-(b_{sm} + b_m)(Q_{m+1} + Q_m)}{2\, gA_m^2\, b_m} \qquad\text{(IV.4b)}$$

$$FR_m = \frac{-(\Delta x)_m |Q_{m+1} + Q_m|}{4\, C_m^2\, A_m^2\, (a_o + h)_m} . \qquad\text{(IV.4c)}$$

On rearranging equation (IV.3), we have

$$H'_{m+1} - H'_m + \left(-AC_m - BRN_m - FR_m \right) Q'_{m+1} + \left(-AC_m + BRN_m - FR_m \right) Q'_m$$

$$= -AC_m \left(Q_{m+1} + Q_m \right), \qquad\text{(IV.5)}$$

so that a comparison of equation (IV.5) with equation (3.8) yields
equations (3.9c), (3.9d), and (3.9e).

The purpose of writing the equation of motion in the form of
equation (IV.3) is that, once all the values at the upper time level
have been calculated, the contributions from the acceleration,
bernoulli, and friction terms to the difference in tide height
$(H'_{m+1} - H'_m)$ may easily be obtained. This method for determining
the relative importance of the various terms in the equations of
motion has been used by Dronkers (1964, p. 197). An example is shown
in Appendix V.

EXAMPLE OF BRANCH-POINT SOLUTION FOR THE
ONE-DIMENSIONAL IMPLICIT METHOD

A branch-point solution will be shown for the river branch scheme discussed in Chapter III. (See Figure II.1.) The application of equations (3.21) and (3.34) to the six river branches yields the following 12 equations (where primed superscripts have been dropped for convenience).

$$H_1 = - p_1^* \, Q_1 + r_1^* + a_1^* \, H_3 \qquad\qquad (V.1a)$$

$$H_3 = - p_3 \, Q_3 + r_3 + a_3 \, H_1 \qquad\qquad (V.1b)$$

$$H_4 = - p_4^* \, Q_4 + r_4^* + a_4^* \, H_8 \qquad\qquad (V.2a)$$

$$H_8 = - p_8 \, Q_8 + r_8 + a_8 \, H_4 \qquad\qquad (V.2b)$$

$$H_9 = - p_9^* \, Q_9 + r_9^* + a_9^* \, H_{13} \qquad\qquad (V.3a)$$

$$H_{13} = - p_{13} \, Q_{13} + r_{13} + a_{13} \, H_9 \qquad\qquad (V.3b)$$

$$H_{14} = - p_{14}^* \, Q_{14} + r_{14}^* + a_{14}^* \, H_{19} \qquad\qquad (V.4a)$$

$$H_{19} = - p_{19} \, Q_{19} + r_{19} + a_{19} \, H_{14} \qquad\qquad (V.4b)$$

$$H_{20} = - p_{20}^* \, Q_{20} + r_{20}^* + a_{20}^* \, H_{22} \qquad\qquad (V.5a)$$

$$H_{22} = - p_{22} \, Q_{22} + r_{22} + a_{22} \, H_{20} \qquad\qquad (V.5b)$$

$$H_{23} = -p_{23}^* Q_{23} + r_{23}^* + a_{23}^* H_{25} \qquad \text{(V.6a)}$$

$$H_{25} = -p_{25} Q_{25} + r_{25} + a_{25} H_{23} \ . \qquad \text{(V.6b)}$$

At this stage we have 24 unknowns.

Next, one puts the branch-point heights equal (equations (3,39a,b,c), (3.40 a,b,c) and (3.41a,b,c)), and expresses the flow rates at both ends of the branches in terms of the heights at both ends. This yields the following 12 equations.

$$Q_1 = (-H_F + r_1^* + a_1^* H_E)/p_1^* \qquad \text{(V.7a)}$$

$$Q_3 = (-H_E + r_3 + a_3 H_F)/p_3 \qquad \text{(V.7b)}$$

$$Q_4 = (-H_E + r_4^* + a_4^* H_D)/p_4^* \qquad \text{(V.8a)}$$

$$Q_8 = (-H_D + r_8 + a_8 H_E)/p_8 \qquad \text{(V.8b)}$$

$$Q_9 = (-H_E + r_9^* + a_9^* H_D)/p_9^* \qquad \text{(V.9a)}$$

$$Q_{13} = (-H_D + r_{13} + a_{13} H_E)/p_{13} \qquad \text{(V.9b)}$$

$$Q_{14} = (-H_D + r_{14}^* + a_{14}^* H_C)/p_{14}^* \qquad \text{(V.10a)}$$

$$Q_{19} = (-H_C + r_{19} + a_{19} H_D)/p_{19} \qquad \text{(V.10b)}$$

$$Q_{20} = (-H_C + r_{20}^* + a_{20}^* H_A)/p_{20}^* \qquad \text{(V.11a)}$$

$$Q_{22} = (-H_A + r_{22} + a_{22} H_C)/p_{22} \qquad \text{(V.11b)}$$

$$Q_{23} = (-H_C + r_{23}^* + a_{23}^* H_B)/p_{23}^* \qquad \text{(V.12a)}$$

$$Q_{25} = (-H_B + r_{25} + a_{25} H_C)/p_{25} \; . \qquad \text{(V.12b)}$$

The number of unknowns have now been reduced to 18.

Next, one makes use of the mass continuity relations (3.36), (3.37), and (3.38) to give the following three equations:

$$C_1 H_E + C_2 H_F + C_3 H_D + C_4 = 0 \qquad \text{(V.13)}$$

$$C_5 H_D + C_6 + C_7 H_E + C_8 H_C = 0 \qquad \text{(V.14)}$$

$$C_9 H_C + C_{10} + C_{11} H_D + C_{12} H_A + C_{13} H_B = 0 \qquad \text{(V.15)}$$

where

$$C_1 = -\frac{1}{p_3} + \frac{1}{p_4^*} + \frac{1}{p_9^*} \; ; \qquad C_2 = \frac{a_3}{p_3} \; ;$$

$$C_3 = -\frac{a_4^*}{p_4^*} - \frac{a_9^*}{p_9^*} \; ; \qquad C_4 = \frac{r_3}{p_3} - \frac{r_4^*}{p_4^*} - \frac{r_9^*}{p_9^*} \; ;$$

$$C_5 = -\frac{1}{p_8} - \frac{1}{p_{13}} + \frac{1}{p_{14}^*} \; ; \qquad C_6 = \frac{r_8}{p_8} + \frac{r_{13}}{p_{13}} - \frac{r_{14}^*}{p_{14}^*} \; ;$$

$$C_7 = \frac{a_8}{p_8} + \frac{a_{13}}{p_{13}} \; ; \qquad C_8 = -\frac{a_{14}^*}{p_{14}^*} \; ;$$

$$C_9 = -\frac{1}{p_{19}} + \frac{1}{p_{20}^*} + \frac{1}{p_{23}^*} \; ; \qquad C_{10} = \frac{r_{19}}{p_{19}} - \frac{r_{20}^*}{p_{20}^*} - \frac{r_{23}^*}{p_{23}^*} \; ;$$

$$C_{11} = \frac{a_{19}}{p_{19}} \; ; \qquad C_{12} = -\frac{a_{20}^*}{p_{20}^*} \; ;$$

$$C_{13} = -\frac{a_{23}^*}{p_{23}^*} \; .$$

On placing $Q_{22} = Q_{25} = 0$ in equations (V.11b) and (V.12b) we obtain

$$C_{14} H_A + C_{15} + C_{16} H_C = 0 \qquad (V.16)$$

$$C_{17} H_B + C_{18} + C_{19} H_C = 0 , \qquad (V.17)$$

where

$$C_{14} = \frac{-1}{P_{22}} ; \quad C_{15} = \frac{r_{22}}{P_{22}} ; \quad C_{16} = \frac{a_{22}}{P_{22}} ;$$

$$C_{17} = \frac{-1}{P_{25}} ; \quad C_{18} = \frac{r_{25}}{P_{25}} ; \quad C_{19} = \frac{a_{25}}{P_{25}} .$$

The original 24 unknowns have now been reduced to the six unknowns that are contained in the five equations (V.13) through (V.17). When H_F is supplied as boundary condition, the five simultaneous equations may be solved to yield the five remaining unknown heights. The process, although straight forward, will be summarized for the sake of completeness. Equations (V.16), (V.17) and (V.13) at once give

$$H_A = - \left(C_{15} + C_{16} H_C \right) / C_{14} \qquad (V.18)$$

$$H_B = - \left(C_{18} + C_{19} H_C \right) / C_{17} \qquad (V.19)$$

and

$$H_D = - \left(C_1 H_E + C_2 H_F + C_4 \right) / C_3 . \qquad (V.20)$$

The next step is to produce a pair of simultaneous equations. The first is easily obtained after the substitution of equation (V.20) into equation (V.14):

$$D_1 H_E + D_2 + D_3 H_C = 0 , \qquad (V.21)$$

where

$$D_1 = C_7 - \frac{C_1 C_5}{C_3} \quad ;$$

$$D_2 = C_6 - \frac{C_5(C_4 + C_2 H_F)}{C_3} \quad ;$$

$$D_3 = C_8 \quad .$$

On substituting equations (V.18) and (V.19) into equation (V.15),
we get

$$\left(C_9 - \frac{C_{12} C_{16}}{C_{14}} - \frac{C_{13} C_{19}}{C_{17}} \right) H_C + \left(C_{10} - \frac{C_{12} C_{15}}{C_{14}} - \frac{C_{13} C_{18}}{C_{17}} \right)$$

$$+ C_{11} H_D = 0 \quad . \tag{V.22}$$

The substitution of equation (V.20) into equation (V.22) yields
the second of the simultaneous equations:

$$D_4 H_C + D_5 + D_6 H_E = 0 \quad , \tag{V.23}$$

where

$$D_4 = C_9 - \frac{C_{12} C_{16}}{C_{14}} - \frac{C_{13} C_{19}}{C_{17}} \quad ;$$

$$D_5 = C_{10} - \frac{C_{12} C_{15}}{C_{14}} - \frac{C_{13} C_{18}}{C_{17}} - \frac{C_{11}(C_4 + C_2 H_F)}{C_3} \quad ;$$

$$D_6 = - \frac{C_1 C_{11}}{C_3} \quad .$$

The solution of equations (V.20) and (V.23) yields

$$H_E = \frac{D_2 D_4 - D_3 D_5}{D_3 D_6 - D_1 D_4} \quad ; \tag{V.24}$$

$$H_C = \frac{D_1 D_5 - D_2 D_6}{D_3 D_6 - D_1 D_4} . \qquad\qquad \text{(V.25)}$$

Thus the procedure for the branch-point solution is to evaluate the constants C_1, C_2, ..., C_{19}, D_1, D_2, ..., D_6, and then to evaluate H_E, H_C, H_D, H_B, and H_A. The remaining unknown heights and flow rates can then be determined.

Some results of interest are shown in Figures V.1, V.2 and V.3. The modulus of the maximum tidal excursions along with the delay of high tide are shown in Figure V.1. Also shown on the same figure are the results of the harmonic method. Some idea of the distortion and change of mean sea level that occur as one proceeds up the inlet can be seen in Figure V.2. An example of an investigation into the contribution of acceleration, convective acceleration and friction terms to the difference in height between the ends of a section (as mentioned in Appendix IV) is shown in Figure V.3.
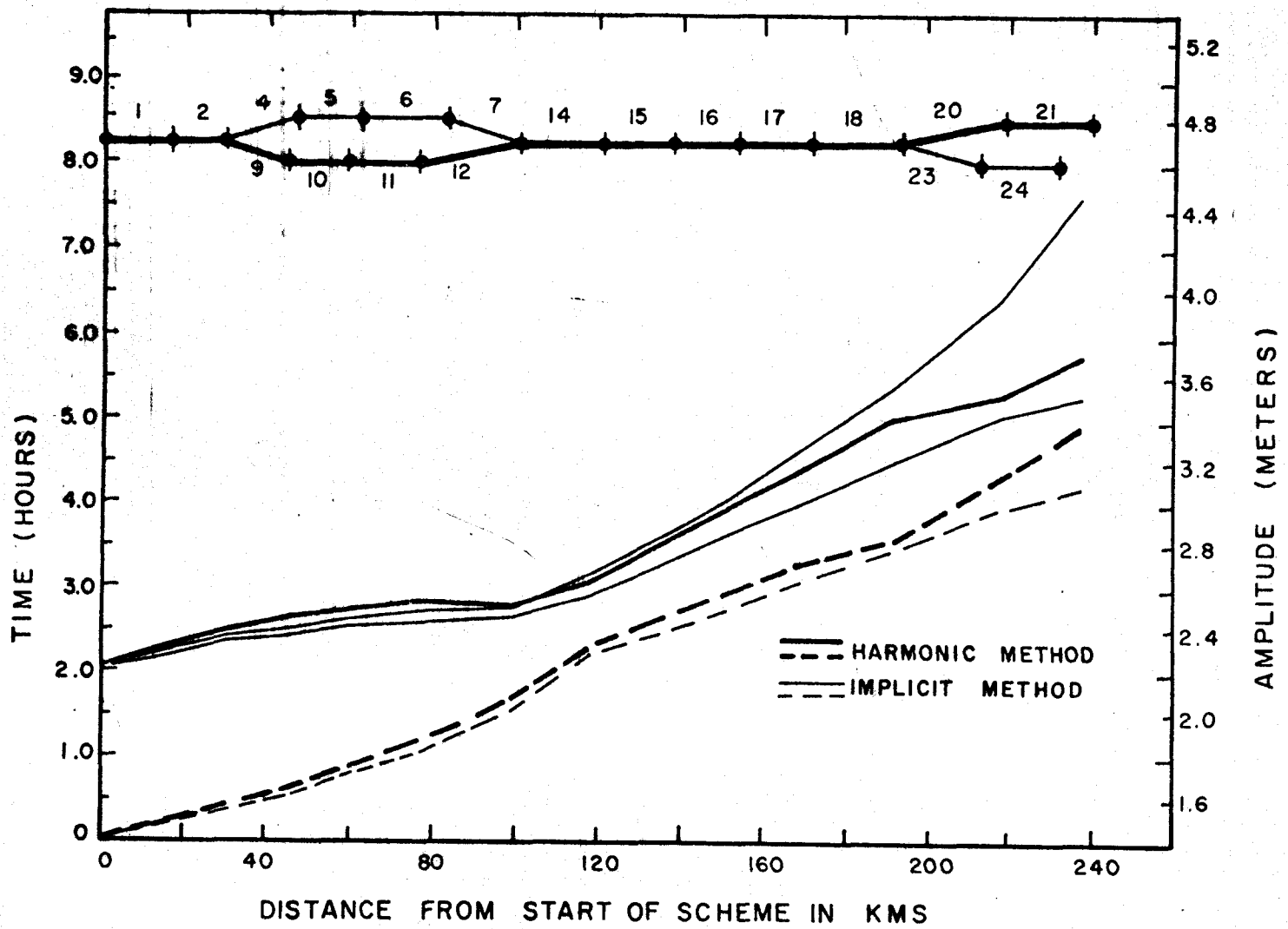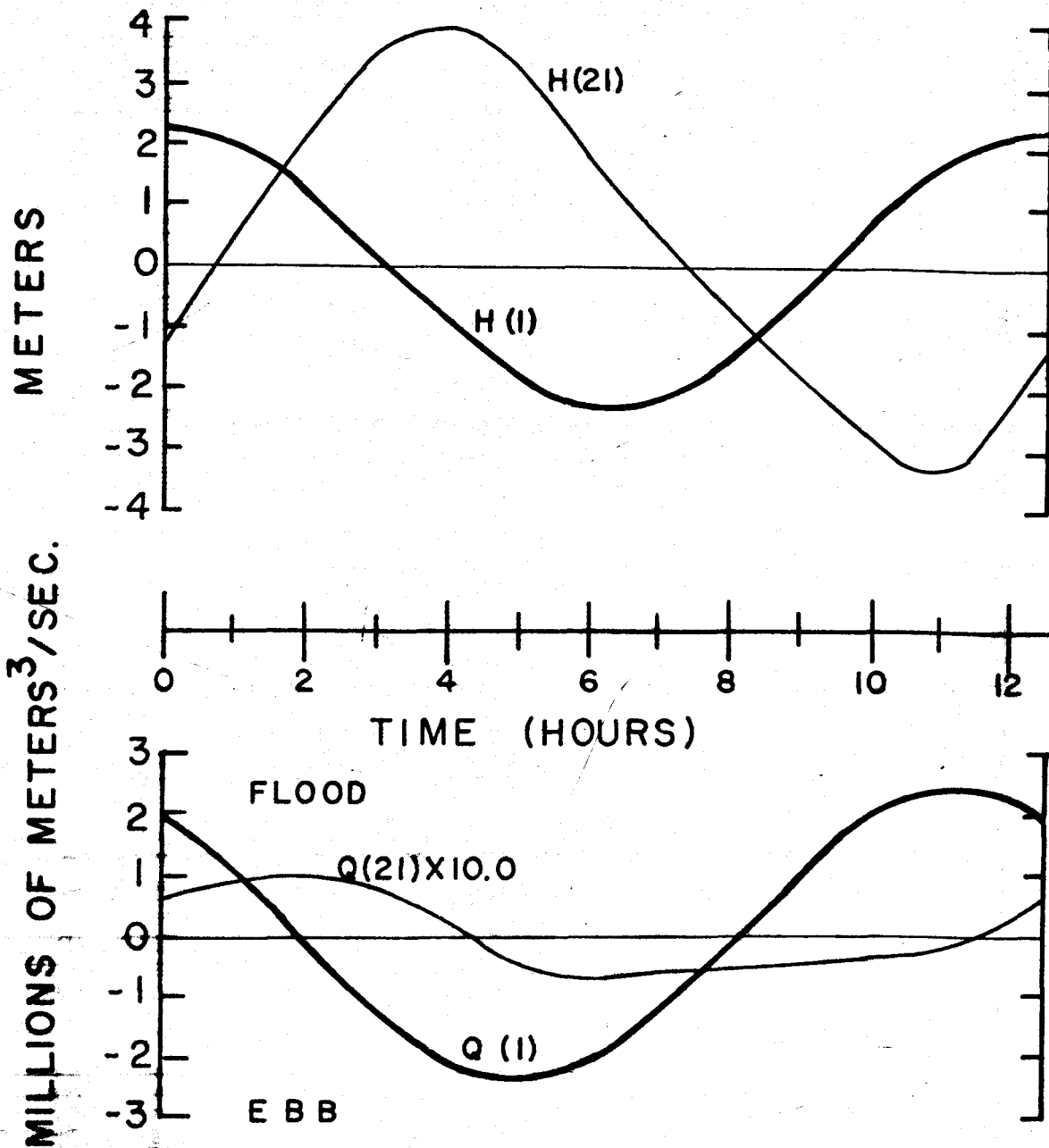
Figure V.1. Results of Harmonic and Implicit Methods.

Figure V.2. Distortion of tide as predicted by Implicit Method.
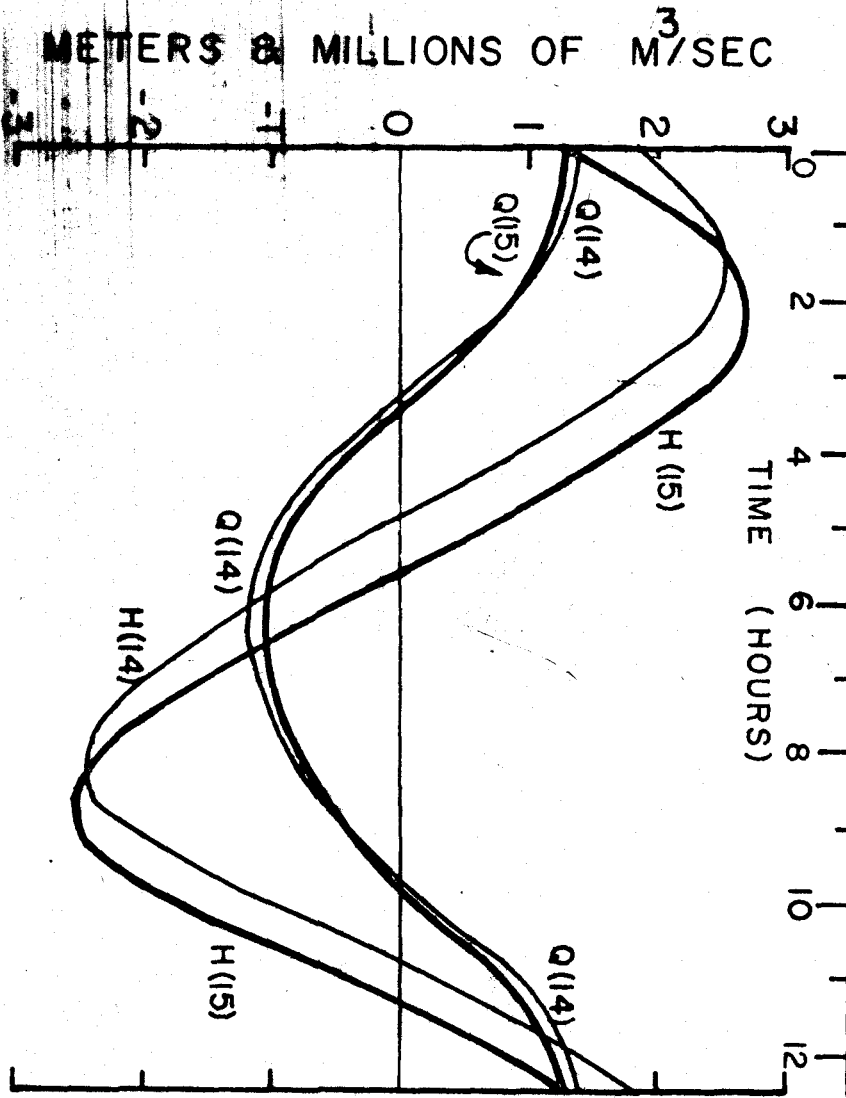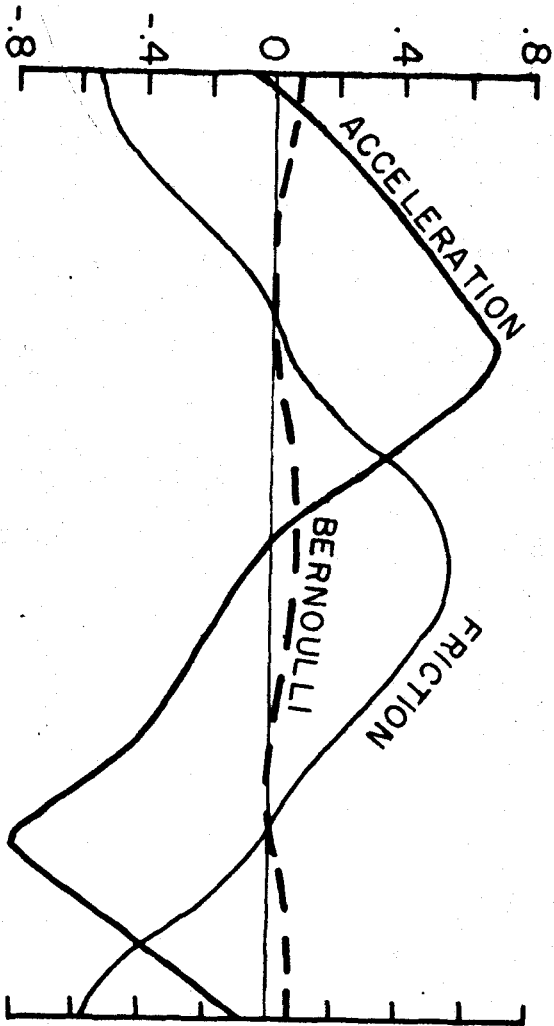
Figure V.3. Contribution of various terms to $(H_{15} - H_{14})$.

COMPACT FORM OF THE FINITE-DIFFERENCE EQUATIONS
FOR THE TWO-DIMENSIONAL IMPLICIT METHOD

First Computation Step.

Equation (4.9) is rewritten as

$$U'_n - U_n = \frac{\tau f}{2} V_m - \frac{\tau g}{2(\Delta x)_m}\left(H'_{m+1,n} - H'_{m-1,n}\right) - R_1 U'_n \quad . \qquad (VI.1)$$

Thus

$$U'_n + \frac{\tau g}{2(\Delta x)_m}\frac{\left(H'_{m+1,n} - H'_{m-1,n}\right)}{(1 + R_1)} = \frac{U_n}{(1 + R_1)} + \frac{\tau f}{2}\frac{V_m}{(1 + R_1)} \quad ,$$

so that, on replacing U'_n by $\dfrac{U'_{m+1,n} + U'_{m-1,n}}{2}$, etc.,

$$U'_{m+1,n} + U'_{m-1,n} + \frac{\tau g}{(\Delta x)_m(1 + R_1)}\left(H'_{m+1,n} - H'_{m-1,n}\right) =$$

$$\frac{\left(U_{m+1,n} + U_{m-1,n}\right)}{(1 + R_1)} + \frac{\tau f}{2(1 + R_1)}\left(V_{m,n+1} + V_{m,n-1}\right).$$

$$(VI.2)$$

This, when compared with

$$U'_{m+1,n} + U'_{m-1,n} + \alpha_m\left(H'_{m+1,n} - H'_{m-1,n}\right) = \beta_m \quad , \qquad (5.1)$$

results in equations (5.3a) and (5.3b).

Equation (4.10) is rewritten as

$$2 H'_n - \left(H_m + H_n\right) + \frac{\tau}{(\Delta x)_m}\left(U'_{m+1,n} d_{m+1,n} - U'_{m-1,n} d_{m-1,n}\right) =$$

$$- \frac{\tau}{(\Delta y)_n}\left(V_{m,n+1} d_{m,n+1} - V_{m,n-1} d_{m,n-1}\right) , \qquad (VI.3)$$

so that

$$H'_{m+1,n} + H'_{m-1,n} + \frac{\tau \, d_{m+1,n}}{(\Delta x)_m} U'_{m+1,n} - \frac{\tau \, d_{m-1,n}}{(\Delta x)_m} U'_{m-1,n} =$$

$$- \frac{\tau}{(\Delta y)_n} \left(V_{m,n+1} \, d_{m,n+1} - V_{m,n-1} \, d_{m,n-1} \right)$$

$$+ \frac{(H_{m,n+1} + H_{m,n-1})}{2} + \frac{(H_{m+1,n} + H_{m-1,n})}{2} . \qquad \text{(VI.4)}$$

This, when compared with

$$H'_{m+1,n} + H'_{m-1,n} + \gamma_m U'_{m+1,n} + \delta_m U'_{m-1,n} = \varepsilon_m , \qquad (5.2)$$

results in equations (5.3c), (5.3d), and (5.3e).

Second Computation Step.

Equation (4.16) is rewritten as

$$\bar{V}'_m - \bar{V}_m = - \frac{\tau f}{2} \bar{U}'_n - \frac{\tau g}{2(\Delta y)_n} \left(H'_{m,n+1} - H'_{m,n-1} \right) - R_2 \, \bar{V}'_m . \quad \text{(VI.5)}$$

Thus

$$\bar{V}'_m + \frac{\tau g}{2(\Delta y)_n} \frac{(H'_{m,n+1} - H'_{m,n-1})}{(1 + R_2)} = \frac{\bar{V}_n}{(1 + R_2)} - \frac{\tau f}{2} \frac{\bar{U}'_n}{(1 + R_2)} ,$$

so that

$$V'_{m,n+1} + V'_{m,n-1} + \frac{\tau g}{(\Delta y)_n (1 + R_2)} \left(H'_{m,n+1} - H'_{m,n-1} \right) =$$

$$\frac{(V_{m,n+1} + V_{m,n-1})}{(1 + R_2)} - \frac{\tau f}{2(1 + R_2)} \left(U'_{m+1,n} + U'_{m-1,n} \right) . \qquad \text{(VI.6)}$$

This, when compared with

$$V'_{m,n+1} + V'_{m,n-1} + \alpha_n \, H'_{m,n+1} - H'_{m,n-1} = \beta_n , \qquad (5.4)$$

results in equations (5.6a) and (5.6b).

Equation (4.14) is rewritten as

$$\bar{H}'_m + \bar{H}'_n - \bar{H}_m - \bar{H}_n + \frac{\tau}{(\Delta y)_n} \left(V'_{m,n+1}\, d_{m,n+1} - V'_{m,n-1}\, d_{m,n-1} \right) =$$

$$- \frac{\tau}{(\Delta x)_m} \left(U'_{m+1,n}\, d'_{m+1,n} - U'_{m-1,n}\, d'_{m-1,n} \right), \qquad \text{(VI.7)}$$

so that

$$H'_{m,n+1} + H'_{m,n-1} + \frac{2\tau\, d_{m,n+1}}{(\Delta y)_n}\, V'_{m,n+1} - \frac{2\tau\, d_{m,n-1}}{(\Delta y)_n}\, V'_{m,n-1} =$$

$$- \frac{2\tau}{(\Delta x)_m} \left(U'_{m+1,n}\, d'_{m+1,n} - U'_{m-1,n}\, d'_{m-1,n} \right) + H_{m,n+1} + H_{m,n-1}$$

$$+ H_{m+1,n} + H_{m-1,n} - H'_{m+1,n} - H'_{m-1,n} . \qquad \text{(VI.8)}$$

This, when compared with

$$H'_{m,n+1} + H'_{m,n-1} + \gamma_n\, V'_{m,n+1} + \delta_n\, V'_{m,n-1} = \epsilon_n , \qquad \text{(5.5)}$$

results in equations (5.6c), (5.6d), and (5.6e).

Third Computation Step.

Equation (4.16) is rewritten as

$$\bar{V}''_m - \bar{V}'_m = - \frac{\tau f}{2}\, \bar{U}'_n - \frac{\tau g}{2(\Delta y)_n} \left(H''_{m,n+1} - H''_{m,n-1} \right) - R_3\, \bar{V}''_m . \qquad \text{(VI.9)}$$

Thus

$$\bar{V}''_m + \frac{\tau g}{2(\Delta y)_n} \frac{\left(H''_{m,n+1} - H''_{m,n-1} \right)}{(1 + R_3)} = \frac{\bar{V}'_m}{(1 + R_3)} - \frac{\tau f}{2} \frac{\bar{U}'_n}{(1 + R_3)} ,$$

so that

$$V''_{m,n+1} + V''_{m,n-1} + \frac{-\tau g}{(\Delta y)_n (1 + R_3)} \left(H''_{m,n+1} - H''_{m,n-1} \right) =$$

$$\frac{V'_{m,n+1} + V'_{m,n-1}}{(1 + R_3)} - \frac{\tau f}{2(1 + R_3)} \left(U'_{m+1,n} + U'_{m-1,n} \right) .$$

$$(VI.10)$$

This, when compared with

$$V''_{m,n+1} + V''_{m,n-1} + \alpha_n \left(H''_{m,n+1} - H''_{m,n-1} \right) = \beta_n , \qquad (5.7)$$

results in equations (5.9a) and (5.9b).

Equation (4.17) is rewritten as

$$2 H''_m - \left(H'_m + H'_n \right) + \frac{\tau}{(\Delta y)_n} \left(V''_{m,n+1} d'_{m,n+1} - V''_{m,n-1} d'_{m,n-1} \right) =$$

$$- \frac{\tau}{(\Delta x)_m} \left(U'_{m+1,n} d'_{m+1,n} - U'_{m-1,n} d'_{m-1,n} \right) , \qquad (VI.11)$$

so that

$$H''_{m,n+1} + H''_{m,n-1} + \frac{\tau d'_{m,n+1}}{(\Delta y)_n} V''_{m,n+1} - \frac{\tau d'_{m,n-1}}{(\Delta y)_n} V''_{m,n-1} =$$

$$- \frac{\tau}{(\Delta x)_m} \left(U'_{m+1,n} d'_{m+1,n} - U'_{m-1,n} d'_{m-1,n} \right)$$

$$+ \frac{\left(H'_{m,n+1} + H'_{m,n-1} \right)}{2} + \frac{\left(H'_{m+1,n} + H'_{m-1,n} \right)}{2} . \qquad (VI.12)$$

This, when compared with

$$H''_{m,n+1} + H''_{m,n-1} + \gamma_n V''_{m,n+1} + \delta_n V''_{m,n-1} = \varepsilon_n , \qquad (5.8)$$

results in equations (5.9c), (5.9d), and (5.9e).

Fourth Computation Step.

Equation (4.19) is rewritten as

$$\bar{U}_n'' - \bar{U}_n' = -\frac{\tau f}{2}\bar{V}_m'' - \frac{\tau g}{2(\Delta x)_m}\left(H_{m+1,n}'' - H_{m-1,n}''\right) - R_4\,\bar{U}_n'' \quad . \quad (VI.13)$$

Thus

$$\bar{U}_n'' + \frac{\tau g}{2(\Delta x)_m}\frac{\left(H_{m+1,n}'' - H_{m-1,n}''\right)}{(1+R_4)} = \frac{\bar{U}_n'}{(1+R_4)} - \frac{\tau f}{2}\frac{\bar{V}_m''}{(1+R_4)} \quad ,$$

so that

$$U_{m+1,n}'' + U_{m-1,n}'' + \frac{\tau g}{(\Delta x)_m(1+R_4)}\left(H_{m+1,n}'' - H_{m-1,n}''\right) =$$

$$\frac{\left(U_{m+1,n}' + U_{m-1,n}'\right)}{(1+R_4)} - \frac{\tau f}{2(1+R_4)}\left(V_{m,n+1}'' + V_{m,n-1}''\right) \quad .$$

$$(VI.14)$$

This, when compared with

$$U_{m+1,n}'' + U_{m-1,n}'' + \alpha_m\left(H_{m+1,n}'' - H_{m-1,n}''\right) = \beta_m \quad , \quad (5.10)$$

results in equations (5.12a) and (5.12b).

Equation (4.20) is rewritten as

$$\bar{H}_m'' + \bar{H}_n'' - \bar{H}_m' - \bar{H}_n' + \frac{\tau}{(\Delta x)_m}\left(U_{m+1,n}''\,d_{m+1,n}' - U_{m-1,n}''\,d_{m-1,n}'\right) =$$

$$- \frac{\tau}{(\Delta y)_n}\left(V_{m,n+1}''\,d_{m,n+1}'' - V_{m,n-1}''\,d_{m,n-1}''\right),$$

$$(VI.15)$$

so that

$$\bar{H}_{m+1,n}'' + H_{m-1,n}'' + \frac{2\tau\,d_{m+1,n}'}{(\Delta x)_m}\,U_{m+1,n}'' - \frac{2\tau\,d_{m-1,n}'}{(\Delta x)_m}\,U_{m-1,n}'' =$$

$$- \frac{2\tau}{(\Delta y)_n}\left(V_{m,n+1}''\,d_{m,n+1}'' - V_{m,n-1}''\,d_{m,n-1}''\right)$$

$$+ H_{m,n+1}' + H_{m,n-1}' + H_{m+1,n}' + H_{m-1,n}' - H_{m,n+1}'' - H_{m,n-1}'' \quad .$$

$$(VI.16)$$

This, when compared with

$$H''_{m+1,n} + H''_{m-1,n} + \gamma_m U''_{m+1,n} + \delta_m U''_{m-1,n} = \epsilon_m \; , \tag{5.11}$$

results in equations (5.12c), (5.12d), and (5.12e).